Redox responsive miktoarm star polymers for drug delivery: Synthetic articulation and exploration of their micellar assemblies

by Victor Lotocki

Department of Chemistry
McGill University, Montreal
August 2020

A thesis submitted to McGill University in partial fulfillment of the requirements of the degree of Master of Science

Acknowledgements

First and foremost, I would like to thank my supervisor Prof. Ashok Kakkar. With his invaluable guidance, I have been able to succeed in my studies and develop myself as a researcher. His kind encouragement and willingness to explore new and interesting topics in polymer chemistry has allowed me to freely conduct research and has shaped my overall research direction. Meanwhile, his patient supervision has always kept me on track and deterred me giving up whenever I got disappointing results. Without his help, I would not have been able to complete this thesis, and for that I am truly grateful.

I am immensely thankful for the advice and contributions of all of my friends and research collaborators that have helped me in these two years including Hossein Yazdani, Qiaochu Zhang, Evan Rizzel Gran, Anastasiia Nyrko, and Parinaz Sabourian. On the subject of my collaborators, it has been an absolute pleasure to work with and discuss science with Prof. Dusica Maysinger. Not only did she give me the opportunity to apply my polymeric systems to drug delivery, but her critical approach to research has been truly eye-opening and has moved me to plan and conduct my own work more analytically.

My fellow lab members and friends Hui Wen Yong, Yu-Chen Wang, Alexandre Moquin, Mojhdeh Baghbanbashi, Ramez Hanna, Harrison Cassidy, and Quentin Gaydon have also all made daily life much more enjoyable and made a large positive impact on my stay in Montreal. I also want to acknowledge the diligent work carried out by my undergraduate research assistants Ari Bao, Brandon Andrade-Gagnon, Anastasiia Nyrko, Qiaochu Zhang, and Annie Tang.

I would have not been able to collect all the data necessary for my project without the help of the many researchers and staff members at McGill. Namely, Nadim Saadé, Adrien Métafiot, and Sharmaine Luk have been instrumental in helping me with polymer characterization through MALDI-TOF and GPC while also providing me with insightful suggestions on how I should develop and prepare my samples. Violeta Toader trained me in DLS, and after the Covid-19-related university closures, helped me greatly by acquiring DLS data in my place. I would also like to thank Jeannie Mui, Kelly Sears, and Prof. Hojatollah Vali for training me to use the TEM and teaching me how to interpret TEM micrographs. After the Covid-19-related closures, their exceptional skill in acquiring TEM micrographs provided me with some final important images needed for my thesis.

Finally, I would like to thank my mother, whose unending love has guided me this far in both my career and in my life.

Abstract

The delivery of lipophilic active pharmaceutical compounds to disease sites continues to be an active area of research due to their poor aqueous solubility and biological stability. The self-assembly of amphiphilic diblock copolymers into micellar nanoparticles has historically enabled the encapsulation of such drugs by solubilizing and stabilizing them within their hydrophobic cores, while hydrophilic coronae provides micelles with aqueous solubility and biological stealth. Miktoarm star polymers are branched architectures in which at least three polymeric arms emanate from a central core junction, and in which at least two of those arms are dissimilar. Such branching architectures form micelles with lower critical micelle concentrations (CMC), higher overall drug loading contents, and more sustained drug release profiles. The synthesis of miktoarm stars has traditionally been carried out by a combination of arm-first and core-first methodologies, in which polymer segments are synthesized first and then grafted to a central core molecule, or in which a heteromultifunctional core is used to initiate the polymerization of different arms respectively. Complications arising from low grafting efficiencies in arm-first methods, and difficulties in selecting different compatible functional groups for polymerization in core-first methods have prompted chemists to use a mixture of these two methods. The simplification of synthetic methods has helped enhance the scope miktoarm stars for applications in biology.

The goals of this thesis were the synthesis of autogenous stimuli-responsive AB_2 (A = polycaprolactone (PCL), B = poly(ethylene glycol) (PEG)) miktoarm star polymers using a mixed arm- and core-first methodologies, a detailed evaluation of their self-assemblies, and the development of drug delivery formulations that promote targeting, and decrease off-targeting. We demonstrated that a combination of ring opening polymerization and Steglich esterification can be used to generate modular “building blocks”, which consist of polymer segments with or without incorporated thioketal and disulfide moieties. The latter are responsive to reactive oxygen species (ROS) or glutathione (GSH) respectively. We demonstrated that the combination of such PEG- and PCL-based building blocks, coupled through efficient copper-catalyzed alkyne-azide cycloaddition (CuAAC) “click” reactions, can greatly simplify the construction of miktoarm stars with different compositions and the pre-determined position based incorporation of stimuli-responsive entities. Tissues surrounding disease sites are associated with high levels of extracellular ROS, while GSH is overproduced intracellularly. Considering this redox gradient,

thioketal and disulfide units were placed in spatially disparate locations near PEG chain ends or adjacent to the miktoarm polymer core junction. ROS-induced oxidative cleavage of thioketal moieties located along PEG backbones facilitates partial outer corona shedding in miktoarm stars self-assembled into micelles, thereby subtly increasing the release of loaded drugs, while keeping micelles intact. Micelles that are taken up intracellularly are exposed to heightened GSH concentrations that can reduce disulfide linkers at miktoarm polymer junctions, resulting in micellar collapse and a significant increase in drug release. This combination of stimuli presents a novel response pathway, through which nanodelivery particles can increasingly promote drug release, as they accumulate at diseased sites and are subsequently taken up by cells. It was also demonstrated that free thiol moieties, which become exposed on micellar surfaces following ROS-induced thioketal cleavage, can further oxidatively couple with each other in a ROS environment, thereby forming micellar networks. Micelles of small (<200 nm) diameters that distribute to tumours through the surrounding leaky vasculature can more efficiently be retained at these disease sites through such network formation, thus promoting drug delivery with decreased off-site targeting.

Résumé

La livraison d'ingrédients pharmaceutiques actifs hydrophobes aux sites de maladies continue d'être un domaine de recherche actif en raison de leur faible solubilité aqueuse et de leur stabilité biologique. Historiquement, l'auto-assemblage de copolymères amphiphiles en nanoparticules micellaires a permis l'encapsulation de ces produits pharmaceutiques en les solubilisant et en les stabilisant dans les noyaux hydrophobes, alors que les couronnes hydrophiles confèrent aux micelles la solubilité aqueuse et la furtivité biologique. Les polymères « miktoarm » sont des architectures ramifiées dans lesquelles au moins trois bras polymériques émanent d'une jonction centrale et dans lesquelles au moins deux de ces bras sont différents. Les architectures ramifiées s'assemblent en micelles avec des faibles concentrations micellaires critiques (CMC), un indice élevé de saturation de médicament et des taux de libération de médicament plus prolongés. La synthèse des polymères miktoarm a été conventionnellement réalisée par une combinaison de méthodologies dites « bras en premier » et « noyau en premier », dans lesquelles les segments polymères sont synthétisés puis greffés sur une molécule centrale, ou dans lesquels un noyau hétéromultifonctionnel est utilisé pour initier la polymérisation de bras polymériques différents respectivement. Les complications qui résultent de la faible efficacité de greffage dans les méthodes bras en premier et les difficultés dans la sélection de groupes fonctionnels différents qui sont compatibles pour la polymérisation avec une méthode noyau en premier ont incité les chimistes à utiliser un mélange de ces deux méthodes. La simplification des méthodes de synthèse a aidé à améliorer l'utilisation des polymères miktoarm pour des applications en biologie.

Les objectifs de cette thèse étaient la synthèse et l'évaluation des polymères miktoarm AB_2 (A = polycaprolactone (PCL), B = polyéthylène glycol (PEG)) sensibles aux stimuli autogènes en utilisant une méthodologie mixte de bras en premier et noyau en premier, une évaluation de leurs auto-assemblages et le développement de formulations d'administration de médicaments qui favorisent le ciblage et réduisent le hors-ciblage. Nous avons démontré qu'une combinaison de polymérisation par ouverture de cycle et d'estérification de Steglich a été utilisée pour synthétiser des « blocs de construction » modulaires, qui sont constitués de segments polymériques avec ou sans des groupes fonctionnels thiocétal et disulfure. Ces derniers sont sensibles respectivement aux dérivés réactifs de l'oxygène (DRO) et au glutathion (GSH). Nous avons démontré que la combinaison des blocs de construction à base de PEG et PCL, conjugués par des cycloadditions

alcyne-azoture catalysées par du cuivre (I), peut simplifier la construction des polymères miktoarm et l'incorporation d'entités sensibles aux stimuli. Les tissus entourant les sites de la maladie sont associés avec des niveaux élevés de DRO extracellulaires, tandis que le GSH est surproduit à l'intérieur des cellules. En raison de cette différence d'oxydoréduction, les groupes thiocétal et disulfure ont été placés à des emplacements spatialement éloignés près des extrémités de la chaîne de PEG ou à côté de la jonction du noyau polymère miktoarm. Le clivage oxydatif induit par les DRO des groupes thiocétaux situés le long de la chaîne de PEG a causé une perte partielle de la couronne dans les polymères miktoarm auto-assemblés en micelles, accélérant ainsi subtilement la libération des médicaments chargés, tandis que les micelles restent assemblées. Les micelles qui sont absorbées dans les cellules sont exposées à des concentrations élevées de GSH qui peuvent réduire les liaisons disulfures aux jonctions polymères miktoarm, résultant en un désassemblage micellaire et une augmentation significative de la libération des médicaments. Cette combinaison de stimuli présente une nouvelle voie de réponse, avec laquelle les nanoparticules peuvent de plus en plus favoriser la libération de médicaments lorsqu'elles s'accumulent dans des sites malades et sont ensuite absorbées par les cellules. Il a également été démontré que les groupes thiol libres, exposés sur les surfaces micellaires après un clivage thiocétal induit par les DRO, peuvent se lier par oxydation et former des réseaux micellaires. Les micelles de petits diamètres <200 nm qui peuvent déplacer vers les tumeurs à travers le système vasculaire poreux environnant peuvent être conservées plus efficacement sur les sites de la maladie grâce à la formation d'un réseau, favorisant la livraison de médicaments avec une réduction du ciblage hors-site.

Table of Contents

Acknowledgements ii
Abstract iii
Résumé v
Table of Contents vii
List of Figures xi
List of Tables xiv
List of Schemes xv
List of Abbreviations xvi
Contributions of Authors xxii

Chapter 1: Miktoarm star polymers: Branched architectures in drug delivery 1
1.1 Introduction 1
1.2. Synthetic Approaches to Miktoarm Star Polymers 6
1.2.1 Chlorosilane Based Synthesis 7
1.2.2 Core-First Synthesis 9
1.2.3 Arm-First Synthesis 11
1.2.4 In-Out Synthesis 13
1.2.5 Miktoarm Polymer Characterization 16
1.3. Amphiphilic Miktoarm Star Polymers: Self-Assembly 18
1.3.1 Micelle Characteristics: CMC and Stability 20
1.3.2 Micelle Drug Loading and Release 22
1.3.3 Non-spherical Micelles 23
1.3.4 Polymersomes 24
1.4. Drug Delivery 26
1.4.1 pH-Responsive Drug Delivery 28
1.4.2 Temperature-Responsive Drug Delivery 33
1.4.3 Redox-Responsive Drug Delivery 35
1.4.4 Light- and Dual-Responsive Drug Delivery 39
1.4.5 Polyplex Delivery 41
1.5. Conclusions and Future Perspective 44
1.6. References 46

Chapter 2: Miktoarm star polymers with environment-selective ROS/GSH responsive locations: From modular synthesis to tuned drug release through micellar partial corona shedding and/or core disassembly 56
2.1 Introduction 56
2.2 Materials and Methods 60
2.2.1 Synthesis 60
2.2.2 GPC Analyses 70
2.2.3 Preparation of Blank Micelles 71
2.2.4 CMC Determination 71
2.2.5 Drug Loading 71
2.2.6 Drug Release 72
2.2.7 Transmission Electron Microscopy 72
2.2.8 Cell Culture 72
2.2.9 Measurement of Intracellular and Extracellular ROS with CellROX® Deep Red 72
2.3 Results and Discussion 73
2.3.1 Building Block Synthesis 73
2.3.2 Miktoarm star polymers syntheses 76
2.3.3 Self-Assembly 78
2.3.4 Drug Loading 80
2.3.5 Stimulus Response 81
2.3.6 Drug Release 84
2.3.7 Effectiveness of curcumin-incorporated micelles to scavenge ROS in glioblastoma cells 87
2.4 Conclusions 89
2.5 References 90

Chapter 3: Evaluation of resveratrol loading and release from ROS- and GSH-responsive AB_2 miktoarm star polymer micelles 96
3.1 Introduction 96
3.2 Materials and Methods 99
3.2.1. Miktoarm Polymer Synthesis 99
3.2.2 Blank Micelle Preparation 101
3.2.3 Resveratrol-loaded Micelle Preparation 101

3.2.4 Calculation of Encapsulation Efficiency and Loading Capacity 101
3.2.5 CMC Determination 102
3.2.6 Resveratrol Release Profiles 102
3.2.7 Transmission Electron Microscopy 102
3.3 Results & Discussion 103
3.4 Conclusions and Future Work 106
3.5 References 107

Chapter 4: Autogenous ROS-induced miktoarm star polymer micelle coupling for enhanced retention and drug delivery 110
4.1 Introduction 110
4.2 Materials and Methods 112
4.2.1 Synthesis 113
4.2.2 GPC Analyses 115
4.2.3 Preparation of Blank Micelles 115
4.2.4 CMC Determination 115
4.2.5 Drug Loading 116
4.2.6 Drug Release 116
4.2.7 Transmission Electron Microscopy 116
4.3 Results and Discussion 117
4.3.1 Synthesis of miktoarm star polymer μ1B 117
4.3.2 Self-Assembly 119
4.3.3 ROS Response 120
4.3.4 Drug Loading and Release 124
4.4 Conclusions 125
4.5 References 125

Chapter 5: Conclusions and Future Perspective 129
5.1 Conclusions and Contributions to Original Knowledge 129
5.2 Future Perspectives 130

Appendix A 133
A.1. Synthetic Schemes 133
A.2. Supplementary Tables & Figures 138
A.3. NMR and Mass Spectra 152
Appendix B 175
Appendix C 176
C.1. Supplementary Tables & Figures 176
C.2 NMR and Mass Spectra 180
Appendix D
Publication: Sabourian, P.; Ji, J.; Lotocki, V.; Moquin, A.; Hanna, R.; Frounchi, M.; Maysinger, D.; Kakkar A. Facile Design of Autogenous Stimuli-Responsive chitosan/hyaluronic Acid Nanoparticles for Efficient Small Molecules to Protein Delivery. *J Mater. Chem. B* **2020**, *8,* 7275-7287.; and Electronic Supporting Information 186

List of Figures

Figure 1.1. Miktoarm polymer architectures of varied compositions. 3

Figure 1.2. Examples of core-first synthesis (left) and arm-first synthesis (right) with examples of functionalities, monomers, and polymers. 7

Figure 1.3. Schematic representation of PEG-PHLG CCS polymer synthesis using an in-out methodology. Reprinted with permission from reference 61. Copyright 2016 Royal Society of Chemistry. 16

Figure 1.4. Aqueous self-assembly of AB_2 miktoarm polymers into micelles and polymersomes, depending on polymer hydrophilic fraction (red = hydrophobic, blue = hydrophilic). 19

Figure 1.5. Cartoon schematic (left) and comparative TEM micrograph (right) of a polymersome assembled from a PEG-$PHis_2$ miktoarm star polymer with emphasis on its hydrophobic bilayer. Reprinted with permission from reference 43. Copyright 2012 Royal Society of Chemistry. 25

Figure 1.6. Fluorescent micrographs of macrophages treated with (A) curcumin-loaded PEG-PCL-TIF micelles, (B) unloaded PEG-PCL-TIF micelles, and (C) TIF control. Relative fluorescence intensities of macrophages treated with control media, TIF-loaded PEG-PCL micelles, curcumin-loaded PEG-PCL-TIF micelles, unloaded PEG-PCL-TIF micelles, free TIF, and free curcumin as a function of (D) treatment time and (E) dose concentration. Reprinted with permission from reference 49. Copyright 2014 John Wiley and Sons. 27

Figure 1.7. Representation of PEG-PAA-PCL miktoarm polymer self-assembly and pH-responsive morphological changes. 30

Figure 1.8. Schematic representation of the effect of (a) physiological pH and (b) acidic pH on the morphology of self-assembled PEG-PCL-P2VP micelles. Reprinted with permission from reference 29. Copyright 2012 Elsevier. 32

Figure 1.9. Schematic illustration of the micellar self-assembly of $(BA)(AC)_2$ miktoarm star polymers. Reprinted with permission from reference 65. Copyright 2016 John Wiley and Sons. 35

Figure 1.10. (A) Scheme of $A(AB)_3$ (P140, P160), $A_2(AB)_2$ (P240), and $A_3(AB)$ (P340) assembly into micelles, their response to GSH, (B) their size distributions from DLS, and (C) a representative TEM micrograph of $A_2(AB)_2$ (P240) micelles. Reprinted with permission from reference 57. Copyright 2015 Royal Society of Chemistry. 37

Figure 1.11. Self-assembly and dual UV/temperature response of PEG-PNBM-PNIPAM miktoarm star polymers. Reprinted with permission from reference 66. Copyright 2017 Elsevier. 40

Figure 1.12. Representation of (A) temperature and UV-induced morphological response of PAzo- $PDEAA_3$ micelles and (B) the corresponding proposed Nile Red release. Reprinted with permission from reference 46. Copyright 2013 Royal Society of Chemistry. 41

Figure 1.13. Independent release of anionic FITC-dextran and cationic rhodamine B from PEG-$qPDMAEMA_4$ micelle/tannic acid-derived microcapsule cores and shells. Reprinted with permission from reference 64. Copyright 2014 American Chemical Society. 44

Figure 2.1. Tuned environment-selective ROS/GSH response and drug release using assemblies from AB_2 miktoarm star polymers. 58

Figure 2.2. CMCs of (A) diblock copolymer b1 and (B) its miktoarm star polymer analogue μ1. 79

Figure 2.3. (A-E) TEM miktoarm star polymers μ1-4, the diblock copolymer b1, and their respective (F-J) TEM size distributions and (K-O) DLS size distributions. 80

Figure 2.4. (A) Time resolved ^1H NMR study of ROS response in μ1 with corresponding insets from boxed areas focused on thioketal peaks; GPC-monitored molecular weight change upon (B) ROS-cleavage in μ1, and (C) GSH-cleavage in μ4. 82

Figure 2.5. Sizes of μ1 micelles measured using DLS over 72 hours of incubation with 200 mM H_2O_2. 84

Figure 2.6. Curcumin release profiles of micelles assembled from polymer (A) μ1, (B) μ2, (C) μ3, (D) μ4, and (E) b1. 86

Figure 2.7. U251N glioblastoma cells were pre-treated with ROS inducer, menadione (MenD, 50 μM) for 1 hour, or glutathione inhibitor, L-buthionine-sulfoximine (BSO, 100 μM) for 24 hours. Following pre-treatment, cells were treated with free curcumin (Cur, 15 μM) or curcumin-loaded μ1 (μ1: 2.44 μM; Cur: 15 μM) for 6 hours. CellROX Deep Red (Ex/Em. = 640/665 nm) was added to a final concentration of 5 μM, 30 minutes before the end of the treatment. (B) Cells were fixed and labeled with Hoechst 33342 nuclear dye prior to being imaged with Leica DMI4000B microscope at 20x objective. Intracellular ROS content was assessed by measuring fluorescence intensity of cells. Shown is the average fluorescence intensity per cell relative to untreated control (RFI). 207 to 364 cells were analysed per condition from two independent experiments. Scale bar represents 40 μm. (C-F). The relative fluorescence intensity from (C), (E) cell lysate and (D), (F) cell culture media, was quantified using a spectrofluorometer. Shown are RFI (relative to control) of U251N cell lysate and DMEM media. Student's t-test, c*ondition vs. control: *p<0.05; **p<0.01, ***p<0.001* 88

Figure 3.1. (A) Structure and schematic of μ1 summarizing its extracellular ROS response. The oxidative cleavage of thioketal linkers located in the upper coronae of μ1 enables an increase in drug release kinetics upon exposure to ROS, while preserving overall micellar morphology. (B) Structure and cartoon schematic of μ4 summarizing its intracellular GSH response. The

reduction of the disulfide linker at the polymer arm junction in μ4 causes a burst release of encapsulated drugs. 98

Figure 3.2. TEM micrographs of resveratrol loaded μ1 at (A) low and (B) high magnifications. TEM micrographs of resveratrol loaded μ4 at (D) low and (E) high magnifications. The size distributions of μ1 micelles (C) and μ4 micelles (F) were determined by relating the size of each imaged micelle to the scale bar in Figures 3.2B and 3.2E. 105

Figure 3.3. Release profiles of resveratrol loaded (A) μ1 and (B) μ4 over 12 hours of dialysis against pH 7.4 PBS. The buffer and dialyzed solutions contained 200 mM H_2O_2 or 10 mM GSH in stimulus responsive studies. 106

Figure 4.1. Cartoon schematic of self-assembled miktoarm star micelles undergoing ROS-induced free thiol group exposure and disulfide coupling. 112

Figure 4.2. TEM micrographs of μ1B micelles with (A) 50 nm, and (B) 100 nm scale bars. (C) Size distribution of micelles in Figure 4A. 119

Figure 4.3. The results of treating 2 mg/mL micellar solutions of μ1B with (blue) H_2O_2 and (orange) H_2O_2 and $CuCl_2$ after a week of reaction time. 121

Figure 4.4. NMR spectra of the reaction of (A) TKDA and (B) μ1B micelles with 200 mM H_2O_2 in D_2O over 48 hours. 122

Figure 4.5. NMR spectra of the reaction of (A) TKDA and (B) μ1B micelles with 200 mM H_2O_2 in D_2O-based pH 7.4 PBS over 48 hours. 122

Figure 4.6. TEM micrographs of μ1B micelles after (A) 0, (B) 12, and (C) 24 hours of 200 mM H_2O_2 treatment. 123

Figure 4.7. Miktoarm polymer μ1B micelles coupling to form (A) linear and (B) globular superstructures. 123

Figure 4.8. Release profile of curcumin from μ1B micelles in pH 7.4 PBS with (black circles) and without (blue triangles) 200 mM H_2O_2 treatment. 124

List of Tables

Table 1.1. Miktoarm star polymers in drug delivery 3

Table 2.1. Critical micelle concentrations and sizes of self-assemblies from miktoarm star polymers (μ1-μ4) and linear diblock copolymer (b1). 79

Table 2.2. Encapsulation efficiencies and loading capacities of curcumin in micelles from their corresponding miktoarm star polymers (μ1-μ4) and linear diblock co-polymer (b1). 81

Table 3.1. Physical characteristics of μ1, μ4, and derived micelles. Molecular weights were estimated as the sum of M_n values of PEG and PCL-core components of the miktoarm polymers as determined by MALDI-TOF. Hydrophobic content was calculated as the MW fraction of the PCL-core component in each polymer. CMCs were determined using encapsulated pyrene fluorescence ratios. Diameters and polydispersities of micelles were determined *via* dynamic light scattering (DLS). 103

Table 3.2. Physical characteristics of resveratrol loaded μ1 and μ4 micelles. Diameters and polydispersities of micelles were determined *via* dynamic light scattering (DLS). Encapsulation efficiencies and loading capacities of resveratrol were calculated according to Equations 1 and 2. 104

List of Schemes

Scheme 1.1. Development of an ABC miktoarm polymer based on PI, PS, and PB, using the chlorosilane method. 8

Scheme 1.2. Core-first synthesis of an ABC miktoarm polymer (A = PCL, B = PS, C = PtBA) from a multifunctional core, using varied polymerization techniques. 10

Scheme 1.3. Core-first synthesis of an AB_2 miktoarm polymer (A = PLLA, B = PNAM) from a multifunctional core using ROP and RAFT. 11

Scheme 1.4. Synthesis of an ABC (A = PEG, B = PNIPAM, C = PDEAEMA) miktoarm star polymer using sequential arm-first (Steglich esterification, CuAAC "click" coupling) and core-first (core-initiated ATRP) methods. 13

Scheme 1.5. In-out synthesis of A_xB_y (A = PCL, B = PS) CCS polymers and their subsequent alkaline hydrolysis. 15

Scheme 1.6. Structure and $^1O_2$-response of PEG-PCL_2 miktoarm star polymers with β-aminoacrylate junctions to 660 nm light in the presence of Ce6. 38

Scheme 2.1. Syntheses of building blocks. For full details, see Schemes A.1-A.5. 74

Scheme 2.2. Syntheses of miktoarm star polymers μ1 - μ4 and the diblock co-polymer b1, and their corresponding ^{1}H NMR spectra in $CDCl_3$. For full details, see Schemes A.1-A.5. 77

Scheme 3.1. Synthesis of μ1. Full synthetic and characterization details available in Chapter 2.2.1. 100

Scheme 3.2. Synthesis of μ4. Full synthetic and characterization details available in Chapter 2.2.1. 101

Scheme 4.1. Synthesis of miktoarm star polymer μ1B (**6**). 117

Scheme 4.2. The successive oxidative cleavage and disulfide bridge formation of a thioketal functional group exposed to H_2O_2. 121

List of Abbreviations

4PBA	(4-(prop-2-yn-1-yloxy)phenyl)methanol
4PB-PCL	(4-(prop-2-yn-1-yloxy)benzyl)-PCL
Alq_3	Aluminum tris(8-hydroxyquinoline)
ATRP	Atom Transfer Radical Polymerization
b1	(PEG-TK-TEG)-block-PCL
BGA	2-Bromoglutaric Acid
BODIPY	Boron-dipyrromethene
Bpy	2,2‘-bipyridine
BSA	Bovine Serum Albumin
BSO	L-buthionine-sulfoximine
CAC	Critical Aggregation Concentration
CCS	Core-Crosslinked Star
$CDCl_3$	Deuterated chloroform
Ce6	Chlorin-e6
CMC	Critical Micelle Concentration
CoQ10	Coenzyme Q10
CPT	Camptothecin
CuAAC	Copper-Catalyzed Alkyne-Azide Cycloaddition
Cur	Curcumin
DBU	1,8-diazabicyclo[5.4.0]undec-7-ene
DCC	Dicyclohexylcarbodiimide
DCM	Dichloromethane
DI	Deionized
DIPC	*N,N′*-Diisopropylcarbodiimide
DLS	Dynamic light scattering
DMAP	4-dimethylaminopyridine

DMEM	Dulbecco’s modified Eagle’s media
DMSO	Dimethyl sulfoxide
DMSO-d6	Deuterated dimethyl sulfoxide
DOX	Doxorubicin
DP	Degree of polymerization
DPBA	(3,5-bis(prop-2-yn-1-yloxy)phenyl)methanol
DPB-PCL	(3,5-bis(prop-2-yn-1-yloxy)benzyl)-PCL with $[M_0]/[I] = 20$
DPB-PCL’	(3,5-bis(prop-2-yn-1-yloxy)benzyl)-PCL with $[M_0]/[I] = 18$
DPB-DS-PCL-Hx	DS-PCL-Hx conjugated to DPBA
DPTS	1,4-Dimethylpyridinium p-toluenesulfonate
DS	Disulfide
DS-Hex	3-((3-(hexyloxy)-3-oxopropyl)disulfaneyl)propanoic acid
DS-PCL-Hx	Hexanol-initiated polycaprolactone conjugated to 3,3′-Dithiodipropionic acid
DTT	Dithiothreitol
DVB	Divinylbenzene
Đ	Polydispersity index
EDC	1-Ethyl-3-(3-dimethylaminopropyl)carbodiimide
EDTA	Ethylenediaminetetraacetic acid
EE	Encapsulation efficiency
EEP	2-Ethoxy-2-oxo-1,3,2-dioxaphospholane
EPR	Enhanced Permeability and Retention Effect
ESI	Electrospray ionization
EVBA	6,6′-(ethane-1,2-diylbis(oxy))bis(3-vinylbenzaldehyde)
FA	Folic Acid
FBS	Fetal bovine serum
FITC	Fluorescein isothiocyanate

FTIR	Fourier-transform infrared spectroscopy
GPC	Gel permeation chromatography
GSH	Glutathione
HPLC	High-performance liquid chromatography
LC	Loading capacity
LCST	Lower Critical Solution Temperature
LD	Lipid Droplets
λ_{em}	Emission wavelength
λ_{ex}	Excitation wavelength
mPEG	Poly(ethylene glycol) monomethyl ether
mPEG-N_3	Azido-poly(ethylene glycol) monomethyl ether
mPEG-OTs	Tosylated poly(ethylene glycol) monomethyl ether
MALDI-TOF	Matrix-Assisted Laser Desorption/Ionization-Time Of Flight
Me_6TREN	Tris(2-(dimethylamino)ethyl)amine
MenD	Menadione
M_n	Number average molecular weight
MS	Mass spectrometry
MTX	Methotrexate
MW	Molecular weight
M_w	Weight average molecular weight
MWCO	Molecular weight cut-off
µ1	µ(PEG-TK-TEG)$_2$PCL
µ1B	µ(PEG-TK-TrEG)$_2$PCL
µ2	µ(PEG-TK-TEG)$_2$PCL-DS
µ3	µ(PEG-TK-TEG)$_2$DS-PCL
µ4	µ(PEG)$_2$DS-PCL
NCA	N-carboxyanhydride

NHS	N-Hydroxysuccinimide
NMR	Nuclear magnetic resonance
OA	Oleic acid
P2MP	Poly(2-methyl-1,3-pentadiene)
P2VP	Poly(2-vinylpyridine)
P4MS	Poly(4-methyl styrene)
PAA	Poly(acrylic acid)
PAzo	Azobenzene side chain-containing polymer
PB	Polybutadiene
PBA	Poly(butyl acrylate)
PBLA	Poly(benzyl-l-aspartate)
PBLG	Poly(γ-benzyl-L-glutamate)
PBS	Phosphate-buffered saline
PCL	Polycaprolactone
PCL-Hx	Hexanol-initiated polycaprolactone
PDEAA	Poly(*N*,*N*-diethylacrylamide)
PDEAEMA	Poly(2-(diethylamino)ethyl methacrylate
PDI	Polydispersity index
pDNA	Plasmid DNA
PDLA	Poly(D-lactic acid)
PEG	Poly(ethylene glycol)
PEG-N_3	Azido-poly(ethylene glycol)
PEG-OTs	Monotosylated poly(ethylene glycol)
PG	Polyglycerol
PGA	Poly(glutamic acid)
PHis	Polyhistidine
PHLG	Poly(β-hydroxyethylenediamine-L-glutamate)

PI	Polyisoprene
PLA	Poly(lactic acid)
PLGA	Poly(lactide-co-glycolide)
PLL	Poly(L-lysine)
PLLA	Poly(L-lactic acid)
PMDETA	*N*,*N*,*N* ′,*N* ″,*N* ″-Pentamethyldiethylenetriamine
PMAA	Poly(methacrylic acid)
PMMA	Poly(methyl methacrylate)
PNAM	Poly(N-acryloylmorpholine)
PNBM	Poly(2-nitrobenzyl methacrylate)
PNIPAM	Poly(N-isopropyl acrylamide)
POEGMA	Poly(oligo(ethylene glycol) monomethyl ether methacrylate)
PPE	Polyphosphoester
PPEGMA	Poly(poly(ethylene glycol) methyl ether methacrylate)
PPG	Poly(propylene glycol)
PS	Polystyrene
PtBA	Poly(*tert*-butyl acrylate)
PTMC	Poly(trimethylene carbonate)
PUA	Poly(undecylenic acid)
PVDF	Poly(vinylidene fluoride)
qPDMAEMA	Quaternized poly(2-(dimethylamino)ethyl methacrylate)
RAFT	Reversible Addition-Fragmentation Chain Transfer
RFI	Relative fluorescence intensity
RhDex	Rhodamine B Isothiocyanate-Dextran
RI	Refractive index
ROP	Ring Opening Polymerization
ROS	Reactive Oxygen Species

RPM	Revolutions per minute
SEC	Size Exclusion Chromatography
SET-LRP	Single Electron Transfer Living Radical Polymerization
SFRP	Stable Free Radical Polymerization
tBMA	*tert*-butyl methacrylate
TEG	Tetraethylene glycol
TEM	Transmission electron microscopy
THF	Tetrahydrofuran
TIF	Tetraiodofluorescein
TK	Thioketal
TK-TEG	18,18-dimethyl-15-oxo-2,5,8,11,14-pentaoxa-17,19-dithiahenicosan-21-oic acid
TK-TrEG	15,15-dimethyl-12-oxo-2,5,8,11-tetraoxa-14,16-dithiaoctadecan-18-oic acid
TKDA	2,2'-(propane-2,2-diylbis(sulfanediyl))diacetic acid
TNF-α	Tumour necrosis factor-α
TPPBr	Triphenylphosphonium Bromide
TrEG	Triethylene glycol
UV-Vis	Ultraviolet–visible
XRD	X-ray diffraction

Contributions of Authors

All syntheses, characterizations, and experiments described in this thesis were performed primarily by the author except where noted. The work presented in Chapters 2 and 3 was done as a collaboration between the Department of Chemistry and the Department of Pharmacology and Therapeutics at McGill University. Hossein Yazdani provided assistance in some of the syntheses and characterizations required for the building blocks of miktoarm star polymers μ1-4 and helped to perform the curcumin and resveratrol release experiments for miktoarm star polymer μ1. Anastasiia Nyrko aided in synthesizing miktoarm star polymer μ4. Qiaochu Zhang performed the CuAAC "click" reaction for block copolymer b1 and performed its curcumin release study. Evan Rizzel Gran and Qiaochu Zhang performed the μ1 ROS scavenging study in glioblastoma cells. Prof. Dusica Maysinger conceived and oversaw the experiments performed at the Department of Pharmacology and Therapeutics. Professor Ashok Kakkar oversaw all other experiments and helped to revise this thesis.

Appendix D is a paper written in a collaboration between the Department of Chemistry and the Department of Pharmacology and Therapeutics at McGill University and the Department of Chemical and Petroleum Engineering at the Sharif University of Technology in Iran. The author contributed to the synthesis and characterization of thioketal diacid and some of the derived chitosan nanoparticles as well as to writing the paper. The reference can be found below.

Sabourian, P.; Ji, J.; Lotocki, V.; Moquin, A.; Hanna, R.; Frounchi, M.; Maysinger, D.; Kakkar A. Facile Design of Autogenous Stimuli-Responsive chitosan/hyaluronic Acid Nanoparticles for Efficient Small Molecules to Protein Delivery. *J Mater. Chem. B* **2020**, *8*, 7275-7287.

Chapter 1: Miktoarm star polymers: Branched architectures in drug delivery

Abstract

Delivering active pharmaceutical agents to disease sites using polymeric soft nanoparticles continues to be a topical area of research. It is becoming increasingly evident that the composition of amphiphilic macromolecules plays a significant role in developing efficient nanoformulations. Branched architectures with asymmetric polymeric arms emanating from a central core junction have provided a pivotal venue to tailor their key parameters. The build-up of miktoarm stars offers vast polymer arm tunability, aiding in the development of macromolecules with adjustable properties, and allows facile inclusion of endogenous stimulus-responsive entities. Miktoarm star-based micelles have been demonstrated to exhibit denser coronae, very low critical micelle concentrations, high drug loading contents, and sustained drug release profiles. With significant advances in chemical methodologies, synthetic articulation of miktoarm polymer architecture, and determination of their structure-property relationships, are now becoming streamlined. This is helping advance their implementation into formulating efficient therapeutic interventions. This review brings into focus important discoveries in the syntheses of miktoarm stars of varied compositions, their aqueous self-assembly, and contributions their formulations are making in advancing the field of drug delivery.

1.1 Introduction

A majority of active pharmaceutical agents fail to provide expected relief upon administration as 90% of drugs in the discovery pipeline have very poor water solubility and low bioavailability.[1-3] These and other related shortcomings, including untargeted accumulation and systemic toxicity, have necessitated the development of nanocarriers for efficient therapeutic interventions. In particular, much progress has been made in the development of polymeric soft nanoparticles over the last 30 years, and it has contributed significantly to enhancing drug solubility, stability, long circulation times, and targeting specific locations in the body.[4] To achieve a free energy minimum, amphiphilic polymers with distinct hydrophilic and hydrophobic blocks self-assemble in an aqueous medium, into a range of supramolecular structures, including micelles and polymersomes.[5, 6] Such nanoparticles can accumulate at disease sites using the enhanced

permeation and retention (EPR) effect,[7-9] resulting from the porous leaky vasculature typical of unhealthy cancerous tissue and its deficient lymphatic drainage.[10-12]

Micelles are supramolecular assemblies that constitute the majority of polymeric nanocarriers, and are characterized by their distinct core-corona build-up. The outer hydrophilic corona contributes to the solubility and stability of micellar structures in aqueous media,[9] and in the majority of the nanoparticles, it is almost exclusively composed of, or based on, poly(ethylene glycol) (PEG). PEG owes its ubiquity to its ability to confer aqueous solubility, stealth, and compatibility with biological systems by avoiding immunogenic response and premature elimination.[4] Using their hydrophobic cores, micelles can load a variety of cargo, including small hydrophobic drugs and biomolecules. A key parameter which is intrinsic to the function of polymeric micelles as drug delivery vehicles is the critical micelle concentration (CMC). At concentrations below their CMC, amphiphilic polymers are disordered. At concentrations at or above the CMC, the continued addition of amphiphiles leads to the formation of their self-assemblies (micelles). Upon administration and introduction into the aqueous biological environment (typically blood), micelles are subject to immense dilution, and low CMCs are required for long circulation times.[4, 13] Micellar drug delivery formulations based on diblock or graft copolymers generally have CMC in a range of 10^{-4} - 10^{-7} M.[14-17] Another parameter of importance is the micelle size, which is typically expected to be below 200 nm. Given the vasculature and tissue pore sizes, such small diameters can significantly improve micellar circulation and biological distribution, and aid in disease site targeting due to the EPR effect.[10-12]

One of the more fascinating and advantageous approaches to improving polymer-based drug delivery has come from adjusting the architecture of polymeric backbones. Miktoarm polymers (sometimes known as heteroarm star polymers) are a class of star polymers with asymmetric branching in which there are at least 3 branching strands originating from a shared core.[18, 19] Their compositions differ from slight variations in molecular weight, to having completely different repeating units and chemical configurations. Due to their asymmetry, miktoarm variants are categorized in the form: $A_xB_yC_z$, where A, B and C are examples of polymeric chains, and the subscript denotes their number (Figure 1.1). The branching architectures of miktoarm polymers have contributed distinct properties to their aqueous self-assemblies, compared to those from their linear diblock copolymer counterparts, including very low CMCs, smaller sizes, and most

importantly the ability to encapsulate large amounts of drug molecules.[20-25] In addition, the tunability offered by having multiple branching segments has led to the synthesis of a variety of micelle structures that incorporate polymeric arms with stimulus-responsive units and biological targeting moieties. These are in addition to conferring aqueous solubility and maintaining micelle stability. Table 1.1 below provides a brief summary, in chronological order of their discovery, of the different types of miktoarm polymeric architectures and their assemblies, used for the delivery of a variety of pharmaceutics.[21, 25, 26] It shows the diversity in their composition, and the potential of targeting these formulations to desired sites through the introduction of various stimuli.

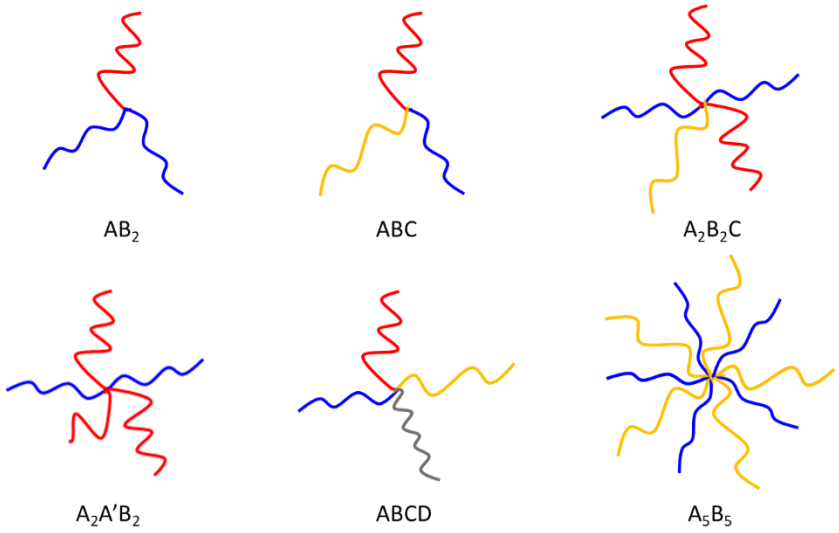

Figure 1.1. Miktoarm polymer architectures of varied compositions.

Table 1.1. Miktoarm star polymers in drug delivery

Polymeric arms[1]	**Architecture**	**Stimulus**	**Cargo**	**Encapsulation Efficiency (%)**	**Loading Capacity (%)**	**Year**	**Citation**
PNIPAM, PUA	AB_2	Temperature	Prednisone acetate	27.7	N/A	2006	27
PEG, PCL, P2VP	ABC	pH	Nile Red	N/A	N/A	2006, 2009, 2012	28-30
PMMA, PNIPAM	AB_3	Temperature	Prednisone acetate	55	N/A	2007	31

PEG, PTMC	AB_2		Indomethacin	27.3-56.6	9.1-21.4	2008	32
PEG, PCL	A_2B_2		Ibuprofen	26.8-89.7	7.3-20.3	2009	33
PEG, PLLA	AB_2		Doxorubicin Hydrochloride	72	N/A	2009	34
PEG, PLLA, PDLA	ABC, AB_2		Paclitaxel	N/A	5.0-11.6	2009	35
PCL, PEG	$A_{14}B_7$		Ibuprofen	7.7-46.0	2.3-13.8	2010	36
PEG, PCL	A_2B		Nimodipine	23-70	2.3-7.0	2010	24
PEG, PCL	AB_{10}		Prednisone acetate	21.1-44.5	2.1-4.3	2010	37
PNIPAM, PLL	AB_2		Prednisone acetate	18.6-21.4	2.1-2.5	2010	38
PEG, PS, PCL	ABC		Disperse Red 1	N/A	0.4-2.1	2010	39
PEG, PCL	AB_2, $A(BA)_2$		Rhodamine B isothiocyanate-Dextran	40-57	N/A	2011	40
PEG, Niacin, BODIPY	A_2B, ABC		Niacin	N/A	N/A	2011	41
PEG, PCL, TPPBr	ABC		Coenzyme Q10	83-85	8.3-8.5	2012	42
PEG, PHis	AB_2	pH	5(6)-carboxyfluorescein	N/A	0.92-1.42 μL mg^{-1}	2012, 2014	43, 44
PCL, PEG, PLL	ABC		Paclitaxel, plasmid DNA	N/A	5.0	2013	45
PAzo, PDEAA	AB_3	UV light, Temperature	Nile Red	N/A	N/A	2013	46
PEG, PCL	A_2B		Curcumin	48.5-65.0	4.6-6.5	2014	47
PCL, PBLA, PEG	ABC		Doxorubicin	56.2	11.2	2014	48
PEG, PCL, TIF	ABC		Curcumin	39.2-55.9	3.9-5.6	2014	49
PCL, PDEAEMA-*co*-PPEGMA	$A_2(BC)_2$	pH	Doxorubicin	N/A	10	2014	50
PCL, PDEAEMA-*co*-PPEGMA	$A_3(BC)_3$	pH	Doxorubicin	29.4-71.4	9.5-19.6	2014	51

PEG, PGA	AB_2	pH	Doxorubicin	N/A	16.2-18.2	2014	52
PAzo, PEG	AB_3	UV light	Nile Red, Rhodamine B	N/A	N/A	2014	53
PEG, PCL	AB_2		Doxorubicin	41.6-72.7	6.1-16.1	2015	54
PCL, PEG	AB_3		Curcumin	17.3-27.6	11.4-13.3	2015	55
PEG, PAA, PCL	ABC	pH	Naproxen	58.2-72.8	9.7-12.1	2015	56
PEG, PEG-*b*-PCL	$A(AB)_3$ $A_2(AB)_2$ $A_3(AB)$	Redox	Camptothecin	N/A	3.6-10.8	2015	57
PEG, PMMA	AB_2	Redox	Methotrexate	64	16	2015	58
PCL, PCL-*b*-PEG	$A(AB)_3$		Doxorubicin	52.8-54.6	8.8-9.1	2016	59
PEG, PCL	AB_2		Doxorubicin	24.7	5.6	2016	60
PEG, PHLG	$A_{16}B_{23}$ CCS		siRNA	N/A	N/A	2016	61
PEG, P(MMA-*co*-MAA)	AB_2	pH	Methotrexate	48.7-82.3	10.3-16.5	2016	62
PCL, P(MAA-*co*-MMA)	A_2B_6	pH	Doxorubicin, Camptothecin	DOX: 42-60 CPT: 6	DOX: 14-20 CPT: 2	2016	63
PEG, qPDMAEMA	AB_4	pH, Ionic strength	Rhodamine B, FITC-dextran	N/A	N/A	2016	64
PPEGMA, PMMA, PNIPAM	$(BA)(AC)_2$	Temperature	Celecoxib	N/A	8.8	2016	65
PEG, PNBM, PNIPAM	ABC	UV light, Temperature	Nile Red	N/A	N/A	2017	66
PEG, PGA	AB_3		Lysozyme	N/A	N/A	2017, 2018	67, 68
PVDF, PS, PEG	$(AB)_2C_2$		Nile Red	N/A	N/A	2018	69
PCL, POEGMA	A_2B, A_2B_2, AB_3, A_3B		Doxorubicin	34.3-62.9	4.4-8.1	2018	70
PEG, PCL	AB_2		Curcumin, Methotrexate	CUR: 93.8-94.2	CUR: 14.1 MTX:	2018	71

				MTX: 72.9-75.7	10.9-11.4		
PLLA, PNAM	AB_2		Doxorubicin	55.6-78.7	9.4-13.6	2018	72
PEG, PLL	AB_2	Redox	pDNA	N/A	N/A	2018	73
PEG, PCL	AB_2	Redox	Chlorin e6, Doxorubicin	Ce6: 77.7-82.1 DOX: 16.2-29.2	Ce6: 15.5-16.4 DOX: 3.2-5.8	2018	74
PLGA, PEG	AB_2		Ibuprofen	51.5-76.5	1.7-7.0	2019	75
PEG, PGA	AB_3		Lysozyme	N/A	N/A	2019	76
OA, PEG	AB_2	pH	Vancomycin	39.6	3.6	2020	77
PEG, PCL	AB_2		Baicalein	94.3-94.7	12.4	2020	78

[1]Polymer segment order corresponds to the order of letters in the Architecture column

1.2. Synthetic Approaches to Miktoarm Star Polymers

Given the asymmetric nature of miktoarm stars, their construction requires careful selection of high yield methodologies for the build-up of individual arms on a branched core. Akin to the divergent and convergent synthetic methodologies pioneered by Tomalia and Fréchet for the synthesis of hyperbranched dendrimers,[79, 80] the construction of branched miktoarm polymers can be mostly broken down to two methods: arm-first and core-first (Figure 1.2). These involve the independent synthesis of separate polymeric arms before attachment to a core molecule, or polymerization initiated on a hetero-multifunctional core respectively.[21] Depending on the necessary reaction conditions, cores may be functionalized separately, or have certain moieties blocked, in order to initiate polymerization from specific locations. Alternatively, in arm-first approaches, pre-synthesized polymers with conjugating end moieties can be coupled to these cores using esterification/amidation-based coupling, or, more recently, “click” chemistry.[81] Both arm-first and core-first methods present their own advantages depending on whether a miktoarm polymer is densely branched, requires precise arm lengths, needs to be synthesized with ease, etc. However, it has become more common recently to assemble miktoarm stars using a mixture of arm- and core-first approaches. Such an approach can best accommodate varied conditions required for the construction of desired branched architectures. For example, considering that one of the most widely studied applications of miktoarm polymers is in biology, and especially as soft

nanoparticle-based drug delivery, PEG has become an increasingly featured component of miktoarm polymers. Thus, it is often much simpler to purchase PEG of a desired molecular weight, modify it to contain a reactive end group, and couple it to cores which have been used for the initiation of hydrophobic polymer polymerization.[32-37, 40, 41]

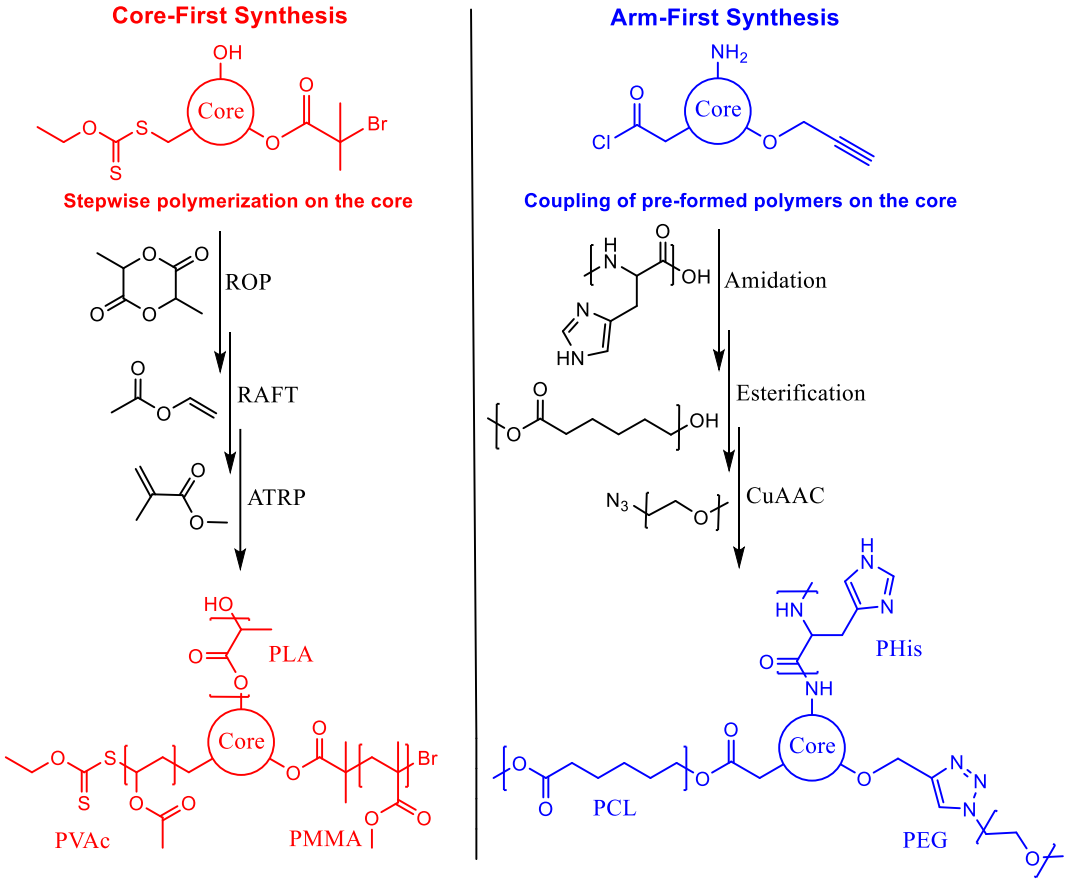

Figure 1.2. Examples of core-first synthesis (left) and arm-first synthesis (right) with examples of functionalities, monomers, and polymers.

1.2.1 Chlorosilane Based Synthesis

Hadjichristidis and coworkers were the first to prepare polymers with asymmetric branching based on an arm-first method using chlorosilane cores.[82-87] Dubbed ”miktoarm” after the Greek word μικτός (miktos) or “mixed”, these polymers had a variety of branches emanating from a single core. More specifically, the first example of such a polymer was a construct made of polyisoprene (PI), polystyrene (PS), and polybutadiene (PB). Due to the increasing reactivity of the polymer anion termini in the order of PB > PI > PS, and the steric hindrance that follows the opposite trend, the miktoarm synthetic methodology was designed such that PI (with intermediate reactivity)

would first be linked to a large excess of a chlorosilane core. Then, relying on the inability of the second PS arm to undergo complete reaction with PI-linked chlorosilane, PS was attached second, followed by excess PB which would undergo complete exchange with the remaining Cl on the chlorosilane core (Scheme 1.1).[88]

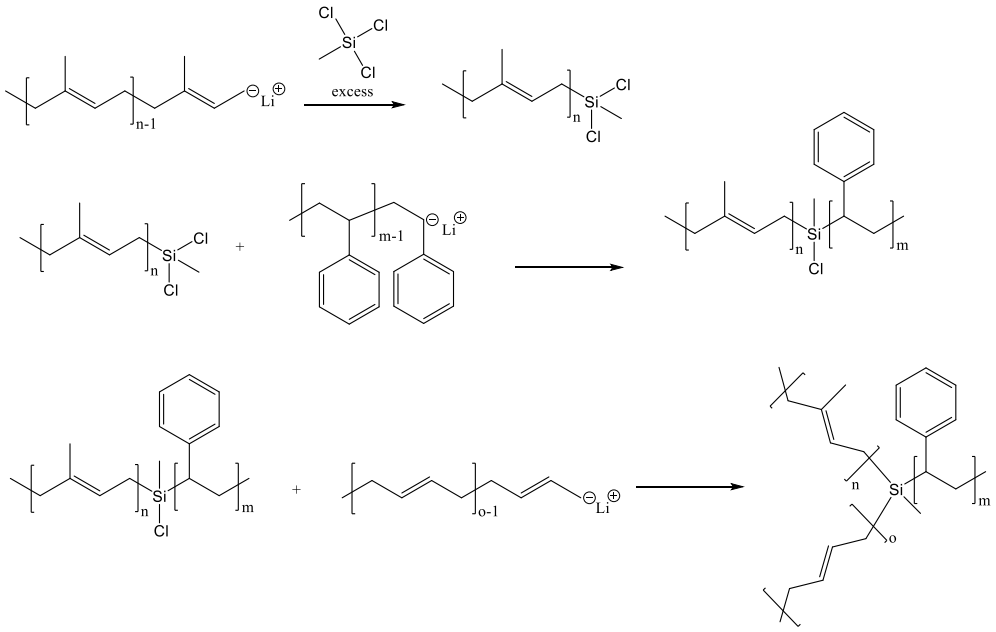

Scheme 1.1. Development of an ABC miktoarm polymer based on PI, PS, and PB, using the chlorosilane method.

While this PB-PI-PS star, as described above, is mostly recognized as the first synthesized miktoarm polymer, a few years prior to this, Pennisi and Fetters had reported A_2A' polymers based on PS and PB arms with differing molecular weights, synthesized using a chlorosilane core-based approach.[86] Then in 1990, an AB_2-type miktoarm polymer was prepared by the single grafting of PS end-capped with chlorosilane, onto the middle of a PI chain.[89]

Iatrou and Hadjichristidis further took advantage of relative polymer chain reactivities to synthesize a variety of branched polymers. Using a tetrachlorosilane core, they were able to sequentially add anionic PS, poly(4-methyl styrene) (P4MS), PI, and PB lithium salts, following each step with a titration, and confirming the ABCD miktoarm star end product *via* size exclusion chromatography (SEC). By swapping the middle components in the sequential addition with PS and PB respectively, an A_2B_2 miktoarm polymer was prepared.[90]

Due to the possible manipulations of chlorosilane cores in developing miktoarm architectures, more methodologies soon followed. While many of these included alterations of polymer addition onto trichlorosilane or tetrachlorosilane cores,[91-98] one of the more interesting examples was the synthesis of an A_8B_8 (A = PS, B = PI) miktoarm polymer based on a core with 16 active chlorosilane bonds (called Si-Cl_{16} for simplicity). This core was synthesized by transforming a tetravinylsilane initial core with methyldichlorosilane using vinylmagnesium bromide. PS, which was made into a living polymer chain with BuLi, was carefully reacted with Si-Cl_{16} to produce PS_8-(Si-Cl_8). After product confirmation by SEC, the remaining chlorosilane bonds were used to link living PI chains to yield a PS_8PI_8 miktoarm polymer.[99] Hadjichristidis and coworkers later used a different chlorosilane linker containing 6 Si-Cl bonds, 1,2-bis(trichlorosilyl)ethane, as the core for an AB_5 (A = PS, B = poly(2-methyl-1,3-pentadiene) (P2MP)) miktoarm polymer. To avoid multiple PS conjugations, a living PS chain was slowly added dropwise to the core in solution after which P2MP was used to completely react with the remaining chlorosilane bonds.[100] Chlorosilane based synthesis has found great success over the years, and it paved the way for other miktoarm polymers. This methodology is well suited for the introduction of nonpolar polymeric chains, and has largely been used with chains that have living anionic ends.

1.2.2 Core-First Synthesis

This methodology, as the name suggests, involves initiating polymerization from a core, and incorporates standard polymerization techniques that do not involve coupling or conjugation of separately synthesized polymeric chains. It includes methods such as atom transfer radical polymerization (ATRP), reversible addition-fragmentation chain transfer (RAFT), anionic/cationic polymerization, and ring opening polymerization (ROP). A notable early example demonstrating the flexibility and power of core-first methods was the synthesis of a trifunctional initiator molecule, with a (2,2,6,6-Tetramethylpiperidin-1-yl)oxyl (TEMPO) group for the stable free radical polymerization (SFRP) of styrene, a bromoisobutyrate for ATRP of *t*-butyl acrylate, and a free OH for ROP of caprolactone (Scheme 1.2).[101] Each of these polymerization methods could be applied to a wide variety of different monomers. For example, substituting caprolactone with ethylene oxide for ROP would yield a PEG chain in the place of PCL, thus making an amphiphilic miktoarm polymer suitable for aqueous self-assembly.

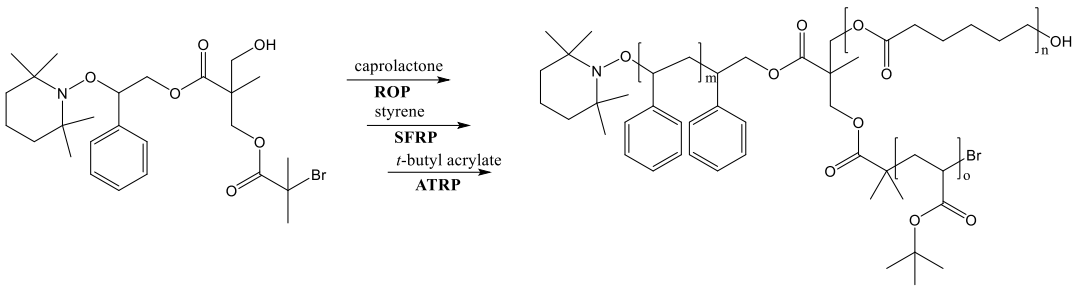

Scheme 1.2. Core-first synthesis of an ABC miktoarm polymer (A = PCL, B = PS, C = PtBA) from a multifunctional core, using varied polymerization techniques.

Core-first synthesis has also been used to prepare amphiphilic miktoarm polymers for drug delivery. A series of A_2B, A_2B_2, AB_3, and A_3B (A = polycaprolactone (PCL), B = poly(oligo(ethylene glycol) monomethyl ether methacrylate) (POEGMA)) miktoarm polymers, were synthesized from pentaerythritol and 1,1,1-tris(hydroxymethyl)ethane, tetrafunctional and trifunctional cores bearing 4 or 3 hydroxyls, respectively. Protecting/deprotecting strategies were used to functionalize these cores with α-bromoisobutyryl bromide, an ATRP initiator. Unfunctionalized OH positions were then used to initiate the polymerization of caprolactone, after which ATRP of OEGMA was carried out at the remaining Br activated positions. The miktoarm polymers were found to have no significant cytotoxicities, could be self-assembled into micelles, and were able to efficiently encapsulate and deliver doxorubicin (DOX) to cells. Interestingly, the most hydrophobic $PCL_3POEGMA$ derived micelles had the lowest CMC, the highest DOX encapsulation efficiency, and the best therapeutic efficiency for DOX release.[70]

Core-first methods are compatible with a variety of polymerization reactions. An AB_2 (A = poly(L-lactide) (PLLA), B = poly(N-acryloylmorpholine) (PNAM)) miktoarm polymer was prepared using a 1,1,1-tris(hydroxymethyl)ethane core, as in the above study. However, 2-bromopropionyl bromide and potassium ethyl xanthogenate were sequentially coupled onto two of the core's hydroxy groups, to yield a multifunctional core containing two RAFT initiating groups and a free hydroxy group. The latter was employed to initiate the ROP of L-lactide, and subsequently the two RAFT initiating ends were used for the polymerization of N-acryloylmorpholine to give the final AB_2 polymer (Scheme 1.3).[72] Since most amphiphilic polymers use PEG to confer aqueous solubility, PNAM is an interesting substitute noted for its low cytotoxicity, and promising properties including its high aqueous solubility and low cytotoxicity.[102, 103]

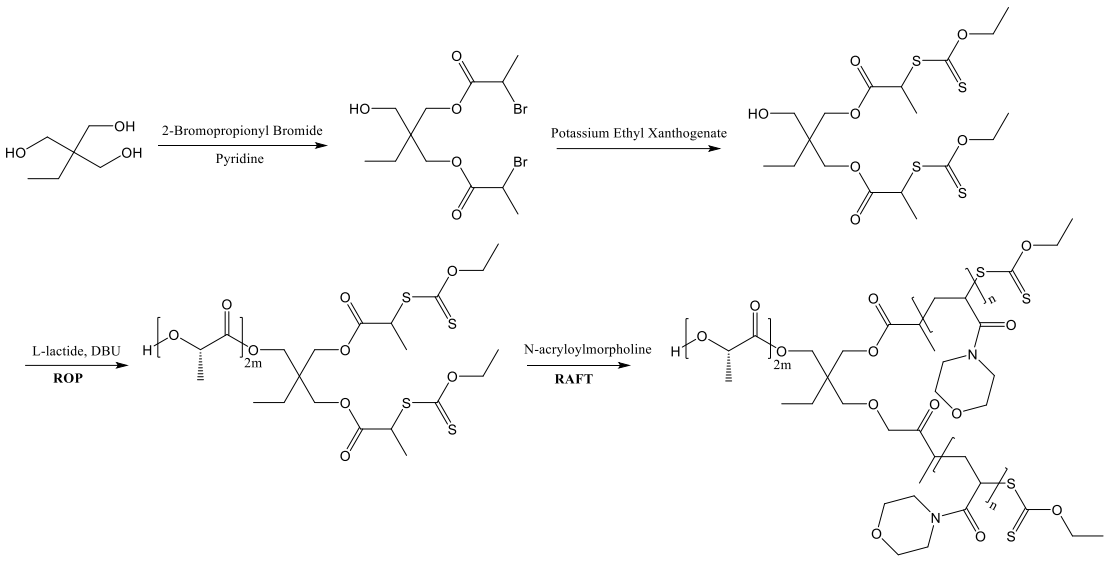

Scheme 1.3. Core-first synthesis of an AB_2 miktoarm polymer (A = PLLA, B = PNAM) from a multifunctional core using ROP and RAFT.

In another study, a "macro-core" was used to couple methoxy PEG to a highly branched polyglycerol (PG). The ROP of caprolactone was then performed using the PG terminal hydroxy ends as initiators to yield an AB_{10} (A = PEG, B = PCL) miktoarm polymer, with good loading efficiency and sustained release of prednisone acetate, an adrenocortical hormone drug.[37] The methodology used in this procedure can be argued to be of a mixed type, and in fact, most miktoarm polymer syntheses in drug delivery do use a combination of core-first and arm-first methods. Due to the complexity in preparing hetero-multifunctional cores for polymerization initiation without side reactions, mixed methodologies are often more practical.

1.2.3 Arm-First Synthesis

Arm-first syntheses generally comprise methodologies in which polymer chains are individually prepared, and then attached to a single core. In fact, the chlorosilane-based miktoarm polymers described above belong to arm-first methodology. This approach is advantageous due to the great control over the properties of individual chains, and the freedom to use reaction conditions that would normally be incompatible in the presence of other polymers. The most important aspect of these syntheses is the necessity to use a coupling or conjugation reaction to link a completed polymer chain to the core. This can generally be achieved using i) a condensation reaction between a terminal alcohol/amine and acid; and ii) "click" coupling chemistry. Due to the unlikelihood of complete reaction between polymer terminal ends, which can generally be associated with steric

factors, condensations are conducted using catalysts. For example, Steglich famously described an esterification procedure that uses a combination of dicyclohexylcarbodiimide (DCC) and 4-dimethylaminopyridine (DMAP) as a coupling reagent and catalyst respectively.[104]

Depending on the reaction conditions, necessary workup, and catalyst solubility, a variety of combinations of coupling reagents have been employed, including but not limited to: 1-Ethyl-3-(3-dimethylaminopropyl)carbodiimide (EDC), N,N′-Diisopropylcarbodiimide (DIC), DCC, N-Hydroxysuccinimide (NHS), 1,4-Dimethylpyridinium p-toluenesulfonate (DPTS), and DMAP. For example, an AB_2 miktoarm polymer was prepared with two PEG segments conjugated to a benzyl core using click chemistry, and niacin coupled to the benzyl alcohol on the core, using EDC/DMAP coupling chemistry. The niacin conjugated structure was seen to localize within cellular lipid droplets (LD), and inhibit the activity of the LD-localized enzyme, DGAT2.[41] Another AB_2 (A = PEG, B = PLLA) miktoarm polymer was synthesized by first activating an acid-terminated PEG with NHS/DCC, to couple it with the free amine of serinol, thereby providing a PEG-core structure where the core has two free hydroxy groups available for ROP. L-Lactide was subsequently polymerized using these terminal alcohols as initiators to give the final miktoarm polymer.[34]

Click coupling is the other widely used form of chemical conjugation applied in developing miktoarm polymer architectures. The term “click chemistry”, while having older roots, is now widely used to refer mainly to the copper-catalyzed alkyne-azide cycloaddition (CuAAC) coupling reaction, first demonstrated by Sharpless.[105] Due to this reaction’s atom economy, tendency to only form the 1,4 isomer, complete or near-complete reaction progression, tolerance of other functional groups, and capacity to be adapted into an immense variety of reaction conditions, it has found significant usage in polymer coupling, in general.[81] An example of its use in miktoarm polymer synthesis can be found in one of the first miktoarm polymers used in drug delivery. An α-methoxy-ω-epoxy poly(ethylene glycol) was exposed to sodium azide in the presence of ammonium chloride in order to produce a methoxy PEG-core structure with primary azide and hydroxy functional groups. A propargyl alcohol-initiated PCL chain was then combined with this PEG, and reacted in the presence of 1,8-diazabicyclo[5.4.0]undec-7-ene (DBU) and CuI, to “click” the two polymers together. The remaining hydroxy functional group was used for the ROP of 2-Ethoxy-2-

oxo-1,3,2-dioxaphospholane (EEP), thus forming an ABC (A = PEG, B = PCL, C = polyphosphoester (PPE)) miktoarm star.[106]

Most researchers rarely limit themselves to one type of conjugation or even only arm-first syntheses. Instead, arm-first and core-first methods are typically combined to attain the desired miktoarm star polymer. For example, both Steglich esterification and CuAAC coupling were combined with a core-first methodology. Propargyl alcohol and $mPEG_{2000}$ were coupled to 2-bromoglutaric acid (BGA), in this sequence, through DCC/DMAP catalyzed Steglich esterifications to yield the desired PEG_{2000}(-alkynyl)-Br macroinitiator. The latter was used for the ATRP of *N* -isopropylacrylamide (NIPAM) with tris(2-(dimethylamino)ethyl)amine (Me_6TREN) and CuCl,. Finally, azido-terminated poly(2-(diethylamino)ethyl methacrylate (PDEAEMA), prepared earlier through ATRP, was "clicked" to the alkynyl group of the PEG-PNIPAM diblock, using CuAAC coupling with *N,N,N ′,N ″,N ″*-Pentamethyldiethylenetriamine (PMDETA) and CuBr, giving the ABC (A = PEG, B = PNIPAM, C = PDEAEMA) miktoarm star polymer (Scheme 1.4).[107]

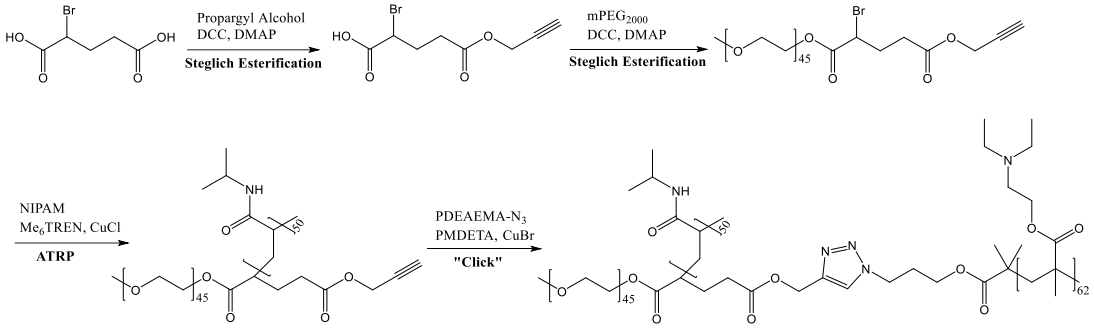

Scheme 1.4. Synthesis of an ABC (A = PEG, B = PNIPAM, C = PDEAEMA) miktoarm star polymer using sequential arm-first (Steglich esterification, CuAAC "click" coupling) and core-first (core-initiated ATRP) methods.

1.2.4 In-Out Synthesis

Synthesis of miktoarm polymers using "in-out" methodologies does not strictly fall into either core-first or arm-first methods. In-out syntheses typically involve the preparation of polymeric macroinitiators, and subsequently crosslinking them using small molecules such as those containing divinyl functionalities. Miktoarm polymers prepared in this manner form densely core-crosslinked star (CCS) A_xB_y architectures, comprised of two different arm variants. The first

known example of such a miktoarm polymer involved the synthesis of vinylbenzyl terminated PS and PI by coupling living anionic PS and PI with *p*-chloromethylstyrene. These macroinitiators were then copolymerized in benzene with n-BuLi as an initiator to yield A_xB_y (A = PS, B = PI) miktoarm stars. The latter were reported to undergo microphase separation, with individual domains being smaller than those observed with the analogous diblock copolymers.[108] While this study did not use polymeric arms compatible with drug delivery, such microdomain sizes suggest potentially beneficial micelle sizes and properties for such architectures.

An example of a typical in-out methodology involved modification of PCL with 2-bromoisobutyryl bromide to form PCL-Br, a macroinitiator for ATRP, which was subsequently core-crosslinked with divinylbenzene (DVB) to give a PCL star polymer with ATRP-active ends. The latter were then used for the polymerization of styrene to yield an A_xB_y (A = PCL, B = PS) CCS polymer. The PCL chains in this miktoarm star were able to undergo biodegradation through hydrolysis in alkaline conditions (Scheme 1.5).[109] Using a poly(butyl acrylate) (PBA) macroinitiator for ATRP, Matyjaszewski's group was similarly able to demonstrate ATRP-enabled core crosslinking using DVB. This was followed by using the resulting Br-capped ends to initiate polymerization of PS. A biodegradable miktoarm polymer was similarly synthesized by exchanging a few components from their earlier miktoarm polymer. Poly(methyl methacrylate) (PMMA) polymerization was initiated using 2-bromoisobutyrate and CuBr/2,2'-bipyridine (bpy) as a catalyst. The resulting chain was then core crosslinked using bis(2-methacryloyloxyethyl) disulfide, a divinyl molecule containing a degradable disulfide linkage. Subsequent ATRP of BA led to the formation of a biodegradable A_xB_y (A = PBA, B = PMMA) miktoarm polymer. Reduction, and resulting degradation of the miktoarm polymer, was triggered by its incubation in 0.08 M Bu_3P/THF solution, and complete cleavage was seen in 40 hours.[110] While not carried out under biological conditions, a comparison can be made to the reductive power of intracellular glutathione (GSH), present at roughly 10 mM concentrations, which can cleave disulfide functional groups.[111-113]

A similar study approached the idea of biodegradable CCS polymers, which included arm-degradable A_x, partially arm-degradable A_xB_y, and core-degradable B_y (A = PCL, B = PS/PMMA). Beginning with a bifunctional core, 2-hydroxyethyl 2'-methyl-2'-bromopropionate, which had both ROP and ATRP active ends, arm-degradable polymers were synthesized by the sequential ROP of CL, and core-crosslinking using DVB. This resulted in a PCL-CCS polymer which could

be degraded through hydrolysis. A non-degradable analogue was synthesized by using the initiator for the ATRP of MMA/St first, followed by DVB crosslinking. Most interestingly, however, was the capacity to make partially arm-degradable A_xB_y polymers using this approach.[114] This opens up the possibility of synthesizing miktoarm polymer-based drug delivery systems with tuned biological responses that can be adjusted to provide a good sustained release of drug cargo.

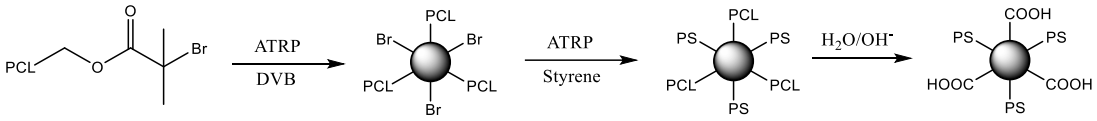

Scheme 1.5. In-out synthesis of A_xB_y (A = PCL, B = PS) CCS polymers and their subsequent alkaline hydrolysis.

To date, there has been one CCS miktoarm star that has been evaluated for drug delivery. Trithiocarbonate-terminated polyethylene glycol (PEG-DMPA), a PEG-based RAFT macroinitiator, was synthesized from α-methoxy-ω-hydroxy PEG. It was core crosslinked with 6,6′-(ethane-1,2-diylbis(oxy))bis(3-vinylbenzaldehyde) (EVBA), a divinyl linker with pendant aldehyde functionalities, in the presence of aluminum tris(8-hydroxyquinoline) (Alq_3), a fluorescent crosslinker, to yield a CCS with PEG arms, short aldehyde pendants, and a crosslinked fluorescent core. The aldehyde groups were used to couple with aminooxy end-functionalized poly(γ-benzyl-l-glutamate) (PBLG), a polypeptide, through the aldehyde-aminooxy click reaction. After an aminolysis step with β-hydroxyethylenediamine, the PBLG arms were converted to PHLG which is cationic at physiological pH (Figure 1.3). The resulting charged miktoarm polymers were found to be biocompatible and were able to bind siRNA through electrostatic interactions. Due to their surface charge, the miktoarm polymers were easily taken up by cancer cells where they could deliver their siRNA cargo. At the same time, the fluorescent miktoarm cores provided efficient tracking.[61]

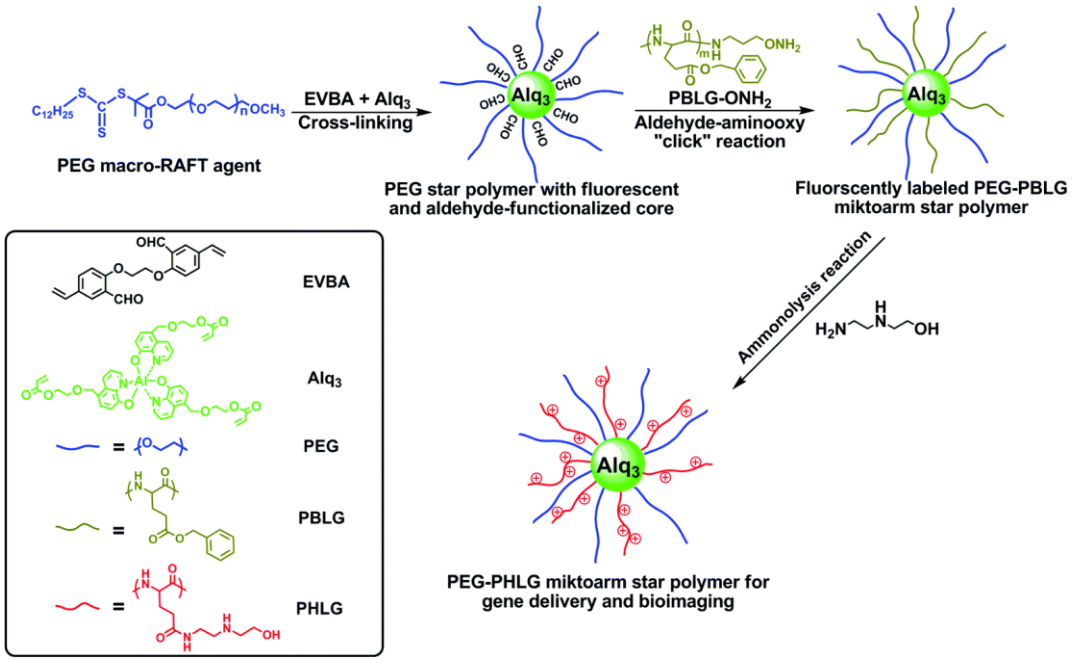

Figure 1.3. Schematic representation of PEG-PHLG CCS polymer synthesis using an in-out methodology. Reprinted with permission from reference 61. Copyright 2016 Royal Society of Chemistry.

1.2.5 Miktoarm Polymer Characterization

Owing to their branched architecture, the characterization of miktoarm polymers is important to establish their compositions, and it requires careful consideration and interpretation of data. Almost universally, the characterization of miktoarm star build-up is obtained through a combination of NMR spectroscopy and GPC chromatography. Despite its prowess in characterizing polymer homoarms, MALDI-TOF has not been successfully employed for the characterization of miktoarm polymers.[53, 67, 115]

Many of the earlier miktoarm polymers, generally synthesized using chlorosilane-based methodologies, had ABC type structure, which was simple to elucidate. For example, as discussed in section 2.1, the construction of the first miktoarm polymer required separate anionic polymerization of PI, PS, and PB arms, each of which were characterized using NMR and GPC. The stepwise conjugation of the polymers with living anionic ends, onto a chlorosilane core, was then followed by GPC, and a downwards shift in retention time, upon addition of each arm, was observed. The inclusion of each arm was further determined using ^{1}H NMR, and through this combination, miktoarm polymer's overall composition could be accurately calculated.[88] Due its

reliability and simplicity, this characterization methodology has been applied in recent ABC type miktoarm polymers, which have been used for applications in drug delivery.[41, 45] For example, the synthesis of a PEG-PNBM-PNIPAM miktoarm polymer, which involved sequential ATRP of NBM, and CuAAC of alkynyl-PNIPAM onto a PEG(-Br)-N_3 macroinitiator, was followed stepwise, using GPC, ^{1}H NMR, as well as FT-IR.[66]

Characterization of miktoarm polymers with AB_n composition, typically involve characterization using a careful comparison of ^{1}H NMR peak integrations, together with the analysis of their GPC chromatograms. For example, in an AB_2 polymer, where B segments are added by click chemistry, the relative integrations of B-derived protons become double, compared to those from the A segment. Analysis of its GPC chromatogram showed a unimodal peak, implying that there are no unconjugated segments.[24, 38, 42, 46, 53, 55]

Often, miktoarm polymer development is carried out using polymerization from heteromultifunctional cores. Where there are equivalent initiating functional groups present in multifunctional or polymer segment-conjugated cores, it is generally assumed that the polymerization is initiated from every such functional group present. For example, in the development of a PEG-PLA_2 miktoarm polymer from a PEG macroinitiator conjugated to a serinol core, L-Lactide ROP was initiated from both hydroxyls present in the core.[34] In such cases, GPC is used to verify A and B segment addition. The ^{1}H NMR is then used to verify the overall polymer structure and calculate the degree of polymerization (DP) of A and B arms.[32, 34, 40, 43, 44, 46, 54, 62, 65, 67, 71, 72, 74] Such strategies have been applied to other miktoarm star architectures, including A_2B_2, A_3B_3, and ABC.[46, 50, 116]

Depending on the core structure, ^{1}H NMR spectra can also provide more accurate confirmation of initiator usage, with the disappearance of the corresponding protons.[59, 63] For example, ethyl-β-d-glucopyranoside, a sugar containing 1 secondary and 3 primary hydroxyls, was used to initiate the ROP of caprolactone, specifically at its secondary hydroxyl group, with the aid of the catalyst Novozyme 435. After the hydroxyl group was terminated with vinyl acetate, caprolactone ROP was initiated from the remaining hydroxyl groups, using a $Sn(Oct)_2$ catalyst. PEG was then conjugated to free PCL-OH ends. In addition to standard GPC characterization, ROP from specific sugar hydroxyl groups was verified due to their inequivalent ^{1}H NMR peak shifts. While not a

quantitative measure, FT-IR can also be used to verify the presence of functional groups derived from each arm composing a miktoarm polymer.[52, 58, 73, 78]

In one unique example, partially deprotonated PEG was used to initiate the ROP of glycidol to yield a short hyperbranched oligoglycidol with 10 hydroxyl groups, for the ROP of caprolactone, which was followed by integration of the ^{1}H NMR spectra. Based on the assumption that each hydroxyl group will be active, caprolactone ROP was subsequently carried out to yield the 10 PCL arms, and verified again using both NMR and GPC.[37]

1.3. Amphiphilic Miktoarm Star Polymers: Self-Assembly

As discussed earlier, most pharmaceutical agents have inadequate bioavailability when administered directly,[2, 3] and thus, polymeric nanocarriers provide an important tool for drug delivery. Amphiphilic block copolymers and lipids have been extensively studied as potential platforms for loading and delivering drug cargo to targeted diseased sites within the body.[7, 117] When introduced into aqueous media, the exposure to the newly polar environment forces amphiphilic polymers to undergo microphase separation, during which chains segregate into distinct polar and non-polar phases.[118] The overall assembly that results from the sequestering of chains, is generally guided by the total fraction of each polar/non-polar chain segment within the amphiphilic polymer, as well as its overall topology.[119] Although conditions vary, it is commonly accepted that for micelle formation, an amphiphilic polymer must have a hydrophilic fraction $f >$ 0.45, and for polymersomes, $f = 0.35 \pm 0.1$ (Figure 1.4).[120, 121] While micelles are characterized by their hydrophobic cores and hydrophilic coronae, polymersomes distinctly have a hydrophilic core, surrounded by a hydrophobic layer, enclosed within a hydrophilic corona. These domains make such nanostructures suitable for the physical encapsulation, prolonged retention, and delivery of poorly-water soluble drugs, thus increasing their bioavailability and overall therapeutic efficiency. Some of the important parameters typical of nanocarriers used for drug delivery applications include their size, CAC/CMC, biocompatibility, drug loading, and drug release.[8, 25, 122] While much of the familiarity surrounding the effects of polymer self-assembly on drug delivery is derived from work on amphiphilic linear diblock copolymers, miktoarm star polymers with asymmetric branching polymer segments have increasingly been shown to possess superior micelle properties, while also being more tunable due to their varied syntheses and number of unique constituent segments.[21, 122]

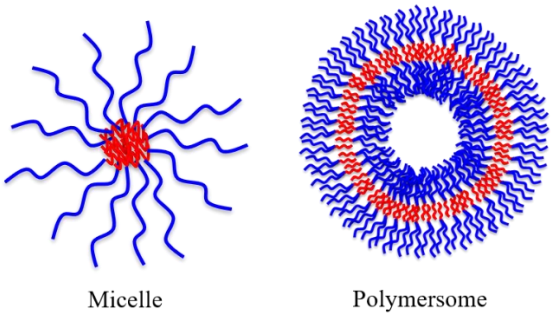

Figure 1.4. Aqueous self-assembly of AB_2 miktoarm polymers into micelles and polymersomes, depending on polymer hydrophilic fraction (red = hydrophobic, blue = hydrophilic).

As discussed earlier, micelle diameters below 200 nm are necessary to improve their biological distribution and disease site accumulation, commonly through the EPR effect.[12] Self-assembled structures from miktoarm star polymers can, in general, have similar sizes to those from linear block copolymers,[52] and scale similarly with increasing hydrophobic segment size relative to hydrophilic blocks.[24, 56, 62] The branched architecture of miktoarm star offers potential for tuning, and this was explored in a study of three copolymers using biocompatible PEG and PCL arms, with different AB, BAB, and AB_2 (A = PEG, B = PCL) diblock, triblock, and miktoarm topologies, but with similar hydrophilic/hydrophobic ratios.[60] XRD was used to study PEG and PCL crystallinities, and it was found that the relative crystallinity of PCL chains decreased in the sequence AB>BAB>AB_2, as the arms became more sterically restricted. PEG crystallinity was found to be severely limited in the BAB triblock as a result of the adjacent PCL arms, and it was similar in AB and AB_2 copolymers. This was further evidenced by the measurement of C=O vibrations using FTIR at 1726 and 1736 cm^{-1}, for crystalline and amorphous PCL regions, respectively. Such variations in crystallinity accounted for the differences in micellar diameters, where AB, BAB, and AB_2 copolymers had sizes of 43, 74, and 53 nm, respectively. On the other hand, one can design miktoarm star polymers to have a larger proportion of hydrophilic to hydrophobic arms, so that the relatively large volumes of the hydrophilic groups force a constricted micellar curvature, resulting in smaller diameters.[123, 124] An AB_3 (A = PMMA, B = PNIPAM) miktoarm star for prednisone acetate delivery was designed for this purpose, and it formed spherical micelles of roughly 50 nm, considerably lower than the 190 nm diameters of the equivalent linear diblock analogues.[31, 125] Depending on the polarity of the majority of branches, miktoarm polymers can have different properties. Increased hydrophobic branching can diminish core crystallinity due to imperfect packing, with an insignificant increase in size, and such an effect

has been demonstrated to be beneficial for drug loading.[126] On the other hand, increased hydrophilic branching can lead to lower nanoparticle sizes.

1.3.1 Micelle Characteristics: CMC and Stability

There are several methodologies that have been employed for studying aqueous self-assembly of amphiphilic polymers, including co-solvent evaporation, thin film, dialysis, and oil/water emulsion methods.[127] In the co-solvent evaporation and dialysis methods, the amphiphilic polymer is solubilized in a miscible organic solvent, added to water slowly, and then the organic phase is removed through evaporation or dialysis, triggering self-assembly. In the oil/water emulsion method, the polymer is dissolved in a water-immiscible organic phase, followed by the addition of water, and evaporation of the organic phase. Regardless of the method, the lowest concentration at which the hydrophobic segments of amphiphiles will begin to sequester is known as the critical aggregation concentration (CAC), or the critical micelle concentration (CMC) for micelles. Amphiphilic polymers in solution exist as unimers below their CMC and partition to the air/solution interface. Continuously increasing polymer concentrations past the CMC leads to the formation of a separate phase composed of the self-assembled polymers, which is accompanied by a decrease of free energy of the system.[128] Due to the large dilution that polymeric micelles undergo upon administration into the body, having a very low CMC not only represents general stability of micelles, but it is integral in maintaining their morphology, and in preserving their function.[4]

The methods for determining a polymer's CMC include tensiometry, conductometry, and fluorescence spectrometry which measures the absorbance and emission spectra of encapsulated hydrophobic dyes. The onset of CMC is seen as a sudden shift in the rate of change of a measured variable as a function of polymer concentration.[128] The CMCs of miktoarm star polymer-based assemblies is often determined through fluorescence spectroscopy, using the hydrophobic fluorophore pyrene, or somewhat less commonly, Nile Red. With pyrene, for example, its partitioning from the aqueous phase (below the CMC) towards micelle interiors (above the CMC), is reflected by an increase in fluorescence intensity and a red-shift of its (0,0) vibronic band.[129] Consequently, the CMC can be found as a change in the intensity ratio of I_{338}-I_{339} / I_{333}-I_{336} in the excitation spectra.[51, 130] Importantly, the CMCs attained in miktoarm star assemblies (10^{-7} - 10^{-9} M) have generally been found to be lower than those of diblock copolymers (10^{-4} - 10^{-7} M), though

it should be noted that most diblock systems have CMCs closer to 10^{-7} M.[4, 14-17, 20-25, 75] Incorporation of additional arms in miktoarm star polymers allows for further stabilization of micelles, leading to lower CMCs. This normally involves tailoring miktoarm stars to have a larger proportion of hydrophobic to hydrophilic segments, so that self-assembly is more energetically favourable. For example, in a study comparing AB and AB_2 (A = PEG, B = poly(glutamic acid (PGA)) polymers with conjugated DOX, the miktoarm star CMCs were lower at 5.4 mg/L compared to the diblock polymer's 9.0 mg/L.[52] Similarly, AB_3 miktoarm star polymers (A = PMMA, B = PNIPAM) were found to have considerably lower CMCs of 10 mg/L than their diblock equivalents (50 mg/L).[31, 125]

With miktoarm polymers, as in the case of more conventional block copolymers, CMCs tend to decrease with increasing hydrophobic chain length. This is generally attributed to the favourable de-solvation and aggregation of hydrophobic segments in aqueous media.[131] It has been well documented for miktoarm star polymers, especially those containing PCL, in varied systems including ABC (PEG-PCL-TPPBr) (triphenylphosphonium bromide), and PEG-PCL-PAA, as well as more complex $A(AB)_3$, $A_2(AB)_2$, and $A_3(AB)$ (A = PEG, B = PCL) systems.[42, 56, 57] One interesting example was of an AB_2 (A = PEG, B = P(MAA-co-MMA) miktoarm star, where poly(methacrylic acid) (PMAA) was a pH-responsive unit. Polymers containing higher hydrophobic PMMA to hydrophilic PMAA content ratios led to more compact and stable micelles and lower CMCs, with the trade-off that they were comparatively less pH-responsive.[62] While hydrophobicity tends to decrease CMCs, they generally increase with increasing hydrophilic block sizes.[56, 72]

Rather than strictly increasing hydrophobic block sizes, one study attempted to change the ratio of hydrophilic and hydrophobic segments through four different A_2B, A_2B_2, AB_3, and A_3B (A = PCL, B = POEGMA) miktoarm star polymers.[70] It was found that increasing the number of PCL arms to POEGMA resulted in the largest increase in micelle stability, with a minimum CMC of 2.66 mg/L for the A_3B miktoarm star. Interestingly, despite PCL/POEGMA ratios, the 4-armed miktoarm stars collectively had lower CMCs than the 3-armed A_2B miktoarm star. This reciprocated an earlier study where more arms in star polymers increased micelle stability.[132] Similarly, the 3-armed star had the highest diameter of 73 nm, and the size decreased with the number of PCL arms in 4-armed miktoarm star polymers to 28 nm.

1.3.2 Micelle Drug Loading and Release

As mentioned earlier, most pharmaceutical agents have poor water solubility and low bioavailability.[2, 3] Loading drugs into self-assembled polymeric micelles can help resolve this issue by providing solvation, enabling prolonged gradual release, and through the EPR effect, facilitate passive targeting to disease sites.[7, 12, 117] Owing to their tailorable architecture, superior CMCs, improve drug loading, and sustained drug release, there has been much recent interest in miktoarm star polymer-based assemblies for drug delivery.[21, 25, 26] Drug incorporation into micelles has been shown to have varied effects on the size of miktoarm micelles, where it can lower, increase, or have a negligible effect upon drug encapsulation.[24, 42, 47-49] Though generally, a decrease in size has been attributed to good polymer-drug compatibility.[47, 49, 57] One of the beneficial effects of including multiple branching arms as in miktoarm stars, is in increasing drug loading content into their self-assemblies. For example, AB_3 (A = PMMA, B = PNIPAM) self-assembled miktoarm polymers were used to load prednisone acetate with encapsulation efficiencies of 50%, compared to 11% with the corresponding linear diblock copolymers.[31, 125] Improved drug loadings were also seen in AB_2 type miktoarm stars with A = PNIPAM, B = poly(undecylenic acid) (PUA), and A = PEG, B = poly(trimethylene carbonate) (PTMC).[27, 32, 133]

Micellar drug retention has generally been associated with more sustained drug release and dampening burst release,[32, 48, 55, 70] which has the benefit of increasing drug bioavailability. This could be the result of strong interactions and more sites of association between encapsulated drug and multiple hydrophobic chains.[27, 52, 70, 133] In a study of $A(AB)_3$, $A_2(AB)_2$, and $A_3(AB)$ (A = PEG, B = PCL) miktoarm stars, camptothecin loading percentages ranged from 3.6 to 10.8%, with higher loadings in assemblies of miktoarm stars with more PCL blocks.[57] A higher degree of branching in polymer-based nanocarriers is imperative in improving their therapeutic efficiency.

It has been argued that the branching architecture of miktoarm stars has favourable effects on drug loading and release properties, and increasing hydrophobic chain length can lead to an increase in drug encapsulation and prolonged drug release.[32, 48, 62] However, long hydrophobic segments may also prohibit micellar hydrophilic surface coverage.[13, 52, 134] This has been mainly a concern for diblock copolymers, and it can be lessened by making use of the branched architectures. For example, in a study of AB_2 (A = poly(lactide-co-glycolide) (PLGA), B = PEG) miktoarm stars, increasing the length of PLGA arms was shown to result in total cumulative ibuprofen release to

be between 10 and 60%.[75] In another study using AB_2 (A = PCL, B = PEG) miktoarm stars, nimodipine loading efficiencies, scaled between 23 and 70%, with variations in PCL length in $PEG775_2$–PCL5800 and $PEG775_2$–PCL19000. However, the drug release was found to be between 93 and 85% of their loaded cargo respectively, showing that PCL size or drug loading efficiency had little effect on drug release.[24] Interestingly, increasing the hydrophilic chain length of a miktoarm star polymer can also promote drug loading as was shown for a miktoarm star with two hydrophilic PNAM chains and a hydrophobic poly(L-lactide) (PLLA) arm.[72]

1.3.3 Non-spherical Micelles

Due to a wide range of the hydrophilic fractions ($f > 0.45$) that conventionally permit amphiphilic polymers to form spherical micelles, and as a result of their simple morphology, micelles constitute the bulk of assemblies that have been explored for drug delivery. However, through the alteration of hydrophilic fractions of constituent amphiphilic polymers, it is possible to assemble nanocarriers with different morphologies. When the hydrophilic fraction is lower than 0.45, polymers tend to form polymersomes, inverted nanostructures, and cylindrical micelles amongst other morphologies.[120, 121] This rule is not universally followed, as for example, in a study with AB (A = PEG, B = PCL) type diblock copolymers, spherical micelles were obtained with PEG fractions of 0.5, 0.3, and 0.17. AB_2 polymers with hydrophilic PEG fractions of 0.55, 0.32, and 0.20, instead formed fiber-like cylindrical micelles at $f \leq 0.32$.[54] Generally, the transition from spherical to cylindrical micelles occurs as the hydrophilic fraction of the constituent polymers decreases, as a result of a change in the curvature. The increase in size of the hydrophobic segment decreases the interfacial curvature, resulting in fiber-like micelles. Unlike linear AB block co-polymers, the miktoarm stars transitioned to form cylindrical assemblies at higher hydrophilic fractions as a result of the lateral crowding of PCL arms. Additionally, owing to their branching, miktoarm stars had generally lower CMCs except in the case of the 0.2 fraction polymers; and higher DOX loading efficiencies, reaching 73%, as opposed to 55% for diblock co-polymers. A comparison of DOX release between the cylindrical f_{PEG} = 0.32 micelles and spherical 0.30 micelles, showed 27 and 48% cumulative release, respectively. Another AB_2 (A = PEG, B = PCL) miktoarm star containing a β-aminoacrylate junction, was found to form spherical micelles at f_{PEG} = 0.71, cylindrical micelles at f_{PEG} = 0.56-0.33, and platelet-like structures for f_{PEG} = 0.23. Interestingly, loading the f_{PEG} = 0.56 polymers with chlorin-e6 (Ce6) and DOX resulted in a spherical morphology.[74]

Rather than assembling a structure defined by fractional hydrophilicity, $(AB)_2C_2$ (A = PS, B = poly(vinylidene fluoride) (PVDF), C = PEG) miktoarm stars were observed to self-assemble into 99 nm micelles in aqueous solution with distinct wrinkled cores.[69] PVDF in the micellar inner core blocks had both lipo-philicity and -phobicity. Cryo-TEM evaluation revealed that micelles had a "frustrated" wrinkled core due to the resultant immiscibility of PVDF and PS. As a proof of concept for drug delivery, these micelles were loaded with Nile Red, and due to imperfect packing of PS and PVDF, the cargo could be encapsulated in empty pockets within the core, potentially allowing for high loading of drugs.

1.3.4 Polymersomes

While micellar systems have been the main focus of miktoarm star-based formulations for drug delivery, polymersomes remain an interesting and valuable option. This is due to the fact that they can load both hydrophilic and hydrophobic drugs as a result of their unique morphologies. Part of the reason why polymersomes have been more seldom explored in drug delivery is that amphiphilic polymers, including miktoarm polymers, are synthesized with hydrophilic/hydrophobic ratios that favour micelle formation upon self-assembly. As stated earlier, hydrophilic fractions of 0.35 ± 0.1 generally favor the formation of polymersomes.[120, 121] Such approximations are difficult to apply universally, especially when considering the variably branched architectures of miktoarm polymers. A comparison of AB and AB_2 (A = PEG, B = PLLA) polymers with varying hydrophilic PEG volume fractions revealed that self-assembly of miktoarm star polymers into polymersomes, is much more tolerant of more varied volume fractions. Polymersome formation was observed for PEG volume fractions of $f = 0.2{-}0.7$, much broader than the range of 0.2-0.4 for the linear diblock counterparts.[34] In another example, an AB_3 (A = PAzo, B = PEG) miktoarm star polymer with an azobenzene-containing 4-isobutyloxyazobenzene side chain on the polymethacrylate arm, had a 78/22 hydrophobic/hydrophilic ratio, slightly outside the typical range for polymersome formation, yet it was still well suited for polymersome assembly. Although their spherical nature can be easily established using electron microscopy or a combination of DLS and SLS, it is often necessary to specifically distinguish them from spherical micelles. To this end, TEM and cryo-TEM micrographs can determine whether particles are polymersomes due to the visual presence of thin outer membranes (Figure 1.5).[43, 53]

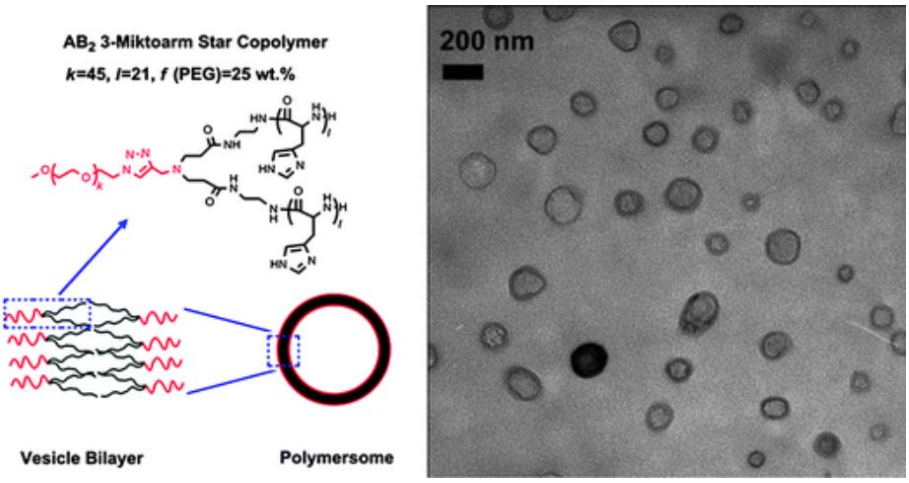

Figure 1.5. Cartoon schematic (left) and comparative TEM micrograph (right) of a polymersome assembled from a PEG-PHis$_2$ miktoarm star polymer with emphasis on its hydrophobic bilayer. Reprinted with permission from reference 43. Copyright 2012 Royal Society of Chemistry.

An AB$_2$ (A = PEG, B = PCL) miktoarm polymer-based polymersome was used for the dual loading of both hydrophobic curcumin and hydrophilic methotrexate HCl, with encapsulation efficiencies of 14.13 and 10.93% respectively. The nanocarriers showed a large burst release of methotrexate HCl unless co-loaded with curcumin. Curcumin was found to have an additional effect in combating multidrug resistance, as a small loading of it had a significant effect on enhancing methotrexate cytotoxicity.[71] Thus far, there has not been enough research to determine whether miktoarm architectures promote drug encapsulation specifically in polymersomes. However, in one study, linear AB and miktoarm star AB$_2$ and A(BA)$_2$ A = PEG, B = PCL) polymer-based assemblies were used to load rhodamine B isothiocyanate-Dextran (RhDex), with encapsulation efficiencies of roughly 45 and 40% for their AB and AB$_2$ polymers based systems, respectively. It showed good consistency between the two architectures, but with higher loading in the diblock. On the other hand, complete drug release occurred at 9 and 14 days for the AB and AB$_2$ polymers respectively, suggesting enhanced drug retention conferred by branching.[40]

Trends relating to physical properties of polymersomes do show some differences to those in micelles. For example, an increase in hydrophobic block size had the effect of hindering drug release, even in the case of those loaded in the hydrophilic core.[34] In comparing polymersomes of AB and AB$_2$ (A = PEG, B = PLLA) type architectures, CACs were found to be consistently lower for polymersomes assembled from miktoarm polymers, and were also found to decrease with hydrophobic block size.[34] Though conversely, in a study using AB and AB$_2$ (A = PEG, B = PCL)

polymers, it was found that there was a small free energy ($\Delta G°$) penalty associated with sequestering more PCL arms into the hydrophobic polymersome bilayer, and consequently AB_2 stars had slightly higher CACs than AB diblock copolymers.[40]

An interesting property of polymersomes is that they are capable of mimicking the architecture of cellular phospholipid bilayers. Assembly of branched AB_2 miktoarm polymers as structural components in polymersomes can better replicate these cellular phospholipid bilayers.[43] A study compared AB_2 (A = PEG, B = polyhistidine (PHis)) miktoarm stars to liposomes and incorporated cholesterol into the assembled polymersomes to enhance stability.[44] A combination of DLS and SLS studies showed that loading these polymersomes with 1 and 5% wt. cholesterol, increased their size from 72 to 92 to 129 nm, while maintaining their polydispersity index (PDI) and morphology. Additionally, polymersome half-life increased considerably to 15 hours from 1 hour in blood plasma concentrations of bovine serum albumin (BSA). The incorporation of cholesterol also increased the rigidity of the polymersome interface, slightly delaying the release of 5(6)-carboxyfluorescein, and these nanoparticles showed better cellular uptake.

1.4. Drug Delivery

Aqueous self-assembly of amphiphilic asymmetric branched architectures has intrigued the scientific community, due to its potential in tuning core-corona architectures in the resulting aggregates. It has been demonstrated that, compared to linear diblock copolymers, which have been extensively employed in drug delivery, the branching architecture of miktoarm star polymers affords enhanced micellar stabilities, lower CMCs, and could encapsulate hydrophobic drugs with much higher efficiencies and loading capacities.[21-23, 25, 54, 67] Asymmetric arm build-up of miktoarm stars has promoted the development of several unique systems which take advantage of having multiple polymer arms, each with specific effects. For example, using high yield reactions and a combination of ring-opening and stitching methodologies, a variety of AB_2 and ABC (A = PEG, B = Niacin and C = BODIPY) type miktoarm polymers have been prepared through the design of cores on which orthogonal reaction sequences could be easily carried out.[41] Using imaging studies, their intracellular localization into lipid droplets was demonstrated, and the niacin conjugated nanostructures supressed bacterial endotoxin stimulated nitric oxide production in microglia.

In another study, tetraiodofluorescein (TIF), a fluorescent dye, containing ABC (A = PEG, B = PCL, C = TIF) miktoarm star was synthesized, by sequential click coupling of mPEG and propargylated TIF to a central core, and ROP of caprolactone on the third junction.[49] The miktoarm star polymers formed micelles in an aqueous medium with a diameter of about 115 nm and a CMC of 0.43 mg/L. These micelles showed a cumulative release of 66% over 7 days. When macrophages were treated with them and imaged using fluorescence microscopy after labelling them with Hoechst 33342, the nanocarriers were clearly visible upon uptake into the cells (Figure 1.6). The nanodelivery system was found to decrease LPS-induced nitric oxide release in stressed macrophages, demonstrating their anti-inflammatory properties.

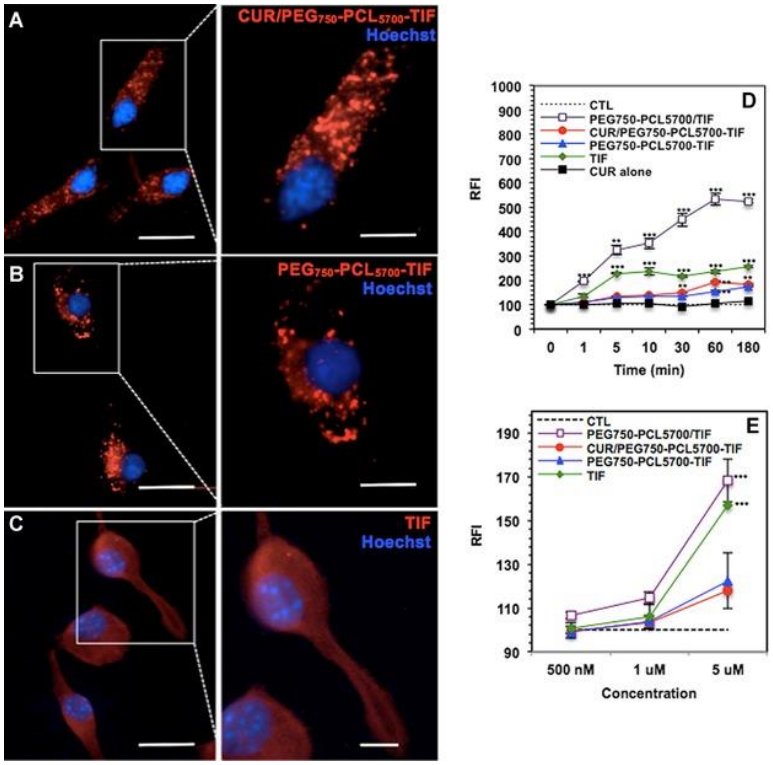

Figure 1.6. Fluorescent micrographs of macrophages treated with (A) curcumin-loaded PEG-PCL-TIF micelles, (B) unloaded PEG-PCL-TIF micelles, and (C) TIF control. Relative fluorescence intensities of macrophages treated with control media, TIF-loaded PEG-PCL micelles, curcumin-loaded PEG-PCL-TIF micelles, unloaded PEG-PCL-TIF micelles, free TIF, and free curcumin as a function of (D) treatment time and (E) dose concentration. Reprinted with permission from reference 49. Copyright 2014 John Wiley and Sons.

A series of mitochondria-targeting ABC (A = PEG, B = PCL, C = triphenylphosphonium bromide (TPPBr)) miktoarm star polymers were developed for coenzyme Q10 (CoQ10) delivery.[42] The star polymers with molar masses ranging from 6,000 to 12,000, formed micelles with a size range of

26.7-43 nm, and encapsulation efficiencies of 83-85%. Fluorescein isothiocyanate (FITC) labeled miktoarm stars-based micelles with the TPPBr functionalities at the corona surface showed significant localization in mitochondria in neurons and glia cells, compared to polymers without any mitochondria targeting moiety. Furthermore, MTT assays and confocal micrographs showed that miktoarm stars carrying CoQ10 improved mitochondrial metabolic activity within 24 hours and reduced mitochondrial damage from reactive oxygen species (ROS) in primary hippocampal cultures.

Miktoarm polymers could also be designed to lead to more stable self-assembled micelles by including stereochemically opposing arms as hydrophobic segments.[35] In this regard, AB_2 and ABC-type miktoarm star polymers were synthesized based on cyclic carbonate-functionalized PEG, on which ring-opening of the carbonate was carried out with an amine-functionalized silyl protecting groups. The order and extent of ROP could be controlled to yield miktoarm stars with a combination of poly(D-lactic acid) (PDLA) and PLLA- based hydrophobic segments. The linear diblock analogs of these which were composed of PEG and either PLLA or PDLA, had CMCs of 24.0 and 25.1 mg/L. The addition of another hydrophobic segment (PLLA or PDLA) in the branched miktoarm polymers, reduced these CMCs to 19.1 and 20.0 mg/L. The branched miktoarm architectures with both PLLA and PDLA as hydrophobic arms had opposing stereochemistry, allowing stabilization through complexation within the core. This had the effect of further reducing CMCs to 15.1 mg/L. The introduction of these stereochemically opposing arms also led to the reduction in size from 221.6 nm (for PEG-PDLA-PDLA) to 160.0 nm (for PEG-PLLA-PDLA). With paclitaxel as a model drug, the miktoarm micelles showed a cumulative release of 55% over 10 days. Stereocomplexation was also demonstrated to promote a much more sustained release of about 35% over this time period.

1.4.1 pH-Responsive Drug Delivery

The design of drug delivery nanocarriers often involves careful tailoring of polymer constituents for enhanced micellar stability, and the introduction of endogenous stimuli-responsive functional groups. For example, there is a considerable variation of pH in blood, tissue, stomach (1.5-3.5), the small intestine (5.5-6.8), the colon (6.4–7.0), as well as in the intracellular endosomal (5.5-6.0) and lysosomal (4.5-5.0) environments. One could use pH stimulus in drug delivery, and the constituent polymers must be resistant to degradation in these environments, and must have a pK_a

adapted to targeted delivery.[135] Polymers used for pH-responsive drug delivery, such as PDEAEMA or poly(methacrylic acid) (PMAA), are often weakly basic. It should also be noted that, while not inherent to nanodelivery systems, acidic conditions can also increase drug release from miktoarm polymers due to drug protonation, resulting in increased aqueous solubility.[72]

An $A_3(BC)_3$ (A = PCL, B = PDEAEMA, C = poly(poly(ethylene glycol) methyl ether methacrylate) (PPEGMA)) miktoarm polymer was synthesized by combining ROP of caprolactone, and sequential ARGET-ATRP of DEAEMA and PEGMA, using a multifunctional dipentaerythritol core.[51] PCL was the biocompatible hydrophobic block that would form the core of self-assembled micelles, PDEAEMA was the pH-responsive entity, which at a pH lower than 6.9 became protonated, leading to hydrophilic/hydrophobic switch. The PPEGMA block provided a hydrophilic shell, which imparted biological stability. At pH > 8, the PDEAEMA chains were found to be completely deprotonated, and as a result collapsed to form the hydrophobic core with PCL. A decrease in pH to 4 led to gradual increase in micelle size due to both PDEAEMA chain expansion upon becoming soluble, and electrostatic repulsion between the now positively charged chains. At pH of 7.4, 6.5, and 5.0, TEM micrographs showed that micelles had diameters of 100-180, 250-350, and >500 nm respectively. DOX-loaded $A_3(BC)_3$ star-based micelles with an encapsulation efficiency of 42-71%, showed steady drug release curves, culminating in 27-40% over 96 hours. Decreasing the pH of the release medium to 6.5 and 5.0 increased the cumulative release to 44-59% and 85-100%, respectively. Generally, micelles with larger PDEAEMA fractions showed greater response to pH, as one would expect. $A_2(BC)_2$ (A = PCL, B = PDEAEMA, C = PPEGMA) stars were also synthesized by the same group, and these polymers self-assembled to slightly smaller (63 nm) micelles.[50] Drug release at pH = 7.4, 6.5, and 5.0 showed cumulative DOX release of 82, 50, and 36% respectively. While the cytotoxicity of unloaded micelles was negligible, DOX-loaded micelles exhibited similar anti-tumor efficiencies to free DOX in HepG2 cancer cells.

A series of ABC (A = PEG, B = PCL, C = PAA) star polymers that would assemble into micelles with hydrophobic cores and mixed PEG/PAA hydrophilic coronae with pH sensitivity imparted by PAA (Figure 1.7), have also been synthesized.[56] At low pH, the COOH group on the backbone of PAA arms became increasingly protonated and resulted in hydrogen-bonding complexation with PEG arms in micellar coronae, and a decrease in micelle size. In the pH range from 6 to 10,

PAA arms became progressively ionized, and formed larger swollen micelles, from the loss of PEG/PAA corona complexation and repulsive forces between adjacent PAA arms. The average particle size increased from 51 to 154 nm at pH 2.2 to 10. The ABC miktoarm polymers had 58-73% encapsulation of naproxen, a model hydrophobic drug, and its cumulative release from the ABC miktoarm star micelles was 65-89% over 24 hours, at pH 7.4. Adjusting the pH to 2.2, and therefore compressing the micelles, resulted in greater drug retention, with cumulative naproxen release coming to roughly 35-50%. This suggests that naproxen would be retained under gastric conditions and released in the intestine, making the micelles suitable for oral administration.

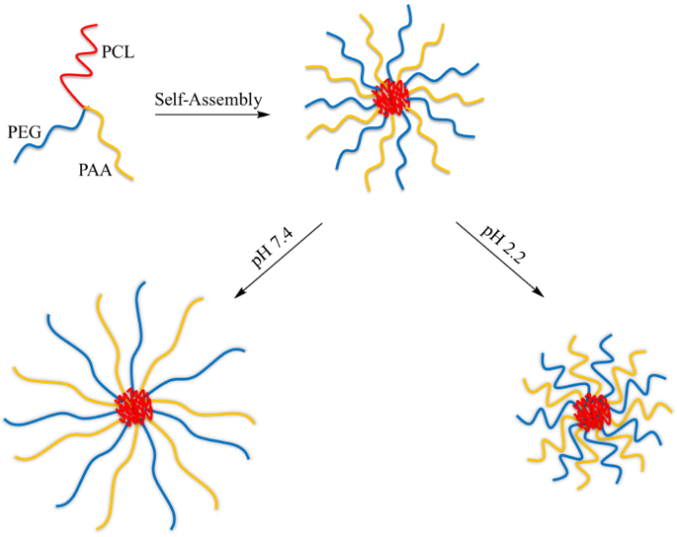

Figure 1.7. Representation of PEG-PAA-PCL miktoarm polymer self-assembly and pH-responsive morphological changes.

A miktoarm star with 8 arms, A_2B_6 (A = PCL, B = PMMA-*co*-PMAA was prepared using D-(−)-salicin (a β-glucoside) as a heterofunctional initiator.[63] It was functionalized with 6 bromoester groups and 2 hydroxyl groups, and the miktoarm star was constructed using ROP of caprolactone and ATRP of tert-butyl methacrylate (tBMA)/MMA, initiated by the hydroxyl and bromoester groups, respectively. The t-butyl groups were then removed through acidolysis to give PCL_2(PMMA-*co*-PMAA)$_6$ stars. Upon self-assembly, the CMC was reported to be as low as 15 mg/L, yet in some samples an additional higher point was found at 411 mg/L. TEM micrographs revealed the presence of dandelion-shaped superstructures with coronae surrounding dark spheres above the CMC. Two anticancer drugs, DOX and camptothecin (CPT), were loaded into the micellar structures with encapsulation efficiencies of up to 60 and 6% respectively, and the drug

loaded micelles were found to be larger than 200 nm in diameter. Due to the pH sensitivity of PMAA, the release rates of both drugs were slower at pH 7.4 than pH 5.0, at which point the chains became ionized and caused micelle swelling.

Another example of a miktoarm star drug delivery system using PMAA as a pH-responsive unit had the composition of AB_2 (A = PEG, B = P(MAA-*co*-MMA).[62] The polymer was synthesized by conjugating a bromoisobutyrate ATRP initiator to a dihydroxy benzoic acid core, followed by mPEG-OH coupling, and ATRP of MMA and tBMA. Acidolysis with TFA afforded the PEG-P(MAA-*co*-MMA)$_2$ miktoarm star polymer. The MAA content of the hydrophobic block was carefully controlled during copolymerization to tune the pH-sensitivity of miktoarm stars and two PEG-P(MMA$_9$-*co*-MAA$_{35}$)$_2$ and PEG-P(MMA$_{24}$-*co*-MAA$_{25}$)$_2$ miktoarm stars were synthesized. Higher MMA content led to higher (82.3%) encapsulation of methotrexate (MTX), an antineoplastic agent with significant chemotherapeutic activity, and the micelles exhibited a greater pH-induced MTX release (98% release after 48 hours at pH 1.2), compared to 33% at pH 7.4.

Taking advantage of poly(2-vinylpyridine) (P2VP), containing basic units with a pK_a of roughly 5.9, a variety of pH-sensitive ABC-type (A = PEG, B = PCL, C = P2VP) miktoarm stars were synthesized.[28-30] Due to the presence of P2VP, these polymers formed micelles with positive (+12.5 mV) zeta potentials upon aqueous self-assembly, thus indicating the presence of protonated P2VP arms in the coronae alongside PEG. Deprotonation through NaOH addition resulted in a micelle diameter change from 54 to 37 nm, due to the collapse of P2VP branches into micelle cores. This was attributed to the unique architecture of the star polymers, as well as the loss of electrostatically repelling chains in the corona (Figure 1.8). A titration indicated that the pK_a was 5.0, corresponding closely to that for P2VP, and was neutral at physiological pH.[28] In a follow-up study, P2VP blocks were biotinylated so that, upon administration, the labelled ABC micelles would contain biotin in the core.[29] Exposure to low pH in a tumour environment would protonate P2VP chains and shift conjugated biotin to the micellar corona, where it would aid in tumor targeting. Interestingly, the passive uptake effect of cationic micelles due to electrostatic interactions with negatively charged cell surfaces is so effective that the inclusion of biotin was unnecessary for astrocyte and 9L cell internalization. Loading of micelles with Nile Red as a model hydrophobe verified their efficacy in drug delivery. While 24% sustained release was seen after 6

hours at pH 7, an acidic pH 5, mimicking the endosomal environment, caused burst release with a cumulative release of 64% after 6 hours.

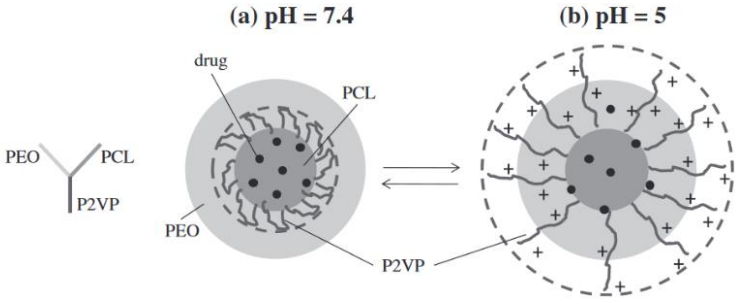

Figure 1.8. Schematic representation of the effect of (a) physiological pH and (b) acidic pH on the morphology of self-assembled PEG-PCL-P2VP micelles. Reprinted with permission from reference 29. Copyright 2012 Elsevier.

Rather than using intrinsically pH-responsive polymers, linear and miktoarm star polymers of AB and AB_2 compositions respectively (A = PEG, B = PGA) were prepared with DOX conjugated via an acid-labile hydrazone linker.[52] To achieve this, ROP of benzyl-L-glutamate was carried out on mPEG with either one or two primary amino groups. This was followed by the ester-amide exchange aminolysis of the benzyl protecting groups on the PGA blocks and then the linker was conjugated to neutralized DOX. The micelles were also loaded with DOX, and it was observed that miktoarm star polymers had nearly twice the drug loading, as compared to their linear analogues. This may be related to the increased number of sites in the PGA blocks for association. pH-dependent DOX release was seen in both AB and AB_2 polymer micelles as a result of acid-catalyzed hydrazone linker cleavage. While all micelles showed a similar 45% cumulative release within 72 hours at pH 7.4, AB_2 micelles showed 15% faster release compared to AB micelles at pH 5.0, and 25% faster release than micelles at physiological pH. These DOX release rates also contributed to a larger tumor-suppressive effect when micelles were incubated with HeLa cells.

Another use of the pH-responsive hydrazone functional group was in linking the constituents of an AB_2 (A = oleic acid (OA), B = PEG) miktoarm star for antibacterial drug delivery.[77] The hydrazone linker itself was formed from the combination of a hydrazide functionalized G1 oleodendrimer with PEG-CHO, and its efficient hydrolysis was initially confirmed via incubation of the AB_2 star in phosphate-buffered saline at pH 6.0. It resulted in fragmentation, observed using ESI, which showed peaks related to the cleaved oleic acid segment. The miktoarm star polymers self-assembled into 130 nm micelles with 6 mg/L CMC, and were used to load vancomycin, an

antibiotic, with an encapsulation efficiency of 39.6%, showing good compatibility with the micellar core. Drug release experiments showed the benefit of the hydrazone linker, as the cumulative release of drug-loaded micelles reached 100% at pH 6.0 in 48 hours, due to hydrazone linker cleavage (and subsequent micellar disassembly), as opposed to 86% release at pH 7.4. It allowed for antibacterial activity for 52 hours when tested against *S. aureus*, while unloaded vancomycin was only effective for 18 hours. The nanocarriers were also shown to be more effective in depleting bacterial growth in a skin infection model.

AB_2 (A = PEG, B = PHis) type pH-sensitive miktoarm star polymers for self-assembly into polymersomes were prepared.[43] Using a 150 mM NaCl solution, it was found that the miktoarm star effectively buffers in a pH range of 5-7, with an effective pKa of 6, which is in the endolysosomal pH range. Shifting pH from physiological pH at 7.4 down to 6.8, 6.0, and 5.0 was also associated with morphological transitions to cylindrical micelles, spherical micelles, and finally, soluble unimers. The polymersomes showed encapsulation of 5(6)-carboxyfluorescein, a fluorescent hydrophilic dye, similar to that for liposomes, and a drug release profile indicating about 70% release in 72 hours. Decreasing the pH below 6.8, and thus triggering structural changes, resulted in complete burst release within a few hours, and it showed good sensitivity to the endosomal pH range.

1.4.2 Temperature-Responsive Drug Delivery

Higher temperatures at disease sites provide another venue to target and control the release of encapsulated drugs from nanoparticles. In addition, heat can be applied from external sources in order to trigger the nanoformulation response. Polymers used in temperature-responsive systems typically feature a lower critical solution temperature (LCST) near the physiological temperature, above which a polymer becomes immiscible. The most common temperature-responsive polymer used with drug delivery systems, and the only one used in miktoarm star-based drug delivery systems is poly(N-isopropylacrylamide) (PNIPAM), due to its availability, biological compatibility, and well-studied LCST in the range of 30-35 °C.[136]

In a very early example, an AB_2 (A = PNIPAM, B = poly(undecylenic acid) (PUA)) miktoarm star was synthesized that had an LCST of 31 °C, very close to accepted values for PNIPAM.[27] Upon loading prednisone acetate, a common anti-inflammatory drug, it was reported that at temperatures below LCST, even after 150 hours, more than 80% of the drug remained intact. However,

significantly faster release rates were seen above the LCST of PNIPAM. In a later study, similar AB_3 miktoarm star polymers (A = PMMA, B = PNIPAM) were synthesized,[31] and below the LCST of PNIPAM, these formed spherical micelles in a size range of 50 nm, and with a CMC of 10 mg/mL. Prednisone acetate was stabilized in the PMMA cores of the micelles, and there was a total cumulative release of 55% at room temperature, compared to a 90% release above LCST. In such cases, the conversion of PNIPAM to a hydrophobic polymer above its LCST results in its collapse from the micellar corona into the core. As a result of the morphological transformation, an increase in the cumulative release of prednisone takes place.[27, 31]

While the previous examples deal with the corona/core switch of PNIPAM, one could also stabilize its position in micellar coronae *via* crosslinking. Crosslinking the micellar shells of assembled AB_2 (A = PNIPAM, B = poly(L-lysine) (PLL)) miktoarm star polymers would not lead to micellar collapse following the temperature increase above the LCST of PNIPAM, and the effect on drug delivery would be more subtle.[38] In such a system, shell crosslinking of drug loaded micelles was carried out using glutaraldehyde, and the permeability of the shell could be controlled by the extent of its reaction. The effect of restricted shell permeability was seen through prednisone acetate release, where the cumulative release from 50 and 100% crosslinked micelles was 17.1 and 22.8% after 170 hours. Increasing the temperature to 38 °C, above the LCST of PNIPAM, led to cumulative releases of 44.7 and 51.2% over the same time period, showing an accelerated yet still very sustained release.

$(BA)(AC)_2$ (A = PMMA, B = PPEGMA, C = PNIPAM) miktoarm polymers were synthesized through a combination of CuAAC coupling with ATRP, on a 1-azido-2,3-propanediol core (Figure 1.9).[65] These miktoarm stars contained only hydrophobic blocks emanating from the core junction, with hydrophilic chains being linked to hydrophobic PMMA chain-ends. While it was speculated that this structure may result in especially low CMCs, it was measured at 2 mg/L, in line with most other miktoarm star polymers. An interesting aspect of this miktoarm star architecture stemmed from the inclusion of PNIPAM arms, which, upon micellar self-assembly at room temperature, were found to be in the coronae of micelles alongside PPEGMA, but collapsed into the PMMA cores at physiological temperatures. When the temperature was further increased above the LCST at 42 °C, it resulted in micellar aggregation. Celecoxib, a hydrophobic drug, was loaded into the micelles with 8.8% encapsulation efficiency, and in 48 hours, 73% of celecoxib was released from

micelles at 25 °C. However, upon increasing the temperature to 37 °C, the release rate was found to be faster (89% drug release over 48 hours). This was explained using the general effect of temperature on release kinetics, as well as dissociation of the drug from PMMA, as PNIPAM began to permeate the core.

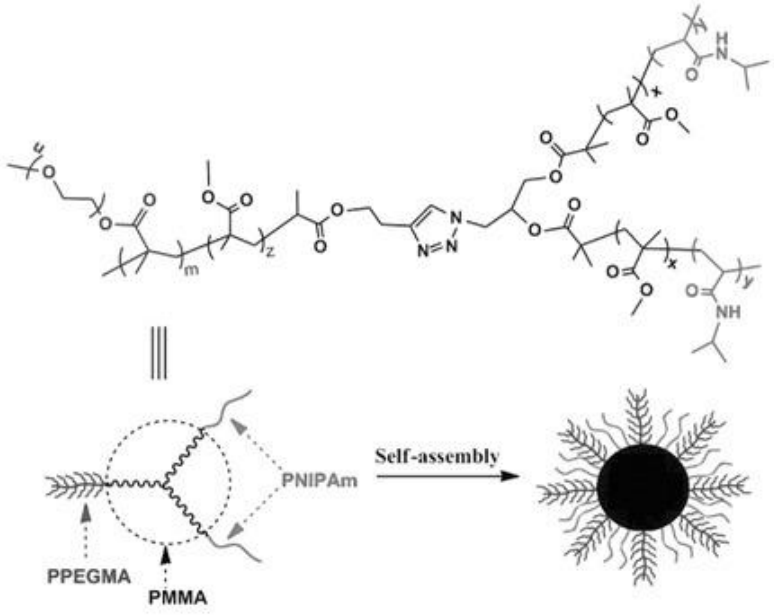

Figure 1.9. Schematic illustration of the micellar self-assembly of $(BA)(AC)_2$ miktoarm star polymers. Reprinted with permission from reference 65. Copyright 2016 John Wiley and Sons.

1.4.3 Redox-Responsive Drug Delivery

Oxidative stress is characteristic of many pathologies such as neurodegenerative disorders, cancer, and diabetes, which results in heightened concentrations of reactive oxygen species (ROS), including hydrogen peroxide (H_2O_2), superoxide (O_2^-), hydroxy radicals (·OH), and singlet oxygen ($^1O_2$).[137] While normally present as regulators in redox-dependent signal transduction,[138] elevated ROS concentrations at diseased sites are a sign of insufficient activity from the endogenous antioxidant defense mechanisms. One aspect of this system is the antioxidant glutathione (GSH), which is oxidized to glutathione disulfide (GSSG) upon exposure to ROS.[139] In cancer, tumour cells are known to contain elevated GSH levels that are thought to aid in tumour cell proliferation.[139] Additionally, evidence suggests that GSH protects cancer cells against chemotherapeutic drugs.[140] While a variety of cleavable polymer linkers have been applied to ROS-responsive drug delivery, including those based on thioketals, diselenides, phenylboronic acids and esters, and vinyldithioethers,[137] interestingly, only the β-aminoacrylate was used as a

specifically $^1O_2$-labile linker in miktoarm polymers.[74] Much effort has been devoted in developing miktoarm stars responsive to GSH that is present at elevated concentrations intracellularly at disease sites. In preparing GSH-responsive systems, polymers are typically conjugated using disulfide linkers that can be cleaved through thiol-disulfide exchange. GSH can also participate in thiol-thioester exchange, facilitating polymer cleavage, and it is reactive to acrylates *via* Michael additions, which can be used to prepare GSH conjugates.[141, 142]

An example of a miktoarm star containing a GSH-responsive linker was prepared using an AB_2 (A = PEG, B = PMMA) build-up, based on a dihydroxy-benzoic acid core with cystamine, a disulfide linker, connecting the core and the hydrophilic PEG arm.[58] The dihydroxy functionalities on the core were coupled to bromoisobutyrate ATRP initiators and used to polymerize PMMA. Aqueous self-assembly of these polymers led to micelles with a diameter of 130 nm and CMC of 0.91 mg/L. As a substitute for GSH which would be present biologically, 10 mM of dithiothreitol (DTT) was used (mimicking intracellular GSH concentrations) to reduce the disulfide linker present in the micelles. This treatment resulted in a micelle size shift to 300 nm after 2 hours, and >1000 nm after 24h, as a result of aggregation of unlinked polymer chains, while no significant size change was seen in untreated samples. MTX was encapsulated with 64% efficiency, and the nanocarriers showed 22% release in 48 hours with no clear burst release. Meanwhile, DTT treatment, causing complete micellar dissociation, resulted in a much more significant (95%) release in 48 hours.

A series of miktoarm polymers based on a core with 4 branching PEG arms have been prepared, by selectively carrying out the ROP of caprolactone on individual PEG ends to yield $A(AB)_3$, $A_2(AB)_2$, and $A_3(AB)$ (A = PEG, B = PCL) stars (Figure 1.10).[57] PEG blocks were end-conjugated to folic acid (FA) while PEG-PCL ones were conjugated to camptothecin (CPT) via dithiodipropionic acid, a GSH-cleavable disulfide bearing linker. Incubation with GSH not only led to the cleavage of CPT conjugated directly to miktoarm stars, but also to a several hundred nanometer increase in micellar diameter, which was associated with core destabilization from the linker cleavage. Faster CPT release was seen in micelles that had the highest CPT content (more points of conjugation), with 76%, 69%, and 54% release coming from $A(AB)_3$, $A_2(AB)_2$, and $A_3(AB)$ micelles respectively. Cellular uptake of CPT was investigated with SKOV-3 cells that overexpressed FA receptors. Micelles with the highest FA surface density (those with free PEG

arms conjugated to FA) were expected to enable higher cellular uptake. The $A_2(AB)_2$ micelles promoted the CPT uptake the most at 25%, and 11 and 15-20% in $A(AB)_3$ and $A_3(AB)$ micelles respectively, suggesting a compromise between FA surface density and CPT-loading. Considering CPT loading, GSH-sensitivity, and cellular uptake, PEG_2-$(PEG\text{-}PCL)_2$ micelles were the most optimal as anti-tumor agents.

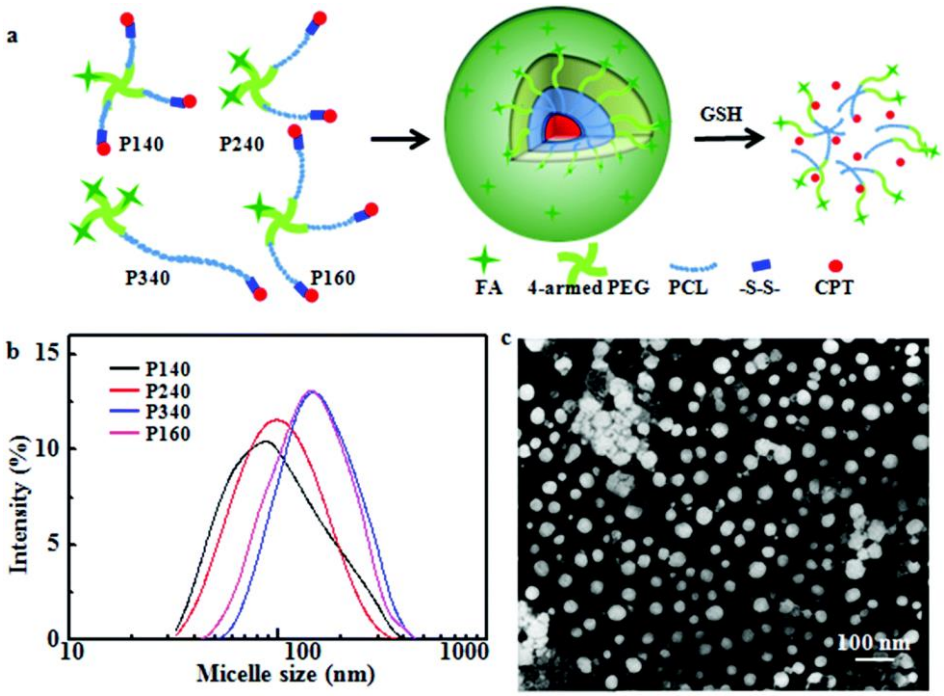

Figure 1.10. (A) Scheme of $A(AB)_3$ (P140, P160), $A_2(AB)_2$ (P240), and $A_3(AB)$ (P340) assembly into micelles, their response to GSH, (B) their size distributions from DLS, and (C) a representative TEM micrograph of $A_2(AB)_2$ (P240) micelles. Reprinted with permission from reference 57. Copyright 2015 Royal Society of Chemistry.

AB_2 (A = PEG, B = PLL) type miktoarm stars have been prepared using N-carboxyanhydride (NCA) ROP on a PEG-based macroinitiator, with or without bioreducible disulfide linkages conjugating the polymeric arms.[73] The disulfide linker-containing system employed cystamine, which was conjugated directly to the PEG macroinitiator, and its NH_2 end was employed for ROP. PLL is cationic at physiological pH, and it can electrostatically bind with negatively charged biomolecules such as plasmid DNA (pDNA). It was demonstrated that a 5:1 wt. ratio of miktoarm polymer to pDNA was sufficient for complete binding. Miktoarm star/pDNA polyplexes were prepared using this ratio, and these formed spherical particles of 57.67 and 142.62 nm diameters, with or without reducible disulfide linkers, respectively. These sizes were constant when incubated with fetal bovine serum for 24 hours, indicating good nanoparticle stability and applicability for

intravenous administration. This was in contrast to complexes of pDNA with just PLL arms, which grew to about 450 nm after 24 hours. The significance of the effect of the linkers or the reasons for the disparate sizes is not fully understood. Unlike the non-bioreducible polyplexes, pDNA bound to miktoarm stars was released in response to DTT, a reducing agent substitute for biological GSH. The in vitro transfection efficiency of miktoarm polyplexes containing disulfide linkers into HeLa cells, was observed to be much higher than that of the non-reducible polyplexes due to the intracellular reduction of these linkers.

A $^1O_2$-responsive miktoarm star of AB_2 (A = PEG, B = PCL) composition has been prepared, using the ROP of caprolactone from a PEG macroinitiator, containing a β-aminoacrylate junction.[74] The latter was found to be 100% in the E-configuration, and its $^1O_2$ induced cleavage was confirmed under red light laser irradiation, after exposure to the $^1O_2$-generating photosensitizer, chlorin e6 (Ce6) (Scheme 1.6). Ce6 and DOX were loaded into the micelles with 78 and 29% efficiencies respectively. Irradiation of these Ce6/DOX co-loaded samples led to the disruption of micelles into irregular aggregates, which triggered 68% DOX release after 24 hours, as opposed to only 26% in the dark. Accordingly, laser irradiation of co-loaded AB_2 micelles resulted in large DOX uptake into the cytoplasmic regions of MDA-MB-231 cells, more so than even free DOX, while micelles kept in the dark maintained good cargo retention.

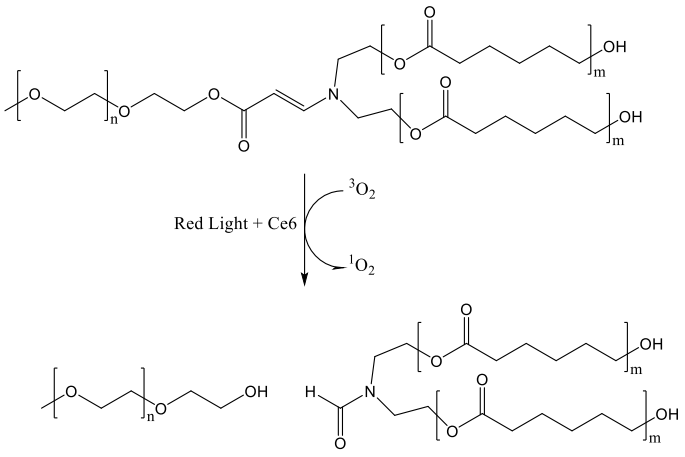

Scheme 1.6. Structure and $^1O_2$-response of PEG-PCL_2 miktoarm star polymers with β-aminoacrylate junctions to 660 nm light in the presence of Ce6.

1.4.4 Light- and Dual-Responsive Drug Delivery

Light is an advantageous non-invasive exogenous stimulus that can be directed to a target site, and it provides an intriguing platform for drug delivery. However, since UV light is often used to trigger such systems, safety risks as well as low tissue penetration are matters of concern. The two main categories of light-responsive polymers that have been explored in drug delivery are those which undergo photochemical cleavage or photoisomerization.[143] For such UV-light induced cleavage, moieties such as pyrenylmethyl esters, coumarinyl esters, and *o*-nitrobenzyls have been incorporated into polymeric systems.[143, 144]

For example, the *o*-nitrobenzyl group was introduced into an ABC (A = PEG, B = poly(2-nitrobenzyl methacrylate) (PNBM), C = PNIPAM) miktoarm star, which could change its micellar morphology, in response to both light and temperature, due to its sensitive PNBM and PNIPAM arms respectively (Figure 1.11).[66] It is well known that the LCST of PNIPAM is 32 °C, but it was found to be 42 °C in the miktoarm polymer,[145] which was attributed to the low MW of the PNIPAM block as well as its clustering with PEG in the micellar coronae. Heating an aqueous micelle solution past this temperature increased micelle diameters from 97 to 142 nm, as PNIPAM chains aggregated with PNBM in the core. UV light irradiation was able to cleave and convert the *o*-nitrobenzyl functionalities into *o*-nitrobenzaldehyde and the carboxylic acid, proceeding through a Norrish II type intramolecular rearrangement. This rearrangement does not require an aqueous solvation, and as a result can occur in micellar cores.[66, 146, 147] In the case of PNBM, UV-induced cleavage of *o*-nitrobenzyl moieties in its side chains converted the polymer to the now hydrophilic PMAA. DLS studies showed that the nanoparticle diameters increased by about 15 nm and had much wider dispersities. Using Nile Red as model cargo, below the LCST and without UV stimulus, its release was found to be negligible, while raising the solution temperature past the LCST only increased the cumulative release of Nile Red to 4.6% after 30 minutes. In contrast, UV irradiation of the sample led to 64% release, showing the much stronger effect of converting the constituent polymer of the hydrophobic core into a hydrophilic chain.

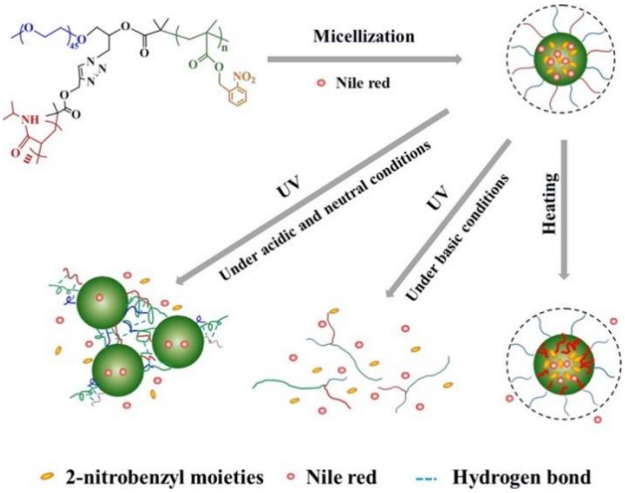

Figure 1.11. Self-assembly and dual UV/temperature response of PEG-PNBM-PNIPAM miktoarm star polymers. Reprinted with permission from reference 66. Copyright 2017 Elsevier.

In the photoisomerization category, azobenzenes, which are known for their ability to transition from trans to cis isomers upon UV irradiation, with an accompanying local polarity increase, are by far the most commonly employed functionalities.[143, 144] This differentiates azobenzene-containing drug carriers from photocleavable systems as they can transition between their "on" and "off" states, which can allow more precise tuning of drug release at desired sites.[46]

A series of azobenzene containing AB_3 miktoarm star polymers (A = PAzo, B = poly(*N*,*N*-diethylacrylamide) (PDEAA)) have been synthesized.[46] Using a trifunctional-azido ATRP initiator, the polymerization of an azobenzene-containing methacrylate yielded a PAzo-core structure. It was then coupled with three PDEAA arms using click chemistry to form a miktoarm polymer. The effect of temperature on the miktoarm polymer assemblies was first assessed with DSC, through which an LCST of 27 °C was determined. PDEAA became hydrophobic above this temperature and resulted in a collapse of the micelle. Temperature reversal led to a partial reassembly. Irradiation of the dual-responsive PAzo-$PDEAA_3$ micelles also resulted in reversible morphological distortion, as well as an 8 nm increase in their D_h. While one might assume that temperature-associated changes would lead to cargo release, Nile Red was found to be associated within the collapsed micellar structure. Micelle deformation from UV irradiation successfully promoted Nile Red release (Figure 1.12).

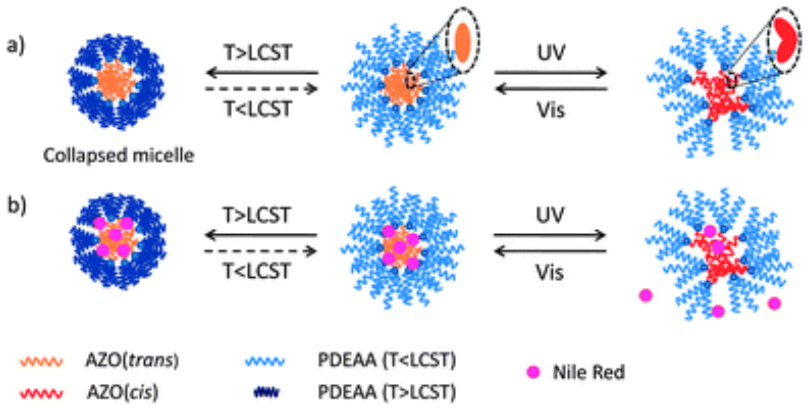

Figure 1.12. Representation of (A) temperature and UV-induced morphological response of PAzo- $PDEAA_3$ micelles and (B) the corresponding proposed Nile Red release. Reprinted with permission from reference 46. Copyright 2013 Royal Society of Chemistry.

Another AB_3 (A = PAzo, B = PEG) miktoarm polymer with an azobenzene-containing 4-isobutyloxyazobenzene side chain on the polymethacrylate arm has been synthesized, using a three-armed PEG macroinitiator for ATRP of the PAzo arm.[53] It formed polymersomes with diameters reported to be approximately 640 nm on average, about double that of the previously reported values. UV-vis spectra showed two absorption bands: the azobenzene *trans* π-π^* transition centered at 360 nm, and the *cis* n-π^* transition at 450 nm. Irradiation with a mercury low pressure UV lamp showed complete trans-cis isomerization within 5 minutes, and at rest, a cis-trans reversal occurred within 24 hours. Irradiation caused a morphological transition of the polymersomes to a 'wrinkled' state, accompanied by a 170 nm decrease in nanoparticle diameter. The permeability of the miktoarm star polymersomes after irradiation resulted in the efficient release of encapsulated hydrophobic Nile Red or hydrophilic Rhodamine B probes.

1.4.5 Polyplex Delivery

Polymeric systems have provided a viable avenue for the delivery of genes and proteins as polyionic complexes, or polyplexes.[148] Owing to the negatively charged backbone of nucleic acids and some peptides, cationic polymer segments are often used as complexing agents for stabilization and drug delivery. As miktoarm polymers contain multiple branched segments, they can be tuned such that disparate arms can be used for complexation within the same drug delivery system. In such an example, self-assembled micelles from ABC (A = PEG, B = PLL, C = PCL) miktoarm polymers, with PEG and PLL comprising the hydrophilic corona, and PCL forming the core, were prepared.[45] Whereas PEG and PCL were used to maintain the integrity of micelles by

acting as corona-stabilizing hydrophilic and core-stabilizing hydrophobic segments respectively, PLL was used for pDNA complexation. Upon self-assembly, the 31 nm micelles were capable of loading the hydrophobic paclitaxel, while being complexed with pDNA, enabling their codelivery. *In vitro* studies showed a burst release of paclitaxel initially, but reached 65% cumulative release within 60 hours. Unfortunately, blank micelles led to significant HeLa cell death, in which 61% of cells survived 6 μg/mL polymer concentrations. Paclitaxel loading led to a further 20% reduction in cell survival. It was found that PEG-PLL-PCL miktoarm stars formed polyplexes with pDNA through electrostatic interactions at N/P (polymer amino (N) / nucleic acid phosphate (P)) ratios higher than 2. Binding affinities were found to be similar for paclitaxel loaded and unloaded micelles. Zeta potentials were measured for N/P ratios 0.5-32, and were found to change to positive values at N/P = 2. However, these continued to steadily rise afterwards indicating further structural change/binding. *In vitro* cell transfection experiments on HeLa cells revealed improved transfection in paclitaxel loaded micelles, likely due to their anti-mitotic effects.

The first example of the use of core-crosslinked miktoarm stars micelles for drug/nucleic acid delivery was for micelles that contained PEG and poly(β-hydroxyethylenediamine-L-glutamate) (PHLG) arms in their coronae.[61] Core-crosslinked polymers prepared by radical polymerization are often symmetrical.[149] The inclusion of mixed arms, as in miktoarm stars, can yield more efficient drug delivery systems, as in this case where PEG confers solubility and PHLG was used for polyplex formation. The pK_a of these miktoarm stars was determined to be 8.6, thus leading to protonation of PHLG terminal amino groups at physiological pH. Due to its cationic arms, the miktoarm polymer formed a complex with negatively charged siRNA. Gel electrophoresis showed that complexes were formed at N/P ratios higher than 16, at which point, bands representing unbound siRNA were no longer seen. Flow cytometry of Cy3-labeled siRNA and Alq_3-labeled miktoarm star cores showed that most siRNA was taken up into A549 cancer cells as a complex with miktoarm stars.

Linear (AB) and AB_3 miktoarm stars (A = PEG, B = PGA) were synthesized based on the NCA ROP of PGA from a PEG macroinitiator, in order to study the effect of polymer topology on lysosome protein complexing.[67] Having an isoelectric point at pH 11.3, lysozyme has a net positive charge at physiological pH which allows for its complexation with polyanions such as PGA, which is negatively charged at physiological pH. No protein complexation was seen at pH 2, where PGA

miktoarm blocks contained completely protonated carboxylic acid groups. Complexation at pH 7.4 depended heavily on polymer topology as well as the polymer/protein ratio. At ratios of >1, complete complexation was seen for the linear AB polymers, whereas a ratio higher than 2.5 was needed for AB_3 miktoarm stars, with the same hydrophilic/hydrophobic ratio. Interestingly, lysozyme complexation in AB_3 miktoarm stars containing B blocks, each being the same MW as the B block in the linear copolymer, showed only marginal improvement. Based on tryptophan fluorescence, it was found that no detectable protein unfolding occurred when bound to the polymers, and so, lysozyme's structural conformation was conserved. Despite this, lower enzymatic activity was observed for bound lysozyme, with a more noticeable decrease in lytic activity at higher polymer/protein ratios. When assessed using *Micrococcus lisodeikticus*, the lysozyme showed decreased cleavage of *N*-acetylmuramic acid and *N*-acetylglucosamine in cell walls, due to obstructed access of substrates to its active site.

AB_3 (A = PEG, B = PGA) miktoarm polymers have also been prepared for the pulmonary delivery of complexed lysozyme as a dry powder.[68, 76] The miktoarm star/lysozyme nanocomplexes were synthesized at a molar charge ratio of 2.5, with mannitol, trehalose, and leucine as aerosol excipients. Fine particle fractions of up to 68% were seen for powders consisting of the polyplexes with trehalose and leucine. Trehalose was used as a bulk agent in formulating the dry powders, which aided in stabilizing the 3D protein structure of lysozyme through the formation of hydrogen bonds. Leucine functioned as a dispersion enhancer, which was essential in forming powders with spherical morphology and an average diameter of 2.5 μm, which is ideal for inhalation. The complexes were found to be well incorporated into dry powders with encapsulation efficiencies between 80 and 100%, while retaining enzymatic activity. Additionally, conjugation of vitamin B_{12}, cobalamin, to PEG termini via CuAAC click coupling, allowed targeting of B_{12}-receptors in epithelial cells containing the vitamin B_{12}-internalization receptor (CD320), *in vitro* and *in vivo*.[76] This significantly increased the cellular internalization of miktoarm star/lysozyme complexes compared to those without conjugated B12. Using the Calu-3 epithelial cell model, it was further established that the topology of miktoarm star polyplexes resulted in greater lysozyme internalization compared to linear complexes, despite a slightly stronger immunogenic response. Dry powders that incorporated the polymer/protein polyplexes showed non-homogenous dispersion in mouse lungs, yet deposition data showed that delivered lysozyme was present in the lungs 14 hours after administration, in contrast to the B_{12}-lacking non-targeting polyplexes.

Although not a strict example of polyplex-based delivery, a system composed of cationic bis-hydrophilic AB_4 miktoarm stars (A = PEG, B = quaternized poly(2-(dimethylamino)ethyl methacrylate) (qPDMAEMA)) was combined with anionic poly(styrenesulfonate) to form stable polymersomes with inter-polyelectrolyte complexes.[64] Their hydrophilic interiors allowed the encapsulation of rhodamine B, a cationic dye molecule, and as a result of the polymersomes' polyelectrolyte complexes, there was no obvious leakage of rhodamine B from their cores, but when dialyzed against a 2M NaCl solution, complete release was seen in 5 hours. These polymersomes were used to construct multilayered microcapsules by the sequential adsorption of tannic acid and polymersome layers, on the surface of bare negatively charged silica nanoparticles, followed by silica core dissolution. PEG chains were able to strongly interact with tannic acid layers because of hydrogen bonding. A change of pH from 5 to 9 resulted in a microcapsule size change from 4.51 to 4.12 μm, which resulted in the opening of microcapsule pores (greater permeability) that could accommodate FITC-dextran in its shell at pH 5 (or below 7). Loading FITC-dextran in 8-layer microcapsule shells and subsequently switching the pH back to 9 resulted in the desorption of the dextran from the shell and its loading into the microcapsule cores. This way, both anionic FITC-dextran and cationic rhodamine B could be loaded in the microcapsule and polymersome interiors. These microcapsules could then be controlled to release either of their loaded cargoes through environmental changes in ionic strength or pH (Figure 1.13).

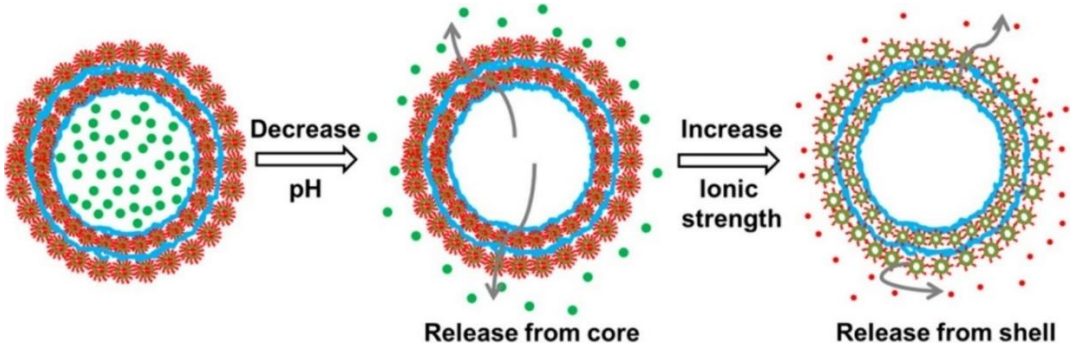

Figure 1.13. Independent release of anionic FITC-dextran and cationic rhodamine B from PEG-qPDMAEMA$_4$ micelle/tannic acid-derived microcapsule cores and shells. Reprinted with permission from reference 64. Copyright 2014 American Chemical Society.

1.5. Conclusions and Future Perspective

Miktoarm star polymers are beginning to make a significant contribution to advancing the scope of drug delivery using polymeric soft nanoparticles, due to their advantageous properties, compared to the traditionally employed, and most widely studied amphiphilic block copolymers.

Advances in the synthesis of miktoarm stars using high yield methodologies has facilitated designing formulations with better therapeutic outcomes. Methods including arm-first and core-first were initially explored for their syntheses, and were centered around either coupling/grafting pre-synthesized polymeric segments onto a central core, or direct polymerization from a heteromultifunctional core, respectively. These methods individually suffer from drawbacks such as sterically induced incomplete grafting in arm-first methods, and difficulty in core initiator preparation as well as polymerization control in core-first methods. Generally, it is best suited to combine these to tailor the overall composition of miktoarm star polymers. One of the most commonly used hydrophilic components in miktoarm stars is poly(ethylene glycol), which is commercially available in varied molecular weights, can be easily functionalized at its ends, and can be covalently linked to core molecules using highly efficient stitching methodologies, including click chemistry and condensation coupling. In-out synthesis, while a viable approach to the construction of miktoarm stars, has not been largely explored in delivering active agents, due to limitations of their self-assembled structures in drug loading in the densely packed cores.

Due in large part to their unique branching architecture, which can accommodate a variety of task-specific polymer segments, miktoarm star-based self-assemblies are formed at very low CMCs, and show high loading efficiencies, with a sustained drug release. Polymer arm tunability has permitted developing micellar formulations which could target specific organelles or cell receptors, or respond to a variety of autogenous stimuli. The ease with which branching stars can be synthetically articulated continues to offer a platform for the development of multi-stimuli-responsive systems that could deliver drugs with biological cues extra- and intracellularly. It is expected that researchers will continue to design miktoarm constructs possessing polymer segments, which upon self-assembly i) can switch between micellar cores and coronae, in response to a stimuli, and without structural collapse; ii) form wrinkled cores, resulting from immiscible core polymer blocks, and increase the number of binding pockets for drug cargo. Considering that noticeable progress has been made in the design and synthesis of miktoarm stars, our understanding of the structure-property relationships of their aqueous self-assembly should continue to be the next focus. This will certainly enhance our efficacy in pharmaceutical interventions in high morbidity rate diseases. Another area of growth is in theranostics, where miktoarm polymers are ideally suited to make a major contribution, due to the ease with which diverse functions, diagnostics, and delivery can be easily introduced *via* their structural build-up.

1.6. References

1. Loftsson, T.; Brewster, M. E., Pharmaceutical applications of cyclodextrins: basic science and product development. *J. Pharm. Pharmacol.* **2010,** *62* (11), 1607-1621.
2. Tran, S.; DeGiovanni, P.-J.; Piel, B.; Rai, P., Cancer nanomedicine: a review of recent success in drug delivery. *Clin. Transl. Med.* **2017,** *6* (1), 44.
3. Croy, S. R.; Kwon, G. S., Polymeric Micelles for Drug Delivery. *Curr. Pharm. Des.* **2006,** *12* (36), 4669-84.
4. Lu, Y.; Zhang, E.; Yang, J.; Cao, Z., Strategies to improve micelle stability for drug delivery. *Nano Res.* **2018,** *11* (10), 4985-4998.
5. Haag, R.; Kratz, F., Polymer Therapeutics: Concepts and Applications. *Angew. Chem. Int.l Ed.* **2006,** *45* (8), 1198-1215.
6. Li, J.; Mooney, D. J., Designing hydrogels for controlled drug delivery. *Nat. Rev. Mater.* **2016,** *1* (12), 16071.
7. Kim, S.; Shi, Y.; Kim, J. Y.; Park, K.; Cheng, J.-X., Overcoming the barriers in micellar drug delivery: loading efficiency, in vivo stability, and micelle–cell interaction. *Expert Opin. Drug Del.* **2010,** *7* (1), 49-62.
8. Kaditi, E.; Mountrichas, G.; Pispas, S.; Demetzos, C., Block Copolymers for Drug Delivery Nano Systems (DDnSs). *Curr. Med. Chem.* **2012,** *19* (29), 5088-5100.
9. Gaucher, G.; Dufresne, M.-H.; Sant, V. P.; Kang, N.; Maysinger, D.; Leroux, J.-C., Block copolymer micelles: preparation, characterization and application in drug delivery. *J. Control. Release* **2005,** *109* (1), 169-188.
10. Mirza, A. Z.; Siddiqui, F. A., Nanomedicine and drug delivery: a mini review. *International Nano Lett.* **2014,** *4* (1), 94.
11. Farokhzad, O. C.; Langer, R., Nanomedicine: Developing smarter therapeutic and diagnostic modalities. *Adv. Drug Del. Rev.* **2006,** *58* (14), 1456-1459.
12. Moghimi, S. M.; Hunter, A. C.; Murray, J. C., Long-Circulating and Target-Specific Nanoparticles: Theory to Practice. *Pharmacol. Rev.* **2001,** *53* (2), 283.
13. Allen, C.; Maysinger, D.; Eisenberg, A., Nano-engineering block copolymer aggregates for drug delivery. *Colloids Surf. B* **1999,** *16* (1), 3-27.
14. Yoshida, E., Control of Micellar Size and Critical Micelle Concentration for "Nonamphiphilic" Poly(vinyl phenol)-block-Polystyrene Diblock Copolymers. *Polym. J.* **2003,** *35* (12), 965-971.
15. Lo, C.-L.; Lin, S.-J.; Tsai, H.-C.; Chan, W.-H.; Tsai, C.-H.; Cheng, C.-H. D.; Hsiue, G.-H., Mixed micelle systems formed from critical micelle concentration and temperature-sensitive diblock copolymers for doxorubicin delivery. *Biomaterials* **2009,** *30* (23), 3961-3970.
16. Kosa, S. A.; Al-Harbi, L. M.; Baloch, M. K.; Ullah, I.; El-Mossalamy, E. H., Impact of Block Length and Temperature over Self-Assembling Behavior of Block Copolymers. *Int. J. Polym. Sci.* **2016,** *2016*, 7.
17. Kulthe, S. S.; Choudhari, Y. M.; Inamdar, N. N.; Mourya, V., Polymeric micelles: authoritative aspects for drug delivery. *Des. Monomers Polym.* **2012,** *15* (5), 465-521.
18. Hadjichristidis, N., Synthesis of miktoarm star (μ-star) polymers. *J. Polym. Sci. Part A: Polym. Chem.* **1999,** *37* (7), 857-871.
19. Hadjichristidis, N.; Iatrou, H.; Pitsikalis, M.; Mays, J., Macromolecular architectures by living and controlled/living polymerizations. *Prog. Polym. Sci.* **2006,** *31* (12), 1068-1132.
20. Sharma, A.; Kakkar, A., Designing Dendrimer and Miktoarm Polymer Based Multi-Tasking Nanocarriers for Efficient Medical Therapy. *Molecules* **2015,** *20* (9), 16987-17015.

21. Khanna, K.; Varshney, S.; Kakkar, A., Miktoarm star polymers: advances in synthesis, self-assembly, and applications. *Polym. Chem.* **2010,** *1* (8), 1171-1185.
22. Pispas, S.; Hadjichristidis, N.; Potemkin, I.; Khokhlov, A., Effect of Architecture on the Micellization Properties of Block Copolymers: A2B Miktoarm Stars vs AB Diblocks. *Macromolecules* **2000,** *33* (5), 1741-1746.
23. Hadjichristidis, N.; Pitsikalis, M.; Iatrou, H.; Driva, P.; Sakellariou, G.; Chatzichristidi, M., 6.03 - Polymers with Star-Related Structures: Synthesis, Properties, and Applications. In *Polymer Science: A Comprehensive Reference*, Matyjaszewski, K.; Möller, M., Eds. Elsevier: Amsterdam, 2012; pp 29-111.
24. Soliman, G. M.; Sharma, R.; Choi, A. O.; Varshney, S. K.; Winnik, F. M.; Kakkar, A. K.; Maysinger, D., Tailoring the efficacy of nimodipine drug delivery using nanocarriers based on A2B miktoarm star polymers. *Biomaterials* **2010,** *31* (32), 8382-8392.
25. Wais, U.; Liu, J.; He, T.; Zhang, H., CHAPTER 5 Micellar and Emulsion-Assisted Drug Delivery: Comparison of Miktoarm Star Polymers and Block Copolymers. In *Miktoarm Star Polymers: From Basics of Branched Architecture to Synthesis, Self-assembly and Applications*, The Royal Society of Chemistry: 2017; pp 116-149.
26. Aghajanzadeh, M.; Zamani, M.; Rostamizadeh, K.; Sharafi, A.; Danafar, H., The role of miktoarm star copolymers in drug delivery systems. *J. Macromol. Sci. Part A* **2018,** *55* (7), 559-571.
27. Li, Y.-Y.; Zhang, X.-Z.; Cheng, H.; Kim, G.-C.; Cheng, S.-X.; Zhuo, R.-X., Novel Stimuli-Responsive Micelle Self-Assembled from Y-Shaped P(UA-Y-NIPAAm) Copolymer for Drug Delivery. *Biomacromolecules* **2006,** *7* (11), 2956-2960.
28. Butsele, K. V.; Fustin, C. A.; Gohy, J. F.; Jérôme, R.; Jérôme, C., Self-Assembly and pH-Responsiveness of ABC Miktoarm Star Terpolymers. *Langmuir* **2009,** *25* (1), 107-111.
29. Cajot, S.; Van Butsele, K.; Paillard, A.; Passirani, C.; Garcion, E.; Benoit, J. P.; Varshney, S. K.; Jérôme, C., Smart nanocarriers for pH-triggered targeting and release of hydrophobic drugs. *Acta Biomater.* **2012,** *8* (12), 4215-4223.
30. Butsele, K. V.; Stoffelbach, F.; Jérôme, R.; Jérôme, C., Synthesis of Novel Amphiphilic and pH-Sensitive ABC Miktoarm Star Terpolymers. *Macromolecules* **2006,** *39* (17), 5652-5656.
31. Wei, H.; Zhang, X.; Cheng, C.; Cheng, S.-X.; Zhuo, R.-X., Self-assembled, thermosensitive micelles of a star block copolymer based on PMMA and PNIPAAm for controlled drug delivery. *Biomaterials* **2007,** *28* (1), 99-107.
32. Zhang, H.-H.; Huang, Z.-Q.; Sun, B.-W.; Guo, J.-X.; Wang, J.-L.; Chen, Y.-Q., Y-shaped poly(ethylene glycol) and poly(trimethylene carbonate) amphiphilic copolymer: Synthesis and for drug delivery. *J. Polym. Sci. Part A: Polym. Chem.* **2008,** *46* (24), 8131-8140.
33. Gou, P.-F.; Zhu, W.-P.; Xu, N.; Shen, Z.-Q., Synthesis, self-assembly and drug-loading capacity of well-defined drug-conjugated amphiphilic A2B2 type miktoarm star copolymers based on poly(ε-caprolactone) and poly(ethylene glycol). *J. Polym. Sci. Part A: Polym. Chem.* **2009,** *47* (24), 6962-6976.
34. Yin, H.; Kang, S.-W.; Bae, Y. H., Polymersome Formation from AB2 Type 3-Miktoarm Star Copolymers. *Macromolecules* **2009,** *42* (19), 7456-7464.
35. Nederberg, F.; Appel, E.; Tan, J. P. K.; Kim, S. H.; Fukushima, K.; Sly, J.; Miller, R. D.; Waymouth, R. M.; Yang, Y. Y.; Hedrick, J. L., Simple Approach to Stabilized Micelles Employing Miktoarm Terpolymers and Stereocomplexes with Application in Paclitaxel Delivery. *Biomacromolecules* **2009,** *10* (6), 1460-1468.

36. Gou, P.-F.; Zhu, W.-P.; Shen, Z.-Q., Synthesis, Self-Assembly, and Drug-Loading Capacity of Well-Defined Cyclodextrin-Centered Drug-Conjugated Amphiphilic A14B7 Miktoarm Star Copolymers Based on Poly(ε-caprolactone) and Poly(ethylene glycol). *Biomacromolecules* **2010,** *11* (4), 934-943.
37. Zhang, X.; Cheng, J.; Wang, Q.; Zhong, Z.; Zhuo, R., Miktoarm Copolymers Bearing One Poly(ethylene glycol) Chain and Several Poly(ε-caprolactone) Chains on a Hyperbranched Polyglycerol Core. *Macromolecules* **2010,** *43* (16), 6671-6677.
38. Li, L.-Y.; He, W.-D.; Li, J.; Zhang, B.-Y.; Pan, T.-T.; Sun, X.-L.; Ding, Z.-L., Shell-Cross-Linked Micelles from PNIPAM-b-(PLL)2 Y-Shaped Miktoarm Star Copolymer as Drug Carriers. *Biomacromolecules* **2010,** *11* (7), 1882-1890.
39. Khanna, K.; Varshney, S.; Kakkar, A., Designing Miktoarm Polymers Using a Combination of "Click" Reactions in Sequence with Ring-Opening Polymerization. *Macromolecules* **2010,** *43* (13), 5688-5698.
40. Maglio, G.; Nicodemi, F.; Conte, C.; Palumbo, R.; Tirino, P.; Panza, E.; Ianaro, A.; Ungaro, F.; Quaglia, F., Nanocapsules Based on Linear and Y-Shaped 3-Miktoarm Star-Block PEO-PCL Copolymers as Sustained Delivery System for Hydrophilic Molecules. *Biomacromolecules* **2011,** *12* (12), 4221-4229.
41. Sharma, A.; Khatchadourian, A.; Khanna, K.; Sharma, R.; Kakkar, A.; Maysinger, D., Multivalent niacin nanoconjugates for delivery to cytoplasmic lipid droplets. *Biomaterials* **2011,** *32* (5), 1419-1429.
42. Sharma, A.; Soliman, G. M.; Al-Hajaj, N.; Sharma, R.; Maysinger, D.; Kakkar, A., Design and Evaluation of Multifunctional Nanocarriers for Selective Delivery of Coenzyme Q10 to Mitochondria. *Biomacromolecules* **2012,** *13* (1), 239-252.
43. Yin, H.; Kang, H. C.; Huh, K. M.; Bae, Y. H., Biocompatible, pH-sensitive AB2 miktoarm polymer-based polymersomes: preparation, characterization, and acidic pH-activated nanostructural transformation. *J. Mater. Chem.* **2012,** *22* (36), 19168-19178.
44. Yin, H.; Kang, H. C.; Huh, K. M.; Bae, Y. H., Effects of cholesterol incorporation on the physicochemical, colloidal, and biological characteristics of pH-sensitive AB2 miktoarm polymer-based polymersomes. *Colloids Surf. B* **2014,** *116*, 128-137.
45. Liu, T.; Zhang, Y.-f.; Liu, S.-y., Drug and plasmid DNA co-delivery nanocarriers based on abctype polypeptide hybrid miktoarm star copolymers. *Chin. J. Polym. Sci.* **2013,** *31* (6), 924-937.
46. Blasco, E.; Schmidt, B. V. K. J.; Barner-Kowollik, C.; Piñol, M.; Oriol, L., Dual thermo- and photo-responsive micelles based on miktoarm star polymers. *Polym. Chem.* **2013,** *4* (16), 4506-4514.
47. Soliman, G. M.; Sharma, A.; Cui, Y.; Sharma, R.; Kakkar, A.; Maysinger, D., Miktoarm Star Micelles Containing Curcumin Reduce Cell Viability of Sensitized Glioblastoma. *J. Nanomed. Biother. Discovery* **2014,** *4* (2), 10.
48. Chu, Y.; Yu, H.; Zhang, Y.; Zhang, G.; Ma, Y.; Zhuo, R.; Jiang, X., Synthesis and characterization of biodegradable amphiphilic ABC Y-shaped miktoarm terpolymer by click chemistry for drug delivery. *J. Polym. Sci. Part A: Polym. Chem.* **2014,** *52* (23), 3346-3355.
49. Soliman, G. M.; Redon, R.; Sharma, A.; Mejía, D.; Maysinger, D.; Kakkar, A., Miktoarm Star Polymer Based Multifunctional Traceable Nanocarriers for Efficient Delivery of Poorly Water Soluble Pharmacological Agents. *Macromol. Biosci.* **2014,** *14* (9), 1312-1324.
50. Lin, W.; Nie, S.; Xiong, D.; Guo, X.; Wang, J.; Zhang, L., pH-responsive micelles based on (PCL)2(PDEA-b-PPEGMA)2 miktoarm polymer: controlled synthesis,

characterization, and application as anticancer drug carrier. *Nanoscale Res. Lett.* **2014,** *9* (1), 243.
51. Lin, W.; Nie, S.; Zhong, Q.; Yang, Y.; Cai, C.; Wang, J.; Zhang, L., Amphiphilic miktoarm star copolymer (PCL)3-(PDEAEMA-b-PPEGMA)3 as pH-sensitive micelles in the delivery of anticancer drug. *J. Mater. Chem. B* **2014,** *2* (25), 4008-4020.
52. Sui, B.; Xu, H.; Jin, J.; Gou, J.; Liu, J.; Tang, X.; Zhang, Y.; Xu, J.; Zhang, H.; Jin, X., Self-Assembled Micelles Composed of Doxorubicin Conjugated Y-Shaped PEG-Poly(glutamic acid)2 Copolymers via Hydrazone Linkers. *Molecules* **2014,** *19* (8), 11915-11932.
53. Blasco, E.; Schmidt, B. V. K. J.; Barner-Kowollik, C.; Piñol, M.; Oriol, L., A Novel Photoresponsive Azobenzene-Containing Miktoarm Star Polymer: Self-Assembly and Photoresponse Properties. *Macromolecules* **2014,** *47* (11), 3693-3700.
54. Yoon, K.; Kang, H. C.; Li, L.; Cho, H.; Park, M.-K.; Lee, E.; Bae, Y. H.; Huh, K. M., Amphiphilic poly(ethylene glycol)-poly(ε-caprolactone) AB2 miktoarm copolymers for self-assembled nanocarrier systems: synthesis, characterization, and effects of morphology on antitumor activity. *Polym. Chem.* **2015,** *6* (4), 531-542.
55. Moquin, A.; Sharma, A.; Cui, Y.; Lau, A.; Maysinger, D.; Kakkar, A., Asymmetric AB3 Miktoarm Star Polymers: Synthesis, Self-Assembly, and Study of Micelle Stability Using AF4 for Efficient Drug Delivery. *Macromol. Biosci.* **2015,** *15* (12), 1744-1754.
56. Alizadeh, R.; Ghaemy, M., pH-responsive ABC type miktoarm star terpolymers: Synthesis via combination of click reaction and SET-LRP, characterization, self-assembly, and controlled drug release. *Polymer* **2015,** *66*, 179-191.
57. Zhang, Y.; Chen, M.; Luo, X.; Zhang, H.; Liu, C.; Li, H.; Li, X., Tuning multiple arms for camptothecin and folate conjugations on star-shaped copolymers to enhance glutathione-mediated intracellular drug delivery. *Polym. Chem.* **2015,** *6* (12), 2192-2203.
58. Zhou, Q.-H.; Lin, J.; Li, L.-D.; Shang, L., Biodegradable micelles self-assembled from miktoarm star block copolymers for MTX delivery. *Colloid Polym. Sci.* **2015,** *293* (8), 2291-2300.
59. Zhu, M.-m.; Song, F.; Nie, W.-c.; Wang, X.-l.; Wang, Y.-z., A facile chemoenzymatic synthesis of amphiphilic miktoarm star copolymers from a sugar core and their potential for anticancer drug delivery. *Polymer* **2016,** *93*, 159-166.
60. Chen, Y.; Zhang, Y. X.; Wu, Z. F.; Peng, X. Y.; Su, T.; Cao, J.; He, B.; Li, S., Biodegradable poly(ethylene glycol)–poly(ε-carprolactone) polymeric micelles with different tailored topological amphiphilies for doxorubicin (DOX) drug delivery. *RSC Adv.* **2016,** *6* (63), 58160-58172.
61. Huang, J.; Liang, H.; Cheng, D.; Lu, J., Polypeptide–poly(ethylene glycol) miktoarm star copolymers with a fluorescently labeled core: synthesis, delivery and imaging of siRNA. *Polym. Chem.* **2016,** *7* (9), 1792-1802.
62. Huang, L.-m.; Li, L.-d.; Shang, L.; Zhou, Q.-h.; Lin, J., Preparation of pH-sensitive micelles from miktoarm star block copolymers by ATRP and their application as drug nanocarriers. *React. Funct. Polym.* **2016,** *107*, 28-34.
63. Mielańczyk, A.; Odrobińska, J.; Grządka, S.; Mielańczyk, Ł.; Neugebauer, D., Miktoarm star copolymers from D-(−)-salicin core aggregated into dandelion-like structures as anticancer drug delivery systems: synthesis, self-assembly and drug release. *Int. J. Pharm.* **2016,** *515* (1), 515-526.

64. Xu, W.; Steinschulte, A. A.; Plamper, F. A.; Korolovych, V. F.; Tsukruk, V. V., Hierarchical Assembly of Star Polymer Polymersomes into Responsive Multicompartmental Microcapsules. *Chem. Mater.* **2016,** *28* (3), 975-985.
65. Zhu, J.; Liu, Y.; Xiao, L.; Zhou, P., Temperature-Sensitive (BA)(AC)2 Miktoarm Star Diblock Copolymer Based on PMMA, PPEGMA, and PNIPAm. *Macromol. Chem. Phys.* **2016,** *217* (6), 773-782.
66. Huo, H.; Ma, X.; Dong, Y.; Qu, F., Light/temperature dual-responsive ABC miktoarm star terpolymer micelles for controlled release. *Eur. Polym. J.* **2017,** *87*, 331-343.
67. Nieto-Orellana, A.; Di Antonio, M.; Conte, C.; Falcone, F. H.; Bosquillon, C.; Childerhouse, N.; Mantovani, G.; Stolnik, S., Effect of polymer topology on non-covalent polymer–protein complexation: miktoarm versus linear mPEG-poly(glutamic acid) copolymers. *Polym. Chem.* **2017,** *8* (14), 2210-2220.
68. Nieto-Orellana, A.; Coghlan, D.; Rothery, M.; Falcone, F. H.; Bosquillon, C.; Childerhouse, N.; Mantovani, G.; Stolnik, S., Dry-powder formulations of non-covalent protein complexes with linear or miktoarm copolymers for pulmonary delivery. *Int. J. Pharm.* **2018,** *540* (1), 78-88.
69. Patil, Y.; Bilalis, P.; Polymeropoulos, G.; Almahdali, S.; Hadjichristidis, N.; Rodionov, V., A Novel Poly(vinylidene fluoride)-Based 4-Miktoarm Star Terpolymer: Synthesis and Self-Assembly. *Mol. Pharm.* **2018,** *15* (8), 3005-3009.
70. Wang, M.; Zhang, X.; Peng, H.; Zhang, M.; Zhang, X.; Liu, Z.; Ma, L.; Wei, H., Optimization of Amphiphilic Miktoarm Star Copolymers for Anticancer Drug Delivery. *ACS Biomater. Sci. Eng.* **2018,** *4* (8), 2903-2910.
71. Aghajanzadeh, M.; Zamani, M.; Rashidzadeh, H.; Rostamizadeh, K.; Sharafi, A.; Danafar, H., Amphiphilic Y shaped miktoarm star copolymer for anticancer hydrophobic and hydrophilic drugs codelivery: Synthesis, characterization, in vitro, and in vivo biocompatibility study. *J. Biomed. Mater. Res. Part A* **2018,** *106* (11), 2817-2826.
72. Ramesh, K.; Thangagiri, B.; Mishra, A. K.; Ahn, B.-H.; Gal, Y.-S.; Lim, K. T., AB2-type miktoarm poly(l-lactide)-b-poly(N-acryloylmorpholine) amphiphilic star block copolymers as nanocarriers for drug delivery. *React. Funct. Polym.* **2018,** *132*, 112-119.
73. Kim, Y.; Uthaman, S.; Nurunnabi, M.; Mallick, S.; Oh, K. S.; Kang, S.-W.; Cho, S.; Kang, H. C.; Lee, Y.-k.; Huh, K. M., Synthesis and characterization of bioreducible cationic biarm polymer for efficient gene delivery. *Int. J. Biol. Macromol.* **2018,** *110*, 366-374.
74. Saravanakumar, G.; Park, H.; Kim, J.; Park, D.; Pramanick, S.; Kim, D. H.; Kim, W. J., Miktoarm Amphiphilic Block Copolymer with Singlet Oxygen-Labile Stereospecific β-Aminoacrylate Junction: Synthesis, Self-Assembly, and Photodynamically Triggered Drug Release. *Biomacromolecules* **2018,** *19* (6), 2202-2213.
75. Chong, Y. K.; Zainol, I.; Ng, C. H.; Ooi, I. H., Miktoarm star polymers nanocarrier: synthesis, characterisation, and in-vitro drug release study. *J. Polym. Res.* **2019,** *26* (3), 79.
76. Nieto-Orellana, A.; Li, H.; Rosiere, R.; Wauthoz, N.; Williams, H.; Monteiro, C. J.; Bosquillon, C.; Childerhouse, N.; Keegan, G.; Coghlan, D.; Mantovani, G.; Stolnik, S., Targeted PEG-poly(glutamic acid) complexes for inhalation protein delivery to the lung. *J. Control. Release* **2019,** *316*, 250-262.
77. Sonawane, S. J.; Kalhapure, R. S.; Jadhav, M.; Rambharose, S.; Mocktar, C.; Govender, T., AB2-type amphiphilic block copolymer containing a pH-cleavable hydrazone linkage for targeted antibiotic delivery. *Int. J. Pharm.* **2020,** *575*, 118948.

78. Aghajanzadeh, M.; Andalib, S.; Danafar, H.; Rostamizadeh, K.; Sharafi, A., The effect of baicalein-loaded Y-shaped miktoarm copolymer on spatial memory and hippocampal expression of DHCR24, SELADIN and SIRT6 genes in rat model of Alzheimer. *Int. J. Pharm.* **2020,** *586*, 119546.
79. Tomalia, D. A.; Baker, H.; Dewald, J.; Hall, M.; Kallos, G.; Martin, S.; Roeck, J.; Ryder, J.; Smith, P., Dendritic macromolecules: synthesis of starburst dendrimers. *Macromolecules* **1986,** *19* (9), 2466-2468.
80. Hawker, C. J.; Frechet, J. M. J., Preparation of polymers with controlled molecular architecture. A new convergent approach to dendritic macromolecules. *J. Am. Chem. Soc.* **1990,** *112* (21), 7638-7647.
81. Meldal, M.; Tornøe, C. W., Cu-Catalyzed Azide−Alkyne Cycloaddition. *Chem. Rev.* **2008,** *108* (8), 2952-3015.
82. Hadjichristidis, N.; Fetters, L. J., Star-Branched Polymers. 4. Synthesis of 18-Arm Polyisoprenes. *Macromolecules* **1980,** *13* (1), 191-193.
83. Roovers, J.; Hadjichristidis, N.; Fetters, L. J., Analysis and dilute solution properties of 12- and 18-arm-star polystyrenes. *Macromolecules* **1983,** *16* (2), 214-220.
84. Alward, D. B.; Kinning, D. J.; Thomas, E. L.; Fetters, L. J., Effect of arm number and arm molecular weight on the solid-state morphology of poly(styrene-isoprene) star block copolymers. *Macromolecules* **1986,** *19* (1), 215-224.
85. Nguyen, A. B.; Hadjichristidis, N.; Fetters, L. J., Static light scattering study of high-molecular weight 18-arm star block copolymers. *Macromolecules* **1986,** *19* (3), 768-773.
86. Pennisi, R. W.; Fetters, L. J., Preparation of asymmetric 3-arm polybutadiene and polystyrene stars. *Macromolecules* **1988,** *21* (4), 1094-1099.
87. Bauer, B. J.; Fetters, L. J.; Graessley, W. W.; Hadjichristidis, N.; Quack, G. F., Chain dimensions in dilute polymer solutions: a light-scattering and viscometric study of multiarmed polyisoprene stars in good and .THETA. solvents. *Macromolecules* **1989,** *22* (5), 2337-2347.
88. Iatrou, H.; Hadjichristidis, N., Synthesis of a model 3-miktoarm star terpolymer. *Macromolecules* **1992,** *25* (18), 4649-4651.
89. Mays, J. W., Synthesis of "simple graft" poly(isoprene-g-styrene) by anionic polymerization. *Polym. Bull.* **1990,** *23* (3), 247-250.
90. Iatrou, H.; Hadjichristidis, N., Synthesis and characterization of model 4-miktoarm star co- and quaterpolymers. *Macromolecules* **1993,** *26* (10), 2479-2484.
91. Iatrou, H.; Siakali-Kioulafa, E.; Hadjichristidis, N.; Roovers, J.; Mays, J., Hydrodynamic properties of model 3-miktoarm star copolymers. *J. Polym. Sci. Part B: Polym. Phys.* **1995,** *33* (13), 1925-1932.
92. Pitsikalis, M.; Hadjichristidis, N., Model Mono-, Di-, and Tri-.omega.-Functionalized Three-Arm Star Polybutadienes. Synthesis and Association in Dilute Solutions by Membrane Osmometry and Static Light Scattering. *Macromolecules* **1995,** *28* (11), 3904-3910.
93. Allgaier, J.; Young, R. N.; Efstratiadis, V.; Hadjichristidis, N., Synthesis and Characterization of Polyisoprene/Polybutadiene A2B2 Star Copolymers. *Macromolecules* **1996,** *29* (5), 1794-1797.
94. Sioula, S.; Tselikas, Y.; Hadjichristidis, N., Synthesis of Model 3-Miktoarm Star Terpolymers of Styrene, Isoprene, and Methyl Methacrylate. *Macromolecules* **1997,** *30* (5), 1518-1520.

95. Zioga, A.; Sioula, S.; Hadjichristidis, N., Synthesis and morphology of model 3-miktoarm star terpolymers of styrene, isoprene and 2-vinyl pyridine. *Macromol. Symp.* **2000,** *157* (1), 239-250.
96. Bellas, V.; Iatrou, H.; Hadjichristidis, N., Controlled Anionic Polymerization of Hexamethylcyclotrisiloxane. Model Linear and Miktoarm Star Co- and Terpolymers of Dimethylsiloxane with Styrene and Isoprene. *Macromolecules* **2000,** *33* (19), 6993-6997.
97. Tsoukatos, T.; Hadjichristidis, N., Synthesis of model polycyclohexylene/polyethylene miktoarm star copolymers with three and four arms. *J. Polym. Sci. Part A: Polym. Chem.* **2002,** *40* (15), 2575-2582.
98. Mavroudis, A.; Avgeropoulos, A.; Hadjichristidis, N.; Thomas, E. L.; Lohse, D. J., Synthesis and Morphological Behavior of Model Linear and Miktoarm Star Copolymers of 2-Methyl-1,3-Pentadiene and Styrene. *Chem. Mater.* **2003,** *15* (10), 1976-1983.
99. Avgeropoulos, A.; Poulos, Y.; Hadjichristidis, N.; Roovers, J., Synthesis of Model 16-Miktoarm (Vergina) Star Copolymers of the A8B8 Type. *Macromolecules* **1996,** *29* (18), 6076-6078.
100. Mavroudis, A.; Avgeropoulos, A.; Hadjichristidis, N.; Thomas, E. L.; Lohse, D. J., Synthesis and Morphological Behavior of Model 6-Miktoarm Star Copolymers, PS(P2MP)5, of Styrene (S) and 2-Methyl-1,3-Pentadiene (P2MP). *Chem. Mater.* **2006,** *18* (8), 2164-2168.
101. Tunca, U.; Ozyurek, Z.; Erdogan, T.; Hizal, G., Novel miktofunctional initiator for the preparation of an ABC-type miktoarm star polymer via a combination of controlled polymerization techniques. *J. Polym. Sci. Part A: Polym. Chem.* **2004,** *42* (17), 4228-4236.
102. Chado, G. R.; Holland, E. N.; Tice, A. K.; Stoykovich, M. P.; Kaar, J. L., Modification of Lipase with Poly(4-acryloylmorpholine) Enhances Solubility and Transesterification Activity in Anhydrous Ionic Liquids. *Biomacromolecules* **2018,** *19* (4), 1324-1332.
103. Xu, F.; Li, H.; Luo, Y.-L.; Tang, W., Redox-Responsive Self-Assembly Micelles from Poly(N-acryloylmorpholine-block-2-acryloyloxyethyl ferrocenecarboxylate) Amphiphilic Block Copolymers as Drug Release Carriers. *ACS Appl. Mater. Interfaces* **2017,** *9* (6), 5181-5192.
104. Neises, B.; Steglich, W., Simple Method for the Esterification of Carboxylic Acids. *Angew. Chem. Int. Ed.* **1978,** *17* (7), 522-524.
105. Rostovtsev, V. V.; Green, L. G.; Fokin, V. V.; Sharpless, K. B., A Stepwise Huisgen Cycloaddition Process: Copper(I)-Catalyzed Regioselective "Ligation" of Azides and Terminal Alkynes. *Angew. Chem. Int. Ed.* **2002,** *41* (14), 2596-2599.
106. Yuan, Y.-Y.; Wang, Y.-C.; Du, J.-Z.; Wang, J., Synthesis of Amphiphilic ABC 3-Miktoarm Star Terpolymer by Combination of Ring-Opening Polymerization and "Click" Chemistry. *Macromolecules* **2008,** *41* (22), 8620-8625.
107. Zhang, Y.; Liu, H.; Hu, J.; Li, C.; Liu, S., Synthesis and Aggregation Behavior of Multi-Responsive Double Hydrophilic ABC Miktoarm Star Terpolymer. *Macromol. Rapid Commun.* **2009,** *30* (11), 941-947.
108. Ishizu, K.; Kuwahara, K., Synthesis of heteroarm star copolymers by anionic copolymerization of binary macromonomers. *Polymer* **1994,** *35* (22), 4907-4913.
109. Du, J.; Chen, Y., PCL Star Polymer, PCL-PS Heteroarm Star Polymer by ATRP, and Core-Carboxylated PS Star Polymer Thereof. *Macromolecules* **2004,** *37* (10), 3588-3594.
110. Gao, H.; Tsarevsky, N. V.; Matyjaszewski, K., Synthesis of Degradable Miktoarm Star Copolymers via Atom Transfer Radical Polymerization. *Macromolecules* **2005,** *38* (14), 5995-6004.

111. Zhang, D.; Fourie-O'Donohue, A.; Dragovich, P. S.; Pillow, T. H.; Sadowsky, J. D.; Kozak, K. R.; Cass, R. T.; Liu, L.; Deng, Y.; Liu, Y.; Hop, C. E.; Khojasteh, S. C., Catalytic cleavage of disulfide bonds in small molecules and linkers of antibody- drug conjugates. *Drug Metab. Dispos.* **2019**, dmd.118.086132.
112. Chen, D.; Zhang, G.; Li, R.; Guan, M.; Wang, X.; Zou, T.; Zhang, Y.; Wang, C.; Shu, C.; Hong, H.; Wan, L.-J., Biodegradable, Hydrogen Peroxide, and Glutathione Dual Responsive Nanoparticles for Potential Programmable Paclitaxel Release. *J. Am. Chem. Soc.* **2018,** *140* (24), 7373-7376.
113. Luo, C.; Sun, J.; Liu, D.; Sun, B.; Miao, L.; Musetti, S.; Li, J.; Han, X.; Du, Y.; Li, L.; Huang, L.; He, Z., Self-Assembled Redox Dual-Responsive Prodrug-Nanosystem Formed by Single Thioether-Bridged Paclitaxel-Fatty Acid Conjugate for Cancer Chemotherapy. *Nano Lett.* **2016,** *16* (9), 5401-5408.
114. Wiltshire, J. T.; Qiao, G. G., Selectively Degradable Core Cross-Linked Star Polymers. *Macromolecules* **2006,** *39* (26), 9018-9027.
115. Levi, A. E.; Fu, L.; Lequieu, J.; Horne, J. D.; Blankenship, J.; Mukherjee, S.; Zhang, T.; Fredrickson, G. H.; Gutekunst, W. R.; Bates, C. M., Efficient Synthesis of Asymmetric Miktoarm Star Polymers. *Macromolecules* **2020,** *53* (2), 702-710.
116. Li, H.; Yang, D.; Gao, Y.; Li, H.; Xu, J., Dual responsive macroemulsion stabilized by Y-shaped amphiphilic AB2 miktoarm star copolymers. *RSC Adv.* **2015,** *5* (117), 96377-96386.
117. Englert, C.; Brendel, J. C.; Majdanski, T. C.; Yildirim, T.; Schubert, S.; Gottschaldt, M.; Windhab, N.; Schubert, U. S., Pharmapolymers in the 21st century: Synthetic polymers in drug delivery applications. *Prog. Polym. Sci.* **2018,** *87*, 107-164.
118. Brown, R. A.; Masters, A. J.; Price, C.; Yuan, X. F., 6 - Chain Segregation in Block Copolymers. In *Comprehensive Polymer Science and Supplements*, Allen, G.; Bevington, J. C., Eds. Pergamon: Amsterdam, 1989; pp 155-198.
119. Ryan, A. J.; Mai, S.-M.; Fairclough, J. P. A.; Hamley, I. W., Structures of amphiphilic block copolymers in their liquid and solid states. In *Amphiphilic Block Copolymers*, Alexandridis, P.; Lindman, B., Eds. Elsevier Science B.V.: Amsterdam, 2000; pp 151-167.
120. Discher, D. E.; Ahmed, F., POLYMERSOMES. *Annu. Rev. Biomed. Eng.* **2006,** *8* (1), 323-341.
121. Kedracki, D.; Abraham, J. N.; Prado, E.; Nardin, C., Self-Assembly of Biohybrid Polymers. In *Macromolecular Self-assembly*, 2016; pp 193-229.
122. Kakkar, A.; Traverso, G.; Farokhzad, O. C.; Weissleder, R.; Langer, R., Evolution of macromolecular complexity in drug delivery systems. *Nat. Rev. Chem.* **2017,** *1* (8), 63.
123. Oliver, R. C.; Lipfert, J.; Fox, D. A.; Lo, R. H.; Doniach, S.; Columbus, L., Dependence of Micelle Size and Shape on Detergent Alkyl Chain Length and Head Group. *PLoS One* **2013,** *8* (5), e62488.
124. Breyton, C.; Gabel, F.; Abla, M.; Pierre, Y.; Lebaupain, F.; Durand, G.; Popot, J.-L.; Ebel, C.; Pucci, B., Micellar and biochemical properties of (hemi)fluorinated surfactants are controlled by the size of the polar head. *Biophys. J.* **2009,** *97* (4), 1077-1086.
125. Wei, H.; Zhang, X.-Z.; Zhou, Y.; Cheng, S.-X.; Zhuo, R.-X., Self-assembled thermoresponsive micelles of poly(N-isopropylacrylamide-b-methyl methacrylate). *Biomaterials* **2006,** *27* (9), 2028-2034.
126. Gou, J.; Feng, S.; Xu, H.; Fang, G.; Chao, Y.; Zhang, Y.; Xu, H.; Tang, X., Decreased Core Crystallinity Facilitated Drug Loading in Polymeric Micelles without Affecting Their Biological Performances. *Biomacromolecules* **2015,** *16* (9), 2920-2929.

127. Aliabadi, H. M.; Lavasanifar, A., Polymeric micelles for drug delivery. *Expert Opin. Drug Del.* **2006,** *3* (1), 139-162.
128. Chakraborty, T.; Chakraborty, I.; Ghosh, S., The methods of determination of critical micellar concentrations of the amphiphilic systems in aqueous medium. *Arab. J. Chem.* **2011,** *4* (3), 265-270.
129. Liu, R.; Forrest, M. L.; Kwon, G. S.; Zhihong, X. X., Polymeric Micelles in Water-Insoluble Drug Delivery. In *Water-insoluble drug formulation*, 3 ed.; Liu, R., Ed. CRC Press: Boca Raton, FL, 2008.
130. Huang, X.; Xiao, Y.; Lang, M., Synthesis and self-assembly behavior of six-armed block copolymers with pH- and thermo-responsive properties. *Macromol. Res.* **2011,** *19* (2), 113-121.
131. Chen, L.-J.; Lin, S.-Y.; Huang, C.-C., Effect of Hydrophobic Chain Length of Surfactants on Enthalpy−Entropy Compensation of Micellization. *J. Phys. Chem. B* **1998,** *102* (22), 4350-4356.
132. Zhao, S.; Yang, H.; Zuo, C.; Sun, L.; Ma, L.; Wei, H., pH-sensitive drug release of star-shaped micelles with OEG brush corona. *RSC Adv.* **2016,** *6* (112), 111217-111225.
133. Soppimath, K. S.; Tan, D. C.-W.; Yang, Y.-Y., pH-Triggered Thermally Responsive Polymer Core–Shell Nanoparticles for Drug Delivery. *Adv. Mater.* **2005,** *17* (3), 318-323.
134. Li, H.; Diao, M.; Zhang, S.; Wang, K.; Xue, C., Novel Polymeric Micelles of AB2 Type α-Methoxy-Poly(ethylene glycol)-b-Poly(γ-benzyl-L-glutamate)2 Copolymers as Tamoxifen Carriers. *J. Nanosci. Nanotechnol.* **2009,** *9* (8), 4805-4811.
135. Zhu, Y.-J.; Chen, F., pH-Responsive Drug-Delivery Systems. *Chem. Asian J.* **2015,** *10* (2), 284-305.
136. Karimi, M.; Sahandi Zangabad, P.; Ghasemi, A.; Amiri, M.; Bahrami, M.; Malekzad, H.; Ghahramanzadeh Asl, H.; Mahdieh, Z.; Bozorgomid, M.; Ghasemi, A.; Rahmani Taji Boyuk, M. R.; Hamblin, M. R., Temperature-Responsive Smart Nanocarriers for Delivery Of Therapeutic Agents: Applications and Recent Advances. *ACS Appl. Mater. Interfaces* **2016,** *8* (33), 21107-21133.
137. Ye, H.; Zhou, Y.; Liu, X.; Chen, Y.; Duan, S.; Zhu, R.; Liu, Y.; Yin, L., Recent Advances on Reactive Oxygen Species-Responsive Delivery and Diagnosis System. *Biomacromolecules* **2019,** *20* (7), 2441-2463.
138. Burhans, W. C.; Heintz, N. H., The cell cycle is a redox cycle: Linking phase-specific targets to cell fate. *Free Radic. Biol. Med.* **2009,** *47* (9), 1282-1293.
139. Ballatori, N.; Krance, S. M.; Notenboom, S.; Shi, S.; Tieu, K.; Hammond, C. L., Glutathione dysregulation and the etiology and progression of human diseases. *Biol. Chem.* **2009,** *390* (3), 191-214.
140. Balendiran, G. K.; Dabur, R.; Fraser, D., The role of glutathione in cancer. *Cell Biochem. Funct.* **2004,** *22* (6), 343-352.
141. Quinn, J. F.; Whittaker, M. R.; Davis, T. P., Glutathione responsive polymers and their application in drug delivery systems. *Polym. Chem.* **2017,** *8* (1), 97-126.
142. Wang, X.; Liu, L.; Luo, Y.; Shi, H.; Li, J.; Zhao, H., Comb-Shaped Glycopolymer/Peptide Bioconjugates by Combination of RAFT Polymerization and Thiol-Ene "Click" Chemistry. *Macromol. Biosci.* **2012,** *12* (11), 1575-1582.
143. Linsley, C. S.; Wu, B. M., Recent advances in light-responsive on-demand drug-delivery systems. *Ther. Deliv.* **2017,** *8* (2), 89-107.
144. Zhou, Y.; Ye, H.; Chen, Y.; Zhu, R.; Yin, L., Photoresponsive Drug/Gene Delivery Systems. *Biomacromolecules* **2018,** *19* (6), 1840-1857.

145. Wei, H.; Cheng, S.-X.; Zhang, X.-Z.; Zhuo, R.-X., Thermo-sensitive polymeric micelles based on poly(N-isopropylacrylamide) as drug carriers. *Prog. Polym. Sci.* **2009,** *34* (9), 893-910.
146. Corrie, J. E.; Barth, A.; Munasinghe, V. R.; Trentham, D. R.; Hutter, M. C., Photolytic cleavage of 1-(2-nitrophenyl)ethyl ethers involves two parallel pathways and product release is rate-limited by decomposition of a common hemiacetal intermediate. *J. Am. Chem. Soc.* **2003,** *125* (28), 8546-54.
147. Gaplovsky, M.; Il'ichev, Y. V.; Kamdzhilov, Y.; Kombarova, S. V.; Mac, M.; Schwörer, M. A.; Wirz, J., Photochemical reaction mechanisms of 2-nitrobenzyl compounds: 2-Nitrobenzyl alcohols form 2-nitroso hydrates by dual proton transfer. *Photochem. Photobiol. Sci.* **2005,** *4* (1), 33-42.
148. Zhang, S.; Xu, Y.; Wang, B.; Qiao, W.; Liu, D.; Li, Z., Cationic compounds used in lipoplexes and polyplexes for gene delivery. *J. Control. Release* **2004,** *100* (2), 165-180.
149. Blencowe, A.; Tan, J. F.; Goh, T. K.; Qiao, G. G., Core cross-linked star polymers via controlled radical polymerisation. *Polymer* **2009,** *50* (1), 5-32.

Chapter 2: Miktoarm star polymers with environment-selective ROS/GSH responsive locations: From modular synthesis to tuned drug release through micellar partial corona shedding and/or core disassembly

Abstract

Branched architectures with asymmetric polymeric arms, provide an advantageous platform for the construction of tailored nanocarriers for therapeutic interventions. We have developed simple and adaptable synthetic methodologies to amphiphilic miktoarm star polymers in which spatial location of reactive oxygen species (ROS) and glutathione (GSH) responsive entities, is articulated to be on the corona shell surface or inside the core. The design of such architectures is facilitated through versatile building blocks and selected combinations of ring-opening polymerization, Steglich esterification and alkyne-azide click reactions. Soft nanoparticles from aqueous self-assembly of these stimuli responsive miktoarm stars, have low critical micelle concentrations and high drug loading efficiencies. Partial corona shedding upon response to ROS is accompanied by an increase in drug release, without significant changes to overall micelle morphology. The location of the GSH responsive unit plays an important role in drug release and micelle disassembly. Curcumin loaded soft nanoparticles show higher efficiencies in preventing ROS generation in extracellular and cellular environments and in ROS scavenging in human glioblastoma cells. The ease in synthetic elaboration and an understanding of structure-property relationships in stimuli responsive nanoparticles offers a facile venue for well-controlled drug delivery based on the extra- and intracellular concentrations of ROS and GSH.

2.1 Introduction

Despite achievements in drug design and discovery, progress in the delivery of biologically active compounds to desired sites has been relatively slow, and this has been attributed to their poor bioavailability.[1] Molecular modifications of bioactive agents to improve their solubility in aqueous media, however, has sometimes resulted in decreased biological activity.[2] Nanotechnological approaches have been applied instead to avoid chemical modifications and retain pharmacological effects of promising pharmaceutics. Different formulations which employ nanometer size vehicles to encapsulate drugs and retain them for a prolonged time period in blood circulation have been developed and have reduced cargo concentrations at unwanted locations.[1, 3-5] Macromolecule-based soft nanostructures have offered great potential and generally employ self-assembled

amphiphilic block co-polymers or lipids for delivery.[6, 7] Such soft nanoparticles often have PEGylated coronas and hydrophobic cores. Considering the sizes of the vasculature and tissue pores, micelles with diameters of less than 200 nm can markedly improve biological distribution due to the enhanced permeability and retention effect (EPR).[8]

Through a detailed evaluation of micelle-based formulations for drug delivery, it has been well documented that the overall structural composition and architecture of amphiphilic polymers play an important role in drug loading capacities and critical micelle concentrations (CMC). Introduction of soft nanoparticles to an aqueous biological environment subjects them to immense dilution, and the CMC is generally desired to be kept at or below 1 μM concentrations.[6] Asymmetric star polymers, frequently referred to as miktoarm star polymers, have provided an advantageous platform to address these issues.[9-14] The volume occupied by hydrophilic poly(ethylene glycol) (PEG) segments in soft nanoparticles from branched miktoarm star polymers can significantly exceed that of the nearby hydrophobic segment, compared to that in assemblies from conventional block co-polymers. This architectural disparity leads to smaller diameters, very low CMCs, and most importantly the ability to encapsulate large amounts of drug molecules.[9-12] In light of the significant opportunities provided by these branched architectures in a diverse range of applications, there has been tremendous effort devoted to developing novel strategies for their construction, which can lead to better control over their overall composition.[15-20] These synthetic articulations will also continue to strengthen designing miktoarm star-polymer based formulations with a desired combination of properties for efficient therapeutic interventions.[15, 21-26]

Some pathologies are associated with oxidative stress which occurs due to the excess of reactive oxygen species (ROS), including hydrogen peroxide (H_2O_2), superoxide (O_2^-), hydroxy radicals (·OH), and singlet oxygen ($^1O_2$) that is inadequately opposed by endogenous antioxidant defense. Oxidative stress-induced damage is one of the contributors to the slow biological deterioration in aging,[27] and a topical area of research in developing ROS-responsive nanocarriers.[28-31] The ROS concentration in the extracellular environment is significantly enhanced at affected diseased sites, and glutathione (GSH) is generally very highly concentrated intracellularly. We considered these differences for the development of a redox environment-selective drug delivery system.[32-36] As elaborated in Chapter 1, there are currently few examples of GSH-responsive miktoarm polymers, and no examples of general ROS-responsive miktoarm polymers. In addition, we were intrigued

to examine if soft nanoparticles in which ROS-sensitive thioketal (TK) moieties are incorporated into micellar coronas, could accommodate small changes in their morphology through *partial outer corona shedding* in response to extracellular concentrations of ROS, while enhancing drug release rates (Figure 2.1). While, there are reports of stimuli responsive systems in which complete micellar corona depletion has been used to enhance drug release, there are no such examples for partial depletion.[32, 33, 37] Using this design, our aim was to show that the overall micellar structure remains intact upon extracellular response to ROS, which will subsequently enter the cells, while subtly increasing drug release. Micellar-core containing disulfide (DS) linkers will then help deliver drug cargo at sites with high GSH concentrations, and will also enable micellar disassembly (Figure 2.1).[34, 38]

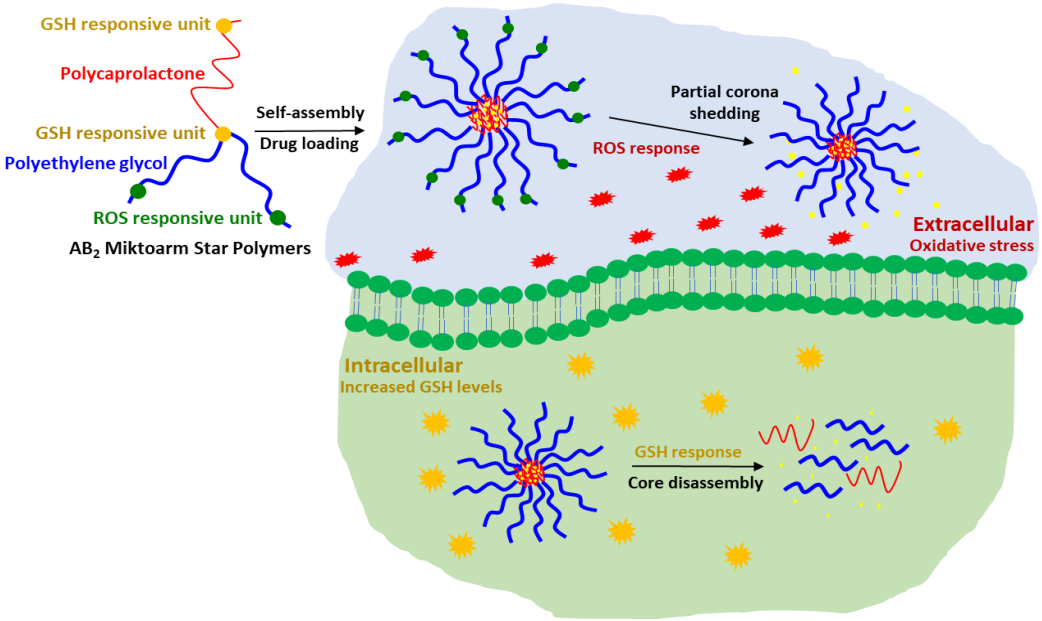

Figure 2.1. Tuned environment-selective ROS/GSH response and drug release using assemblies from AB_2 miktoarm star polymers.

Considering the role that ROS-induced oxidative damage plays in age-related diseases, senolytic agents have become an active area of research. We employed curcumin for drug loading and release studies, as it can be easily acquired and has been shown to extend the lifespan & increase the health of several model organisms.[39] While the exact mechanisms are not well understood, it is known that curcumin has a broad anti-inflammatory effect that involves down-regulating NF-κB gene products, thereby suppressing cytokines and TNF-α expression.[40, 41]

We report herein a facile mixed arm- and core-first methodology to a variety of AB_2 (A = polycaprolactone (PCL), B = PEG) type amphiphilic miktoarm star polymers with tailored spatial distribution of ROS and GSH responsive groups for extra- and intracellular response and drug delivery. Of the constituent polymeric arms for the branched structures, we chose polyethylene glycol (PEG) as the hydrophilic component since it has been widely used in drug delivery systems to confer aqueous solubility as well as stealth to the resulting micellar nanostructures.[42] Polycaprolactone (PCL), the hydrophobic polymeric arm, is biocompatible.[43, 44] We optimized the synthesis of AB_2 type miktoarm star polymers using a simple and modular synthetic methodology, which employed the desired building blocks with a combination of "stitching" (*via* Steglich esterification and the copper catalyzed alkyne-azide cycloaddition "click" (CuAAC) reaction) and ring-opening polymerization.[45-49] The ROS-responsive TK units were precisely incorporated near the outer terminal ends of the PEG arms, which will subsequently become micellar corona. GSH-responsive DS links were added to desirable sites within the polymeric architecture at i) the terminal end of the hydrophobic PCL chain, and ii) the focal junction where the PCL chain is covalently linked to the branched structure. A model diblock copolymer was also synthesized for direct comparison with the miktoarm star polymers. We demonstrate that self-assemblies from the branched architectures i) have very low CMCs and carry a high load of curcumin cargo; ii) shed their upper corona *partially* in response to oxidative stress; and iii) disassemble in response to GSH. In addition, the spatial location of DS units in the miktoarm star polymer assemblies plays an important role in drug release: the PCL chain-end located GSH responsive unit does not influence drug release profile, while the one covalently linking the PCL arm to the focal point of the polymer architecture, leads to a marked increase in drug release. Such micellar disassembly not only leads to rapid drug release directly at a targeted site, but additionally accelerates biodegradation of the separated PCL and PEG segments. Using CellROX® Deep Red, a fluorogenic probe for oxidative stress, we evaluated and confirmed the ROS scavenging behaviour of our drug delivery system in human glioblastoma cells.[50] Curcumin-loaded micelles containing only ROS-responsive moieties significantly decreased *in vitro* ROS production, and were more effective in scavenging ROS.

2.2 Materials and Methods

Poly(ethylene glycol) monomethyl ether 2000 was obtained from TCI Chemicals, tetraethylene glycol monomethyl ether and ε-caprolactone monomer from Acros Organics, Dulbecco's modified Eagle's media, penicillin-streptomycin, CellROX® Deep Red, and Hoechst 33342 nuclear dye from ThermoFisher Scientific, and all were used as received. Fetal bovine serum and U251N human glioblastoma cells were obtained from Wisent and the American Type Culture Collection respectively. All other chemicals and reagents used in this study were used as received from Sigma-Aldrich.

Nuclear magnetic resonance (NMR) spectra were variously acquired on Bruker AVIIIHD 400 and 500 MHz NMR Spectrometers, both equipped with BBFO+ SmartProbes, and a Varian Inova 500 MHz NMR Spectrometer equipped with a HCN probe. Mass spectrum determinations were conducted and analyzed on a Bruker MALDI Autoflex III-TOF and on an Exactive Plus Orbitrap-API (Thermo Scientific) high-resolution mass spectrometer. Dynamic light scattering (DLS) was performed on a Brookhaven 90Plus Particle Size Analyser equipped with a 40 mW red diode laser operating at 658 nm. TEM images were taken on a FEI Tecnai 12 BioTwin 120 kV TEM equipped with an AMT XR80 CCD Camera System located at the Facility for Electron Microscopy Research (FEMR) at McGill University. UV-Vis absorption spectra were taken on a Varian Cary 50 UV-Vis Spectrophotometer. Fluorescence spectra were collected on a Cary Eclipse Fluorescence Spectrophotometer. Fluorescence imaging of cells was performed on a Leica DMI 4000B microscope. Gel permeation chromatography (GPC) was performed on a Waters Breeze system with HPLC grade tetrahydrofuran (THF) as the mobile phase. GPC analyses were performed at the Department of Chemical Engineering at McGill University.

2.2.1 Synthesis

(3,5-bis(prop-2-yn-1-yloxy)phenyl)methanol (DPBA). This reaction was performed following a literature procedure.[1] 3,5-dihydroxybenzyl alcohol (1.0g, 7.14mmol), propargyl bromide (80% solution in toluene, 1.6mL, 14.28mmol), K_2CO_3 (1.28g, 9.28mmol) and [18]-Crown-6 (catalytic) were dissolved in acetone, and added to a 3-neck flask equipped with a condenser. The reaction mixture was brought to reflux and stirred for 12 hours under a nitrogen atmosphere. Upon completion, the solvent was removed under reduced pressure and the remaining mixture was extracted with DCM from water three times. The combined DCM extracts were dried with $MgSO_4$

and the solution volume was minimized before being passed through a silica gel column with a 1:1 hexanes:ethyl acetate eluent. The pure product was collected and dried *in vacuo* to yield a white solid (1.25 g, 81%).

^{1}H NMR (400 MHz, $CDCl_3$): δ_H (ppm) 1.60 (1H, s, OH), 2.55 (2H, t, $^{4}J_{HH}$ = 2.4 Hz, C≡CH), 4.68 (2H, s, CH_2-OH), 4.71 (4H, d, $^{4}J_{HH}$ = 2.3 Hz, CH_2-C≡C), 6.57 (1H, t, $^{4}J_{HH}$ = 2.3 Hz, H–Ar), 6.67 (2H, d, $^{4}J_{HH}$ = 2.5 Hz, H–Ar). ^{13}C{^{1}H}-NMR (100 MHz, $CDCl_3$): δ_C (ppm) 55.9, 65.1, 75.7, 78.4, 101.5, 106.2, 143.6, 158.8

3,5-bis(prop-2-yn-1-yloxy)benzyl PCL (DPB-PCL). Compound **3** was prepared by adapting a ring opening polymerization methodology from the literature.[2] DPBA (**2**, 0.2g, 0.925mmol) and distilled ε-caprolactone (2.07 mL, 18.7mmol) were dissolved in dry toluene and added to a warm 3-neck flask equipped with a condenser. While stirring under nitrogen atmosphere, the reaction mixture was brought to reflux and Tin(II)2-ethylhexanoate (0.076 mL, 0.187mmol) was added through a rubber septum. After 12 hours of stirring, the flask was let to cool before toluene was removed under reduced pressure. The mixture was re-dissolved in minimal amount of DCM and dropped into ice cold methanol to precipitate the pure product. The product was collected by filtration and dried *in vacuo* to obtain an off-white solid (1.43 g, 61%)

^{1}H NMR (400 MHz, $CDCl_3$): δ_H (ppm) 1.40 (56H, m, (-OOC-C-C-CH_2-)$_{28}$), 1.66 (112H, m, (-OOC-C-CH_2-C-CH_2-)$_{28}$), 2.33 (56H, t, $^{3}J_{HH}$ = 7.6 Hz, (-OOC-CH_2)$_{28}$), 2.55 (2H, t, $^{4}J_{HH}$ = 2.4 Hz, C≡CH), 3.66 (2H, t, $^{3}J_{HH}$ = 6.4 Hz, -OOC-CH_2-), 4.08 (56H, t, $^{3}J_{HH}$ = 6.8 Hz, (-CH_2-OOC-)$_{28}$), 4.69 (4H, d, $^{4}J_{HH}$ = 2.4 Hz, CH_2-C≡C), 5.07 (2H, s, CH_2-OH), 6.59 (1H, t, $^{4}J_{HH}$ = 2.4 Hz, H–Ar), 6.61 (2H, d, $^{4}J_{HH}$ = 2.4 Hz, H–Ar). ^{13}C{^{1}H}-NMR (125 MHz, $CDCl_3$): δ_C (ppm) 24.5, 25.5, 28.3, 34.1, 55.9, 64.1, 75.7, 107.5, 173.5. MS: MALDI-TOF M_n = 2839.05; M_w = 3321.40; PDI = 1.17; DP = 24.90

PEG-OTs. Monotosylation of PEG was carried out by adaptation and modification of a literature procedure.[3] Ag_2O was first freshly prepared by adding a 9mL 85 ºC aqueous solution of NaOH (0.24g, 5.89mmol) quickly to a separate 85 ºC aqueous solution of $AgNO_3$ (1.0g, 5.89mmol). A brown solid product immediately formed and was then filtered and washed with hot water and methanol before drying under reduced pressure. A 3-neck flask containing a solution PEG 2050 (2.95g, 1.44mmol), Ag_2O (0.500g, 2.16mmol), and KI (0.0478g, 0.288mmol) in DCM was prepared and cooled in an ice bath. Then, p-toluenesulfonyl chloride (0.288g, 1.51mmol) was

added while stirring under a nitrogen atmosphere. The reaction was continuously stirred over 12 hours to completion. The reaction solution was opened to air and centrifuged at 4500 RPM for 20 min to remove Ag_2O. The remaining solution was then concentrated in DCM and dropped into a flask containing ice cold ether to precipitate the purified product. The product was filtered and dried under reduced pressure to yield a white fluffy powder (2.23 g, 70 % yield).

^{1}H NMR (400 MHz, $CDCl_3$): δ_H (ppm) 2.44 (3H, s, CH3), 2.75 (1H, brs, OH), 3.63 (182H, m, PEG), 4.15 (2H, t, J=4 Hz, CH2-OTs), 7.34 (2H, d, $^3J_{HH}$ = 8Hz, H–Ar), 7.79 (2H, d, $^3J_{HH}$ = 8.0 Hz, H–Ar). $^{13}C\{^1H\}$-NMR (125 MHz, $CDCl_3$): δ_C (ppm) 21.5, 61.3, 68.4, 69.1, 70.1, 70.3, 70.5, 72.5, 127.8, 129.7, 132.9, 144.6.

PEG-N_3. Ts-PEG 2050 (**5**, 1.8g, 0.823mmol) and NaN_3 (0.43g, 6.58mmol) were added to a round bottom flask containing anhydrous ethanol, which was equipped with a condenser. The reaction mixture was brought to reflux and stirred for 24 hours under a nitrogen atmosphere. The flask was then opened to air and left to cool. Ethanol was removed from the system under reduced pressure, and the mixture was extracted 4 times from water with chloroform before drying with $MgSO_4$. The product was then concentrated in DCM and precipitated by dropwise addition to ice cold diethyl ether. After filtration and drying *in vacuo*, a white solid product was obtained (1.48 g, 87%).

^{1}H NMR (400 MHz, $CDCl_3$): δ_H (ppm) 2.48 (1H, brs, OH), 3.40 (2H, t, $^3J_{HH}$ = 4.8 Hz, CH_2-N_3), 3.66 (180, m, PEG), 3.74 (2H, t, $^3J_{HH}$ = 4.8 Hz, CH_2-OH). $^{13}C\{^1H\}$-NMR (125 MHz, $CDCl_3$): δ_C (ppm) 50.6, 61.6, 69.9, 70.3, 70.52, 70.58, 70.61, 70.65, 72.48.

2,2'-(propane-2,2-diylbis(sulfanediyl))diacetic acid (TKDA). In a three-neck flask under a nitrogen atmosphere, mercaptoacetic acid (25mL, 0.358mol) was dissolved in acetone (45mL, 0.607mol). While cooling in an ice bath, 40 mL HCl were added dropwise to the solution through a rubber septum, and the reaction mixture was left to stir for 12 hours. Upon completion, the flask was cooled once more in an ice bath and the precipitate filtered. The crude product was washed sequentially with cold water and cold hexanes to obtain a pure white product (33.54g, 83%).

^{1}H NMR (400 MHz, $CDCl_3$): δ_H (ppm) 1.65 (6H, s, CH_3), 3.56 (4H, s, CH_2). $^{13}C\{^1H\}$-NMR (100 MHz, DMSO-d_6): δ_C (ppm) 30.6, 33.6, 56.7, 171.7.

18,18-dimethyl-15-oxo-2,5,8,11,14-pentaoxa-17,19-dithiahenicosan-21-oic acid (TK-TEG). Steglich esterification was carried out by an adaptation and modification of a published

methodology.[4] TKDA (1.0g, 4.46mmol) and DMAP (0.109g, 0.897mmol) were added to a 3-neck flask and dissolved with a 1:1 mixture of dry diethyl ether and dry DCM. Upon cooling in an ice bath, solutions of TEG (0.179mL, 0.97mmol) and DCC (0.231g, 1.13mmol) in dry DCM were simultaneously added dropwise to the reaction mixture over 1.5 hours while stirring under a nitrogen atmosphere. Upon completion, the 3-neck flask was cooled in an ice bath and any formed precipitate was filtered off. The crude product was then extracted from water with DCM 3 times and dried under $MgSO_4$. The crude was concentrated in DCM and passed through a silica gel column with a 8:1 DCM:methanol eluent to remove any remaining impurities, and the solvent was removed under reduced pressure to yield a colourless oil (0.178 g, 48%).

^{1}H NMR (400 MHz, $CDCl_3$): δ_H (ppm) 1.63 (6H, s), 3.40 (3H, s), 3.44 (2H, s), 3.51 (2H, s), 3.57 (2H, m), 3.68 (10H, m), 3.75 (2H, m), 4.29 (2H, m). $^{13}C\{^1H\}$-NMR (125 MHz, $CDCl_3$): δ_C (ppm) 24.7, 25.4, 30.1, 32.9, 33.2, 33.5, 57.2, 58.9, 64.4, 68.9, 70.3, 70.4, 70.52, 70.53, 70.57, 71.9, 170.2, 172.3. MS: ESI m/z: (M+Na) Calculated for $C_{16}H_{30}O_8S_2Na$ 437.52 g/mol, Found 437.13 g/mol.

N_3-PEG-TK-TEG. The esterification procedure was adapted and modified as required based on a literature methodology.[5] N_3-PEG (0.76g, 0.362mmol), TK-TEG (0.15g, 3.62mmol), and DPTS (0.10g, 3.62mmol) were dissolved in dry DCM in a three-neck flask. A solution of DIPC (0.070mL, 4.52mmol) in dry DCM was added dropwise to the flask over 1.5 hours while continuously stirring under nitrogen atmosphere. The reaction was then continued to run for 24 hours. After the reaction was complete, the flask was stored in a freezer at 0 ºC overnight and the formed precipitate was discarded. The crude product was passed through a silica gel column with a 8:1 DCM:methanol eluent to remove any remaining impurities and then dried *in vacuo* to yield an off-white solid (0.438 g, 49%).

^{1}H NMR (400 MHz, $CDCl_3$): δ_H (ppm) 1.63 (6H, s, $2CH_3$), 3.39 (5H, m, CH_2-N_3, OCH_3), 3.45 (4H, s, S-CH_2-C=O), 3.67 (196H, m, PEG and TEG), 4.28 (4H, m, CH_2-O-C=O). $^{13}C\{^1H\}$-NMR (125 MHz, $CDCl_3$): δ_C (ppm) 30.2, 32.9, 50.7, 57.2, 58.9, 64.7, 68.9, 70.0, 70.5, 71.9, 170.4. MS: MALDI-TOF M_n = 2371.85; M_w = 2400.18; PDI = 1.01; DP = 53.87

μ(PEG-TK-TEG)$_2$PCL (μ1). The copper catalyzed alkyne-azide click reaction was adapted and modified as required based on a procedure method.[6, 7] N_3PEG-TK-TEG (**10**) (0.600g, 0.253mmol), DPB-PCL (**3**) (0.359g, 0.126mmol), and CuBr (0.041g, 0.286mmol) were dissolved in a round

bottom flask containing dry THF. While stirring the reaction mixture under nitrogen atmosphere, PMDETA (0.060mL, 0.286mmol) was added, and the reaction was continuously stirred for 24 hours. The completed reaction mixture was then concentrated under reduced pressure and passed through a silica gel column with a 8:1 DCM:methanol eluent to remove CuBr and PMDTA. Remaining unreacted polymers were removed via dialysis through a 3.5 kD membrane in aqueous medium over 24 hours. The pure product was then removed from the dialysis bag and isolated by removing water under pressure, to yield a pale brown solid (0.400 g, 42%).

^{1}H NMR (500 MHz, $CDCl_3$): δ_H (ppm) 1.42 (56H, m), 1.63 (12H, s), 1.67 (112H), 2.32 (56H, t, $^{3}J_{HH}$ = 7.7 Hz), 3.40 (6H, s), 3.46 (8H, s), 3.66 (392H, s), 3.91 (4H, t, $^{3}J_{HH}$ = 4.6 Hz), 4.08 (56H, t, $^{3}J_{HH}$ = 6.6 Hz), 4.29 (4H, t, $^{3}J_{HH}$ = 5.2 Hz), 4.58 (4H, t, $^{3}J_{HH}$ = 5.3 Hz), 5.07 (2H, s), 5.20 (4H, s), 6.62 (2H, s), 6.64 (1H, s) 7.87 (2H, s). ^{13}C{^{1}H}-NMR (125 MHz, DMSO-d_6): δ_C (ppm) 24.5, 25.5, 28.3, 30.3, 33.0, 34.1, 50.2, 59.2, 61.9, 64.1, 69.2, 70.6, 72.2, 123.9, 143.6, 170.7, 173.5.

3-((3-(hexyloxy)-3-oxopropyl)disulfaneyl)propanoic acid (DS-Hex). Steglich esterification was carried out by an adaptation and modification of a published methodology.[4] 3,3-dithiodipropionic acid (1.22g, 5.82mmol) and DMAP (0.119g, 0.970mmol) were dissolved in a 3-neck flask containing dry DCM and cooled in an ice bath. Solutions of DCC (0.300g, 1.46mmol) and hexanol (0.122mL, 0.970mmol) in dry DCM were then simultaneously added dropwise to the reaction mixture over 1.5 hours while stirring under nitrogen atmosphere. The reaction was continuously stirred over 12 hours as the mixture gradually warmed to room temperature. The solution was filtered to remove any precipitate formed during the reaction and then the solvent was removed under reduced pressure to obtain a crude product. The pure product was isolated by washing with cold hexanes 3 times and removing hexanes from the combined washes under reduced pressure to give a white solid (0.040g, 14 %).

^{1}H NMR (400 MHz, $CDCl_3$): δ_H (ppm) 0.92 (3H, t, $^{3}J_{HH}$ = 6.8 Hz, CH_3), 1.34 (6H, m, $3CH_2$), 1.65 (2H, m, CH_2), 2.76 (2H, t, $^{3}J_{HH}$ = 7.32 Hz, CH_2COO-), 2.83 (2H, t, $^{3}J_{HH}$ = 7.32 Hz, CH_2COOH), 2.96 (4H, m, CH_2-S-S-CH_2), 4.12 (2H, t, $^{3}J_{HH}$ = 6.84 Hz, COO-CH_2). ^{13}C{^{1}H}-NMR (100 MHz, $CDCl_3$): δ_C (ppm) 14.0, 22.5, 25.5, 28.5, 30.9, 31.4, 32.7, 33.2, 33.6, 34.1, 65.0, 171.9, 176.2. MS: ESI m/z: (M - H) Calculated for $C_{12}H_{21}O_4S_2$ 293.42 g/mol, Found 293.09 g/mol.

μ(PEG-TK-TEG)2PCL-DS (μ2). μ(PEG-TK-TEG)$_2$PCL (0.25g, 0.0330mmol), DS-Hex (0.023g, 0.0781mmol), and DPTS (0.022g, 0.0788mmol) were dissolved in a 3-neck flask

containing dry DCM. While stirring under nitrogen atmosphere, a solution containing DIPC (0.015mL, 0.0969mmol) in dry DCM was added dropwise over 1.5 hours. After 24 hours of continuous stirring, the solution was concentrated and left in a freezer at 0 ºC. The precipitate was filtered, and the crude product was extracted from water with DCM three times. The combined organic extracts were washed with a 5% $NaHCO_3$ solution. The DCM in the recovered extract was removed *in vacuo*, and the remaining mixture was dialyzed in aqueous medium against a 3.5 kD membrane. The product was removed from inside the membrane and isolated after removal of water under reduced pressure. The remaining product was washed with ice cold water, and then centrifuged at 4000 RPM for 15 minutes at 4 ºC. The supernatant was discarded, and this process was repeated 2 more times to give the pure product as a light brown solid (0.162g, 62%).

^{1}H NMR (500 MHz, $CDCl_3$): δ_H (ppm) 0.87 (3H, t, $^3J_{HH}$ = 7.0 Hz), 1.39 (60H, m), 1.61 (12H, s), 1.65 (114H, m), 2.30 (56H, t, $^3J_{HH}$ = 7.5 Hz), 2.74 (4H, m), 2.93 (4H, m), 3.37 (6H, s), 3.43 (8H, s), 3.63 (392H, m), 3.87 (4H, t, $^3J_{HH}$ = 4.5 Hz), 4.05 (58H, t, $^3J_{HH}$ = 6.5 Hz), 4.08 (4H, t, $^3J_{HH}$ = 7 Hz), 4.26 (4H, t, $^3J_{HH}$ = 4.5 Hz), 4.99 (2H, s), 5.18 (4H, s), 6.43-6.61 (3H, m, H-Ar), 7.84 (2H, s). ^{13}C{^{1}H}-NMR (125 MHz, $CDCl_3$): δ_C (ppm) 13.9, 22.5, 24.5, 24.6, 25.5, 28.3, 30.30, 33.0, 33.9, 34.1, 34.2, 41.2, 57.3, 59.0, 60.2, 60.3, 64.1, 64.5, 68.9, 70.5, 72.0, 170.5, 173.5.

PCL-Hx. Compound **16** was prepared by adapting a ring opening polymerization methodology from the literature.[2] Hexanol (0.2mL, 1.61mmol) and distilled ε-caprolactone (3.56mL, 32.1mmol) were dissolved in dry toluene and added to a warm 3-neck flask equipped with a condenser. While stirring under nitrogen atmosphere, the reaction mixture was brought to reflux and Tin(II)2-ethylhexanoate (0.13mL, 0.401mmol) was added through a rubber septum. After 12 hours of stirring, the flask was allowed to cool before the toluene was removed under reduced pressure. The mixture was redissolved in minimal DCM and dropped into ice cold methanol to precipitate the pure product. The product was collected by filtration and dried *in vacuo* to give an off-white solid (3.112 g, 81%).

^{1}H NMR (400 MHz, $CDCl_3$): δ_H (ppm) 0.89 (5H, m, CH_3-CH_2), 1.32 (6H, m, CH_2-CH_2-CH_2), 1.39 (56H, m, (-OOC-C-C-CH_2-)$_n$), 1.65 (114H, m, (-OOC-C-CH_2-C-CH_2-)$_n$), 2.32 (56H, t, $^3J_{HH}$ = 7.64 Hz, (-OOC-CH_2)$_n$), 3.66 (2H, t, $^3J_{HH}$ = 6.52 Hz, -OOC-CH_2-), 4.07 (56H, t, $^3J_{HH}$ = 6.64 Hz, (-CH_2-OOC-)$_n$). ^{13}C{^{1}H}-NMR (125 MHz, $CDCl_3$): δ_C (ppm) 11.8, 13.91, 13.96, 22.49, 22.58, 24.5, 25.6,

25.2, 25.4, 25.50, 25.55, 28.32, 28.38, 28.4, 28.5, 29.6, 31.3, 31.7, 32.3, 34.0, 34.1, 34.2, 47.3, 62.5, 63.7, 64.1, 64.7, 64.4, 173.4, 173.52, 173.55, 173.6, 173.4.

DS-PCL-Hx. Steglich esterification was carried out by an adaptation and modification of a published methodology.[4] 3,3′-Dithiodipropionic acid (0.6g, 2.85mmol) and DMAP (0.061g, 0.500mmol) were dissolved in a 3-neck flask containing dry DCM and dry THF. The solution was cooled in an ice bath while under a nitrogen atmosphere. While stirring, DCC (0.106g, 0.500mmol) and Hex-PCL (1.02g, 0.500mmol) were separately yet simultaneously added dropwise over 1.5 hours. The reaction mixture was left to react overnight. Upon completion, the mixture was filtered to remove any formed precipitate. The solvent was removed under reduced pressure, and the crude product was washed with DCM. The DCM solution was recovered via filtration, and the solvent was removed *in vacuo* to recover the pure product as an off-white solid (0.9707g, 94%).

^{1}H NMR (400 MHz, $CDCl_3$): δ_H (ppm) 0.91 (5H, m, CH_3-CH_2), 1.33 (6H, m, $3CH_2$), 1.41 (56H, m, (-OOC-C-C-CH_2-)$_n$), 1.67 (112H, m, (-OOC-C-CH_2-C-CH_2-)$_n$), 2.33 (56H, t, $^{3}J_{HH}$ = 7.60 Hz, (-OOC-CH_2)$_n$), 2.74-2.82 (4H, m, CH_2COO-), 2.97 (4H, m, CH_2-S-S-CH_2), 4.08 (56H, t, $^{3}J_{HH}$ = 6.40 Hz, (-CH_2-OOC-)$_n$), 4.13 (2H, t, $^{3}J_{HH}$ = 6.40 Hz, COO-CH_2). ^{13}C{^{1}H}-NMR (125 MHz, $CDCl_3$): δ_C (ppm) 14.0, 22.5, 24.5, 25.53, 25.58, 28.3, 28.6, 31.4, 33.1, 33.3, 34.12, 34.18, 47.3, 63.8, 64.1, 64.5, 171.7, 173.5.MS: MALDI-TOF M_n = 2058.17; M_w = 2379.46; PDI = 1.16; DP = 18.05

DPB-DS-PCL-Hx. Steglich esterification was carried out by an adaptation and modification of a published methodology.[4] DS-PCL-Hx (0.5g, 0.243mmol), DPBA (0.158g, 0.729mmol), and DMAP (0.090g, 0.729mmol) were dissolved in a 3-neck flask containing dry DCM. The solution was cooled in an ice bath while under a nitrogen atmosphere. While stirring, DCC (0.150g, 0.729mmol) was added dropwise over 1.5 hours. The reaction mixture was left to react for 24 hours. Upon completion, the mixture was filtered to remove any formed precipitate. The mixture was concentrated, left in the freezer overnight, and any formed crystals were removed. The solvent was removed under reduced pressure, and the crude product was washed with methanol 3 times. The pure product was left to dry in a vacuum desiccator overnight to yield the pure the pure product as an off-white solid (0.430g, 72%).

^{1}H NMR (400 MHz, $CDCl_3$): δ_H (ppm) 0.90 (5H, m, CH_3-CH_2), 1.33 (6H, m, $3CH_2$), 1.40 (56H, m, (-OOC-C-C-CH_2-)$_n$), 1.67 (112H, m, (-OOC-C-CH_2-C-CH_2-)$_n$), 2.33 (56H, t, $^{3}J_{HH}$ = 7.64 Hz,

(-OOC-CH_2)$_n$), 2.57 (2H, t, $^4J_{HH}$ = 2.50 Hz, C≡CH), 2.72-2.84 (4H, m, CH_2COO-), 2.92-2.99 (4H, m, CH_2-S-S-CH_2), 4.08 (56H, t, $^3J_{HH}$ = 6.50 Hz, (-CH_2-OOC-)$_n$), 4.12 (2H, t, $^3J_{HH}$ = 7.00 Hz, COO-CH_2), 4.70 (4H, d, $^4J_{HH}$ = 2.50 Hz, CH_2-C≡C), 5.11 (2H, s, Ar-CH_2-OOC), 6.60 (1H, t, H–Ar), 6.63 (2H, d, H–Ar). $^{13}C\{^1H\}$-NMR (125 MHz, $CDCl_3$): δ_C (ppm) 14.0, 22.5, 24.5, 25.5, 28.3, 28.6, 31.4, 33.0, 34.13, 34.19, 55.9, 64.1, 64.5, 75.8, 107.5, 158.8, 173.5, 173.6. MS: MALDI-TOF M_n = 2464.48; M_w = 2671.70; PDI = 1.08; DP = 21.62

μ(PEG-TK-TEG)2DS-PCL (μ3). The copper catalyzed alkyne-azide click reaction was adapted and modified as required based on a literature procedure.[6, 7] N_3-PEG-TK-TEG (0.560g, 0.236mmol), DPB-DS-PCL-Hx (0.250g, 0.101mmol), were dissolved in a three-neck flask containing dry THF. Separately, CuBr (0.0408g, 0.284mmol) and PMDETA (0.060mL, 0.284mmol) were dissolved in dry THF and then added to the flask containing the polymeric starting materials. The reaction mixture was stirred under N_2 for 24 hours at 35 ºC. Upon completion, THF was removed under reduced pressure, the product was placed in water, and added to a 3.5 kD dialysis membrane. The product was dialyzed against 100 mL of water containing 300 mg of EDTA overnight. The remaining product was collected from the membrane, washed with ice cold water, and then centrifuged at 4000 RPM for 15 minutes at 4 ºC. The supernatant was discarded, and the washing/centrifugation process was repeated 2 more times to give the pure product as a light brown solid (0.980g, 84%).

^1H NMR (500 MHz, $CDCl_3$): δ_H (ppm) 0.87 (5H, m), 1.39 (60H, m), 1.62 (12H, s), 1.66 (114H, m), 2.31 (56H, t, $^3J_{HH}$ = 7.50 Hz), 2.74 (4H, m), 2.92 (4H, m), 3.39 (6H, s), 3.45 (8H, s), 3.66 (486H, m), 3.79 (4H, t, $^3J_{HH}$ = 5.00 Hz), 4.07 (62H, t, $^3J_{HH}$ = 6.50 Hz), 4.27 (4H, t, $^3J_{HH}$ = 4.50 Hz), 5.31 (4H, s), 6.44-6.56 (3H, m, H-Ar), 7.73 (2H, s). $^{13}C\{^1H\}$-NMR (125 MHz, $CDCl_3$): δ_C (ppm) 14.0, 22.5, 24.5, 25.54, 25.59, 28.3, 28.6, 30.3, 31.4, 33.0, 31.4, 33.0, 34.12, 34.18, 50.6, 59.0, 61.7, 64.1, 64.51, 64.56, 68.9, 70.5, 173.5.

mPEG-OTs. PEG_{2000} methyl ether (1.5g, 0.750mmol) was added to a 3-neck flask and dissolved in THF. The flask was placed under nitrogen atmosphere, and a concentrated aqueous solution containing NaOH (0.09g, 2.25mmol) was added. Subsequently, a solution of *p*-toluenesulfonyl chloride (0.43g, 2.25mmol) in THF was added dropwise to the reaction mixture over 1 hour. After letting it stir overnight, the solvent was removed from the flask under reduced pressure, and the product was extracted with DCM from water 3 times. The combined organic extracts were dried

under $MgSO_4$. The solution was filtered to remove the drying agent, concentrated, and then dropped into ice cold diethyl ether under vigorous stirring. The pure precipitated product was obtained by filtration as a white solid (1.30g, 81%).

^{1}H NMR (500 MHz, $CDCl_3$): δ_H (ppm) 2.46 (3H, s, CH_3), 3.39 (3H, s, OCH_3), 3.63 (182H, m, PEG), 4.17 (2H, t, J=4.50 Hz, CH_2-OTs), 7.36 (2H, d, $^3J_{HH}$ = 8.00 Hz, H–Ar), 7.81 (2H, d, $^3J_{HH}$ = 8.00 Hz, H–Ar).

mPEG-N_3. Ts-PEG_{2000} (1.30g, 0.603mmol) and NaN_3 (0.12g, 1.85mmol) were added to a 3-neck flask containing anhydrous ethanol which was equipped with a condenser. The reaction mixture was brought to reflux and stirred for 24 hours under nitrogen atmosphere. The flask was then opened to air and let cool. Ethanol was removed from the system under reduced pressure, and the mixture was extracted 4 times from ice cold water with chloroform before drying with $MgSO_4$. The product was then concentrated in DCM and precipitated by dropwise addition to ice cold diethyl ether. After filtration and drying *in vacuo*, a white solid product was obtained (0.62 g, 52%).

^{1}H NMR (500 MHz, $CDCl_3$): δ_H (ppm) 3.38 (3H, s, OCH_3), 3.39 (2H, t, $^3J_{HH}$ = 5.00 Hz, CH_2-N_3), 3.66 (180, m, PEG), 3.78 (2H, t, $^3J_{HH}$ = 4.50 Hz, CH_2-O), 4.06 (2H, t, $^3J_{HH}$ = 6.50 Hz, CH_2-O). ^{13}C{^{1}H}-NMR (125 MHz, $CDCl_3$): δ_C (ppm) 50.6, 59.0, 70.0, 70.5, 70.65, 70.68, 70.7, 71.9.

μ(PEG)2DS-PCL (μ4). The copper catalyzed alkyne-azide click reaction was adapted and modified as required based on a literature procedure.[6, 7] $mPEG_{2000}$-N_3 (0.030g, 0.0146mmol) and DPB-DS-PCL-Hx (0.018g, 0.00731mmol) were dissolved in a round bottom flask containing dry THF. Separately, CuBr (0.0025g, 0.0174mmol) and PMDETA (0.0030g, 0.0174mmol) were dissolved in dry THF and then added to the flask containing the polymer starting materials. The reaction mixture was stirred under N_2 for 24 hours at 35 ºC. Upon completion, THF was removed under reduced pressure, the product was placed in water, and then placed in a 3.5 kD dialysis membrane. The product was dialyzed against 100 mL of water containing 50 mg of EDTA overnight. The remaining product was collected from inside the membrane, washed with ice cold water, and then centrifuged at 4000 RPM for 15 minutes at 4 ºC. The supernatant was discarded, and this process was repeated 2 more times to give the pure product as a pale brown solid (0.039g, 82%).

^{1}H NMR (500 MHz, $CDCl_3$): δ_H (ppm) 0.91 (5H, m), 1.40 (60H, m), 1.66 (114H, m), 2.33 (56H, t, $^{3}J_{HH}$ = 7.50 Hz), 2.75 (4H, m), 2.95 (4H, m), 3.40 (6H, s), 3.68 (260H, m), 3.80 (4H, t, $^{3}J_{HH}$ = 4.50 Hz), 4.08 (58H, t, $^{3}J_{HH}$ = 7.00 Hz), 5.32 (6H, s), 6.53 (1H, s, H–Ar), 6.58 (2H, s, H–Ar), 7.75 (2H, s). $^{13}C\{^{1}H\}$-NMR (125 MHz, $CDCl_3$): δ_C (ppm) 15.2, 24.5, 25.5, 28.3, 29.7, 34.1, 50.9, 53.4, 59.0, 64.1, 65.8, 70.5, 173.5.

(4-(prop-2-yn-1-yloxy)phenyl)methanol (4PBA). This reaction was adapted and modified from a literature procedure.[1] 4-hydroxybenzyl alcohol (1.1g, 8.86mmol), Propargyl Bromide (0.987mL, 8.86mmol) (80% solution in toluene), K_2CO_3 (1.225g. 8.86mmol), and [18]-Crown-6 (catalytic) were dissolved in acetone and added to a 3-neck flask equipped with a condenser. The reaction mixture was brought to reflux and stirred for 12 hours under a nitrogen atmosphere. Upon completion, the reaction solvent was removed under reduced pressure and the remaining mixture was extracted with DCM from water three times. The combined DCM extracts were dried with $MgSO_4$ and the solution volume was minimized before being passed through a silica gel column with a 1:1 hexanes:ethyl acetate eluent. The pure product was collected and dried *in vacuo* to yield an off-white solid (1.137 g, 79%).

^{1}H NMR (400 MHz, $CDCl_3$): δ_H (ppm) 1.64 (1H, s, OH), 2.54 (2H, t, $^{4}J_{HH}$ = 2.40 Hz, C≡CH), 4.65 (2H, s, CH_2-OH), 4.72 (2H, d, $^{4}J_{HH}$ = 2.40 Hz, CH_2-C≡C), 6.99 (2H, d, $^{3}J_{HH}$ = 8.80 Hz, H–Ar), 7.33 (2H, d, $^{3}J_{HH}$ = 8.80 Hz, H–Ar).

4-(prop-2-yn-1-yloxy)benzyl PCL (4PB-PCL). Compound **26** was prepared by adapting a ring opening polymerization methodology from the literature.[2] 4PBA (0.2g, 1.23mmol) and distilled ε-caprolactone (2.76mL, 24.9mmol) were dissolved in dry toluene and added to a warm 3-neck flask equipped with a condenser. While stirring under nitrogen atmosphere, the reaction mixture was brought to reflux and Tin(II)2-ethylhexanoate (0.080mL, 0.249mmol) were added through a rubber septum. After 12 hours of stirring, the flask was allowed to cool before the toluene was removed under reduced pressure. The mixture was redissolved in minimal DCM and dropped into ice cold methanol to precipitate the pure product. The product was collected by filtration and dried *in vacuo* to give an off-white solid (1.46g, 48%).

^{1}H NMR (400 MHz, $CDCl_3$): δ_H (ppm) 1.40 (34H, m, (-OOC-C-C-CH_2-)$_n$), 1.66 (68H, m, (-OOC-C-CH_2-C-CH_2-)$_n$), 2.32 (34H, m, OOCCH_2-)$_n$) 2.55 (1H, t, $^{4}J_{HH}$ = 2.40 Hz, C≡CH), 3.67 (2H, t, $^{3}J_{HH}$ = 6.40 Hz, CH_2OH), 4.08 (32H, t, $^{3}J_{HH}$ = 6.80 Hz, (-CH_2-OOC-)$_n$), 4.71 (2H, d, $^{4}J_{HH}$ = 2.40

Hz, CH_2-C≡C), 5.07 (2H, s, Ar-CH_2-O), 6.98 (2H, d, $^3J_{HH}$ = 8.40 Hz, H–Ar), 7.32 (2H, d, $^3J_{HH}$ = 8.40 Hz, H–Ar). $^{13}C\{^1H\}$-NMR (125 MHz, $CDCl_3$): δ_C (ppm) 24.5, 25.4, 28.3, 34.1, 55.8, 64.1, 65.8, 75.6, 114.9, 129.1, 129.9, 173.5. MS: MALDI-TOF M_n = 2036.85; M_w = 2126.42; PDI = 1.04; DP = 17.87

(PEG-TK-TEG)-block-PCL (b1). The copper catalyzed alkyne-azide click reaction was adapted and modified as required based on a literature procedure.[6, 7] N_3-PEG-TK-TEG (0.116g, 0.0491mmol), (0.100g, 0.0491mmol) 4PB-PCL, and CuBr (0.0106g, 0.0737mmol) were dissolved in a round bottom flask containing dry THF. While stirring the reaction mixture under nitrogen atmosphere, PMDETA (0.015mL, 0.0737mmol) was added, and the reaction was continuously stirred at 35 ℃ for 24 hours. The completed reaction mixture was then concentrated under reduced pressure. The crude product was purified by dialysis through a 3.5 kD membrane against a solution of 250 mg of EDTA for 24 h and then precipitated in ice-cold ethyl ether. The final product was collected by vacuum filtration and left to dry under reduced pressure, to give an off white solid (0.199g, 92%).

^1H NMR (500 MHz, $CDCl_3$): δ_H (ppm) 1.40 (H, m), 1.63 (12H, s), 1.67 (100H, m), 2.32 (50H, t, $^3J_{HH}$ = 7.50 Hz), 3.40 (4H, s), 3.46 (3H, s), 3.66 (414H, s), 4.08 (50H, t, $^3J_{HH}$ = 6.50 Hz), 4.29 (4H, m), 5.01 (2H, s), 5.32 (2H, s), 6.72 (2H, d, $^3J_{HH}$ = 8.50 Hz), 7.20 (2H, d, $^3J_{HH}$ = 8.50 Hz), 7.87 (2H, s). $^{13}C\{^1H\}$-NMR (125 MHz, $CDCl_3$): δ_C (ppm) 24.5, 25.5, 28.3, 30.3, 32.3, 34.1, 59.0, 64.1, 64.5, 68.9, 70.5, 129.9, 173.5.

2.2.2 GPC Analyses

Miktoarm and diblock polymers were prepared for GPC by dissolution in HPLC grade THF. A mobile phase flow rate of 0.3 mL/min was used for a GPC equipped with 3 Waters Styragel HR columns (HR1 with a molar mass measurement range of 1 x 10^2 - 5 x 10^3 g/mol, HR2 with a molar mass measurement range of 5 x 10^2 - 2 x 10^4 g/mol and HR4 with a molar mass measurement range of 5x10^3 - 6x10^5 g/mol) and a guard column was used. The columns were heated to 40 °C during the analysis. The molar masses were determined by calibration with linear narrow molar mass distribution PMMA standards (PSS Polymer Standards Service GmbH, molar masses ranging from 682 g/mol to 1,520,000 g/mol) and the GPC was equipped with a differential refractive index (RI 2414) detector.

2.2.3 Preparation of Blank Micelles

Blank micelles were prepared by the co-solvent evaporation method.[51] In a typical preparation, 2 mg of the polymer was dissolved in 1 mL of THF, and then injected together into 2 mL of DI water at a rate of 1 drop/s. The mixture was left to stir vigorously overnight while the organic phase evaporated, leaving behind the self-assembled micelles in water. The micellar solution was filtered through a 0.22 μm PVDF syringe filter. Aliquots of the micelle solutions were tested using DLS to determine the hydrodynamic diameter and polydispersity index of the micelles. All measurements were performed in triplicate at room temperature. Size distributions were obtained as a lognormal distribution.

2.2.4 CMC Determination

Pyrene loaded micelles were similarly prepared by the co-solvent evaporation method. A series of polymer concentrations were prepared in 6 μM solutions of pyrene in THF. These solutions were injected into DI water at a rate of 1 drop/s and left to stir vigorously overnight to evaporate the organic phase and trigger self-assembly. Aliquots were taken and measured directly by fluorescence spectroscopy with an emission wavelength of 390 nm. The peak intensity ratios at 333 and 338 nm for each sample were plotted as a function of polymer concentration to determine the CMC as the point at which an increasing polymer concentration resulted in an increase of the intensity ratio and the slope.

2.2.5 Drug Loading

The procedure for drug loading was similar to the preparation of blank micelles except for the addition of 1 mg of curcumin dissolved in THF. Unencapsulated drug was removed first by centrifuging the micellar solution at 1000 RPM for 5 minutes followed by filtering the supernatant through a 0.22 μm PVDF syringe filter. Aliquots of the drug loaded micellar solutions were tested using DLS to determine their hydrodynamic diameters and dispersities. The concentration and mass of encapsulated drug was determined by acquiring the intensity of the peak at 424 nm using UV-visible spectroscopy and relating values to a drug concentration standard curve (Figure A.1). Encapsulation efficiencies and loading capacities were calculated according to Equations 1 and 2 respectively.

$$EE\ \% = \frac{Loaded\ Drug\ (mg)}{Total\ Drug\ (mg)} \qquad (1)$$

$$LC\ \% = \frac{Loaded\ Drug\ (mg)}{Total\ Drug\ (mg) + Polymer\ (mg)} \qquad (2)$$

2.2.6 Drug Release

Drug loaded micellar solutions were pipetted into 3.5 kD MWCO dialysis tubing and dialyzed against 140 mL of pH 7.4 phosphate-buffered saline (PBS) containing 1% v/v Tween 80. 20 μL aliquots were taken from the dialysis tubing at certain time points to measure the concentration of unreleased drug by UV-visible spectroscopy. These aliquots were diluted with methanol to break apart the micelles and decrease the resultant absorbance signal in order to better measure the drug of interest. A 1 mg/mL drug solution in a 45/40/15 ratio of water/dimethylacetamide/PEG_{750} was used as the control. Released drug, in percent, was plotted as a function of dialysis time.

2.2.7 Transmission Electron Microscopy

In a typical experiment, a 10 μL drop of the 2 mg/mL polymeric micelle solution was dropped onto a carbon-coated copper grid. After 2 minutes, excess solution was removed by absorbing it with a Whatman filter paper carefully placed at the rim of the grid. Afterwards, 10 μL of 2% uranyl acetate was similarly dropped onto the grid, left for 2 minutes, and had its excess absorbed by a Whatman filter paper. The grid was left to dry for an additional 20 minutes before imaging.

2.2.8 Cell Culture

U251N human glioblastoma were cultured in Dulbecco's modified Eagle's media (DMEM, Gibco) supplemented with fetal bovine serum (5% v/v, FBS) and penicillin-streptomycin (1% v/v) at 37oC with 5% CO2 and 95% relative humidity. Cells were seeded 100,000 cells per well (for spectrofluorometric measurements) or 5,000 cells per glass coverslip (for microscopy) and were left to adhere overnight. U251N cells were pre-treated with a ROS inducer, 50 μM menadione (MenD) for 1 hour, or glutathione inhibitor, L-buthionine-sulfoximine (BSO, 100 μM) for 24 hours in serum-deprived media. Following pre-treatment, cells were treated with 15 μM of free curcumin or curcumin-loaded μ1 (μ1: 2.44 μM; curcumin: 15 μM) for 6 hours in serum-deprived media.

2.2.9 Measurement of Intracellular and Extracellular ROS with CellROX® Deep Red

Cells were treated as indicated at 37 ^{o}C. Cells were incubated with CellROX® Deep Red (excitation/emission wavelengths: 640/665 nm) at a final concentration of 5 μM during the last 30 minutes of the treatment period. At the end of the treatment, media was collected. Cells were lysed with DMSO and collected. Fluorescence intensities of media and cell lysate samples were measured by Cary Eclipse fluorescence spectrometer at an emission wavelength at 665 nm (excitation: 640 nm, range: 650 – 700 nm). For fluorescence imaging, cells were fixed, labeled

with Hoechst 33342 nuclear dye (10 μM, 10 min), and imaged with a Leica DMI 4000B microscope at 20x objective. Micrographs were analysed with ImageJ software.

2.3 Results and Discussion

Miktoarm star polymers were designed to be related by PEG and PCL segments as the hydrophilic and hydrophobic components respectively, but they differ through the varied stimuli responsive units introduced into their structures. The synthesis of these branched architectures was initiated by designing building blocks that could help facilitate their spatial location. 2,2'-(propane-2,2-diylbis(sulfanediyl))diacetic acid (thioketal diacid), was synthesized from thioglycolic acid and acetone, and contains a ROS responsive TK moiety with COOH terminal units to link it with the polymeric arms. Miktoarm star polymers (μ1, μ2, μ3), and a linear diblock copolymer (b1) contain this ROS-responsive TK moiety incorporated into their PEG chains, whereas the branched architecture (μ4) without it served as a control (Scheme S.2). Likewise, a 3,3-dithiodipropionic acid (disulfide-diacid) moiety was used to introduce GSH responsive units into the miktoarm star polymers based on their desired responsive properties. With μ2, disulfide (DS) addition consisted of only coupling the finished μ1 to the DS component, whereas in μ3 and μ4, DS was carefully introduced to the terminus of a hexanol initiated PCL before subsequent coupling to the core. This ensured that in μ3 and μ4, the GSH-responsive unit was adjacent to the focal point of the molecule, and in μ2, the DS moiety was located near the terminal end of PCL. Such adjustable placement of responsive moieties necessitates a strict order of segment coupling and synthesis in order to facilitate stimulus responsive cleavage at desired polymeric positions. A summary of the syntheses of these amphiphilic macromolecules is provided below, while full synthetic schemes can be found in Appendix A (Schemes A.1-A.5).

2.3.1 Building Block Synthesis

Miktoarm star polymers μ1-μ4 and diblock copolymer b1 were constructed in a modular fashion that involved the synthesis of 5 different "building blocks" (4, 8, 11, 13, and 15) with varying ROS/GSH responsiveness. The building blocks were then combined to give the desired miktoarm star polymeric structure using CuAAC or esterification-based coupling chemistry (Schemes 2.1-2.2).

PCL-dialkyne core (4). Building block 4, which is utilized for the construction of miktoarm star polymers μ1 and μ2, was prepared from 3,5-dihydroxy benzyl alcohol (1) and propargyl bromide

(2). The propargylation at 3 and 5 hydroxy positions was monitored by the appearance of a C*H*$_2$-C≡C peak at 4.68 and a C≡C*H* peak at 2.55 ppm in its ^{1}H NMR. It was then used as an initiator in the ROP of ε-caprolactone (3) ([M$_0$]/[I] = 20), to yield the hydrophobic component of the miktoarm star polymer (4). Following ROP, the PCL peaks in 4 were clearly visible at 1.39, 1.65, 2.32, and 4.07 ppm. In addition to preserving the alkyne peaks, the new C*H*$_2$O ester was seen at 5.07 ppm.

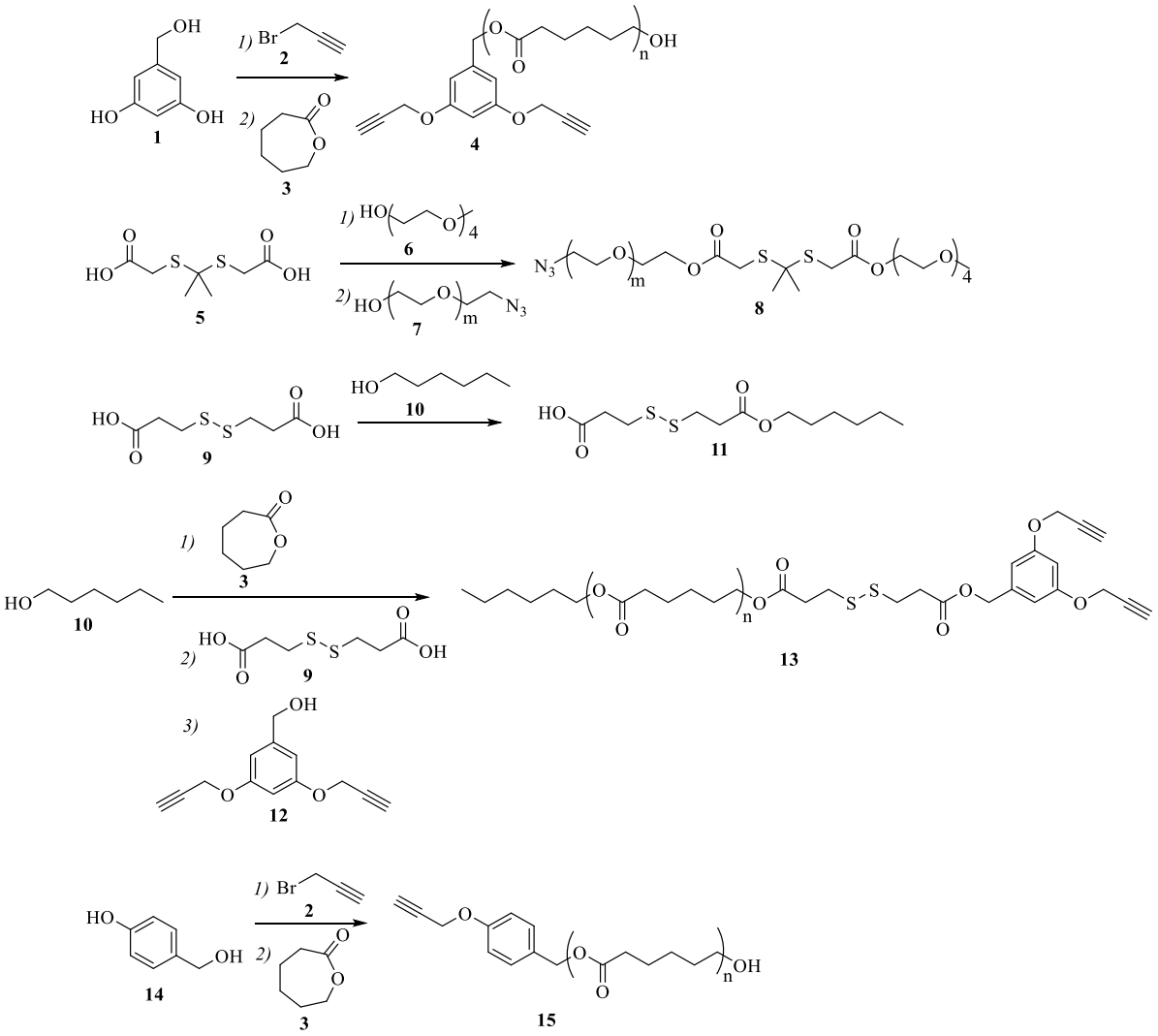

Scheme 2.1. Syntheses of building blocks. For full details, see Schemes A.1-A.5.

ROS-responsive asymmetric thioketal unit (8). The ROS-responsive polymeric arm (8, Scheme 2.1) of μ1, μ2, and μ3 was prepared by the introduction of a thioketal group to one terminal end of PEG. It was achieved by first preparing thioketal diacid (5) from thioglycolic acid, and then

functionalizing it at only one acid end with tetraethylene glycol (TEG) (6). Thioketal diacid 5 was characterized by its two singlet peaks at 1.65 and 3.56 ppm corresponding to C*H*$_3$ and C*H*$_2$ protons respectively. Its monoTEGylation was achieved through the slow addition of excess TEG to a solution containing the diacid and the esterification catalysts DMAP/DCC. Isolation of the monofunctionalized TEG-thioketal compound was done through successive filtration, liquid extractions, and column chromatography. Introduction of TEG to one end of 5 was confirmed by the even splitting of 5's C*H*$_2$ peak to two singlets seen at 3.44 and 3.51 ppm due to the molecule's asymmetric nature. Additionally, the C*H*$_2$O esterification-derived triplet was visible at 4.29 ppm.

Dihydroxy terminated-PEG$_{2050}$ was selectively monotosylated using Ag_2O as a catalyst, and the tosyl group was then substituted with an azide to yield 7.[52] It led to appearance of peaks at 2.44 and 7.34-7.79 ppm corresponding to the C*H*$_3$ and Ar-*H* of the tosyl group, and a triplet for the C*H*$_2$-OTs protons at 4.15 ppm. Replacement of the tosyl group with an azide (N_3) on PEG$_{2050}$ was confirmed by the disappearance of the relevant tosyl peaks and appearance of the C*H*$_2$-N_3 triplet at 3.40 ppm.

MonoTEGylated TK was stitched at its free acid end with 7 *via* Steglich esterification to yield the hydrophilic arm 8. It led to the merging of the peaks from the asymmetric thioketal-flanking C*H*$_2$ protons, originally seen in the TEG-thioketal intermediate, to give one singlet at 3.45 ppm for 8. Additionally, the stepwise evolution of the PEG-based hydrophilic arm 8 was validated by its individual GPC traces (Figure A.2-A.3).

GSH-responsive asymmetric disulfide (11). The dual stimuli responsive μ2 was prepared by first synthesizing 11, a short hydrophobic chain bearing a GSH-responsive disulfide unit terminated with a free acid end. Hexanol (10) was introduced to a large excess of 3,3'-dithiodipropionic acid, 9, and esterified using DMAP/DCC. Monitoring the reaction using ^{1}H NMR showed the appearance of a triplet at 4.12 ppm corresponding to the newly formed ester group. Additionally, the C*H*$_2$ protons adjacent to the acid and ester groups from the original compound 9 became asymmetrical in the monofunctional 11 (Scheme 2.1). These protons have equal, yet distinct signals present at 2.76 and 2.83 ppm as triplets.

PCL-disulfide-dialkyne (13). Synthesis of the GSH-responsive block 13 to be incorporated into μ3 and μ4 required the use of hexanol (10) as an initiator for the ROP of ε-caprolactone (3). The ^{1}H NMR spectrum of the resulting PCL based product depicted characteristic PCL peaks at 1.39,

1.65, 2.32 and 4.07 ppm. Similar to the earlier disulfide group introduction in 11, the resulting product from above was functionalized with 9 to obtain a PCL chain conjugated to a disulfide containing linker and a free acid end. The latter was coupled to the dipropargylated 12, to yield the disulfide-linked PCL-building block 13. The latter was confirmed by the appearance of two equal triplets at 2.76 and 2.80 ppm which correspond to the now asymmetrical C*H*$_2$-S-S-C*H*$_2$ protons. The subsequent conjugation of this product with 12 showed all the 12-derived peaks including a doublet at 4.70 and a *H*-Ar triplet and doublet at 6.60 and 6.63 ppm, as well as the new shifted singlet at 5.11 ppm.

PCL-monoalkyne core (15). For comparison purposes, and to establish any difference in the properties of the soft nanoparticles, we synthesized building block 15 which was incorporated into the model diblock copolymer b1, analogous to the miktoarm star polymer μ1 constructed from 4. Synthetically, the main difference between 15 and 4 lies in the starting molecule, 14, a monohydroxy version of 1, that was prepared using propargyl bromide (2) to give 4-propargyl benzyl alcohol (Scheme 2.1). It was monitored by the appearance of a doublet at 4.72 and a triplet at 2.54 ppm corresponding to the alkyne proton. ROP of caprolactone (3) was conducted through the hydroxy group as an initiator to yield building block 15. Its ^{1}H NMR showed characteristic PCL peaks at 1.40, 1.66, 2.32, and 4.08 ppm, as well as the downfield shift of the C*H*$_2$-OH singlet from 4.65 in 4-propargyl benzyl alcohol to 5.07 ppm in 15.

2.3.2 Miktoarm star polymers syntheses

Using the above building blocks, we constructed the desired amphiphilic polymers through varied conjugations using either copper catalysed alkyne-azide coupling (CuAAC) or esterification reactions (Scheme 2.2).

Miktoarm star polymer μ1. The ROS responsive μ1 was synthesized through the CuAAC coupling of building blocks 4 and 8 (for details see Scheme A.1). The structure of μ1 was confirmed through ^{1}H NMR by its triazole *H* peak at 7.87 ppm, as well as by the triazole ring-flanking C*H*$_2$ protons at 4.58 and 5.20 ppm.

Miktoarm star polymer μ2. Dual stimuli responsive μ2 was prepared by conjugating the GSH responsive disulfide block 11 to the PCL-OH terminal end of μ1 using Steglich esterification (Scheme A.2). It led to the appearance of the two C*H*$_2$-C*H*$_2$-S-S triplets seen in building block 11

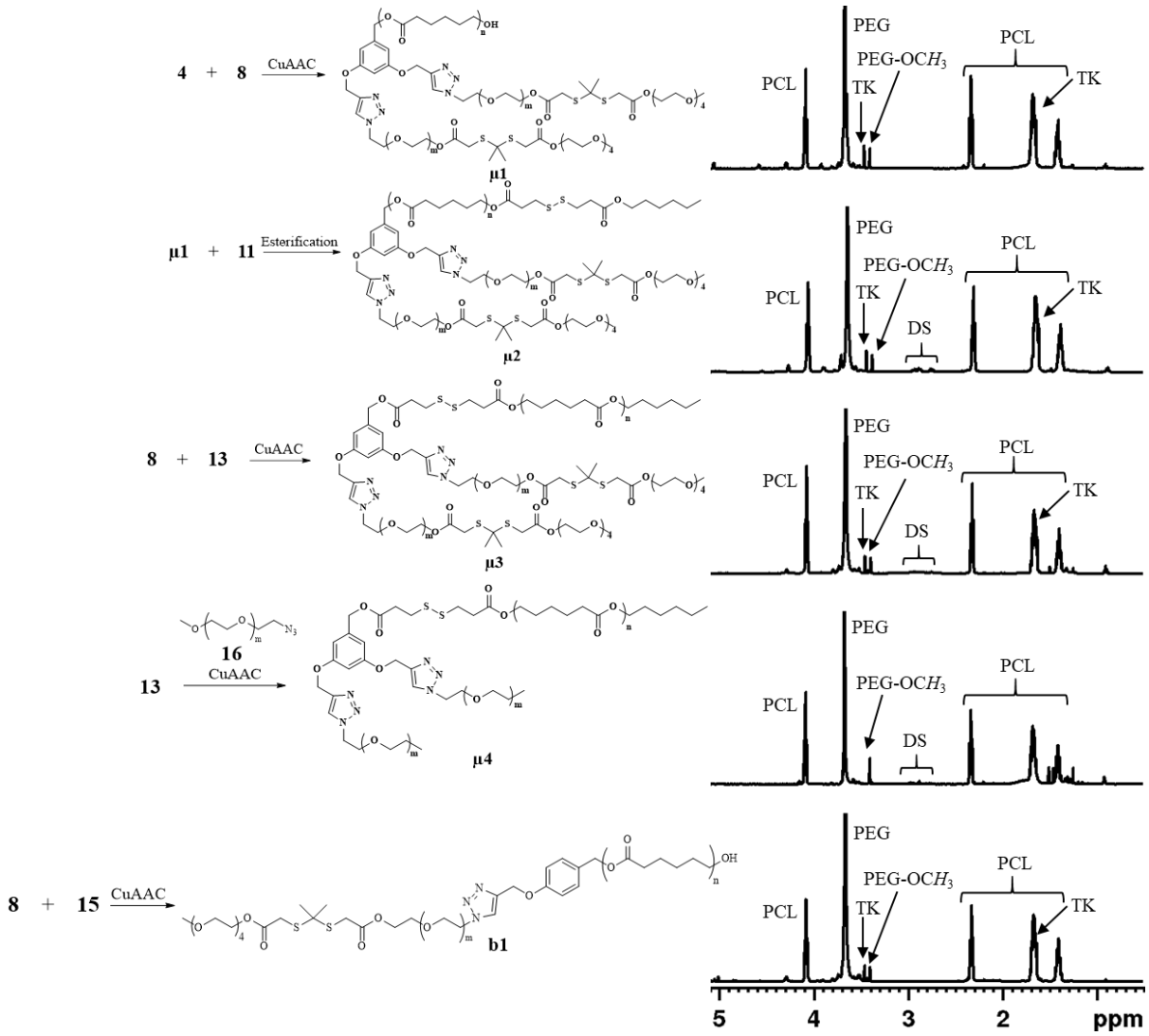

Scheme 2.2. Syntheses of miktoarm star polymers μ1 - μ4 and the diblock co-polymer b1, and their corresponding ^{1}H NMR spectra in $CDCl_3$. For full details, see Schemes A.1-A.5.

clustered around 2.8 ppm. Furthermore, the hexyl group protons were around 0.9 ppm, roughly overlapping with one of the PCL-derived multiplets at 1.39 ppm.

Miktoarm star polymer μ3. The dual stimuli responsive μ3 was synthesized by the CuAAC coupling reaction between the ROS-responsive PEG block 8 and the GSH-responsive PCL block 13 (Scheme A.3). Its ^{1}H NMR showed all of the expected PEG and PCL peaks at roughly the same positions, as well as the appearance of a singlet at 7.73 ppm corresponding to the triazole group formed from the coupling of the azide group in 8 and the terminal alkynes in 13.

Miktoarm star polymer μ4. The GSH-responsive μ4 was constructed using the sequential reaction methodology as described briefly here: PEG_{2000} methyl ether was first

monofunctionalized with tosyl chloride under basic conditions. The monotosylated-PEG was then refluxed with sodium azide to yield the desired azide-PEG hydrophilic arm, 16. Monotosylation of PEG was confirmed by the appearance of peaks at 2.46 ppm and 7.36-7.81 ppm for the C*H*$_3$ and Ar-*H* protons of the tosyl group. A triplet corresponding to C*H*$_2$-OTs was also visible at 4.17 ppm. The substitution of O-Ts with N_3 led to the disappearance of the aforementioned tosyl peaks and appearance of the C*H*$_2$-N_3 triplet at 3.39 ppm. The building block 13 was then coupled with N_3-PEG arm 16 using the CuAAC reaction (Scheme A.4). It preserved the signals derived from both the PEG and PCL-based arms, and the appearance of a new triazole peak at 7.75 ppm.

Diblock polymer b1 was synthesized through the CuAAC coupling of building blocks 8 and 15 (Scheme A.5), and it was verified by the presence of all the relevant peaks from each constituent polymer, as well as the triazole proton at 7.87 ppm.

Miktoarm star polymers µ1-4 and the diblock co-polymer b1 were characterized using NMR and GPC (Figure A.7-A.11).

2.3.3 Self-Assembly

Miktoarm star polymers were soluble in water and organic solvents including acetone, acetonitrile, chloroform, methylene chloride, and tetrahydrofuran. Their aqueous self-assembly was performed using the co-solvent evaporation method (THF/water). The critical micelle concentrations (CMCs) for all the polymers were determined by pyrene fluorescence intensity ratios of 338/333 nm as a function of polymer concentration (Figure 2.2 and Figure A.12-A.16). CMCs were found to be very low (0.21 – 1.2 µM), given the favourable PEG/PCL ratios found in all the polymers (Table 2.1). While CMCs for diblock copolymers have a range from 10^{-4} - 10^{-7} M, we have found in this study and earlier ones that miktoarm star polymers give consistent values in the range of 10^{-7} - 10^{-8} M.[42, 53-57] The disparity among various miktoarm star polymeric architectures (µ1 vs. µ2; and µ1, µ2 vs. µ3, µ4: Table 2.1) may relate to the presence of a disulfide group that can lower the cohesion of micellar cores by decreasing PCL interactions, thus increasing CMC and size.[58-61] The diblock copolymer b1 showed a CMC nearly 6x higher (Figure 2.2, Table 2.1) than that of its analogous miktoarm star polymer, which is in line with those from other block-copolymers, and may be due to the lack of an additional PEG segment, as in a miktoarm star polymer, leading to stabilization of its supramolecular structure (Figure 2.2).[9, 11]

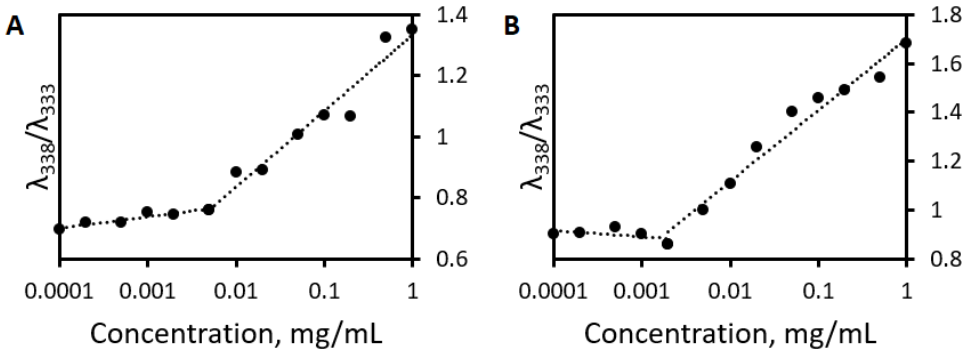

Figure 2.2. CMCs of (A) diblock copolymer b1 and (B) its miktoarm star polymer analogue μ1.

Table 2.1. Critical micelle concentrations and sizes of self-assemblies from miktoarm star polymers (μ1-μ4) and linear diblock copolymer (b1).

			Blank Micelles		Curcumin Loaded	
	Molar Mass[1]	**CMC (μM)**	**Diameter (nm)**	***Đ***	**Diameter (nm)**	***Đ***
μ1	7581	0.21	61.5	0.304	125.9	0.173
μ2	7875	0.44	105.2	0.206	112.3	0.233
μ3	7206	0.90	84.5	0.148	115.7	0.151
μ4	6730	0.77	84.4	0.121	114.7	0.198
b1	4408	1.2	106.4	0.154	129.6	0.159

[1]Molar masses were calculated by summing the mass spectrometry-determined molar masses of constituent building blocks (Table A.1).

Aqueous self-assembly of polymers led to the formation of spherical micelles, as confirmed by TEM (Figure 2.3A-E). Micelle sizes and their distributions were examined with DLS, and all the assembled structures (Table 2.1) were well below 200 nm, a reasonable upper limit used to discern good biological distribution of soft nanoparticles.[8] Curcumin loading consistently increased micelle diameters (Figure A.17-A.21). One would reasonably expect that additional PEG branches in a polymer architecture would decrease the size of derived micelles due to the increase of free space occupied by hydrophilic segments. Following this rationale, diblock copolymer micelles would be expected to be larger than their miktoarm star polymer analogues. Comparison of micellar structures from ROS responsive linear (b1) and miktoarm (μ1) polymeric structures showed that the diblock equivalent of the branched polymer was larger in comparison.

Micelle assemblies were further evaluated using TEM, and images from different miktoarm star polymer assemblies were enumerated and individually measured by relating their diameters to the

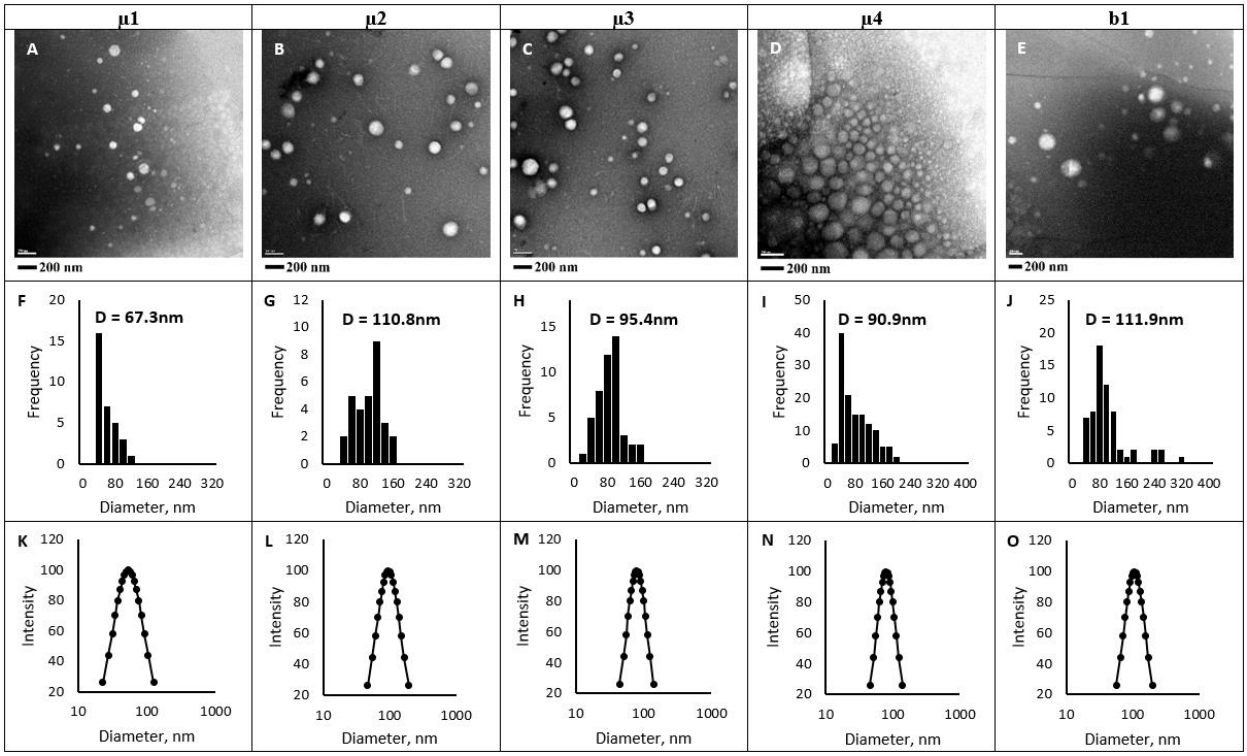

Figure 2.3. (A-E) TEM miktoarm star polymers μ1-4, the diblock copolymer b1, and their respective (F-J) TEM size distributions and (K-O) DLS size distributions.

scale bar. The sizes of spherical micelles derived from μ1-μ4 and b1 roughly corresponded to those obtained from DLS measurements, showing good consistency between these two different techniques (Figure 2.3F-J). The slightly larger sizes seen by TEM may have been the result of sphere flattening upon exposure to the TEM vacuum.[62] In addition, the size distributions seen by TEM paralleled those by DLS, with the TEM-derived ones having a lower normality as a result of the smaller sample size (Figure 2.3K-O).

2.3.4 Drug Loading

Curcumin was chosen as a model drug that is representative of senolytic agents, and it has been shown to have a broad anti-inflammatory response.[39, 40] Considering the purpose of our polymers in specifically targeting sites of oxidative stress, curcumin is additionally appropriate given its role as an antioxidant. With the miktoarm star polymeric architectures reported here, we were able to achieve curcumin encapsulation efficiencies (EEs) of >90%, which are amongst the highest reported values, especially considering the associated loading capacities (LCs) (Table 2.2).[63-68] Encapsulation efficiencies were found to be fairly consistent amongst the miktoarm star polymers. A comparison of the miktoarm star polymer μ1 and the diblock b1 (Table 2.2) fully demonstrates the degree to which a denser corona in micelles from branched architectures can indirectly promote

drug encapsulation. With the additional arm the coronal assemblies are denser, thus stabilizing hydrophobic interactions within micellar cores.[9, 11, 12] Aside from specific polymer-drug structural compatibility, general drug hydrophobicity is the best metric by which one can assess and justify micellar drug loading.[69-72] Thus, curcumin's relatively high hydrophobicity (as seen by its high *log P*) promotes such interactions.[73-75]

Table 2.2. Encapsulation efficiencies and loading capacities of curcumin in micelles from their corresponding miktoarm star polymers (μ1-μ4) and linear diblock co-polymer (b1).

	Encapsulation Efficiency (%)	**Loading Capacity (%)**
μ1	91.8 ± 1.0	31.5 ± 0.23
μ2	92.2 ± 3.9	31.5 ± 0.16
μ3	72.2 ± 8.9	24.1 ± 3.0
μ4	80.4 ± 13	26.5 ± 3.8
b1	42.1 ± 0.59	14.0 ± 0.20

2.3.5 Stimulus Response

The spatial location of the stimulus-responsive units within polymeric architectures, and the degree to which these could influence drug release in the presence of ROS or GSH were subsequently assessed. We were especially intrigued to know if the presence of TK at the end of the hydrophilic PEG segments would change drug release rates in an environment containing elevated ROS levels. After their self-assembly, the ROS response behavior of the μ1 and b1 micelles containing thioketal linkages in their PEG arms was examined using H_2O_2. A 24 hour ^{1}H NMR study in which the blank μ1 micelles were incubated at 37 °C with H_2O_2 in D_2O showed the clear depression of TK-derived C*H*$_3$ and C*H*$_2$ singlets over time with the simultaneous appearance and increase of free thiol S*H* and acetone C*H*$_3$ singlets (Figure 2.4A). Due to the assembly of the polymers as micelles in water, the peaks derived from PCL (2.21 ppm, 1.53 ppm, 1.29 ppm) in the hydrophobic interior take on a broader, less resolved, form. The thioketal C*H*$_3$ is seen as a sharp singlet at 1.55 ppm, overlapping with the broad PCL peak at 1.53. Unlike the ^{1}H NMR of the unassembled μ1 polymer in $CDCl_3$, where the thioketal C*H*$_2$ appears as one singlet, its assembly into micelles splits this signal into two for the variously hydrated halves of the thioketal diacid linker in the micellar corona (3.31 ppm and 3.49 ppm). Following the oxidative cleavage of the thioketal linker in H_2O_2 via successive ^{1}H NMR spectra over time reveals the disappearance of the thioketal C*H*$_3$ at 1.55 ppm

as well as the CH_2 at 3.49 ppm. Interestingly, thioketal cleavage causes similar hydration of resulting CH_2-SH protons which causes them to all merge at the 3.31 ppm position. This is seen by comparing the integration ratio of the 3.31 ppm CH_2 peak to the constant 3.27 ppm TEG-OCH_3 peak. The integration ratio of the two peaks goes from 4.06:6.00 (3.31:3.27 ppm) to 7.48:6.00 over 24 hours of H_2O_2 incubation (Figure A.22). The slightly broader peak at 3.31 ppm makes the immediate comparison by peak height not viable. Since an integration ratio of 8:6 would indicate complete reaction, it suggests that nearly all the ROS-responsive thioketal moieties were cleaved over this time period. Complementing thioketal CH_3 and CH_2 peak disappearance is the appearance of peaks related to the products acetone (CH_3) and the free thiol (SH) at 2.15 and 1.60 ppm respectively. Due to their adjacency to the much more populous PCL peaks, insets are provided on the right in Figure 2.4A for better elucidation. The changes in peaks for the miktoarm star polymer µ1 assembly upon interaction with H_2O_2 can be directly related to the oxidative cleavage of the thioketal diacid molecule similarly incubated in 200 mM H_2O_2. Due to its free nature, complete reaction took place in just over 4 hours (Figure A.23). The diblock co-polymer b1 incubated in H_2O_2 showed a similar reaction behavior by ^{1}H NMR (Figure A.24).

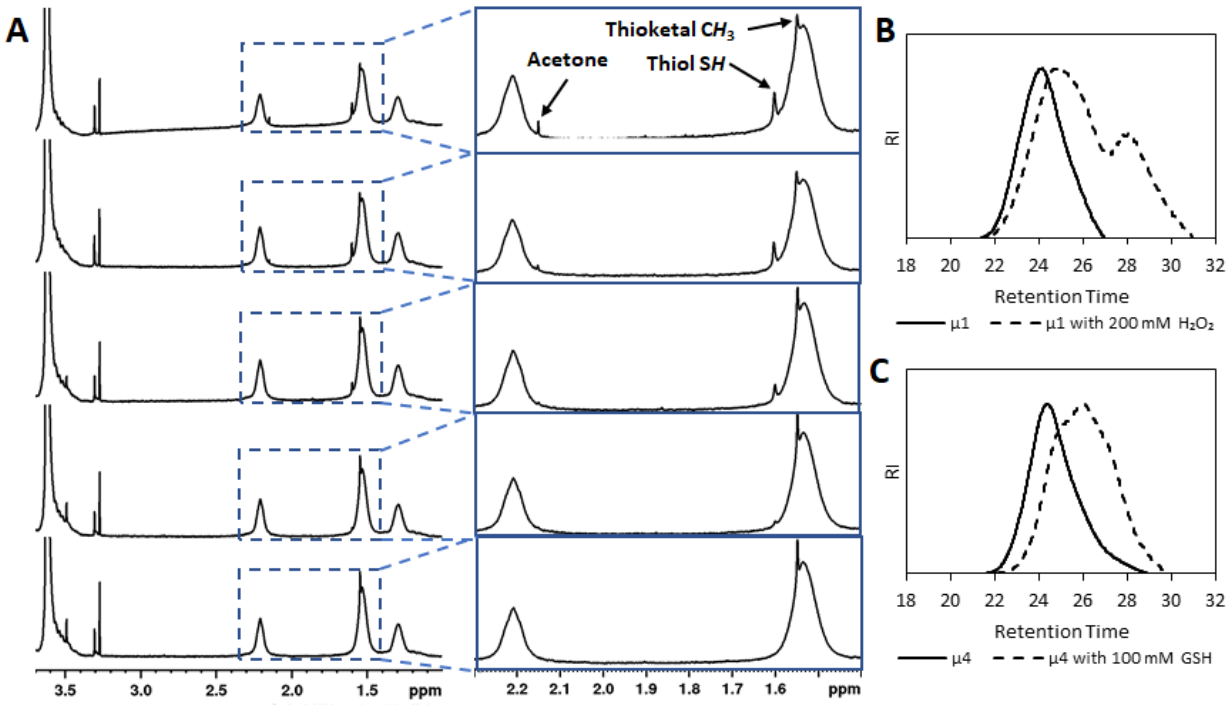

Figure 2.4. (A) Time resolved ^{1}H NMR study of ROS response in µ1 with corresponding insets from boxed areas focused on thioketal peaks; GPC-monitored molecular weight change upon (B) ROS-cleavage in µ1, and (C) GSH-cleavage in µ4.

We subsequently examined the changes in polymeric structure using GPC. Micelles prepared from the aqueous self-assembly of the miktoarm star polymer μ1 were incubated with 200 mM H_2O_2 for a period of 24 hours. Solvent was then removed from the micellar solutions, dissolved (and therefore disassembled) in THF, and then passed through a 0.22 μM syringe filter for analysis. The GPC analysis showed that upon H_2O_2 incubation, polymer molar mass distributions shifted to slightly higher retention times and were followed by newly emerged smaller low molar mass peaks (Figure 2.4B). The block co-polymer b1, which also contains the ROS-sensitive moiety, showed a similar retention time shift corresponding to a slight decrease in molar mass (Figure A.25). These results coupled with the NMR study show that ROS-induced TK degradation leads to the detachment of low molar mass TEG segments from the miktoarm or diblock polymeric units ("*partial corona shedding*") in self-assembled micelles.

Monitoring DS linker cleavage upon exposure to GSH *via* NMR is complicated by the appearance of interfering GSH signals as well as poor resolution of C*H*$_2$-S-S from C*H*$_2$-SH protons in large miktoarm assemblies. We therefore employed GPC analyses as evidence of DS degradation. Miktoarm star polymer μ4 was self-assembled into micelles in an aqueous medium and then incubated with 10 mM GSH for 24 hours. Micellar solutions were then dried, re-dissolved in THF, and passed through a syringe filter. GPC analysis showed that products from the treatment of micelles of μ4 with GSH, had a higher retention time than untreated μ4. The molar mass shift clearly suggested that small polymeric arm structures are formed from the dissociation of core-PEG and PCL segments through disassembly (Figure 2.4C).

To examine if the ROS-responsive micelles would retain their overall structure upon partial corona shedding under oxidative stress, miktoarm star polymer μ1 was self-assembled into micelles, and the micellar diameters were measured by DLS during incubation with 200 mM H_2O_2 over a period of 72 hours. The latter mirrored the exposure of micelles to H_2O_2 during *in vitro* drug release study. Incubated micelles were filtered through a 0.22 μm syringe filter every 24h before measuring their sizes. The diameters of the micellar structures remained relatively consistent (Figure 2.5), demonstrating that the upper corona-shedding does not disrupt the morphology of these micelles.

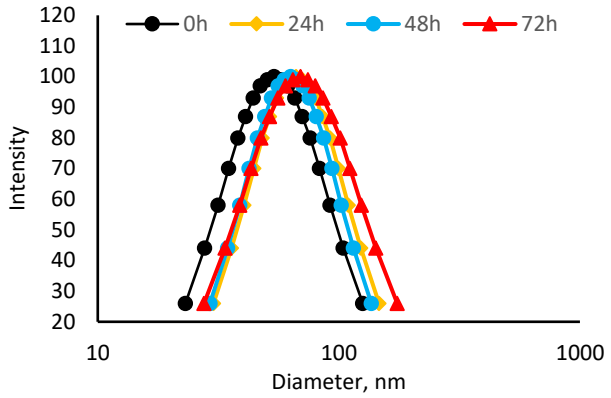

Figure 2.5. Sizes of µ1 micelles measured using DLS over 72 hours of incubation with 200 mM H_2O_2.

2.3.6 Drug Release

Following the experiments confirming structural changes in miktoarm and diblock polymers in response to ROS and GSH, drug loaded polymeric micelles were evaluated for their release kinetics. We were intrigued to examine the role played by the ROS (TK) and GSH (DS) induced bond cleavage and corresponding changes in the micellar corona and core on the release of encapsulated curcumin.

To ascertain that micellar encapsulation of curcumin limited its diffusion out of the structures, a drug release study was also conducted with free curcumin without encapsulation, in which drug solubility was provided by PEG_{750} and dimethylacetamide (Figure A.26). Compared to the free drug (where ~90% of curcumin escaped in about 24h), curcumin release from the micelles without any stimulus was considerably sustained. Roughly 30% of the drug still remained over all the samples after dialysis for 72 hours (Figure 2.6). This result combined with unusually high encapsulation efficiencies suggests good compatibility between curcumin and miktoarm star polymer assemblies.

In polymers containing a TK linker within their PEG arms (µ1, µ2, µ3, and b1), incubation with 200 mM H_2O_2 showed a clear increase in drug release kinetics, suggesting that partial corona shedding leads to the loosening of micellar coronae *via* TK oxidative cleavage. It facilitates the diffusion of drug molecules from within the soft nanoparticles' cores (Figure 2.6A-C, E). In drug loaded micelles, as recent studies have demonstrated, a proportion of the drug molecules is also associated with PEG corona.[51, 79, 80] Thus, "partial corona shedding" would affect drug release both indirectly by aiding in core-to-environment diffusion and directly by freeing drug-associated PEG chains. An interesting distinction can be made between the drug release profiles for miktoarm star

polymer-based and the diblock copolymer micelles. Given its extended and steadier release rate, curcumin diffusion kinetics are heavily influenced by the ROS environment. For example, μ1, μ2, and μ3 miktoarm star polymer-based micelles showed an 10-13% increase in drug release over a dialysis period of 72 hours (Figure 2.6A-C). Notably, b1 micelles showed a smaller 6% increase over this same time period, suggesting that the more loosely packed b1 corona contributes less to limiting the diffusion of encapsulated drug (Figure 2.6E). Provided that drug encapsulation also includes PEG association within the corona, cleavage of a less dense corona would consequently promote drug release to a lesser extent.

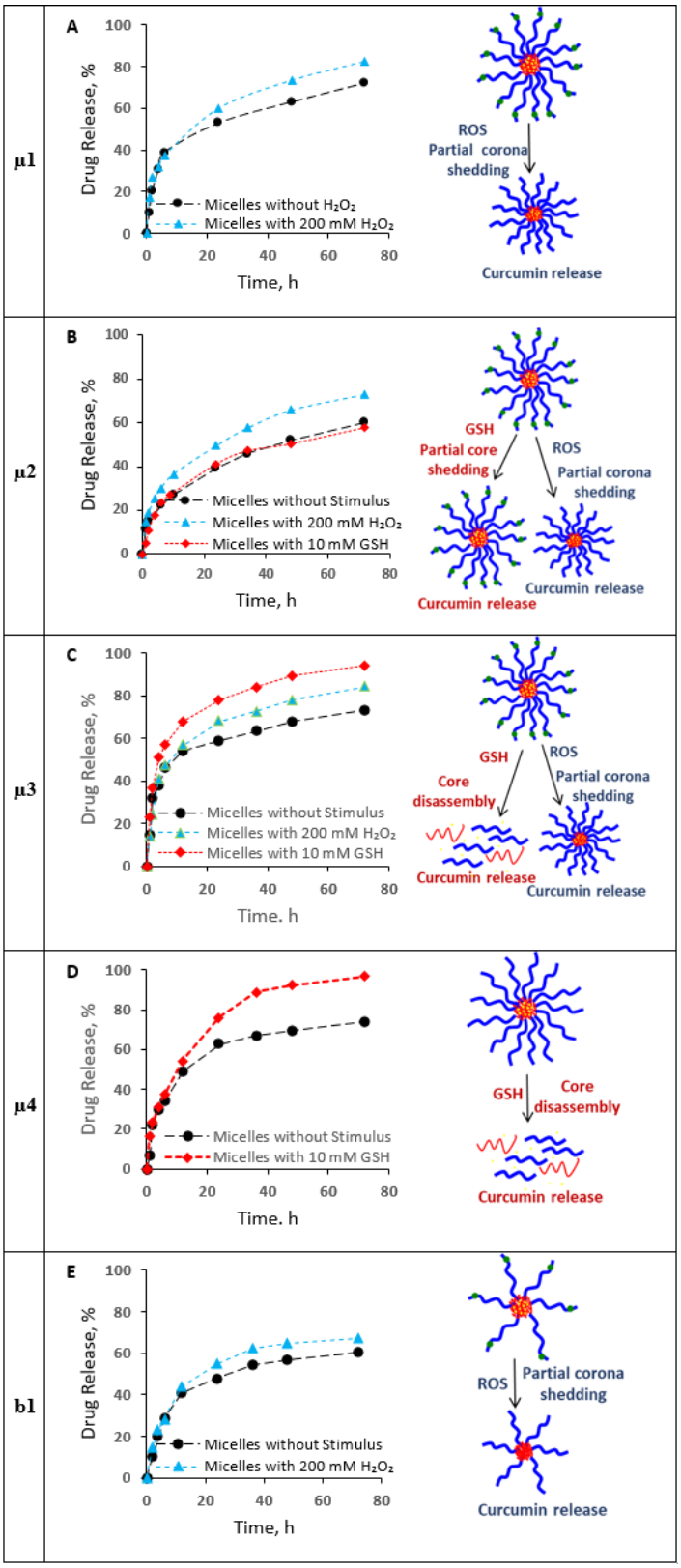

Figure 2.6. Curcumin release profiles of micelles assembled from polymer (A) μ1, (B) μ2, (C) μ3, (D) μ4, and (E) b1.

As ROS-induced partial corona shedding enhanced drug release rates, we continued our investigation by testing a similar core shedding mechanism. Miktoarm star polymer μ2 has a DS group linking a short hydrophobic hexyl unit to the PCL chain end. GSH would cleave the DS, releasing this tail end, and possibly disrupt drug association with micellar cores. Subsequent drug release studies with micelles assembled from μ2 showed that GSH treatment of these micelles showed no significant improvement to release rates, suggesting that while a partial corona shedding mechanism can improve drug release characteristics, a similar partial core-shedding mechanism apparently does not (Figure 2.6B).

In contrast, insertion of a DS unit adjacent to the polymer focal point demonstrated significant influence on drug release upon interaction with GSH. Incubation of micelles of μ3 and μ4 with GSH led to increase in release rates of curcumin by over 20% (Figure 2.6C-D). This result when coupled with the drug release profile for μ2 confirms that spatial location of the GSH responsive unit in miktoarm star polymers plays a crucial role in drug release.

2.3.7 Effectiveness of curcumin-incorporated micelles to scavenge ROS in glioblastoma cells

To assess the ROS scavenging efficiency of the oxidative stress-responsive nanoparticles, U251N human glioblastoma cells were treated with curcumin incorporated or not into μ1 micelles. ROS concentrations were measured using CellROX® Deep Red (λ_{em}, 665 nm). Cell imaging using fluorescence microscopy (Figure 2.7A-B) was complemented with spectrofluorometric measurements of ROS (Figure 2.7C- D). Fluorescence intensities of CellROX® Deep Red were determined in cell lysates and in the cell culture supernatants. Control experiments in cell free media were performed to rule out possible interference with the measurements due to interactions between CellROX® Deep Red and the drug or micelles. There was no significant interference with CellROX® Deep Red fluorescence signals, micelles or drug molecules incorporated into the micelles. (Figure A.27). We treated U251N cells with menadione (MenD) as our positive control for ROS measurements with CellROX® Deep Red.[81, 82] Increased ROS concentrations by menadione showed significant CellROX® fluorescence intensity compared to untreated controls (Figure 2.7A-B). Curcumin, with or without micelle loading, maintained baseline levels of reactive oxygen species comparable to cell control conditions without any drug treatment. Curcumin incorporated into μ1 micelles prevented ROS generation more effectively than free curcumin both within the cells and in the extracellular medium (Figure 2.7C-D). Finally, the effectiveness of

curcumin incorporated in the micelles was determined when cells were deprived from glutathione (by BSO treatment). The ROS-scavenging ability of curcumin was compromised in glutathione-deprived cells. In contrast, curcumin-loaded micelles restored baseline ROS levels (Figure 2.7E-F). These results suggest that curcumin incorporated into micelles may be spared from degradation. However, free curcumin is more susceptible to oxidation in GSH-deprived cells and was less efficient in reducing ROS accumulation due to BSO treatment.[83] These findings suggest that ROS responsive micelles containing curcumin and other drug candidates are suitable stimulus-responsive nanocarriers for ROS scavenging.

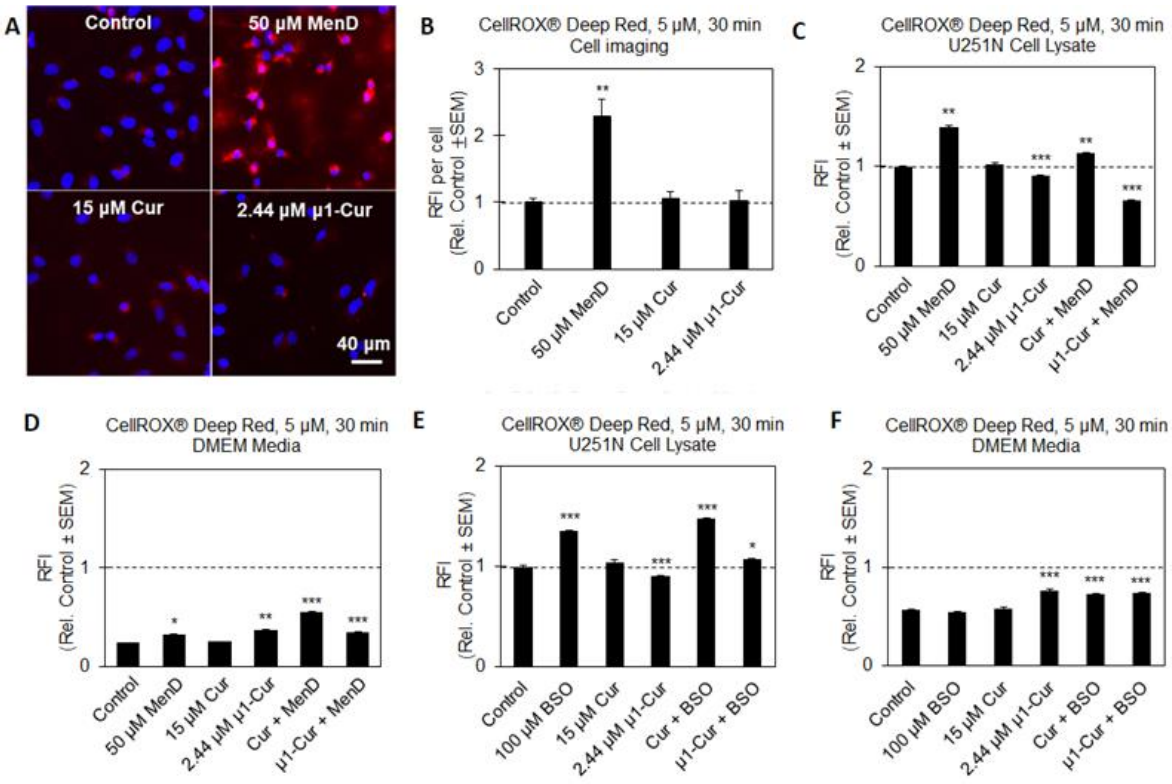

Figure 2.7. U251N glioblastoma cells were pre-treated with ROS inducer, menadione (MenD, 50 µM) for 1 hour, or glutathione inhibitor, L-buthionine-sulfoximine (BSO, 100 µM) for 24 hours. Following pre-treatment, cells were treated with free curcumin (Cur, 15 µM) or curcumin-loaded µ1 (µ1: 2.44 µM; Cur: 15 µM) for 6 hours. CellROX Deep Red (Ex/Em. = 640/665 nm) was added to a final concentration of 5 µM, 30 minutes before the end of the treatment. (B) Cells were fixed and labeled with Hoechst 33342 nuclear dye prior to being imaged with Leica DMI4000B microscope at 20x objective. Intracellular ROS content was assessed by measuring fluorescence intensity of cells. Shown is the average fluorescence intensity per cell relative to untreated control (RFI). 207 to 364 cells were analysed per condition from two independent experiments. Scale bar represents 40 µm. (C-F). The relative fluorescence intensity from (C), (E) cell lysate and (D), (F) cell culture media, was quantified using a spectrofluorometer. Shown are RFI

(relative to control) of U251N cell lysate and DMEM media. Student's t-test, c*ondition vs. control: *p<0.05; **p<0.01, ***p<0.001*

2.4 Conclusions

We have developed a simple and highly versatile methodology to construct environment-selective miktoarm star polymers with tunable placements of stimuli responsive units. Using a mixed arm- and core-first methodology, we demonstrated that our modular miktoarm polymer constructs facilitate the design of smart polymeric architectures for a desired stimulus response, based on the concentrations of active species in extra- and intracellular spaces. We have demonstrated that such soft nanoparticle assemblies respond to reactive oxygen species, shed their upper corona layer *partially*, and accelerate drug release while keeping their overall architectural integrity intact. The denser coronae, lower CMCs, and higher encapsulation efficiencies offered by miktoarm polymers, compared to diblock copolymers, provide a better platform for delivering drugs extracellularly using the novel partial corona shedding route. The curcumin-loaded oxidative stress-responsive micelles from μ1 showed higher efficiencies in preventing ROS-formation and ROS-scavenging in U251 human glioblastoma cells than the free drug, demonstrating the efficacy of our delivery system. The spatial location of the GSH responsive unit has a direct influence on the drug release characteristics of the soft nanoparticles. A small perturbance by *partial* inner core shedding at the hydrophobic end, in response to GSH, did not have a similar subtle effect in enhancing drug release. However, DS incorporation near the core of a polymer leads to micelles that degrade and liberate encapsulated drug in response to GSH. This also expedites PEG and PCL biodegradation. The particular combination of ROS- and GSH-responsive mechanisms, as implemented in μ3, represents a new mode of drug delivery by which release can be promoted in a stepwise fashion, as nanoparticles accumulate at diseased sites and are then taken up by cells. Such synthetic articulation of miktoarm star polymers, their self-assembly into nanoparticles with very low CMCs that carry sufficient amount of active pharmaceutical agents, and their response to stimuli in the external and internal cellular environment, is expected to improve interventions in pathologies associated with disturbed redox states in affected cells and their microenvironments.

2.5 References

1. Tran, S.; DeGiovanni, P.-J.; Piel, B.; Rai, P., Cancer nanomedicine: a review of recent success in drug delivery. *Clin. Transl. Med.* **2017,** *6* (1), 44.
2. Meng, Q.; Hu, H.; Zhou, L.; Zhang, Y.; Yu, B.; Shen, Y.; Cong, H., Logical design and application of prodrug platforms. *Polym. Chem.* **2019,** *10* (3), 306-324.
3. Hunter, A. C.; Moghimi, S. M., Smart polymers in drug delivery: a biological perspective. *Polym. Chem.* **2017,** *8* (1), 41-51.
4. Zhao, J.; Stenzel, M. H., Entry of nanoparticles into cells: the importance of nanoparticle properties. *Polym. Chem.* **2018,** *9* (3), 259-272.
5. Kakkar, A.; Traverso, G.; Farokhzad, O. C.; Weissleder, R.; Langer, R., Evolution of macromolecular complexity in drug delivery systems. *Nat. Rev. Chem.* **2017,** *1* (8), 63.
6. Kim, S.; Shi, Y.; Kim, J. Y.; Park, K.; Cheng, J.-X., Overcoming the barriers in micellar drug delivery: loading efficiency, in vivo stability, and micelle–cell interaction. *Expert Opin. Drug Del.* **2010,** *7* (1), 49-62.
7. Englert, C.; Brendel, J. C.; Majdanski, T. C.; Yildirim, T.; Schubert, S.; Gottschaldt, M.; Windhab, N.; Schubert, U. S., Pharmapolymers in the 21st century: Synthetic polymers in drug delivery applications. *Prog. Polym. Sci.* **2018,** *87*, 107-164.
8. Moghimi, S. M.; Hunter, A. C.; Murray, J. C., Long-Circulating and Target-Specific Nanoparticles: Theory to Practice. *Pharmacol. Rev.* **2001,** *53* (2), 283.
9. Yoon, K.; Kang, H. C.; Li, L.; Cho, H.; Park, M.-K.; Lee, E.; Bae, Y. H.; Huh, K. M., Amphiphilic poly(ethylene glycol)-poly(ε-caprolactone) AB2 miktoarm copolymers for self-assembled nanocarrier systems: synthesis, characterization, and effects of morphology on antitumor activity. *Polym. Chem.* **2015,** *6* (4), 531-542.
10. Khanna, K.; Varshney, S.; Kakkar, A., Miktoarm star polymers: advances in synthesis, self-assembly, and applications. *Polym. Chem.* **2010,** *1* (8), 1171-1185.
11. Pispas, S.; Hadjichristidis, N.; Potemkin, I.; Khokhlov, A., Effect of Architecture on the Micellization Properties of Block Copolymers: A2B Miktoarm Stars vs AB Diblocks. *Macromolecules* **2000,** *33* (5), 1741-1746.
12. Hadjichristidis, N.; Pitsikalis, M.; Iatrou, H.; Driva, P.; Sakellariou, G.; Chatzichristidi, M., 6.03 - Polymers with Star-Related Structures: Synthesis, Properties, and Applications. In *Polymer Science: A Comprehensive Reference*, Matyjaszewski, K.; Möller, M., Eds. Elsevier: Amsterdam, 2012; pp 29-111.
13. Nieto-Orellana, A.; Di Antonio, M.; Conte, C.; Falcone, F. H.; Bosquillon, C.; Childerhouse, N.; Mantovani, G.; Stolnik, S., Effect of polymer topology on non-covalent polymer–protein complexation: miktoarm versus linear mPEG-poly(glutamic acid) copolymers. *Polym. Chem.* **2017,** *8* (14), 2210-2220.
14. Wais, U.; Liu, J.; He, T.; Zhang, H., CHAPTER 5 Micellar and Emulsion-Assisted Drug Delivery: Comparison of Miktoarm Star Polymers and Block Copolymers. In *Miktoarm Star Polymers: From Basics of Branched Architecture to Synthesis, Self-assembly and Applications*, The Royal Society of Chemistry: 2017; pp 116-149.
15. Aghajanzadeh, M.; Zamani, M.; Rostamizadeh, K.; Sharafi, A.; Danafar, H., The role of miktoarm star copolymers in drug delivery systems. *J. Macromol. Sci. Part A* **2018,** *55* (7), 559-571.
16. Zhao, X.; Zhang, J.; Zhao, Y., Synthesis and properties of penta-responsive ABC star quaterpolymers. *Polym. J.* **2020,** *52* (1), 153-163.

17. Li, H.; Li, Y.; Xiao, Y.; Zhang, B.; Cheng, Z.; Shi, J.; Xiong, J.; Li, Z.; Zhang, K., Well-Defined DNA–Polymer Miktoarm Stars for Enzyme-Resistant Nanoflares and Carrier-Free Gene Regulation. *Bioconjugate Chem.* **2020,** *31* (3), 530-536.
18. Karatzas, A.; Haataja, J. S.; Skoulas, D.; Bilalis, P.; Varlas, S.; Apostolidi, P.; Sofianopoulou, S.; Stratikos, E.; Houbenov, N.; Ikkala, O.; Iatrou, H., Marcromolecular Architecture and Encapsulation of the Anticancer Drug Everolimus Control the Self-Assembly of Amphiphilic Polypeptide-Containing Hybrids. *Biomacromolecules* **2019,** *20* (12), 4546-4562.
19. Chong, Y. K.; Zainol, I.; Ng, C. H.; Ooi, I. H., Miktoarm star polymers nanocarrier: synthesis, characterisation, and in-vitro drug release study. *J. Polym. Res.* **2019,** *26* (3), 79.
20. Nieto-Orellana, A.; Li, H.; Rosiere, R.; Wauthoz, N.; Williams, H.; Monteiro, C. J.; Bosquillon, C.; Childerhouse, N.; Keegan, G.; Coghlan, D.; Mantovani, G.; Stolnik, S., Targeted PEG-poly(glutamic acid) complexes for inhalation protein delivery to the lung. *J. Control. Release* **2019,** *316*, 250-262.
21. Zhang, Y.; Bradley, M.; Geng, J., Photo-controlled one-pot strategy for the synthesis of asymmetric three-arm star polymers. *Polym. Chem.* **2019,** *10* (35), 4769-4773.
22. Augustine, D.; Hadjichristidis, N.; Gnanou, Y.; Feng, X., Hydrophilic Stars, Amphiphilic Star Block Copolymers, and Miktoarm Stars with Degradable Polycarbonate Cores. *Macromolecules* **2020,** *53* (3), 895-904.
23. Levi, A. E.; Fu, L.; Lequieu, J.; Horne, J. D.; Blankenship, J.; Mukherjee, S.; Zhang, T.; Fredrickson, G. H.; Gutekunst, W. R.; Bates, C. M., Efficient Synthesis of Asymmetric Miktoarm Star Polymers. *Macromolecules* **2020,** *53* (2), 702-710.
24. Ge, Y.; Chen, C.; Sim, X. M.; Zheng, J.; Goto, A., Synthesis of ABC Miktoarm Star Copolymers via Organocatalyzed Living Radical Polymerization. *Macromol. Rapid Commun.* **2020,** *41* (5), 1900623.
25. Teng, X.; Zhang, P.; Liu, T.; Xin, J.; Zhang, J., Biobased miktoarm star copolymer from soybean oil, isosorbide, and caprolactone. *J. Appl. Polym. Sci.* **2020,** *137* (2), 48281.
26. Skandalis, A.; Pispas, S., Synthesis of (AB)n-, AnBn-, and AxBy-type amphiphilic and double-hydrophilic star copolymers by RAFT polymerization. *J. Polym. Sci. A Polym. Chem.* **2019,** *57* (16), 1771-1783.
27. Burhans, W. C.; Heintz, N. H., The cell cycle is a redox cycle: Linking phase-specific targets to cell fate. *Free Radical Biol. Med.* **2009,** *47* (9), 1282-1293.
28. Ye, H.; Zhou, Y.; Liu, X.; Chen, Y.; Duan, S.; Zhu, R.; Liu, Y.; Yin, L., Recent Advances on Reactive Oxygen Species-Responsive Delivery and Diagnosis System. *Biomacromolecules* **2019,** *20* (7), 2441-2463.
29. Yin, W.; Ke, W.; Chen, W.; Xi, L.; Zhou, Q.; Mukerabigwi, J. F.; Ge, Z., Integrated block copolymer prodrug nanoparticles for combination of tumor oxidative stress amplification and ROS-responsive drug release. *Biomaterials* **2019,** *195*, 63-74.
30. Wei, M.; Gao, Y.; Li, X.; Serpe, M. J., Stimuli-responsive polymers and their applications. *Polym. Chem.* **2017,** *8* (1), 127-143.
31. Sabourian, P.; Tavakolian, M.; Yazdani, H.; Frounchi, M.; van de Ven, T. G. M.; Maysinger, D.; Kakkar, A., Stimuli-responsive chitosan as an advantageous platform for efficient delivery of bioactive agents. *J. Control. Release* **2020,** *317*, 216-231.
32. Chen, D.; Zhang, G.; Li, R.; Guan, M.; Wang, X.; Zou, T.; Zhang, Y.; Wang, C.; Shu, C.; Hong, H.; Wan, L.-J., Biodegradable, Hydrogen Peroxide, and Glutathione Dual Responsive Nanoparticles for Potential Programmable Paclitaxel Release. *J. Am. Chem. Soc.* **2018,** *140* (24), 7373-7376.

33. Yu, L.-Y.; Shen, Y.-A.; Chen, M.-H.; Wen, Y.-H.; Hsieh, P.-I.; Lo, C.-L., The feasibility of ROS- and GSH-responsive micelles for treating tumor-initiating and metastatic cancer stem cells. *J. Mater. Chem. B* **2019,** *7* (19), 3109-3118.
34. Luo, C.; Sun, J.; Liu, D.; Sun, B.; Miao, L.; Musetti, S.; Li, J.; Han, X.; Du, Y.; Li, L.; Huang, L.; He, Z., Self-Assembled Redox Dual-Responsive Prodrug-Nanosystem Formed by Single Thioether-Bridged Paclitaxel-Fatty Acid Conjugate for Cancer Chemotherapy. *Nano Lett.* **2016,** *16* (9), 5401-5408.
35. Yin, W.; Ke, W.; Lu, N.; Wang, Y.; Japir, A. A.-W. M. M.; Mohammed, F.; Wang, Y.; Pan, Y.; Ge, Z., Glutathione and Reactive Oxygen Species Dual-Responsive Block Copolymer Prodrugs for Boosting Tumor Site-Specific Drug Release and Enhanced Antitumor Efficacy. *Biomacromolecules* **2020,** *21* (2), 921-929.
36. Chen, R.; Ma, Z.; Xiang, Z.; Xia, Y.; Shi, Q.; Wong, S.-C.; Yin, J., Hydrogen Peroxide and Glutathione Dual Redox-Responsive Nanoparticles for Controlled DOX Release. *Macromol. Biosci.* **2020,** *20* (2), 1900331.
37. Jazani, A. M.; Arezi, N.; Shetty, C.; Hong, S. H.; Li, H.; Wang, X.; Oh, J. K., Tumor-targeting intracellular drug delivery based on dual acid/reduction-degradable nanoassemblies with ketal interface and disulfide core locations. *Polym. Chem.* **2019,** *10* (22), 2840-2853.
38. Zhang, D.; Fourie-O'Donohue, A.; Dragovich, P. S.; Pillow, T. H.; Sadowsky, J. D.; Kozak, K. R.; Cass, R. T.; Liu, L.; Deng, Y.; Liu, Y.; Hop, C. E.; Khojasteh, S. C., Catalytic cleavage of disulfide bonds in small molecules and linkers of antibody- drug conjugates. *Drug Metab. Dispos.* **2019**, dmd.118.086132.
39. Bielak-Zmijewska, A.; Grabowska, W.; Ciolko, A.; Bojko, A.; Mosieniak, G.; Bijoch, Ł.; Sikora, E., The Role of Curcumin in the Modulation of Ageing. *Int. J. Mol. Sci.* **2019,** *20* (5), 1239.
40. Jacob, A.; Wu, R.; Zhou, M.; Wang, P., Mechanism of the Anti-inflammatory Effect of Curcumin: PPAR-gamma Activation. *PPAR Res.* **2007,** *2007*, 89369-89369.
41. Kulkarni, S. S.; Cantó, C., The molecular targets of resveratrol. *Biochim. Biophys. Acta Mol. Basis Dis.* **2015,** *1852* (6), 1114-1123.
42. Lu, Y.; Zhang, E.; Yang, J.; Cao, Z., Strategies to improve micelle stability for drug delivery. *Nano Res.* **2018,** *11* (10), 4985-4998.
43. Lu, L.; Zhang, Q.; Wootton, D.; Chiou, R.; Li, D.; Lu, B.; Lelkes, P.; Zhou, J., Biocompatibility and biodegradation studies of PCL/β-TCP bone tissue scaffold fabricated by structural porogen method. *J. Mater. Sci. Mater. Med.* **2012,** *23* (9), 2217-2226.
44. Salgado, C. L.; Sanchez, E. M. S.; Zavaglia, C. A. C.; Granja, P. L., Biocompatibility and biodegradation of polycaprolactone-sebacic acid blended gels. *J. Biomed. Mater. Res. Part A* **2012,** *100A* (1), 243-251.
45. Neises, B.; Steglich, W., Simple Method for the Esterification of Carboxylic Acids. *Angew. Chem. Int. Ed.* **1978,** *17* (7), 522-524.
46. Moore, J. S.; Stupp, S. I., Room temperature polyesterification. *Macromolecules* **1990,** *23* (1), 65-70.
47. Rostovtsev, V. V.; Green, L. G.; Fokin, V. V.; Sharpless, K. B., A Stepwise Huisgen Cycloaddition Process: Copper(I)-Catalyzed Regioselective "Ligation" of Azides and Terminal Alkynes. *Angew. Chem. Int. Ed.* **2002,** *41* (14), 2596-2599.
48. Meldal, M.; Tornøe, C. W., Cu-Catalyzed Azide−Alkyne Cycloaddition. *Chem. Rev.* **2008,** *108* (8), 2952-3015.

49. Liu, Q.; Chen, Y., Synthesis of well-defined macromonomers by the combination of atom transfer radical polymerization and a click reaction. *J. Polym. Sci A Polym. Chem.* **2006,** *44* (20), 6103-6113.
50. Grinberg, Y. Y.; Dibbern, M. E.; Levasseur, V. A.; Kraig, R. P., Insulin-like growth factor-1 abrogates microglial oxidative stress and TNF-α responses to spreading depression. *J. Neurochem.* **2013,** *126* (5), 662-672.
51. Moquin, A.; Sturn, J.; Zhang, I.; Ji, J.; von Celsing, R.; Vali, H.; Maysinger, D.; Kakkar, A., Unraveling Aqueous Self-Assembly of Telodendrimers to Shed Light on Their Efficacy in Drug Encapsulation. *ACS Appl. Bio Mater.* **2019,** *2* (10), 4515-4526.
52. Seidler, C.; Ng, D. Y. W.; Wu, Y.; Weil, T., pH responsive supramolecular core-shell protein hybrids. *Supramol. Chem.* **2016,** *28* (9-10), 742-746.
53. Yoshida, E., Control of Micellar Size and Critical Micelle Concentration for "Nonamphiphilic" Poly(vinyl phenol)-block-Polystyrene Diblock Copolymers. *Polym. J.* **2003,** *35* (12), 965-971.
54. Lo, C.-L.; Lin, S.-J.; Tsai, H.-C.; Chan, W.-H.; Tsai, C.-H.; Cheng, C.-H. D.; Hsiue, G.-H., Mixed micelle systems formed from critical micelle concentration and temperature-sensitive diblock copolymers for doxorubicin delivery. *Biomaterials* **2009,** *30* (23), 3961-3970.
55. Kosa, S. A.; Al-Harbi, L. M.; Baloch, M. K.; Ullah, I.; El-Mossalamy, E. H., Impact of Block Length and Temperature over Self-Assembling Behavior of Block Copolymers. *Int. Journal Polym. Sci.* **2016,** *2016*, 7.
56. Kulthe, S. S.; Choudhari, Y. M.; Inamdar, N. N.; Mourya, V., Polymeric micelles: authoritative aspects for drug delivery. *Des. Monomers Polym.* **2012,** *15* (5), 465-521.
57. Soliman, G. M.; Sharma, R.; Choi, A. O.; Varshney, S. K.; Winnik, F. M.; Kakkar, A. K.; Maysinger, D., Tailoring the efficacy of nimodipine drug delivery using nanocarriers based on A2B miktoarm star polymers. *Biomaterials* **2010,** *31* (32), 8382-8392.
58. Maibaum, L.; Dinner, A. R.; Chandler, D., Micelle Formation and the Hydrophobic Effect. *J. Phys. Chem. B* **2004,** *108* (21), 6778-6781.
59. Van Domeselaar, G. H.; Kwon, G. S.; Andrew, L. C.; Wishart, D. S., Application of solid phase peptide synthesis to engineering PEO–peptide block copolymers for drug delivery. *Colloids Surf. B* **2003,** *30* (4), 323-334.
60. Owen, S. C.; Chan, D. P. Y.; Shoichet, M. S., Polymeric micelle stability. *Nano Today* **2012,** *7* (1), 53-65.
61. Gaucher, G.; Dufresne, M.-H.; Sant, V. P.; Kang, N.; Maysinger, D.; Leroux, J.-C., Block copolymer micelles: preparation, characterization and application in drug delivery. *J. Control. Release* **2005,** *109* (1), 169-188.
62. Yu, S.; Azzam, T.; Rouiller, I.; Eisenberg, A., "Breathing" Vesicles. *J. Am. Chem. Soc.* **2009,** *131* (30), 10557-10566.
63. Hasan, M.; Elkhoury, K.; Kahn, C. J. F.; Arab-Tehrany, E.; Linder, M., Preparation, Characterization, and Release Kinetics of Chitosan-Coated Nanoliposomes Encapsulating Curcumin in Simulated Environments. *Molecules* **2019,** *24* (10), 2023.
64. Obeid, M. A.; Khadra, I.; Albaloushi, A.; Mullin, M.; Alyamani, H.; Ferro, V. A., Microfluidic manufacturing of different niosomes nanoparticles for curcumin encapsulation: Physical characteristics, encapsulation efficacy, and drug release. *Beilstein J. Nanotechnol.* **2019,** *10*, 1826-1832.
65. De Leo, V.; Milano, F.; Mancini, E.; Comparelli, R.; Giotta, L.; Nacci, A.; Longobardi, F.; Garbetta, A.; Agostiano, A.; Catucci, L., Encapsulation of Curcumin-Loaded Liposomes for

Colonic Drug Delivery in a pH-Responsive Polymer Cluster Using a pH-Driven and Organic Solvent-Free Process. *Molecules* **2018,** *23* (4), 739.
66. Alqahtani, M. S.; Alqahtani, A.; Al-Thabit, A.; Roni, M.; Syed, R., Novel lignin nanoparticles for oral drug delivery. *J. Mater. Chem. B* **2019,** *7* (28), 4461-4473.
67. Akolade, J. O.; Oloyede, H. O. B.; Salawu, M. O.; Amuzat, A. O.; Ganiyu, A. I.; Onyenekwe, P. C., Influence of formulation parameters on encapsulation and release characteristics of curcumin loaded in chitosan-based drug delivery carriers. *J. Drug Delivery Sci. Technol.* **2018,** *45*, 11-19.
68. Bilas, R.; Sriram, K.; Maheswari, P. U.; Sheriffa Begum, K. M. M., Highly biocompatible chitosan with super paramagnetic calcium ferrite (CaFe2O4) nanoparticle for the release of ampicillin. *Int. J. Biol. Macromol.* **2017,** *97*, 513-525.
69. Basak, R.; Bandyopadhyay, R., Encapsulation of Hydrophobic Drugs in Pluronic F127 Micelles: Effects of Drug Hydrophobicity, Solution Temperature, and pH. *Langmuir* **2013,** *29* (13), 4350-4356.
70. Kabanov, A. V.; Alakhov, V. Y., Pluronic block copolymers in drug delivery: from micellar nanocontainers to biological response modifiers. *Crit. Rev. Ther. Drug Carrier Syst.* **2002,** *19* (1), 1-72.
71. Allen, C.; Maysinger, D.; Eisenberg, A., Nano-engineering block copolymer aggregates for drug delivery. *Colloids Surf. B* **1999,** *16* (1), 3-27.
72. Hurter, P. N.; Scheutjens, J. M. H. M.; Hatton, T. A., Molecular modeling of micelle formation and solubilization in block copolymer micelles. 2. Lattice theory for monomers with internal degrees of freedom. *Macromolecules* **1993,** *26* (19), 5030-5040.
73. Wishart, D. S.; Knox, C.; Guo, A. C.; Shrivastava, S.; Hassanali, M.; Stothard, P.; Chang, Z.; Woolsey, J., DrugBank: a comprehensive resource for in silico drug discovery and exploration. *Nucleic Acids Res.* **2006,** *34* (Database issue), D668-D672.
74. Wishart, D. S.; Feunang, Y. D.; Guo, A. C.; Lo, E. J.; Marcu, A.; Grant, J. R.; Sajed, T.; Johnson, D.; Li, C.; Sayeeda, Z.; Assempour, N.; Iynkkaran, I.; Liu, Y.; Maciejewski, A.; Gale, N.; Wilson, A.; Chin, L.; Cummings, R.; Le, D.; Pon, A.; Knox, C.; Wilson, M., DrugBank 5.0: a major update to the DrugBank database for 2018. *Nucleic Acids Res.* **2018,** *46* (D1), D1074-D1082.
75. Tetko, I. V.; Gasteiger, J.; Todeschini, R.; Mauri, A.; Livingstone, D.; Ertl, P.; Palyulin, V. A.; Radchenko, E. V.; Zefirov, N. S.; Makarenko, A. S.; Tanchuk, V. Y.; Prokopenko, V. V., Virtual Computational Chemistry Laboratory – Design and Description. *J. Comput. Aid. Mol. Des.* **2005,** *19* (6), 453-463.
76. Imanishi, K.; Einaga, Y., Effects of Hydrophilic Chain Length on the Characteristics of the Micelles of Pentaoxyethylene n-Decyl C10E5 and Hexaoxyethylene n-Decyl C10E6 Ethers. *J. Phys. Chem. B* **2005,** *109* (15), 7574-7581.
77. Oliver, R. C.; Lipfert, J.; Fox, D. A.; Lo, R. H.; Doniach, S.; Columbus, L., Dependence of Micelle Size and Shape on Detergent Alkyl Chain Length and Head Group. *PLoS One* **2013,** *8* (5), e62488.
78. Breyton, C.; Gabel, F.; Abla, M.; Pierre, Y.; Lebaupain, F.; Durand, G.; Popot, J.-L.; Ebel, C.; Pucci, B., Micellar and biochemical properties of (hemi)fluorinated surfactants are controlled by the size of the polar head. *Biophys. J.* **2009,** *97* (4), 1077-1086.
79. Li, Z.; Johnson, L. M.; Ricarte, R. G.; Yao, L. J.; Hillmyer, M. A.; Bates, F. S.; Lodge, T. P., Enhanced Performance of Blended Polymer Excipients in Delivering a Hydrophobic Drug through the Synergistic Action of Micelles and HPMCAS. *Langmuir* **2017,** *33* (11), 2837-2848.

80. Li, Z.; Lenk, T. I.; Yao, L. J.; Bates, F. S.; Lodge, T. P., Maintaining Hydrophobic Drug Supersaturation in a Micelle Corona Reservoir. *Macromolecules* **2018,** *51* (2), 540-551.
81. Loor, G.; Kondapalli, J.; Schriewer, J. M.; Chandel, N. S.; Vanden Hoek, T. L.; Schumacker, P. T., Menadione triggers cell death through ROS-dependent mechanisms involving PARP activation without requiring apoptosis. *Free Radical Biol. Med.* **2010,** *49* (12), 1925-1936.
82. Criddle, D. N.; Gillies, S.; Baumgartner-Wilson, H. K.; Jaffar, M.; Chinje, E. C.; Passmore, S.; Chvanov, M.; Barrow, S.; Gerasimenko, O. V.; Tepikin, A. V.; Sutton, R.; Petersen, O. H., Menadione-induced Reactive Oxygen Species Generation via Redox Cycling Promotes Apoptosis of Murine Pancreatic Acinar Cells. *J. Biol. Chem.* **2006,** *281* (52), 40485-40492.
83. Awasthi, S.; Pandya, U.; Singhal, S. S.; Lin, J. T.; Thiviyanathan, V.; Seifert, W. E.; Awasthi, Y. C.; Ansari, G. A. S., Curcumin–glutathione interactions and the role of human glutathione S-transferase P1-1. *Chem. Biol. Interact.* **2000,** *128* (1), 19-38.

Chapter 3: Evaluation of resveratrol loading and release from ROS- and GSH-responsive AB_2 miktoarm star polymer micelles

Abstract

Asymmetrically branching star polymers have shown great promise in drug delivery in general, and better control over cargo loading and release in particular, compared to traditional block copolymer-based nanocarriers. Using our recently developed methodology to stimuli-responsive miktoarm stars, we synthesized ROS- and GSH-responsive AB_2 (A = PCL, B = PEG) miktoarm polymers for examining loading and release characteristics of resveratrol, a common model anti-inflammatory drug. ROS is abundant extracellularly around disease sites, and while responsible for biological oxidative stress, it is commonly targeted to increase the efficacy of targeted drug delivery systems. GSH, on the other hand, is overproduced intracellularly, allowing the use of redox-responsive drug delivery systems with vastly different response mechanisms. Incorporation of a thioketal linker at the terminus of hydrophilic PEG segments in miktoarm stars subtly promoted resveratrol release when self-assembled micelles were treated with H_2O_2 due to the partial corona "shedding" of loaded micelles. Miktoarm star polymers with disulfide linkers adjacent to their core junctions responded to GSH through disulfide reduction, and subsequent disassembly, and PEG and PCL separation. GSH treatment of self-assembled micelles with loaded resveratrol resulted in its significant burst release.

3.1 Introduction

Despite the incredible advancements in drug design and discovery, most drugs either fail or perform inadequately at clinical trials due to their poor bioavailability that is typically attributed to hydrophobicity and early biodegradation.[1, 2] To combat this, nano-delivery systems have been developed that are capable of encapsulating drugs and effectively delivering them to diseased sites.[3, 4] Such systems are often micellar, and they are usually composed of amphiphilic block copolymers where the hydrophobic segment constitutes the core of the micelles and helps to encapsulate drug cargo. The outer corona of micelles is composed of the hydrophilic polymer segment and solubilizes the micelle in aqueous media enabling its biological distribution and drug delivery.[5, 6]

Miktoarm stars integrate at least 3 polymeric chains emanating from a single junction, of which at least 2 are different. These asymmetric star polymers can generally be classified as being of A_nB_m compositions, where A and B represent different polymer chains of varied numbers (n, m). Amphiphilic miktoarm polymers present several key advantages over the more commonly used diblock copolymers in nanomedicine: most notably their low critical micelle concentrations (CMC), smaller diameters and high loading capacities.[7-10] Micelles assembled from AB_n miktoarm polymers where B is the hydrophilic segment have been shown to possess denser coronae than those formed from diblock copolymers.[11] Thus, it follows that incorporating stimulus responsive units into the structure of hydrophilic polymers would enable them to more densely populate the corona of miktoarm polymer micelles. Due to its ubiquity, aqueous solubility, biological compatibility, stealth, and ease of synthetic manipulation, we have used poly(ethylene glycol) (PEG) as the hydrophilic segment of our miktoarm polymers.[12, 13] Hydrophobic polycaprolactone (PCL) provides biocompatibility, biodegradability, and can be synthesized through simple polymerization with a range of miktoarm polymer compatible initiators.[14-16] It was demonstrated in Chapter 2 that such AB_2 type miktoarm polymers (A = PCL, B = PEG) which contain a ROS-responsive thioketal (TK) at the terminal PEG ends, which constitutes upper micellar corona, respond more efficiently to ROS in the aqueous medium than their diblock copolymer counterparts. Incorporation of ROS-responsive units into micellar coronae offers another unique advantage, as diseased sites predominantly contain ROS in their extracellular sites. As described in chapter 2, following the self-assembly and drug loading of ROS-responsive miktoarm polymer (μ1) into micelles, and upon delivery to diseased sites where, in response to high ROS concentrations, the incorporated TK unit gets oxidatively cleaved, enabling upper corona "shedding" (Figure 3.1A). Such partial corona shedding can promote encapsulated drug release while keeping the overall micellar morphology intact, thus permitting a slow and sustained drug release in the extracellular environment.

Compared to ROS, glutathione (GSH) concentrations are low extracellularly and much higher intracellularly. Accordingly, a GSH-responsive miktoarm polymer (μ4) was synthesized in chapter 2, which contained a GSH-responsive disulfide group linking its PCL arm to its central junction. Upon self-assembly, it became a part of the micellar core, yet near the core/corona interface. Administration of the drug loaded μ4 micelles to diseased sites and uptake into cells would result in the reduction of the GSH-responsive disulfide linker present near the miktoarm polymer

junction and cause a burst-release of drug directly at the targeted site (Figure 3.1B). Such miktoarm polymers were highly effective in encapsulating curcumin and its autogenous environment selective release. Using a similar methodology, we prepared AB_2 type miktoarm polymer-based soft nanoparticles, which were loaded with resveratrol. Considering the role that ROS-induced oxidative damage plays in age-related diseases, senolytic agents such as resveratrol have become an active area of research and have been shown to extend the lifespan and increase the health of several model organisms.[17, 18] While these exact mechanisms are not well understood, it is known that resveratrol has a broad anti-inflammatory effect that involves down-regulating NF-κB gene products, thereby suppressing cytokines and TNF-α expression. Importantly, resveratrol also has a well-studied pharmacological profile and exhibits therapeutic effects that aid in chemoprevention and chemotherapy in addition to the elimination of senescent cells that trigger inflammation.[19, 20] Our ROS- and GSH-responsive miktoarm star polymers, developed in chapter 2, provided a platform to carry out a detailed evaluation of the efficacy of resveratrol-loaded formulations in biology. These studies are currently being carried out in collaboration with the group of Professor Dusica Maysinger in the Department of Pharmacology and Therapeutics at McGill University. Due to COVID-19 pandemic which led to slow research ramping in Pharmacology, it was not possible to include these biological evaluations here as these studies are currently underway.

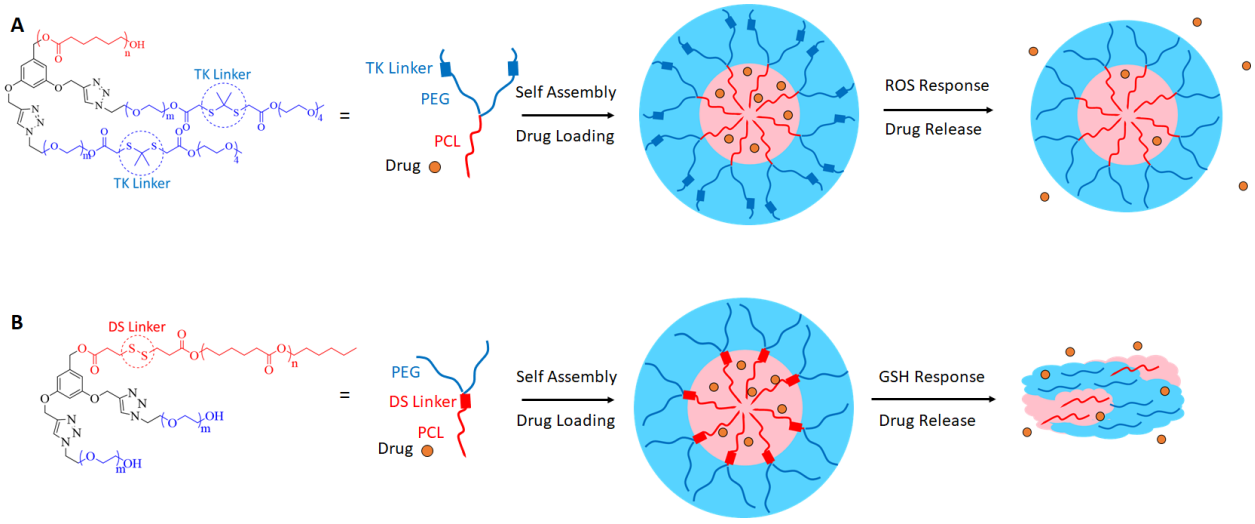

Figure 3.1. (A) Structure and schematic of μ1 summarizing its extracellular ROS response. The oxidative cleavage of thioketal linkers located in the upper coronae of μ1 enables an increase in drug release kinetics upon exposure to ROS, while preserving overall micellar morphology. (B) Structure and cartoon schematic of μ4 summarizing its intracellular GSH response. The reduction of the disulfide linker at the polymer arm junction in μ4 causes a burst release of encapsulated drugs.

3.2 Materials and Methods

AB_2 miktoarm polymers were prepared exactly as described in Chapter 2. The synthesis is summarized below in Chapter 3.2.1. All other chemicals were acquired and used as received from Sigma Aldrich. UV-visible spectroscopy was performed on a Varian Cary 50 UV-Vis Spectrophotometer. Fluoroscence spectrometry was performed on a Cary Eclipse Fluorescence Spectrophotometer. Dynamic light scattering was performed on a Brookhaven 90Plus Particle Size Analyser equipped with a 40 mW red diode laser operating at 658 nm. TEM micrographs were acquired on a FEI Tecnai 12 BioTwin 120 kV TEM equipped with an AMT XR80 CCD Camera System located at the Facility for Electron Microscopy Research (FEMR) at McGill University.

3.2.1. Miktoarm Polymer Synthesis

AB_2 miktoarm polymers were synthesized as described in in Chapter 2.2.1. Miktoarm polymer μ1 synthesis is shown in Scheme 3.1 and explained briefly hereafter. To obtain the PCL arm, **1**, 3,5-dihydroxybenzyl alcohol was propargylated with propargyl bromide, in the presence of K_2CO_3, and a catalytic [18]-Crown-6 in acetone. The propargylated core was then isolated with 3 DCM extractions from water and passed through a silica gel column using 1:1 ethyl acetate:hexanes as the eluent. Ring opening polymerization (ROP) was performed on the now single free OH group with ε-caprolactone, using tin(II)2-ethylhexanoate as a catalyst. The PCL-core structure, **1**, was obtained *via* precipitation in methanol. The TK-containing PEG arms, **2**, were synthesized by asymmetrically conjugating tetraethylene glycol and N_3-PEG to either carboxylic acid group in 2,2'-(propane-2,2-diylbis(sulfanediyl))diacetic acid (thioketal diacid, TKDA) using a DMAP/DCC catalyst system. The product was isolated after each conjugation step through successive filtration and silica gel column chromatography using an eluent of 8:1 DCM:methanol. Finally, μ1 was obtained by through a copper-catalyzed alkyne-azide cycloaddition (CuAAC) "click" reaction between 1 and 2, using CuBr as a catalyst and PMDETA as its ligand. The product was once again passed through a silica gel column 8:1 DCM:methanol and then dialyzed against water using a 3.5 kD membrane to remove all catalysts and unreacted polymers.

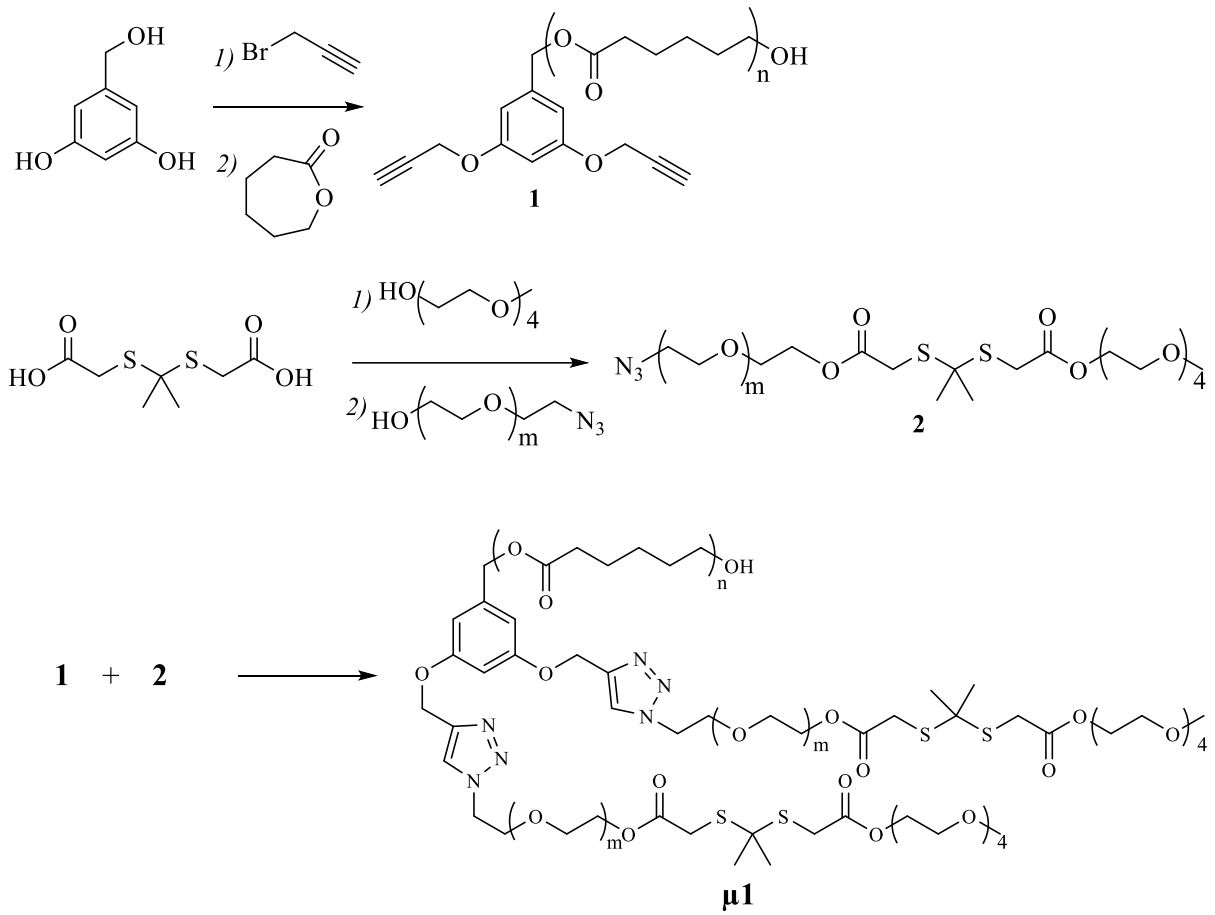

Scheme 3.1. Synthesis of μ1. Full synthetic and characterization details available in Chapter 2.2.1.

The miktoarm polymer μ4 was synthesized according to the procedure in Chapter 2.2.1, and its synthesis is summarized in Scheme 3.2. Briefly, The PCL-core structure, **3**, bearing the GSH-responsive disulfide was synthesized by first carrying out successive ROP of ε-caprolactone initiated by hexanol. Pure PCL obtained via precipitation in methanol. Then 3,3′-dithiodipropionic acid and (3,5-bis(prop-2-yn-1-yloxy)phenyl)methanol were successively conjugated at the hydroxyl end of PCL using DMAP/DCC-catalyzed esterifications and purified by concentrating the product in DCM, filtering off catalysts and excess reactants, and precipitating in methanol. μ4 was assembled using the CuAAC "click" reaction between **3** and N_3-PEG using CuBr and PMDETA as a catalyst and ligand. The product was purified by first dialyzing it against and EDTA solution and then washing it with minimal ice-cold water.

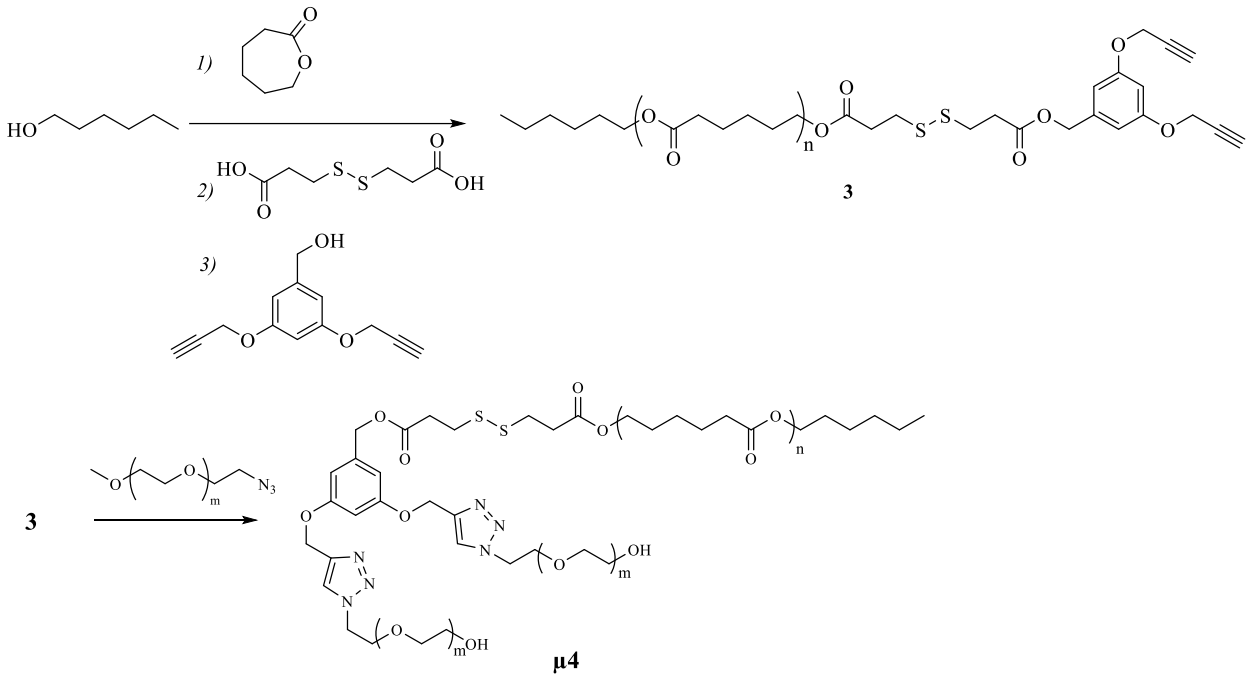

Scheme 3.2. Synthesis of μ4. Full synthetic and characterization details available in Chapter 2.2.1.

3.2.2 Blank Micelle Preparation

In a typical preparation, 0.25 mL of a 4 mg/mL stock solution of the miktoarm polymer in acetone was injected into 1 mL of Milli-Q water at a rate of 1 drop/s. The mixture was left to stir overnight while acetone evaporated. The mixture was filtered through a 0.22 μm PVDF syringe filter and diluted back to 1 mL with water.

3.2.3 Resveratrol-loaded Micelle Preparation

The preparation of resveratrol-loaded micelles was similar to the preparation of blank micelles: 0.25 mL of a 4 mg/mL stock solution of the miktoarm polymer in acetone was mixed with 0.25 mL of a 2 mg/mL stock solution of resveratrol in acetone. The polymer/drug solution was injected into 1 mL of Milli-Q water at a rate of 1 drop/s. The mixture was stirred vigorously overnight while the organic phase evaporated. The mixture was centrifuged for 5 minutes at 1000 RPM and the supernatant was filtered through a 0.22 μm PVDF syringe filter and diluted back to 1 mL with water.

3.2.4 Calculation of Encapsulation Efficiency and Loading Capacity

A 20 μL aliquot of the resveratrol-loaded micelles was diluted to 2 mL with methanol to break up the micelles and solubilize the drug. The solution was measured with UV-vis spectroscopy and the signal at 324 nm was taken to calculate resveratrol concentration. The mass of encapsulated drug

was determined by relating the absorbance signal to a drug concentration standard curve (Figure B.1). Encapsulation efficiencies and loading capacities were calculated according to Equations 1 and 2 respectively.

$$EE\ \% = \frac{Loaded\ Drug\ (mg)}{Total\ Drug\ (mg)} \quad (1)$$

$$LC\ \% = \frac{Loaded\ Drug\ (mg)}{Total\ Drug\ (mg) + Polymer\ (mg)} \quad (2)$$

3.2.5 CMC Determination

Miktoarm polymer solutions in a range of concentrations from 0.0001 – 1 mg/mL were prepared in THF, and pyrene was added to each solution to a concentration of 6 µM. The miktoarm polymer/pyrene mixtures were injected into equal volumes of DI water at a rate of 1 drop/s and stirred vigorously overnight to evaporate the THF and trigger self-assembly. Fluorescence excitation spectra were acquired at λ_{em} = 390 nm, and the peak ratios of λ_{ex} = 338 nm to λ_{ex} = 333 nm were plotted against miktoarm polymer concentration for each sample. The CMC was taken as the concentration at which the 338/333 nm excitation peak ratio begins to increase.

3.2.6 Resveratrol Release Profiles

A solution of resveratrol-loaded micelles was transferred into 3.5 kD MWCO dialysis tubing and dialyzed against 140 mL of pH 7.4 phosphate-buffered saline (PBS) containing 1% v/v Tween 80 to act as a sink. 40 µL aliquots, diluted to 1 mL with methanol, were taken from the tubing at predetermined intervals in order to measure remaining drug concentrations *via* UV-visible spectroscopy. The cumulative released resveratrol percentage was plotted against dialysis time. A 1 mg/mL solution of free resveratrol in a 45/40/15 ratio of water/dimethylacetamide/PEG_{750} was dialyzed in the same manner to act as a control (Figure B.2).

3.2.7 Transmission Electron Microscopy

An 8 µL drop of a 2 mg/mL micelle solution was dropped onto a carbon-coated copper grid. After 2 minutes, excess solution was removed by absorbing it with a Whatman filter paper carefully placed at at 90° angle at the edge of the grid. 8 µL of 2% uranyl acetate was then similarly dropped onto the grid, and its excess was then absorbed using filter paper after 2 minutes of drying. The grid was used for imaging after another 30 minutes.

3.3 Results & Discussion

One of the main factors governing micelle stability is the hydrophilic/hydrophobic ratio of its constituent polymers. For amphiphilic polymers, a fraction of approximately >45% hydrophilic polymer is necessary for stable micelle formation.[21] Bearing in mind that synthetically linking different arms of miktoarm polymers together becomes increasingly more difficult with larger molar masses, we first synthesized PCL segments with molar masses of roughly 2800 and 2500 (for μ1 and μ4 respectively), and matched them with hydrophilic arms based on PEG 2000. This resulted in μ1 and μ4 of very similar hydrophilic content with slightly more separated molar masses (Table 3.1).

While the overall architecture and composition of both miktoarm polymers remains the same, we expected that the difference in their cores (from the DS unit in μ4) and molecular weights would cause a slight variance in their CMCs (Table 3.1). Regardless, the obtained CMCs were still excellent, and well below the point at which micelle disassembly would result from biological administration and dilution, especially when compared to those generally seen in diblock copolymers.[12, 22-24] Micelle diameters were similar for both miktoarm polymers and were lower than 200 nm, a rough limit below which micelles can be distributed biologically and penetrate porous vasculature without issue. [25]

Table 3.1. Physical characteristics of μ1, μ4, and derived micelles. Molecular weights were estimated as the sum of M_n values of PEG and PCL-core components of the miktoarm polymers as determined by MALDI-TOF. Hydrophobic content was calculated as the MW fraction of the PCL-core component in each polymer. CMCs were determined using encapsulated pyrene fluorescence ratios. Diameters and polydispersities of micelles were determined *via* dynamic light scattering (DLS).

	Polymer		**Blank Micelles**			
	Molecular Weight	**Hydrophobic Content (%)**	**CMC (μM)**	**CMC (μg/mL)**	**Diameter (nm)**	**PDI**
μ1	7581	62.6	0.21	1.6	61.5	0.304
μ4	6730	63.4	0.77	5.2	84.4	0.121

Loading of μ1 and μ4-derived micelles with resveratrol significantly increased micellar diameters from their blank formulations. DLS results yielded values of 145 and 122 nm for resveratrol loaded μ1 and μ4 respectively, while TEM results showed lower values of 118.6 and 121.9 nm for loaded μ1 and μ4 respectively (Table 3.2). TEM generally leads to slightly smaller diameters than those measured by DLS, due to their dehydration under vacuum during sample preparation. While this

was clearly apparent for μ1, the TEM micrograph for μ4 showed micellar diameters similar to those seen by DLS (Figure 3.2). Interestingly, loaded resveratrol is seen to crystallize within the cores of micelles, as evidenced by the darker contrast in their more electron-dense centers,[26, 27] yet it is apparent that micelles are not loaded consistently (Figure 3.2A, B, D, E).

Encapsulation efficiencies of resveratrol vary widely for PEG-based micelles, ranging from 1.7-97%. As such, we compared our drug loading characteristics to the loading capacities to those reported in the literature, which were: 0.24%, 3.95%, 5.4%, 7.93%, and 20% for a series of graft and diblock copolymers composed of PEG and either PCL, PLGA, PLA, or polypyrroles. Resveratrol loading capacities for μ1 and μ4 were thus in agreement with previous results, suggesting good compatibility between the drug and miktoarm polymers (Table 3.2).[28-32]

Table 3.2. Physical characteristics of resveratrol loaded μ1 and μ4 micelles. Diameters and polydispersities of micelles were determined *via* dynamic light scattering (DLS). Encapsulation efficiencies and loading capacities of resveratrol were calculated according to Equations 1 and 2.

	Diameter (nm)[a]	**Diameter (nm)[b]**	**PDI[a]**	**Encapsulation Efficiency (%)**	**Loading Capacity (%)**
μ1	145.1	118.6	0.274	31.7 ± 1.2	10.6 ± 0.40
μ4	122.5	121.9	0.149	35.3 ± 9.4	11.8 ± 3.1

[a]Values determined by DLS
[b]Values determined by TEM

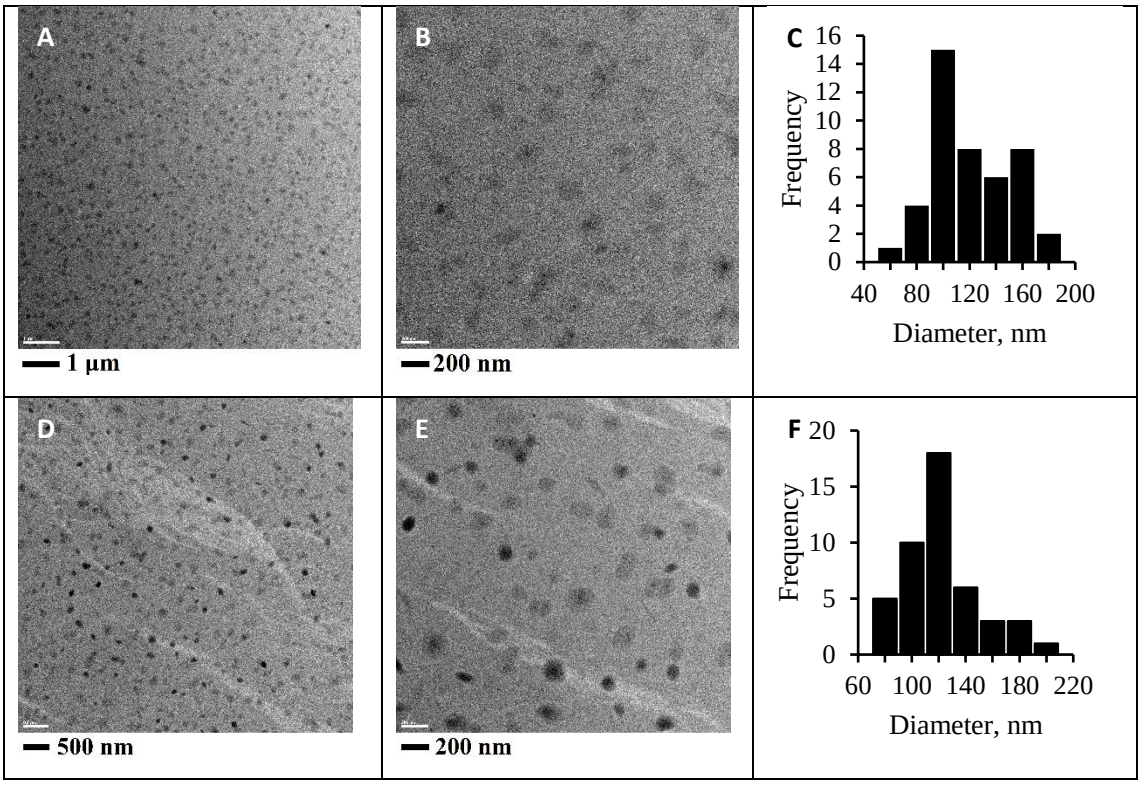

Figure 3.2. TEM micrographs of resveratrol loaded µ1 at (A) low and (B) high magnifications. TEM micrographs of resveratrol loaded µ4 at (D) low and (E) high magnifications. The size distributions of µ1 micelles (C) and µ4 micelles (F) were determined by relating the size of each imaged micelle to the scale bar in Figures 3.2B and 3.2E.

Upon confirming that µ1- and µ4-derived micelles had suitable morphologies and good resveratrol loading capacities, we subsequently studied the effect that ROS and GSH will have on their release characteristics from micelles. To establish that resveratrol encapsulation by µ1 and µ4 micelles restricted their diffusion, free resveratrol was first solubilized in a 45/40/15 ratio of water/dimethylacetamide/PEG_{750} and then dialyzed against pH 7.4 PBS buffer where nearly complete (98%) release was confirmed by UV/visible spectroscopy within 12 hours (Figure 3.3). Furthermore, an absence of micellar retention led to a significant dose dumping effect where 60% of free resveratrol was released within the first hour of dialysis. On the other hand, only 85% and 83% release were seen in µ1 and µ4 micelles respectively over the full 12 hour period, confirming the retention of cargo by micelles.

Treatment of µ1 micelles with 200 mM H_2O_2, a model for general ROS, increased drug release rates by up to 10% compared to untreated micelles (Figure 3.3A). Notably, H_2O_2 treatment led to an overall subtle increase in drug release as one would expect from TK cleavage-induced micellar corona shedding while also contributing to a dose dumping effect within the first 6 hours. Further

treatment saw the release profiles of treated and untreated samples converge as they both approached complete release over 48 hours (Figure B.2A). Treatment of resveratrol loaded μ4 micelles with 10 mM GSH showed a substantially enhanced resveratrol release profile compared to untreated micelles (Figure 3.3B). The reduction of the disulfide group linking PCL to the miktoarm polymer junction by GSH separates the hydrophilic and hydrophobic components of the polymer and causes micellar disassembly. This results in a release rate that is enhanced by up to 20% compared to the untreated sample and is comparable to free resveratrol release. This suggests that a similar burst release would arise in the GSH-rich intracellular environment. Continued exposure to GSH over 48 hours exhibited a slow convergence of the treated and untreated resveratrol release profiles as they approached completion (Figure B.2B).

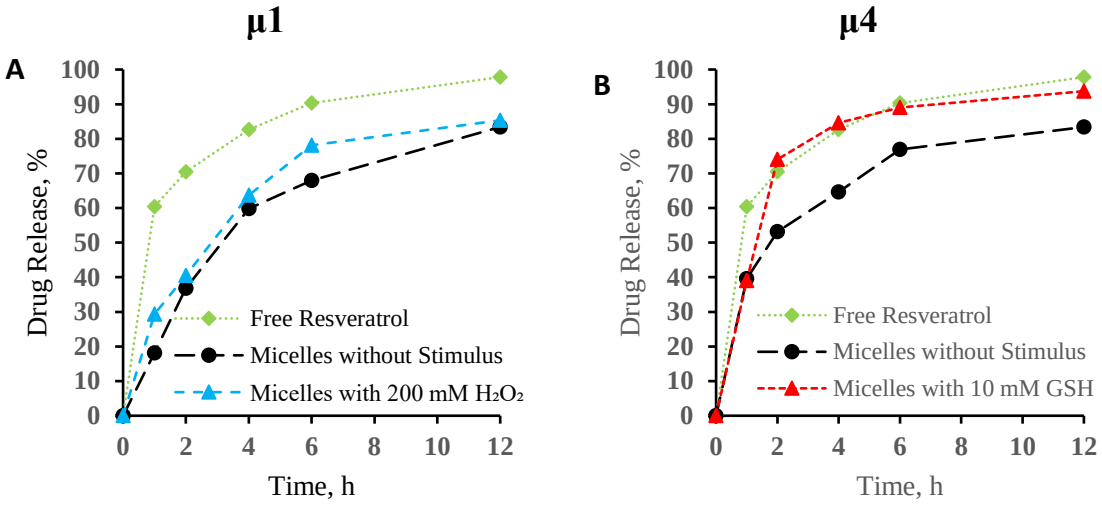

Figure 3.3. Release profiles of resveratrol loaded (A) μ1 and (B) μ4 over 12 hours of dialysis against pH 7.4 PBS. The buffer and dialyzed solutions contained 200 mM H_2O_2 or 10 mM GSH in stimulus responsive studies.

3.4 Conclusions and Future Work

Miktoarm star polymers with AB_2 (A = PCL, B = PEG) architectures were developed as a promising alternative to diblock copolymers due to their superior drug delivery properties. These star polymers self-assemble to form spherical micelles, and were successfully used to load resveratrol, with good encapsulation efficiencies and loading capacities. Resveratrol is a senolytic agent with broad anti-inflammatory effects, and its loading was accompanied by slight (~25 nm) or negligible increases in micelle diameter, and the loaded drug was distributed unevenly between micelles and crystallized within their cores. In order to assess resveratrol release from the

miktoarm polymer-based formulations, prepared using a similar methodology as described in Chapter 2, several drug release studies were conducted. Although it is a hydrophobic drug, resveratrol exhibited a rapid release profile, with >50% release being seen within 4 hours of incubation. It was demonstrated that resveratrol release can be further accelerated in response to opposing redox conditions for μ1 and μ4. μ1 micelles contain ROS-cleavable thioketal linkers near the terminal ends of their PEG arms, and they responded to H_2O_2 by partially shedding their outer coronae to subtly increase the rate of resveratrol release. On the other hand, incubation of μ4 micelles with GSH caused the cleavage of their sensitive disulfide linkers which join the polymers' PEG and PCL segments, causing micellar collapse and an ensuing significant increase in resveratrol release. The μ1 and μ4 micelles respond differently to oxidative stress and therefore have differing efficacies in the disease site extracellular environment where ROS are abundant, and in the intracellular environment where GSH is overproduced. The encouraging drug release studies based on stimulus response prompted our ongoing *in vitro* biological testing, which includes cell viability studies, evaluations of biomarkers for drug-induced cell senescence, as well as ROS/GSH quantification in treated cells. These results could not be included here due to delays related to the COVID-19 pandemic and slower research ramping that followed lab closures.

3.5 References

1. Loftsson, T.; Brewster, M. E., Pharmaceutical applications of cyclodextrins: basic science and product development. *J. Pharm. Pharmacol.* **2010,** *62* (11), 1607-1621.
2. Tran, S.; DeGiovanni, P.-J.; Piel, B.; Rai, P., Cancer nanomedicine: a review of recent success in drug delivery. *Clin. Transl. Med.* **2017,** *6* (1), 44.
3. Patra, J. K.; Das, G.; Fraceto, L. F.; Campos, E. V. R.; Rodriguez-Torres, M. d. P.; Acosta-Torres, L. S.; Diaz-Torres, L. A.; Grillo, R.; Swamy, M. K.; Sharma, S.; Habtemariam, S.; Shin, H.-S., Nano based drug delivery systems: recent developments and future prospects. *J. Nanobiotechnol.* **2018,** *16* (1), 71.
4. Tiwari, G.; Tiwari, R.; Sriwastawa, B.; Bhati, L.; Pandey, S.; Pandey, P.; Bannerjee, S. K., Drug delivery systems: An updated review. *Int. J. Pharm. Investig.* **2012,** *2* (1), 2-11.
5. Kaditi, E.; Mountrichas, G.; Pispas, S.; Demetzos, C., Block Copolymers for Drug Delivery Nano Systems (DDnSs). *Curr. Med. Chem.* **2012,** *19* (29), 5088-5100.
6. Kim, S.; Shi, Y.; Kim, J. Y.; Park, K.; Cheng, J.-X., Overcoming the barriers in micellar drug delivery: loading efficiency, in vivo stability, and micelle–cell interaction. *Expert Opin. Drug Del.* **2010,** *7* (1), 49-62.
7. Sharma, A.; Kakkar, A., Designing Dendrimer and Miktoarm Polymer Based Multi-Tasking Nanocarriers for Efficient Medical Therapy. *Molecules* **2015,** *20* (9), 16987-17015.
8. Khanna, K.; Varshney, S.; Kakkar, A., Miktoarm star polymers: advances in synthesis, self-assembly, and applications. *Polym. Chem.* **2010,** *1* (8), 1171-1185.

9. Hadjichristidis, N.; Pitsikalis, M.; Iatrou, H.; Driva, P.; Sakellariou, G.; Chatzichristidi, M., 6.03 - Polymers with Star-Related Structures: Synthesis, Properties, and Applications. In *Polymer Science: A Comprehensive Reference*, Matyjaszewski, K.; Möller, M., Eds. Elsevier: Amsterdam, 2012; pp 29-111.
10. Pispas, S.; Hadjichristidis, N.; Potemkin, I.; Khokhlov, A., Effect of Architecture on the Micellization Properties of Block Copolymers: A2B Miktoarm Stars vs AB Diblocks. *Macromolecules* **2000,** *33* (5), 1741-1746.
11. Lonsdale, D. E.; Monteiro, M. J., Synthesis and self-assembly of amphiphilic macrocyclic block copolymer topologies. *J. Polym. Sci. A Polym. Chem.* **2011,** *49* (21), 4603-4612.
12. Lu, Y.; Zhang, E.; Yang, J.; Cao, Z., Strategies to improve micelle stability for drug delivery. *Nano Res.* **2018,** *11* (10), 4985-4998.
13. Knop, K.; Hoogenboom, R.; Fischer, D.; Schubert, U. S., Poly(ethylene glycol) in Drug Delivery: Pros and Cons as Well as Potential Alternatives. *Angew. Chem. Int. Ed.* **2010,** *49* (36), 6288-6308.
14. Lu, L.; Zhang, Q.; Wootton, D.; Chiou, R.; Li, D.; Lu, B.; Lelkes, P.; Zhou, J., Biocompatibility and biodegradation studies of PCL/β-TCP bone tissue scaffold fabricated by structural porogen method. *J. Mater. Sci. Mater. Med.* **2012,** *23* (9), 2217-2226.
15. Chen, Y.; Zhang, Y. X.; Wu, Z. F.; Peng, X. Y.; Su, T.; Cao, J.; He, B.; Li, S., Biodegradable poly(ethylene glycol)–poly(ε-carprolactone) polymeric micelles with different tailored topological amphiphilies for doxorubicin (DOX) drug delivery. *RSC Adv.* **2016,** *6* (63), 58160-58172.
16. Khanna, K.; Varshney, S.; Kakkar, A., Designing Miktoarm Polymers Using a Combination of "Click" Reactions in Sequence with Ring-Opening Polymerization. *Macromolecules* **2010,** *43* (13), 5688-5698.
17. Bielak-Zmijewska, A.; Grabowska, W.; Ciolko, A.; Bojko, A.; Mosieniak, G.; Bijoch, Ł.; Sikora, E., The Role of Curcumin in the Modulation of Ageing. *Int. J. Mol. Sci.* **2019,** *20* (5), 1239.
18. Bhullar, K. S.; Hubbard, B. P., Lifespan and healthspan extension by resveratrol. *Biochim. Biophy. Acta Mol. Basis Dis.* **2015,** *1852* (6), 1209-1218.
19. Jacob, A.; Wu, R.; Zhou, M.; Wang, P., Mechanism of the Anti-inflammatory Effect of Curcumin: PPAR-gamma Activation. *PPAR Res.* **2007,** *2007*, 89369-89369.
20. Kulkarni, S. S.; Cantó, C., The molecular targets of resveratrol. *Biochim. Biophys. Acta Mol. Basis Dis.* **2015,** *1852* (6), 1114-1123.
21. Mourya, V.; Inamdar, N.; Nawale, R.; Kulthe, S., Polymeric Micelles: General Considerations and their Applications. *Indian J. Pharm. Res. Educ.* **2015,** *45* (2), 128-138.
22. Yoshida, E., Control of Micellar Size and Critical Micelle Concentration for "Nonamphiphilic" Poly(vinyl phenol)-block-Polystyrene Diblock Copolymers. *Polym. J.* **2003,** *35* (12), 965-971.
23. Lo, C.-L.; Lin, S.-J.; Tsai, H.-C.; Chan, W.-H.; Tsai, C.-H.; Cheng, C.-H. D.; Hsiue, G.-H., Mixed micelle systems formed from critical micelle concentration and temperature-sensitive diblock copolymers for doxorubicin delivery. *Biomaterials* **2009,** *30* (23), 3961-3970.
24. Kosa, S. A.; Al-Harbi, L. M.; Baloch, M. K.; Ullah, I.; El-Mossalamy, E. H., Impact of Block Length and Temperature over Self-Assembling Behavior of Block Copolymers. *Int. J. Polym. Sci.* **2016,** *2016*, 7.
25. Moghimi, S. M.; Hunter, A. C.; Murray, J. C., Long-Circulating and Target-Specific Nanoparticles: Theory to Practice. *Pharmacol. Rev.* **2001,** *53* (2), 283.

26. Moquin, A.; Sturn, J.; Zhang, I.; Ji, J.; von Celsing, R.; Vali, H.; Maysinger, D.; Kakkar, A., Unraveling Aqueous Self-Assembly of Telodendrimers to Shed Light on Their Efficacy in Drug Encapsulation. *ACS Appl. Bio Mater.* **2019,** *2* (10), 4515-4526.
27. Li, X.; Hirsh, D. J.; Cabral-Lilly, D.; Zirkel, A.; Gruner, S. M.; Janoff, A. S.; Perkins, W. R., Doxorubicin physical state in solution and inside liposomes loaded via a pH gradient. *Biochim. Biophys. Acta Biomembr.* **1998,** *1415* (1), 23-40.
28. Moquin, A.; Hanna, R.; Liang, T.; Erguven, H.; Gran, E. R.; Arndtsen, B. A.; Maysinger, D.; Kakkar, A., PEG-conjugated pyrrole-based polymers: one-pot multicomponent synthesis and self-assembly into soft nanoparticles for drug delivery. *Chem. Commun.* **2019,** *55* (66), 9829-9832.
29. Lu, X.; Ji, C.; Xu, H.; Li, X.; Ding, H.; Ye, M.; Zhu, Z.; Ding, D.; Jiang, X.; Ding, X.; Guo, X., Resveratrol-loaded polymeric micelles protect cells from Aβ-induced oxidative stress. *Int. J. Pharm.* **2009,** *375* (1), 89-96.
30. Hu, M.; Zhu, J.; Qiu, L., Polymer micelle-based combination therapy of paclitaxel and resveratrol with enhanced and selective antitumor activity. *RSC Adv.* **2014,** *4* (109), 64151-64161.
31. Sanna, V.; Siddiqui, I. A.; Sechi, M.; Mukhtar, H., Resveratrol-Loaded Nanoparticles Based on Poly(epsilon-caprolactone) and Poly(d,l-lactic-co-glycolic acid)–Poly(ethylene glycol) Blend for Prostate Cancer Treatment. *Mol. Pharm.* **2013,** *10* (10), 3871-3881.
32. Washington, K. E.; Kularatne, R. N.; Biewer, M. C.; Stefan, M. C., Combination Loading of Doxorubicin and Resveratrol in Polymeric Micelles for Increased Loading Efficiency and Efficacy. *ACS Biomater. Sci. Eng.* **2018,** *4* (3), 997-1004.

Chapter 4: Autogenous ROS-induced miktoarm star polymer micelle coupling for enhanced retention and drug delivery

Abstract

Miktoarm stars, or branched stars containing mixed polymeric arms, have been shown to prominently exhibit many properties that have contributed to the development of drug delivery systems with superior therapeutic efficiency, including good polymer arm tunability, low critical micelle concentrations, and high drug loading and sustained release properties amongst others. Through the combination of facile synthetic methods, including ring opening polymerization, Steglich esterifications, and CuAAC "click" coupling, we have developed an AB_2 miktoarm star polymer with hydrophobic A = PCL and hydrophilic B = PEG segments, for the micellar encapsulation and delivery of curcumin to ROS-afflicted disease sites. PEG arms were put together such that ROS-cleavable thioketal linkers were spatially located near their terminal ends, corresponding to the coronal surface of micelles. Incubation of these ROS-responsive miktoarm star polymer micelles with H_2O_2, exposes thiol corona surface groups through thioketal oxidative cleavage, which can further couple with each other to form networked micelle clusters. Such network formation at disease sites is expected to promote the retention of drug delivery systems within them and consequently improve the viability of encapsulated drugs.

4.1 Introduction

The low bioavailability of many pharmaceutical agents is commonly ascribed to their poor aqueous solubility and instability in biological environments.[1, 2] Improvements in nanotechnology and nanomedicine have led to the development of a variety of amphiphilic polymers that can assemble into micelles with distinct hydrophobic/hydrophilic domains. More specifically, lipophilic drugs can be solubilized and stabilized in micellar cores, while being shielded by outer hydrophilic coronae, which also lend biological stealth and aqueous solubility to such nanocarriers.[3-5] Conventionally, micellar drug delivery systems have been assembled from amphiphilic diblock copolymers that consist of linked hydrophilic and hydrophobic polymer segments on a single backbone (linear block-copolymers).[6, 7] With development of facile synthetic methodologies,[8-14] miktoarm star polymers, or branched stars that have mixed polymeric arms, have increasingly been used as drug nanocarriers due to their superior properties including lower CMCs, drug loading

contents, more sustained drug release profiles, and an overall higher segment tunability that enables their more varied use as drug delivery systems.[14-19]

Reactive oxygen species (ROS) including hydrogen peroxide, singlet oxygen, hydroxy radicals, and superoxides are overabundant extracellularly in pathologies including cancer, chronic inflammation, and are contributors to the biological decline seen in aging.[20-23] Consequently, numerous polymeric drug delivery systems have been developed with ROS-sensitive linkers including thioketals, thioethers, diselenides, phenylboronic esters etc., that respond to autogenous ROS to promote drug release at affected sites.[24-27]

The enhanced permeability and retention (EPR) effect describes a mechanism by which micelles are retained at disease sites. Due to the critical nutritional requirements of growing tumours, blood vessel growth is stimulated and develops from abnormally aligned endothelial cells.[28, 29] The leaky structure of tumorous vasculature promotes the accumulation of nanoparticles, and stemming from the defective lymphatic drainage associated with tumour sites, the nanoparticles are retained.[28-32] In light of much research, the EPR effect has proven to be quite controversial, since the delivery of nanoparticle formulations from an injection site far away to a tumour site, and in spite of the high tumor interstitial fluid pressure and poor blood flow, is unlikely. Increased drug delivery from nanocarriers has also not been seen in clinical trials, and the animal models (including mice) used to study the effect have shown a more pronounced effect than human models.[33]

To enhance the efficacy of soft nanoparticles in drug delivery, we designed an AB_2 (A = PCL, B = PEG) miktoarm star polymer from a dipropargylated benzyl alcohol core through a combination of ring opening polymerization, Steglich esterifications and copper-catalyzed alkyne-azide cycloaddition (CuAAC) "click" reactions. Through tandem conjugation chemistry, we were able to place a ROS-responsive thioketal linker near the terminal end of the PEG arms, so that upon self-assembly, the miktoarm star-based micelles would have these thioketals near their surfaces. These linkers are expected to become oxidatively cleaved in response to the extracellular ROS present at tumour sites which would expose free thiol ends that can couple with each other by forming disulfide bridges, in response to the ROS environment. In generating these disulfide links, we aim to evoke an effect whereby micelles that are delivered to tumour sites through the surrounding leaky vasculature couple together to form large networks that are too large to be eliminated back through the same blood vessels (Figure 4.1). To our knowledge, such a mechanism

has not yet been reported in the literature, and we expect that this will amplify the EPR effect and address some of the issues that are currently raised in retaining micelles at such disease sites.

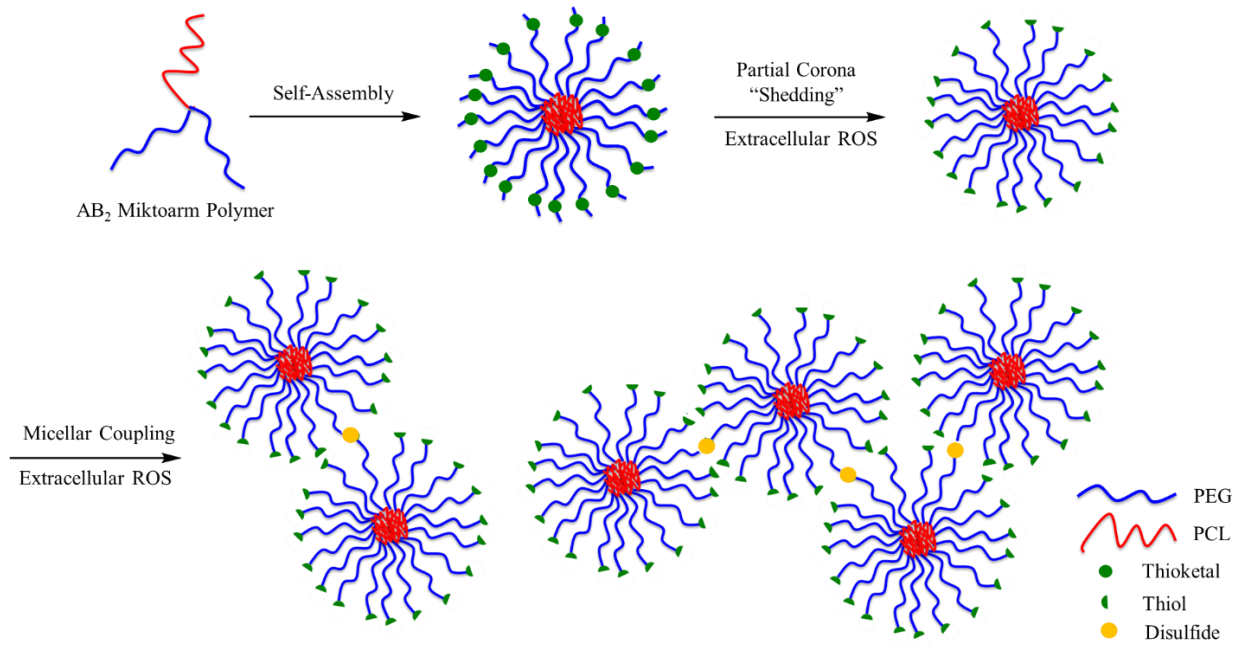

Figure 4.1. Cartoon schematic of self-assembled miktoarm star micelles undergoing ROS-induced free thiol group exposure and disulfide coupling.

4.2 Materials and Methods

(3,5-bis(prop-2-yn-1-yloxy)phenyl)methanol (dipropargyl benzyl alcohol, DPBA), 2,2'-(propane-2,2-diylbis(sulfanediyl))diacetic acid (thioketal diacid, TKDA), and azido-PEG (N_3-PEG) were prepared as described in Section 2.2.1. ε-caprolactone monomer was acquired and used as received from Acros Organics. All other chemicals were purchased and used as received from Sigma Aldrich. Nuclear magnetic resonance (NMR) spectra were acquired on a Bruker AVIIIHD 400 and 500 MHz NMR Spectrometers, both equipped with BBFO+ SmartProbes. Mass spectra were acquired on a Bruker MALDI Autoflex III-TOF, a Bruker Maxis Impact Q-TOF, and a Thermo Scientific ExactivePlus Orbitrap-API mass spectrometer. Dynamic light scattering (DLS) was performed using a Brookhaven 90Plus Particle Size Analyser equipped with a 40 mW red diode laser operating at 658 nm. TEM images were taken on a FEI Tecnai 12 BioTwin 120 kV TEM equipped with an AMT XR80 CCD Camera System located at the Facility for Electron Microscopy Research (FEMR) at McGill University. UV-Vis absorption spectra were taken on a Varian Cary

50 UV-Vis Spectrophotometer. Fluorescence spectra were collected on a Cary Eclipse Fluorescence Spectrophotometer. Gel permeation chromatography (GPC) was performed on a Waters Breeze system with HPLC grade tetrahydrofuran (THF) as the mobile phase at the Department of Chemical Engineering at McGill University.

4.2.1 Synthesis

3,5-bis(prop-2-yn-1-yloxy)benzyl PCL (DPB-PCL'), 2. Compound **2** was prepared by adapting a ring opening polymerization methodology from the literature.[34] 3,5-bis(prop-2-yn-1-yloxy)phenyl)methanol (dipropargyl benzyl alcohol, DPBA (0.2g, 0.925mmol) and distilled ε-caprolactone (1.85 mL, 16.65mmol) were dissolved in dry toluene and added to a warm 3-neck flask equipped with a condenser. While stirring under nitrogen atmosphere, the reaction mixture was brought to reflux and Tin(II)2-ethylhexanoate (0.076 mL, 0.187mmol) was added through a rubber septum. After stirring overnight, the flask was cooled, and toluene was concentrated under reduced pressure. The mixture was then precipitated in ice cold methanol to obtain the product. The pure product was collected by filtration and dried *in vacuo* to obtain an off-white solid (1.21 g, 57%)

^{1}H NMR (400 MHz, $CDCl_3$): δ_H (ppm) 1.40 (36H, m, (-OOC-C-C-CH_2-)$_{18}$), 1.66 (72H, m, (-OOC-C-CH_2-C-CH_2-)$_{18}$), 2.32 (36H, t, $^{3}J_{HH}$ = 7.5 Hz, (-OOC-CH_2)$_{18}$), 2.56 (2H, t, $^{4}J_{HH}$ = 2.4 Hz, C≡CH), 3.66 (2H, t, $^{3}J_{HH}$ = 6.5 Hz, -OOC-CH_2-), 4.08 (36H, t, $^{3}J_{HH}$ = 6.7 Hz, (-CH_2-OOC-)$_{18}$). 4.69 (4H, d, $^{4}J_{HH}$ = 2.4 Hz, CH_2-C≡C), 5.07 (2H, s, CH_2-OH), 6.59 (1H, t, $^{4}J_{HH}$ = 2.2 Hz, H–Ar), 6.61 (2H, d, $^{4}J_{HH}$ = 2.2 Hz, H–Ar).

^{13}C{^{1}H}-NMR (125 MHz, $CDCl_3$): δ_C (ppm) 24.6, 25.5, 28.4, 34.1, 56.0, 64.2, 107.5, 158.8, 173.5.

MALDI-TOF M_n = 1994.45; M_w = 2193.25; PDI = 1.10; DP = 17.50

15,15-dimethyl-12-oxo-2,5,8,11-tetraoxa-14,16-dithiaoctadecan-18-oic acid (TK-TrEG), 4. Steglich esterification was carried out by the adaptation and modification of a published methodology.[35] TKDA (4.0g, 17.9mmol) and DMAP (0.4g, 3.27mmol) were added to a 3-neck flask and dissolved with a 1:1 mixture of dry diethyl ether and dry DCM. Upon cooling in an ice bath, solutions of TrEG (0.476mL, 2.98mmol) and DCC (0.860g, 4.17mmol) in dry DCM were simultaneously, but separately, added dropwise to the reaction mixture over 1.5 hours while stirring under a nitrogen atmosphere. After an overnight reaction the 3-neck flask was cooled in

an ice bath and any formed precipitate was filtered off. The crude product was then extracted from water with DCM 3 times, concentrated, then extracted again from new distilled water with DCM 3 times, and dried under $MgSO_4$. The solvent was then removed under reduced pressure to yield a colourless oil (0.618 g, 56%).

^{1}H NMR (400 MHz, $CDCl_3$): δ_H (ppm) 1.64 (6H, s), 3.41 (3H, s), 3.45 (2H, s), 3.53 (2H, s), 3.59 (2H, m), 3.68 (6H, m), 3.77 (2H, m), 4.31 (2H, m).

^{13}C{^{1}H}-NMR (125 MHz, $CDCl_3$): δ_C (ppm) 30.2, 32.9, 33.2, 57.3, 59.0, 64.5, 69.0, 70.4, 70.4, 70.5, 71.9, 170.2, 173.2.

MS: ESI m/z: (M-H) Calculated for $C_{14}H_{25}O_7S_2$ 369.47 g/mol, Found 369.10 g/mol.

N_3-PEG-TK-TrEG, 5. The esterification procedure was adapted and modified as required based on a literature methodology.[36] N_3-PEG (4.13g, 1.99mmol), TK-TrEG (0.737g, 1.99mmol), and DPTS (0.612g, 2.19mmol) were dissolved in dry DCM in a three-neck flask and cooled in an ice bath. A solution of DIPC (0.462mL, 2.99mmol) in dry DCM was then added dropwise to the flask over 1.5 hours while continuously stirring under nitrogen atmosphere. The reaction continued to run for 24 hours. After the reaction was complete, the flask was stored in a freezer at 0 ºC overnight and the formed precipitate was discarded. The crude product was passed through a silica gel column with a 8:1 DCM:methanol eluent to remove any remaining impurities and then dried *in vacuo* to yield an off-white solid (2.13 g, 44%).

^{1}H NMR (400 MHz, $CDCl_3$): δ_H (ppm) 1.63 (6H, s, CH_3), 3.40 (5H, m, CH_2-N_3, OCH_3), 3.46 (4H, s, S-CH_2-C=O), 3.65 (192H, m, PEG and TrEG), 4.28 (4H, m, CH_2-O-C=O).

^{13}C{^{1}H}-NMR (125 MHz, $CDCl_3$): δ_C (ppm) 30.3, 33.0, 50.7, 57.3, 59.0, 61.7, 64.5, 68.9, 70.0, 70.6, 71.9, 170.5.

MALDI-TOF M_n = 2397.41; M_w = 2465.26; PDI = 1.03; DP = 54.42

μ(PEG-TK-TrEG)$_2$PCL (μ1B), 6. The copper catalyzed alkyne-azide click reaction was adapted and modified as required based on a procedure method.[37, 38] N_3PEG-TK-TrEG (**5**) (0.741g, 0.301mmol), DPB-PCL (**2**) (0.300g, 0.150mmol), and CuBr (0.0540g, 0.376mmol) were dissolved in a round bottom flask containing dry THF. While stirring the reaction mixture under nitrogen atmosphere, PMDTA (0.079mL, 0.376mmol) was added, and the reaction was continuously stirred

for 24 hours. The completed reaction mixture was then concentrated under reduced pressure and dialyzed through a 3.5 kD membrane against 150 mL of DI water with 200mg of EDTA to remove the catalysts over 24 hours. The pure product was then removed from the dialysis bag and isolated by removing water under pressure, to yield a pale brown solid (0.932 g, 90%).

^{1}H NMR (500 MHz, $CDCl_3$): δ_H (ppm) 1.40 (56H, m), 1.63 (12H, s), 1.66 (112H), 2.32 (56H, t, $^{3}J_{HH}$ = 7.7 Hz), 3.40 (6H, s), 3.46 (8H, s), 3.66 (392H, s), 3.81 (4H, t, $^{3}J_{HH}$ = 4.6 Hz), 4.08 (56H, t, $^{3}J_{HH}$ = 6.6 Hz), 4.29 (4H, t, $^{3}J_{HH}$ = 5.2 Hz), 4.99 (2H, s), 5.21 (4H, s), 6.55 (2H, s), 6.58 (1H, s) 7.75 (2H, s).

^{13}C{^{1}H}-NMR (125 MHz, $CDCl_3$): δ_C (ppm) 24.6, 25.5, 28.4, 33.0, 34.1, 64.2, 69.2, 70.6, 72.2, 123.9, 173.6.

4.2.2 GPC Analyses

All polymers were dissolved in HPLC grade THF prior to GPC analysis. A mobile phase flow rate of 0.3 mL/min was used while columns were heated to 40 °C. The GPC was equipped with 3 Waters Styragel HR columns (HR1 with a molar mass measurement range of 1 x 10^2 - 5 x 10^3 g/mol, HR2 with a molar mass measurement range of 5 x 10^2 - 2 x 10^4 g/mol and HR4 with a molar mass measurement range of 5x10^3 - 6x10^5 g/mol) as well as a guard column. PMMA Standards with narrow dispersities (PSS Polymer Standards Service GmbH, molar masses ranging from 682 g/mol to 1,520,000 g/mol) were used to calibrate the GPC, and a differential refractive index (RI 2414) detector was used.

4.2.3 Preparation of Blank Micelles

Blank micelles were prepared using the co-solvent evaporation method.[39] 1 mg of polymer was dissolved in 0.5 mL of acetone and slowly injected into 2 mL of DI water at a rate of 1 drop/s. The resulting solution was left to stir overnight while the organic phase evaporated, triggering the self-assembly of micelles in water. The solutions were then filtered through 0.22 µm PVDF syringe filters. Samples were analyzed using DLS to determine micelle diameters (obtained as lognormal size distributions) and polydispersities.

4.2.4 CMC Determination

Pyrene loaded micelles were prepared by the co-solvent evaporation method. A series of miktoarm star polymer µ1B samples with different concentrations were prepared and mixed with pyrene (6 µM) in THF. The polymer/pyrene solutions were injected into vials containing 2 mL of DI water

at a rate of 1 drop/s and left to stir overnight while the organic phase evaporated. Afterwards, the samples with varying polymer concentrations were measured using fluorescence spectroscopy. Excitation spectra were acquired by setting the emission wavelength to 390. The peak intensity ratio of 338 nm /333 nm was taken for each sample and plotted as a function of polymer concentration. In the resulting plot, the point at which the horizontal slope noticeably increased from further polymer addition was taken as the critical micelle concentration (CMC).

4.2.5 Drug Loading

The drug loading procedure was similar to the procedure for preparing blank micelles. 1 mg samples of polymer and 0.5 mg samples of curcumin were mixed in 1 mL of acetone, and the resulting solution was slowly pipetted into a vial containing 2 mL of DI water at a rate of 1 drop/s. The organic phase was then left to evaporate overnight to allow self-assembly of micelles alongside the encapsulation of curcumin. Unencapsulated drug was removed by first centrifuging the samples at 2500 RPM for 5 and then filtering them through 0.22 μm PVDF syringe filters. The encapsulation efficiencies and loading capacities were measured according to equations 1 and 2 repectively, where the total drug and polymer masses were the initial weighed amounts, and the loaded drug was determined by the UV-Vis absorption spectrum of curcumin. The peak intensity at 424 nm was related to curcumin concentration using a standard curve (Figure A.1).

$$EE\ \% = \frac{Loaded\ Drug\ (mg)}{Total\ Drug\ (mg)} \qquad (1)$$

$$LC\ \% = \frac{Loaded\ Drug\ (mg)}{Total\ Drug\ (mg) + Polymer\ (mg)} \qquad (2)$$

4.2.6 Drug Release

Drug loaded micelle solutions were pipetted into 3.5 kD MWCO dialysis membranes, clipped at either side, and dialyzed against 150 mL of pH 7.4 phosphate-buffered saline (PBS) containing 1% v/v Tween 80 to act as a sink. 20 μL aliquots were taken at regular time intervals, diluted to 1 mL with methanol to disassemble micelles, and their curcumin concentrations were measured using UV-Vis spectroscopy by relating the peak intensity at 424 nm to a standard curve (Figure A.1). The released curcumin was plotted as a percent against dialysis time.

4.2.7 Transmission Electron Microscopy

2 mg/mL polymeric micelle solutions were drop-mounted onto glow discharged carbon-coated copper grids and left to dry for 5 minutes. Afterwards, the excess solution was carefully absorbed

using a Whatman filter paper placed at the edge of the grid. Negative staining was carried out using 2% uranyl acetate solution. The grid was again left to dry and excess solution was removed using a Whatman filter paper.

4.3 Results and Discussion

4.3.1 Synthesis of miktoarm star polymer μ1B

Miktoarm star polymer μ1B was designed as an AB_2 (A = PCL, B = PEG) star with thioketal units linking on the PEG chains near their terminal ends. The synthesis followed the methodology used to synthesize miktoarm star polymer μ1, in general, as described in Chapter 2. The notable differences include the independent synthesis of a smaller sized PCL segment, and the use of a smaller triethylene glycol (TrEG) end group as opposed to tetraethylene glycol (TEG) (Scheme 4.1). The ROP of caprolactone, while efficient, is not consistent enough to closely reproduce PCL chains of similar degrees of polymerization. In addition, the inclusion of hydrophobic chains with lower molecular weight compositions generally results in a smaller micellar diameter, a parameter of significance in developing nanoformulations. Triethylene glycol was used as a cheaper and smaller alternative, and combined with the smaller PCL chain length, the nanoformulations from these AB_2 polymers responded to ROS more quickly than the similar formulations reported in chapter 2.

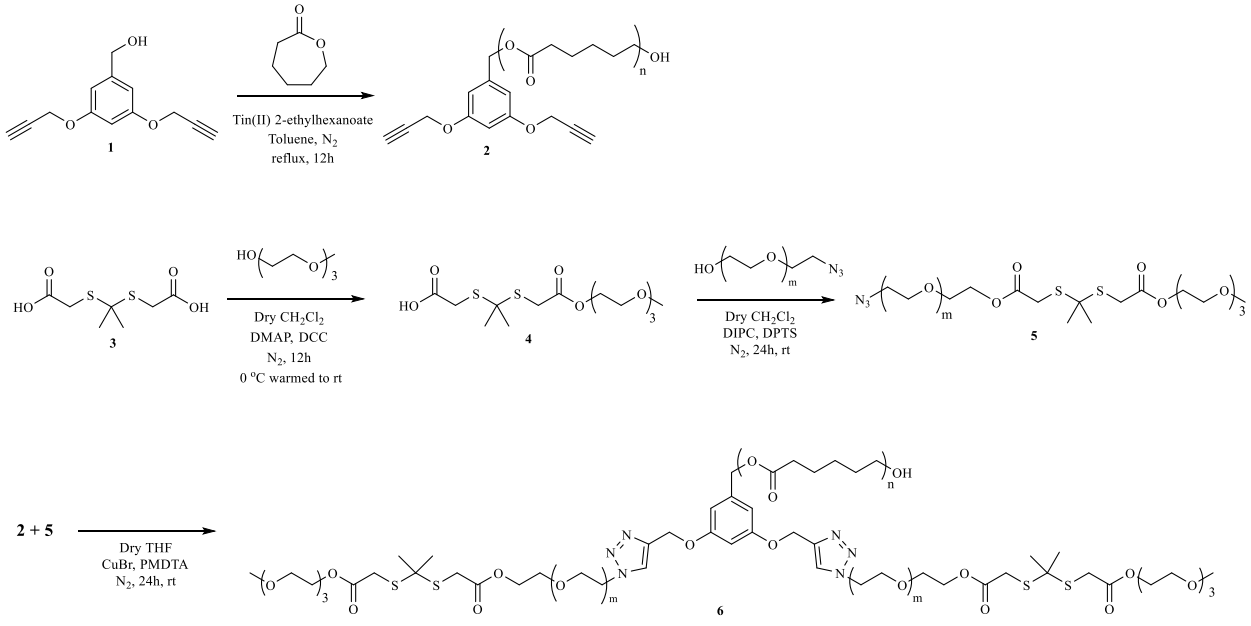

Scheme 4.1. Synthesis of miktoarm star polymer μ1B (**6**).

DPB-PCL' (2). The ring opening polymerization of ε-caprolactone was initiated by the hydroxyl group in DPBA (**1**) with $[M_0]/[I] = 18$ and resulted in the synthesis of hydrophobic PCL. The NMR peaks corresponding to the PCL repeating unit were confirmed at 1.40, 1.66, 2.32, and 4.08 ppm. Protons from the propargyl group from DPBA were preserved in **2** with visible peaks appearing at 2.56 and 4.69 ppm. The CH_2O ester linking the benzyl core to the PCL arm was confirmed with a singlet at 5.07 ppm. A DP of 23 was calculated for **2** by comparing the integrated peak area under the triplet at 4.08 ppm to singlet at 5.07 ppm, while MALDI-TOF gave a DP of 17.5 and a molar mass of 1994 g/mol (Table C.1).

TK-TrEG (4). The ROS-responsive thioketal containing end-group was synthesized by conjugating TrEG to TKDA. Monofunctionalization was achieved by the slow, and independent, addition of DCC and TrEG in a 3-neck flask containing a solution of excess TKDA and DMAP. After successive filtrations and liquid extractions, the pure product was isolated and confirmed by the appearance of split singlets at 3.45 and 3.53 ppm relating to the now asymmetrical CH_2 protons on either side of the thioketal functional group. In addition, the new ester CH_2O peak from the conjugation was confirmed at 4.31 ppm.

N_3-PEG-TK-TrEG (5). The ROS-responsive PEG arm was synthesized through an esterification of the thioketal containing TK-TrEG (**4**) with N_3-PEG, which was synthesized as described in Section 2.2.1. These two segments were coupled using a DIPC/DPTS catalyst system, and the pure product was obtained through successive filtration and silica gel column chromatography. Peaks representing groups present earlier in each unit (**4** and **5**) were once again seen. Notably, the asymmetric CH_2 protons at 3.45 and 3.53 ppm from TK-TrEG (**4**) merged to form one singlet visible at 3.46 ppm, denoting that the thioketal functional group was now equally flanked by similar ester groups. A DP of 54 was calculated for **5** by comparing the integrated peak area under its ester CH_2O triplet at 4.28 ppm to the PEG multiplet at 3.66 ppm, while MALDI-TOF gave a DP of 54.4 and a molar mass of 2397 g/mol (Table C.1).

μ(PEG-TK-TrEG)$_2$PCL (μ1B) (6). The hydrophobic core-PCL arm (**2**) was stitched to two thioketal-containing PEG arms (**5**) by using CuBr and PMDETA as the catalyst and ligand used in CuAAC "click" coupling. After the catalyst system was removed by dialysis against EDTA, the pure miktoarm star polymer μ1B was isolated as a pale brown solid. The conjugation was

confirmed *via* the appearance of a triazole proton at 7.75 ppm alongside the disappearance of alkyne proton signals from the core-PCL unit (**2**).

Polymer segments **2** and **5** as well as the miktoarm star polymer **6** were characterized using GPC and gave single elution peaks with good dispersities (Figure C.1-C.3).

4.3.2 Self-Assembly

The amphiphilic miktoarm star polymer μ1B, containing hydrophobic PCL and hydrophobic PEG arms, was soluble in water and organic solvents, facilitating its self-assembly into micelles. Self-assembly of μ1B was performed using the co-solvent evaporation method, and it led to the formation of spherical micelles, as confirmed by TEM (Figure 4.2A-B). The sizes of these micelles were determined to be 54.0 nm, on average, by DLS, and 31.2 nm by TEM (Figure C.4, Figure 4.2C). The smaller size of micelles in TEM micrographs can be attributed to drying in the vacuum environment. Interestingly, micelles formed from μ1B are significantly smaller than the 64.1 nm micelles formed by μ1 (Table 2.1) as a result of their smaller hydrophobic segment size and an equivalent hydrophilic arm size.[40-42] These micelles were well below 200 nm, a general size limit above which nanoparticles suffer from poor biodistribution.[32]

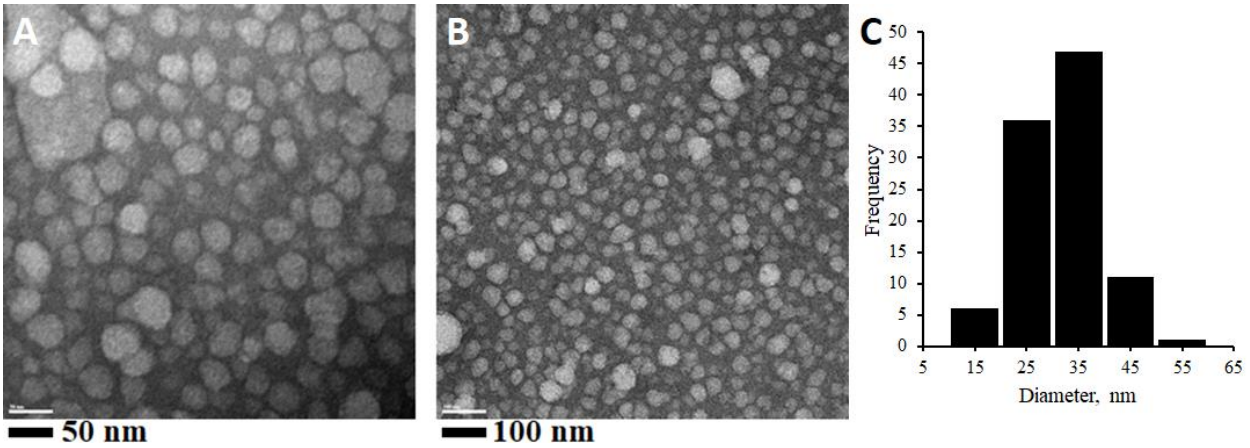

Figure 4.2. TEM micrographs of μ1B micelles with (A) 50 nm, and (B) 100 nm scale bars. (C) Size distribution of micelles in Figure 4A.

The critical micelle concentration for μ1B micelles was determined using the pyrene fluorescence method, where polymer at varying concentrations was used to encapsulate pyrene, a hydrophobic fluorophore. The polymer concentration at which micelles could form and enable the partitioning of pyrene to their relatively less polar cores, resulting in an increase in the excitation wavelength ratio of I_{338}/I_{333}, was denoted as the CMC.[43-45] For μ1B, the CMC was determined to be 3.1 μg/mL,

and it was found to be (Figure C.5) higher than the value of 1.6 μg/mL for μ1 (Figure 2.2). This can be attributed to the lower aggregation stability conferred to μ1B by its shorter hydrophobic PCL arm,[46] yet this CMC was found to be similar to other miktoarm star polymers in general.[3, 40, 47-50]

4.3.3 ROS Response

The viability of thioketal-based ROS-responsive linkers has become well established in developing polymeric micelles for targeted drug delivery.[24-27, 51] Due to its ease of synthesis and straightforward reaction, we opted to use thioketal diacid as a linker to conjugate PEG and TrEG segments in our drug delivery systems. Incubating TKDA with H_2O_2, a model substitute for more general ROS, leads to its oxidative cleavage, forming acetone and 2 equivalents of thiols. However, continued reaction with H_2O_2 can lead to the formation of disulfide bridges from free thiol ends (Scheme 4.2).[51-53] By positioning thioketal groups near the terminal ends of the PEG chains into which they were incorporated, we were able to develop a system in which H_2O_2 could cleave off small TrEG units, keeping micelles intact, and further react to form disulfide bridges with the now exposed free thiol ends. Through this reaction, disulfide bridges could be generated between different micelles in solution, thus forming a network of a large enough size that could not pass through the porous vasculature present at tumour sites. Micelles would be small enough to penetrate tumorous tissue, but when exposed to the extracellular ROS present at those sites, could not escape, thus inducing micelle coupling. It should be noted that due to the distribution of free thiol ends present on micelles and cleaved TrEG units, we expect that that thiol coupling would also take place within partially cleaved micelles, between free TrEG units, and between TrEG units and micelles, but only one point of reaction between micelles would be necessary for network formation. In a preliminary experiment, micelles were self-assembled from a 2 mg/mL concentration of μ1B polymers in aqueous media and were incubated at 37 °C in either 200 mM of H_2O_2 or 200 mM H_2O_2 and 3.2 μM $CuCl_2$, since $CuCl_2$ can catalyze the decomposition of H_2O_2 into other forms of ROS. Interestingly, both samples became clearly turbid over the period of a week, which we suspected was from significant micellar coupling (Figure 4.3).

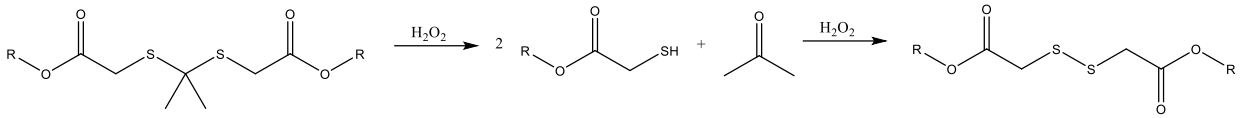

Scheme 4.2. The successive oxidative cleavage and disulfide bridge formation of a thioketal functional group exposed to H_2O_2.

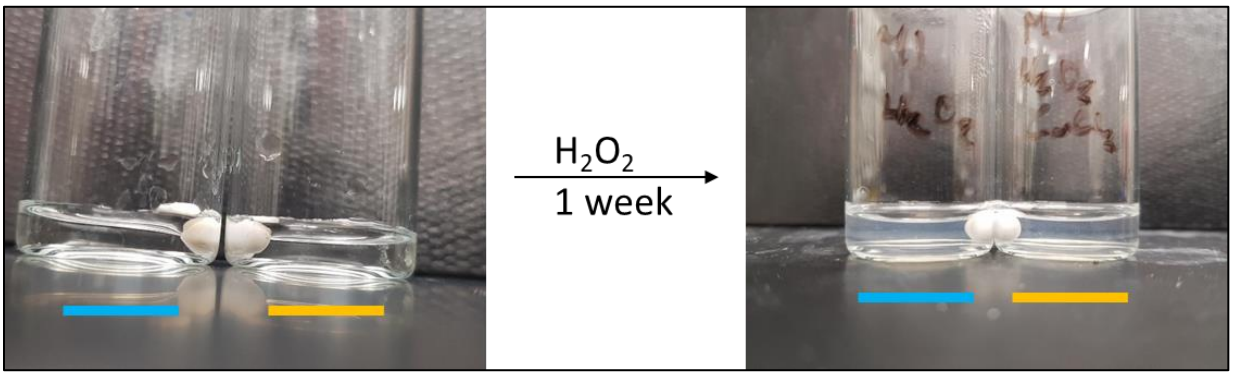

Figure 4.3. The results of treating 2 mg/mL micellar solutions of μ1B with (blue) H_2O_2 and (orange) H_2O_2 and $CuCl_2$ after a week of reaction time.

Micelles were self-assembled in D_2O and their treatment with H_2O_2 was followed *via* NMR in order to elucidate the degree of reaction over time. As a comparison, TKDA itself was also followed under these conditions, and the cleavage of its thioketal group was seen through the decline of its thioketal methyl C*H*$_3$ singlet at 1.54 ppm over a period of about 5 hours. Simultaneously, the cleavage resulted in the formation of acetone, denoted by the singlet at 2.12 ppm, and the shift of TKDA's C*H*$_2$ protons from 3.45 to 3.57 ppm (Figure 4.4A). In the reaction of H_2O_2 with μ1B, a similar trend can be seen, yet it occurs more slowly likely due to the less accessible thioketal groups within the micellar coronae (Figure 4.4B). More specifically, the oxidative cleavage of the thioketal group reduces its C*H*$_3$ peak at 1.55 ppm over approximately 12 hours, and this is accompanied by the simultaneous decrease in the nearby C*H*$_2$ peak at 3.49 ppm. Comparison to the corresponding C*H*$_2$ peak in Figure 4.4A suggests that this peak in facts shifts downfield and overlaps with the immense PEG peak seen at 3.63 ppm. The continued increase in the acetone singlet seen at 2.15 ppm over 24-48 hours suggests that the thioketal group continues to be cleaved past the 12 hour time point, and its C*H*$_3$ singlet is obscured by the overlapping PCL peak (broadened due to the polymer's micellization in water). The formation of free thiol ends on the micellar surface is characterized by the appearance of a thiol S*H* singlet at 1.61 ppm within 1 hour of reaction. Most interestingly, this peak persists over 12 hours and then disappears by the 24 hour time point, suggesting its further oxidation to S-S bonds. A similar disappearance of S*H*

protons was also seen in mercaptoacetic acid, the precursor to TKDA, during H_2O_2 incubation (Figure C.6).

Phosphate-buffered saline (PBS) provides an environment that is isotonic with the human body, and it is ubiquitous in biological research. In order to more closely assess the reaction of μ1B micelles in a biological environment, they were once again assembled in D_2O, and then treated with 200 mM H_2O_2 in pH 7.4 D_2O-based PBS. A control experiment showed that the cleavage of TKDA was much faster in PBS, with the complete reaction occurring within 3 hours, as opposed to 5 in just D_2O (Figure 4.5A). Unlike TKDA, the behaviour of μ1B micelles when treated with 200 mM was not significantly affected by their incubation in PBS (Figure 4.5B).

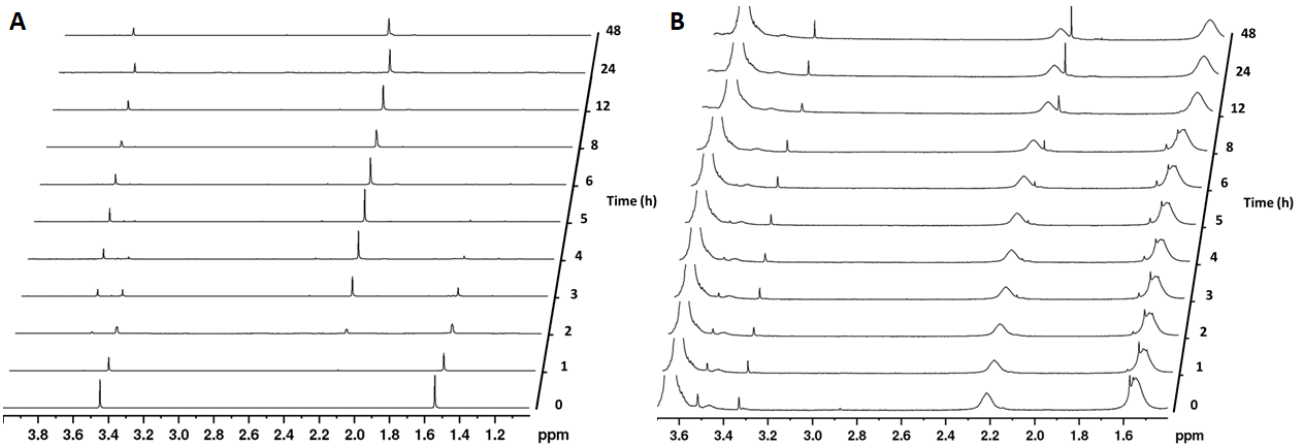

Figure 4.4. NMR spectra of the reaction of (A) TKDA and (B) μ1B micelles with 200 mM H_2O_2 in D_2O over 48 hours.

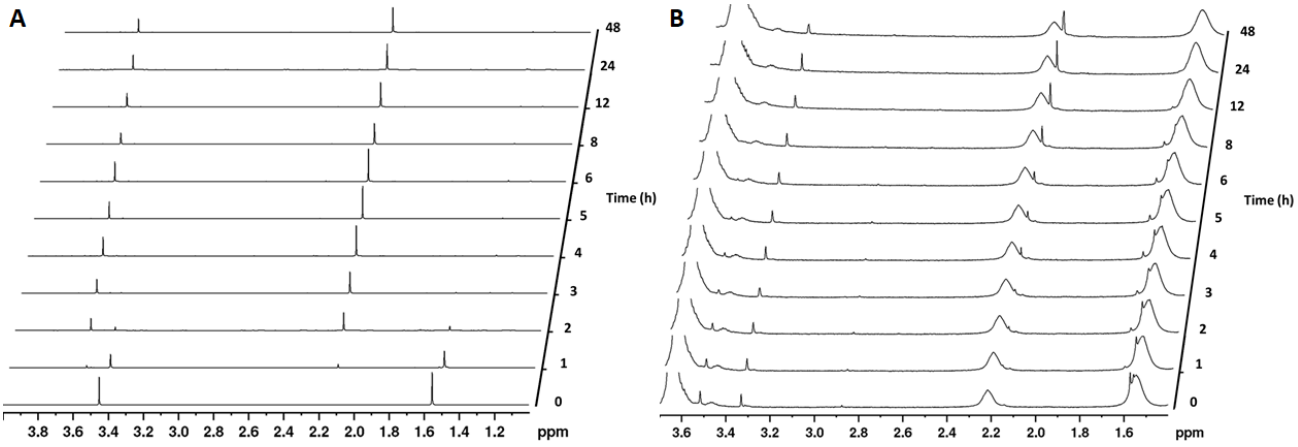

Figure 4.5. NMR spectra of the reaction of (A) TKDA and (B) μ1B micelles with 200 mM H_2O_2 in D_2O-based pH 7.4 PBS over 48 hours.

Given that that the thioketal group in μ1B is largely cleaved by 200 mM of H_2O_2 within 12-24 hours, TEM micrographs were acquired for these micelles at 24 hours, 12 hours, and 0 hours after H_2O_2 treatment (Figure 4.6, Figure C.7). It can be seen that within 12 hours, the nanoparticles transition from disperse spherical micelles to interconnected clusters (Figure 4.6A-B). An additional time point at 24 hours revealed that these networks do not visually progress much more significantly (Figure 4.6C). Micellar network formation is a highly random and disordered process and has shown to form different types of superstructures as seen *via* TEM apart from the cluster mentioned previously. Incubation of μ1B with 200 mM of H_2O_2 for 24 hours at 37 °C had also led to micelles interconnecting in a linear and globular manner, with larger clusters appearing to be "porous" as a result of space not occupied by micelles (Figure 4.7).

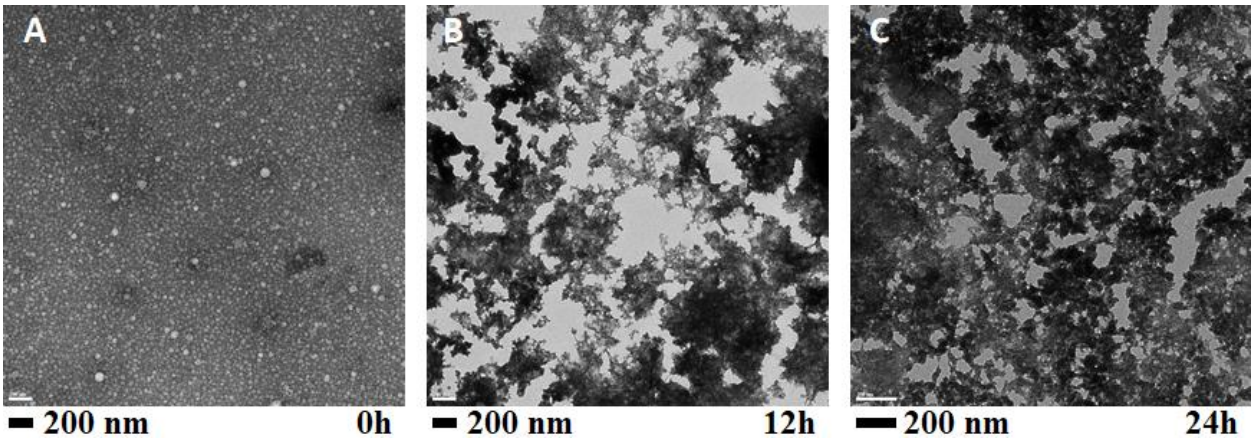

Figure 4.6. TEM micrographs of μ1B micelles after (A) 0, (B) 12, and (C) 24 hours of 200 mM H_2O_2 treatment.

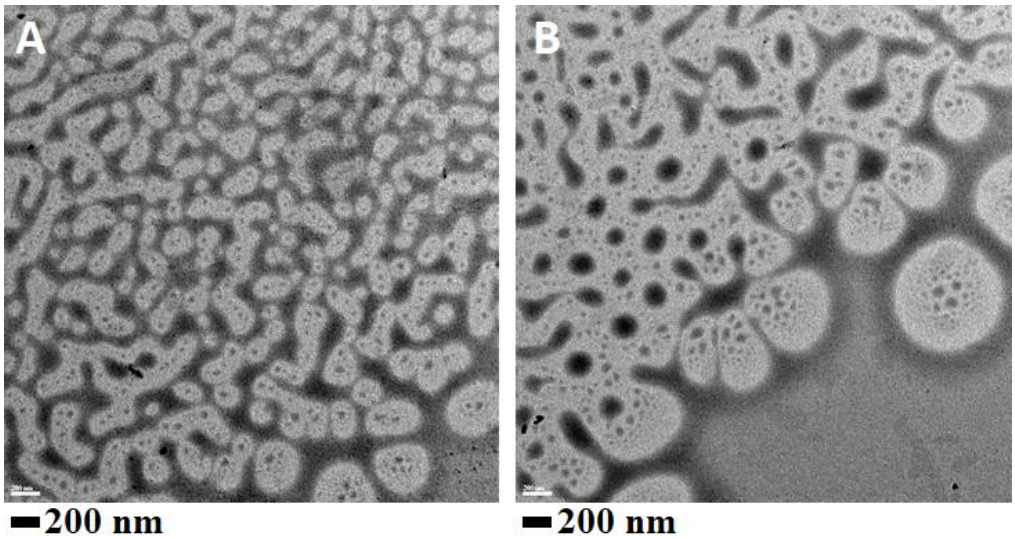

Figure 4.7. Miktoarm polymer μ1B micelles coupling to form (A) linear and (B) globular superstructures.

4.3.4 Drug Loading and Release

Miktoarm micelles with partially cleavable coronae were shown previously to subtly increase drug release rates when exposed to H_2O_2 (Chapter 2.3.6, Chapter 3.3.2) despite their propensity to form network structures under such conditions. While µ1B has slightly shorter TrEG units than the TEG units seen for µ1, we were interested to see the degree to which this can affect drug loading and release. Using co-solvent evaporation from acetone into water, µ1B micelles were loaded with curcumin, a senolytic agent that has been shown to strengthen the well-being of several model organisms,[54] with an encapsulation efficiency of 55.7% ± 16.9 and a loading capacity of 18.6% ± 5.6. While still considerably high, these values are diminished from those seen for µ1 as a result of the lower hydrophobic segment size in µ1B.[41, 55, 56] Curcumin loaded micelles were dialyzed against pH 7.4 PBS with 1% v/v Tween 80 to acquire their drug release profiles. Aliquots were taken at pre-determined time intervals and curcumin concentrations were quantified using UV-vis spectroscopy. H_2O_2 treatment led to an approximately 5%, modest, increase in drug release over 72 hours of dialysis time, with a difference in release profiles being seen after 24 hours (Figure 4.8). Notably, this roughly corresponds with the time point at which the thioketal CH_3 group is no longer visible *via* NMR (Figure 4.4B).

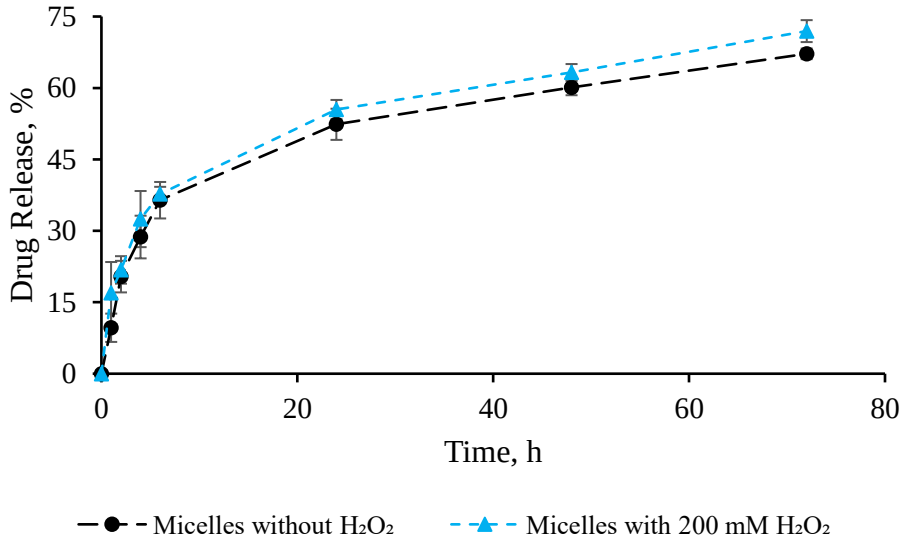

Figure 4.8. Release profile of curcumin from µ1B micelles in pH 7.4 PBS with (black circles) and without (blue triangles) 200 mM H_2O_2 treatment.

4.4 Conclusions

Synthetic tools developed in Chapter 2 were utilised to synthesize an AB_2 (A = PCL, B = PEG) miktoarm star polymer, using simple stitching methodologies including Steglich esterifications and CuAAC "click" coupling. Due in part to its branching architecture, the developed miktoarm star polymer μ1B exhibited a good CMC, curcumin loading content, and a sustained curcumin release profile. Self-assembly resulted in spherical micelles with small sizes suitable for biological administration. We demonstrated that in response to H_2O_2, one of many reactive oxygen species present at disease sites, thioketal linkers located near the terminal ends of μ1B PEG arms were oxidatively cleaved in approximately 24 hours. This stimulus response subtly increased the cumulative release percentage of curcumin, but more interestingly, caused the coupling of micelles through the free thiols present at their surfaces. The formation of micellar networks through such oxidative thiol coupling led to clusters exceedingly larger than single micelles. This study was limited due to restrictions imposed by COVID-19 pandemic, however, it gives a proof-of-concept that miktoarm star polymer based aqueous assemblies that can generate free thiols in biological medium, can be used to promote the accumulation of drug carriers at disease sites where reactive oxygen species are overproduced through the formation of disulfide bonds. The evocation of this novel pathway through an "artificially enhanced" EPR effect in this manner, can improve the localization of drug delivery nanoparticles administered therapeutically.

4.5 References

1. Tran, S.; DeGiovanni, P.-J.; Piel, B.; Rai, P., Cancer nanomedicine: a review of recent success in drug delivery. *Clin. Transl. Med.* **2017,** *6* (1), 44.
2. Bruno, B. J.; Miller, G. D.; Lim, C. S., Basics and recent advances in peptide and protein drug delivery. *Ther. Deliv.* **2013,** *4* (11), 1443-1467.
3. Lu, Y.; Zhang, E.; Yang, J.; Cao, Z., Strategies to improve micelle stability for drug delivery. *Nano Res.* **2018,** *11* (10), 4985-4998.
4. Haag, R.; Kratz, F., Polymer Therapeutics: Concepts and Applications. *Angew. Chem. Int. Ed.* **2006,** *45* (8), 1198-1215.
5. Kim, S.; Shi, Y.; Kim, J. Y.; Park, K.; Cheng, J.-X., Overcoming the barriers in micellar drug delivery: loading efficiency, in vivo stability, and micelle–cell interaction. *Expert Opin. Drug Del.* **2010,** *7* (1), 49-62.
6. Kaditi, E.; Mountrichas, G.; Pispas, S.; Demetzos, C., Block Copolymers for Drug Delivery Nano Systems (DDnSs). *Curr. Med. Chem.* **2012,** *19* (29), 5088-5100.
7. Gaucher, G.; Dufresne, M.-H.; Sant, V. P.; Kang, N.; Maysinger, D.; Leroux, J.-C., Block copolymer micelles: preparation, characterization and application in drug delivery. *J. Control. Release* **2005,** *109* (1), 169-188.

8. Zhao, X.; Zhang, J.; Zhao, Y., Synthesis and properties of penta-responsive ABC star quaterpolymers. *Polym. J.* **2020,** *52* (1), 153-163.
9. Zhang, Y.; Bradley, M.; Geng, J., Photo-controlled one-pot strategy for the synthesis of asymmetric three-arm star polymers. *Polym. Chem.* **2019,** *10* (35), 4769-4773.
10. Augustine, D.; Hadjichristidis, N.; Gnanou, Y.; Feng, X., Hydrophilic Stars, Amphiphilic Star Block Copolymers, and Miktoarm Stars with Degradable Polycarbonate Cores. *Macromolecules* **2020,** *53* (3), 895-904.
11. Levi, A. E.; Fu, L.; Lequieu, J.; Horne, J. D.; Blankenship, J.; Mukherjee, S.; Zhang, T.; Fredrickson, G. H.; Gutekunst, W. R.; Bates, C. M., Efficient Synthesis of Asymmetric Miktoarm Star Polymers. *Macromolecules* **2020,** *53* (2), 702-710.
12. Ge, Y.; Chen, C.; Sim, X. M.; Zheng, J.; Goto, A., Synthesis of ABC Miktoarm Star Copolymers via Organocatalyzed Living Radical Polymerization. *Macromol. Rapid Commun.* **2020,** *41* (5), 1900623.
13. Skandalis, A.; Pispas, S., Synthesis of (AB)n-, AnBn-, and AxBy-type amphiphilic and double-hydrophilic star copolymers by RAFT polymerization. *J. Polym. Sci. A Polym. Chem.* **2019,** *57* (16), 1771-1783.
14. Khanna, K.; Varshney, S.; Kakkar, A., Miktoarm star polymers: advances in synthesis, self-assembly, and applications. *Polym. Chem.* **2010,** *1* (8), 1171-1185.
15. Wais, U.; Liu, J.; He, T.; Zhang, H., CHAPTER 5 Micellar and Emulsion-Assisted Drug Delivery: Comparison of Miktoarm Star Polymers and Block Copolymers. In *Miktoarm Star Polymers: From Basics of Branched Architecture to Synthesis, Self-assembly and Applications*, The Royal Society of Chemistry: 2017; pp 116-149.
16. Sharma, A.; Kakkar, A., Designing Dendrimer and Miktoarm Polymer Based Multi-Tasking Nanocarriers for Efficient Medical Therapy. *Molecules* **2015,** *20* (9), 16987-17015.
17. Pispas, S.; Hadjichristidis, N.; Potemkin, I.; Khokhlov, A., Effect of Architecture on the Micellization Properties of Block Copolymers: A2B Miktoarm Stars vs AB Diblocks. *Macromolecules* **2000,** *33* (5), 1741-1746.
18. Hadjichristidis, N.; Pitsikalis, M.; Iatrou, H.; Driva, P.; Sakellariou, G.; Chatzichristidi, M., 6.03 - Polymers with Star-Related Structures: Synthesis, Properties, and Applications. In *Polymer Science: A Comprehensive Reference*, Matyjaszewski, K.; Möller, M., Eds. Elsevier: Amsterdam, 2012; pp 29-111.
19. Aghajanzadeh, M.; Zamani, M.; Rostamizadeh, K.; Sharafi, A.; Danafar, H., The role of miktoarm star copolymers in drug delivery systems. *J. Macromol. Sci. Part A* **2018,** *55* (7), 559-571.
20. Upsides and Downsides of Reactive Oxygen Species for Cancer: The Roles of Reactive Oxygen Species in Tumorigenesis, Prevention, and Therapy. *Antioxid. Redox Signaling* **2012,** *16* (11), 1295-1322.
21. Chelombitko, M. A., Role of Reactive Oxygen Species in Inflammation: A Minireview. *Moscow Univ. Biol. Sci. Bull.* **2018,** *73* (4), 199-202.
22. Burhans, W. C.; Heintz, N. H., The cell cycle is a redox cycle: Linking phase-specific targets to cell fate. *Free Radical Biol. Med.* **2009,** *47* (9), 1282-1293.
23. Van Raamsdonk, J. M.; Hekimi, S., Deletion of the Mitochondrial Superoxide Dismutase sod-2 Extends Lifespan in Caenorhabditis elegans. *PLoS Genet.* **2009,** *5* (2), e1000361.
24. Ye, H.; Zhou, Y.; Liu, X.; Chen, Y.; Duan, S.; Zhu, R.; Liu, Y.; Yin, L., Recent Advances on Reactive Oxygen Species-Responsive Delivery and Diagnosis System. *Biomacromolecules* **2019,** *20* (7), 2441-2463.

25. Yin, W.; Ke, W.; Chen, W.; Xi, L.; Zhou, Q.; Mukerabigwi, J. F.; Ge, Z., Integrated block copolymer prodrug nanoparticles for combination of tumor oxidative stress amplification and ROS-responsive drug release. *Biomaterials* **2019,** *195*, 63-74.
26. Wei, M.; Gao, Y.; Li, X.; Serpe, M. J., Stimuli-responsive polymers and their applications. *Polym. Chem.* **2017,** *8* (1), 127-143.
27. Sabourian, P.; Tavakolian, M.; Yazdani, H.; Frounchi, M.; van de Ven, T. G. M.; Maysinger, D.; Kakkar, A., Stimuli-responsive chitosan as an advantageous platform for efficient delivery of bioactive agents. *J. Control. Release* **2020,** *317*, 216-231.
28. Golombek, S. K.; May, J.-N.; Theek, B.; Appold, L.; Drude, N.; Kiessling, F.; Lammers, T., Tumor targeting via EPR: Strategies to enhance patient responses. *Adv. Drug Delivery Rev.* **2018,** *130*, 17-38.
29. Matsumura, Y.; Maeda, H., A New Concept for Macromolecular Therapeutics in Cancer Chemotherapy: Mechanism of Tumoritropic Accumulation of Proteins and the Antitumor Agent Smancs. *Cancer Res.* **1986,** *46* (12 Part 1), 6387-6392.
30. Mirza, A. Z.; Siddiqui, F. A., Nanomedicine and drug delivery: a mini review. *Int. Nano Lett.* **2014,** *4* (1), 94.
31. Farokhzad, O. C.; Langer, R., Nanomedicine: Developing smarter therapeutic and diagnostic modalities. *Adv. Drug Delivery Rev.* **2006,** *58* (14), 1456-1459.
32. Moghimi, S. M.; Hunter, A. C.; Murray, J. C., Long-Circulating and Target-Specific Nanoparticles: Theory to Practice. *Pharmacol. Rev.* **2001,** *53* (2), 283.
33. Nichols, J. W.; Bae, Y. H., EPR: Evidence and fallacy. *J. Control. Release* **2014,** *190*, 451-464.
34. Khanna, K.; Varshney, S.; Kakkar, A., Designing Miktoarm Polymers Using a Combination of "Click" Reactions in Sequence with Ring-Opening Polymerization. *Macromolecules* **2010,** *43* (13), 5688-5698.
35. Neises, B.; Steglich, W., Simple Method for the Esterification of Carboxylic Acids. *Angew. Chem. Int. Ed.* **1978,** *17* (7), 522-524.
36. Moore, J. S.; Stupp, S. I., Room temperature polyesterification. *Macromolecules* **1990,** *23* (1), 65-70.
37. Rostovtsev, V. V.; Green, L. G.; Fokin, V. V.; Sharpless, K. B., A Stepwise Huisgen Cycloaddition Process: Copper(I)-Catalyzed Regioselective "Ligation" of Azides and Terminal Alkynes. *Angew. Chem. Int. Ed.* **2002,** *41* (14), 2596-2599.
38. Liu, Q.; Chen, Y., Synthesis of well-defined macromonomers by the combination of atom transfer radical polymerization and a click reaction. *J. Polym. Sci. A Polym. Chem.* **2006,** *44* (20), 6103-6113.
39. Moquin, A.; Sturn, J.; Zhang, I.; Ji, J.; von Celsing, R.; Vali, H.; Maysinger, D.; Kakkar, A., Unraveling Aqueous Self-Assembly of Telodendrimers to Shed Light on Their Efficacy in Drug Encapsulation. *ACS Appl. Bio Mater.* **2019,** *2* (10), 4515-4526.
40. Soliman, G. M.; Sharma, R.; Choi, A. O.; Varshney, S. K.; Winnik, F. M.; Kakkar, A. K.; Maysinger, D., Tailoring the efficacy of nimodipine drug delivery using nanocarriers based on A2B miktoarm star polymers. *Biomaterials* **2010,** *31* (32), 8382-8392.
41. Huang, L.-m.; Li, L.-d.; Shang, L.; Zhou, Q.-h.; Lin, J., Preparation of pH-sensitive micelles from miktoarm star block copolymers by ATRP and their application as drug nanocarriers. *React. Funct. Polym.* **2016,** *107*, 28-34.

42. Alizadeh, R.; Ghaemy, M., pH-responsive ABC type miktoarm star terpolymers: Synthesis via combination of click reaction and SET-LRP, characterization, self-assembly, and controlled drug release. *Polymer* **2015,** *66*, 179-191.
43. Liu, R.; Forrest, M. L.; Kwon, G. S.; Zhihong, X. X., Polymeric Micelles in Water-Insoluble Drug Delivery. In *Water-insoluble drug formulation*, 3 ed.; Liu, R., Ed. CRC Press: Boca Raton, FL, 2008.
44. Huang, X.; Xiao, Y.; Lang, M., Synthesis and self-assembly behavior of six-armed block copolymers with pH- and thermo-responsive properties. *Macromol. Res.* **2011,** *19* (2), 113-121.
45. Lin, W.; Nie, S.; Zhong, Q.; Yang, Y.; Cai, C.; Wang, J.; Zhang, L., Amphiphilic miktoarm star copolymer (PCL)3-(PDEAEMA-b-PPEGMA)3 as pH-sensitive micelles in the delivery of anticancer drug. *J. Mater. Chem. B* **2014,** *2* (25), 4008-4020.
46. Chen, L.-J.; Lin, S.-Y.; Huang, C.-C., Effect of Hydrophobic Chain Length of Surfactants on Enthalpy−Entropy Compensation of Micellization. *J. Phys. Chem. B* **1998,** *102* (22), 4350-4356.
47. Yoshida, E., Control of Micellar Size and Critical Micelle Concentration for "Nonamphiphilic" Poly(vinyl phenol)-block-Polystyrene Diblock Copolymers. *Polym. J.* **2003,** *35* (12), 965-971.
48. Lo, C.-L.; Lin, S.-J.; Tsai, H.-C.; Chan, W.-H.; Tsai, C.-H.; Cheng, C.-H. D.; Hsiue, G.-H., Mixed micelle systems formed from critical micelle concentration and temperature-sensitive diblock copolymers for doxorubicin delivery. *Biomaterials* **2009,** *30* (23), 3961-3970.
49. Kosa, S. A.; Al-Harbi, L. M.; Baloch, M. K.; Ullah, I.; El-Mossalamy, E. H., Impact of Block Length and Temperature over Self-Assembling Behavior of Block Copolymers. *Int. J. Polym. Sci.* **2016,** *2016*, 7.
50. Kulthe, S. S.; Choudhari, Y. M.; Inamdar, N. N.; Mourya, V., Polymeric micelles: authoritative aspects for drug delivery. *Des. Monomers Polym.* **2012,** *15* (5), 465-521.
51. Chen, D.; Zhang, G.; Li, R.; Guan, M.; Wang, X.; Zou, T.; Zhang, Y.; Wang, C.; Shu, C.; Hong, H.; Wan, L.-J., Biodegradable, Hydrogen Peroxide, and Glutathione Dual Responsive Nanoparticles for Potential Programmable Paclitaxel Release. *J. Am. Chem. Soc.* **2018,** *140* (24), 7373-7376.
52. Kirihara, M.; Asai, Y.; Ogawa, S.; Noguchi, T.; Hatano, A.; Hirai, Y., A Mild and Environmentally Benign Oxidation of Thiols to Disulfides. *Synthesis* **2007,** *2007* (21), 3286-3289.
53. He, Y.; Hang, D.; Lu, M., A Simple and Practical Method for the Oxidation of Thiols to Disulfides at Mild Conditions Without Solvents. *Phosphorus Sulfur Silicon Relat. Elem.* **2012,** *187* (9), 1118-1124.
54. Bielak-Zmijewska, A.; Grabowska, W.; Ciolko, A.; Bojko, A.; Mosieniak, G.; Bijoch, Ł.; Sikora, E., The Role of Curcumin in the Modulation of Ageing. *Int. J. Mol. Sci.* **2019,** *20* (5), 1239.
55. Zhang, H.-H.; Huang, Z.-Q.; Sun, B.-W.; Guo, J.-X.; Wang, J.-L.; Chen, Y.-Q., Y-shaped poly(ethylene glycol) and poly(trimethylene carbonate) amphiphilic copolymer: Synthesis and for drug delivery. *J. Polym. Sci. A Polym. Chem.* **2008,** *46* (24), 8131-8140.
56. Chu, Y.; Yu, H.; Zhang, Y.; Zhang, G.; Ma, Y.; Zhuo, R.; Jiang, X., Synthesis and characterization of biodegradable amphiphilic ABC Y-shaped miktoarm terpolymer by click chemistry for drug delivery. *J. Polym. Sci. A Polym. Chem.* **2014,** *52* (23), 3346-3355.

Chapter 5: Conclusions and Future Perspectives

5.1 Conclusions and Contributions to Original Knowledge

Miktoarm star polymers are an emerging class of branched architectures in which mixed polymeric segments emanate from a central core. Advances in arm-first and core-first synthetic methodologies have encouraged the increased development of miktoarm star polymers for a variety of applications, most notably in drug delivery. The inclusion of branched polymeric architecture lends an advantageous platform in drug delivery, as it provides vast tunability of the resulting self-assemblies. Through variations in polymeric segments, a multitude of their properties including core/corona structure, hydrophobic cores, and various biological stimulus-response mechanisms, could be tailored. In addition, miktoarm star polymers based micelles have also been shown to be physically superior to conventional block copolymer-based formulations, in terms of i) lower CMCs, resulting in more stable structures that can resist large dilution upon biological administration; ii) higher drug encapsulation efficiencies; and iii) prolonged drug release profiles that aid in drug bioavailability and activity.

In this thesis, a mixed arm-first and core-first methodology was applied to synthesize a series of AB_2 (A = PCL, B = PEG) stimuli-responsive miktoarm star polymers in a modular fashion. This strategy first consisted of designing several PEG- or PCL-based "building blocks" through highly efficient ring opening polymerizations and Steglich esterifications, which incorporated ROS-responsive thioketal groups (at the terminal ends of PEG arms), and GSH-responsive disulfide groups (adjacent to the core molecules at the PCL junction). The synthetic methodology then employed highly efficient copper-catalyzed alkyne-azide cycloaddition "click" coupling between different blocks, leading to a series of miktoarm star polymers with or without stimuli-responsive entities. These were subsequently self-assembled into spherical micelles with diameters well below 200 nm, an upper limit under which polymeric nanoparticles distribute well through the vasculature. Micelles had very low CMCs, and were able to load senolytic agents, including curcumin and resveratrol, with excellent encapsulation efficiencies. Importantly, the incubation of micelles containing ROS-responsive thioketal moieties on their surfaces with H_2O_2, led to oxidative cleavage of thioketal linkers, and subsequent partial "shedding" of micellar coronae. This subtly increased the rate of drug release while micelles remained largely intact. As elevated levels of ROS are present extracellularly, this effect can pair well with the action of GSH-

responsive disulfide moieties located at the core junction of miktoarm star polymers. Exposure of disulfide containing micelles to GSH, which is overproduced within oxidatively stressed cells, enabled the reductive cleavage of disulfide linkers, thus separating PCL from PEG segments, causing micellar disassembly, and significantly accelerating drug release. While ROS- and GSH-induced effects were shown for both curcumin- and resveratrol-loaded micelles, drug release acceleration was more apparent for curcumin as a result of its more prolonged release profile, which stems from its higher hydrophobicity. Curcumin was additionally shown to efficiently suppress ROS generation in U251 human glioblastoma cells when loaded into ROS-responsive micelles. An added consequence of micellar corona shedding is the exposure of free thiol groups which result directly from thioketal cleavage. Micelles which remain exposed to ROS can link and form networks *via* oxidative thiol coupling. Such network formation occurs within 24 hours of ROS exposure and, following micellar delivery through the leaky vasculature of disease sites, can promote their retention. Following this two-part mechanism of partial corona shedding and network formation, ROS-responsive micelles are expected to promote the targeted delivery of senolytic agents with limited side-effects.

5.2 Future Perspectives

The ROS-responsive miktoarm star polymers investigated in this thesis were produced *via* the incorporation of stimulus-responsive thioketal groups at a spatially distant end of their PEG segments. ROS exposure led to the partial corona shedding of their self-assembled micelles, thus slightly increasing the release rate of loaded drugs. In a similar manner, a series of ROS-responsive miktoarm star polymers can be synthesized in which thioketal linkers are incorporated at varied positions in their PEG backbones. In this study, N_3-PEG_{2000} was coupled to a unit consisting of thioketal diacid conjugated to TEG or TrEG. The process could be reversed, and instead, N_3-PEGs of lower molecular weight could be coupled to thioketal-oligo-ethylene glycols of increasing length, resulting in miktoarm stars with thioketal groups at varying points in their PEG arms. The rate at which the thioketal groups in these miktoarm stars react would be expected to decrease as thioketal placement nears the miktoarm core junction. More interestingly, however, would be the effect of corona shedding in micelles assembled from this series of polymers. In particular, drug release acceleration triggered by thioketal oxidative cleavage could be directly related to thioketal spatial location. While thioketal groups are certainly attractive due to their efficient reaction with extracellular ROS, GSH-responsive disulfide groups could also be incorporated into PEG and

studied in a similar manner. Due to their reductive effect, micellar corona shedding would not be followed by micellar coupling, and corona shedding could be studied in isolation.

Considering the fact that ROS- and GSH-responsive miktoarm star polymers were developed for drug delivery applications, a complete biological evaluation would extend the work described in this thesis and provide further justification for the use of miktoarm star polymers based nanocarriers in drug delivery. The cytotoxicity of empty and drug-loaded micelles could be tested through MTT assays, and the extent of micelle stability could be evaluated in fetal bovine serum or in similar media that can provide a model for intravenous conditions. Quantification of cellular ROS and GSH levels can also be analyzed using the fluorescent probes CellROX Deep Red and monochlorobimane, respectively, and would establish the degree to which loaded miktoarm star polymers contribute to senescent cell elimination.

We have shown, in a preliminary investigation, that the thiol groups exposed on the surface of micelles, when placed in an oxidative ROS environment, can induce coupling of micelles. Such coupling was characterized in miktoarm polymers using NMR spectra. In micelles, we observed an increase in solution turbidity, and it was further investigated using TEM, and it showed the formation of linked micelles. These are very promising preliminary results, which need to be further confirmed by a detailed evaluation, using a combination of techniques. It is possible to image micellar formulations using SEM, which may help visualize the linking of micelles in a more direct manner. This can be combined with Cryo-TEM studies on these micelles. In addition, the number of species in solution is expected to decrease as micelles form larger structures. Their enumeration through particle counting instrumentation, such as SLS or a Coulter counter, can provide another avenue for collecting network formation evidence. Finally, the functional group transition from thioketal to thiol to disulfide can be followed precisely using FT-IR.

Thiol-ene and thiol-yne coupling reactions are well understood “click” chemistry reactions that provide stereoselectivity and give excellent yields. This has led to their common employment in polymer segment conjugation in complex branched or grafted systems. Proof-of-concept experiments in chapter 4 have shown that coupling of micelle surface thiol groups can lead to their linking and the subsequent formation of micelle networks. Given the thermodynamic driving force behind thiol-ene and thiol-yne “click” reactions, they can be applied to micellar network formation in order to improve the efficiency of their coupling. The proof-of-concept of these reactions in

biological medium has already been established in our laboratory. AB_2 (A = PCL, B = PEG) miktoarm star polymers can be developed that, instead of thioketal moieties, contain terminal alkenyl or alkynyl groups. Such polymers would be afforded through the direct conjugation of alkenoic or alkynoic acids to PEG-OH terminal groups *via* Steglich esterification. Micelles could then be co-assembled from polymers containing thioketal ends and those containing alkenyl or alkynyl groups, and the aqueous radical-catalyzed thiol-ene/yne reaction would then be carried out to induce network formation. Alternatively, micelles can be self-assembled separately such that individual micelles would contain only one type of end group. In addition to NMR-based kinetic studies and TEM, which were used to study thiol-thiol oxidative coupling, methods such as SEM and Coulter counter-based nanoparticle sizing and quantification can provide further avenues to characterize the micelle-to-network transition based on thiol-thiol, thiol-ene, and thiol-yne coupling.

Appendix A

A.1. Synthetic Schemes

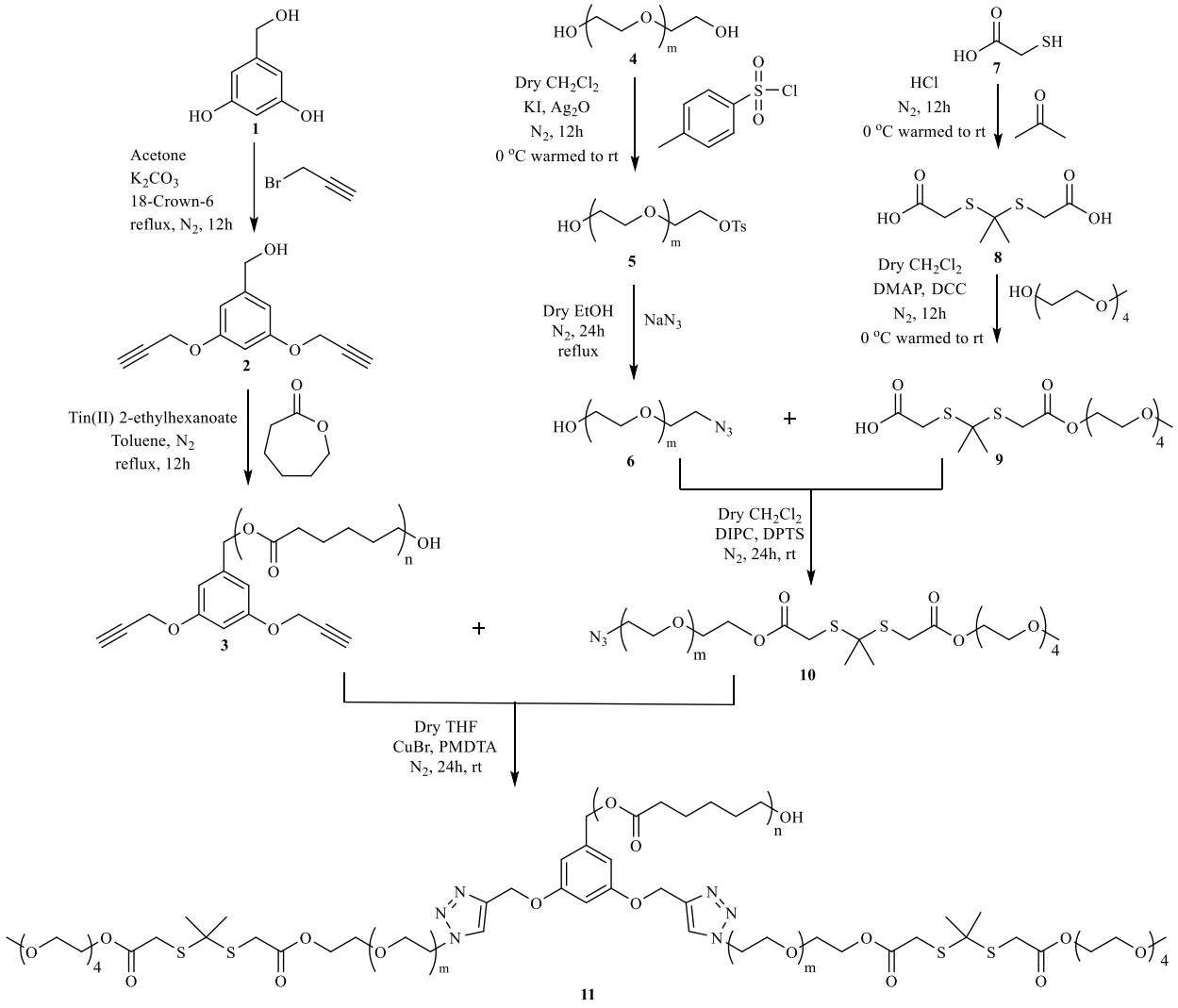

Scheme A.1. Synthesis of μ1.

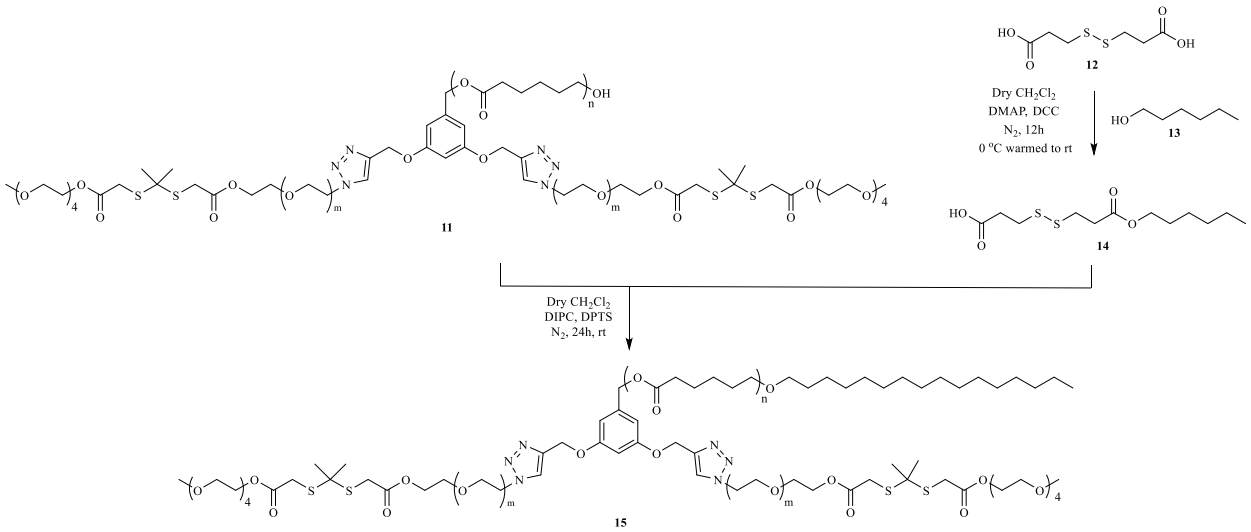

Scheme A.2. Synthesis of μ2.

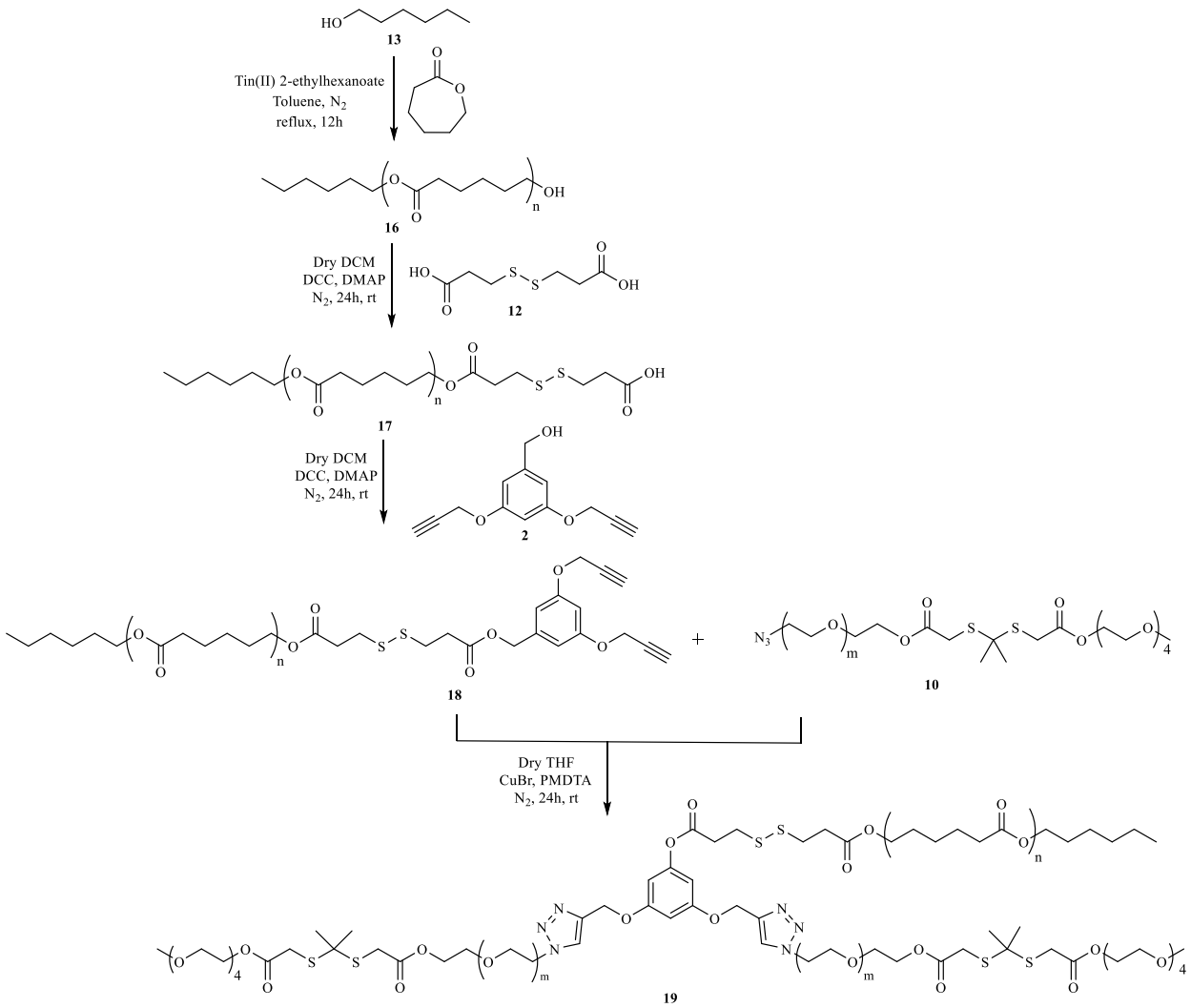

Scheme A.3. Synthesis of μ3.

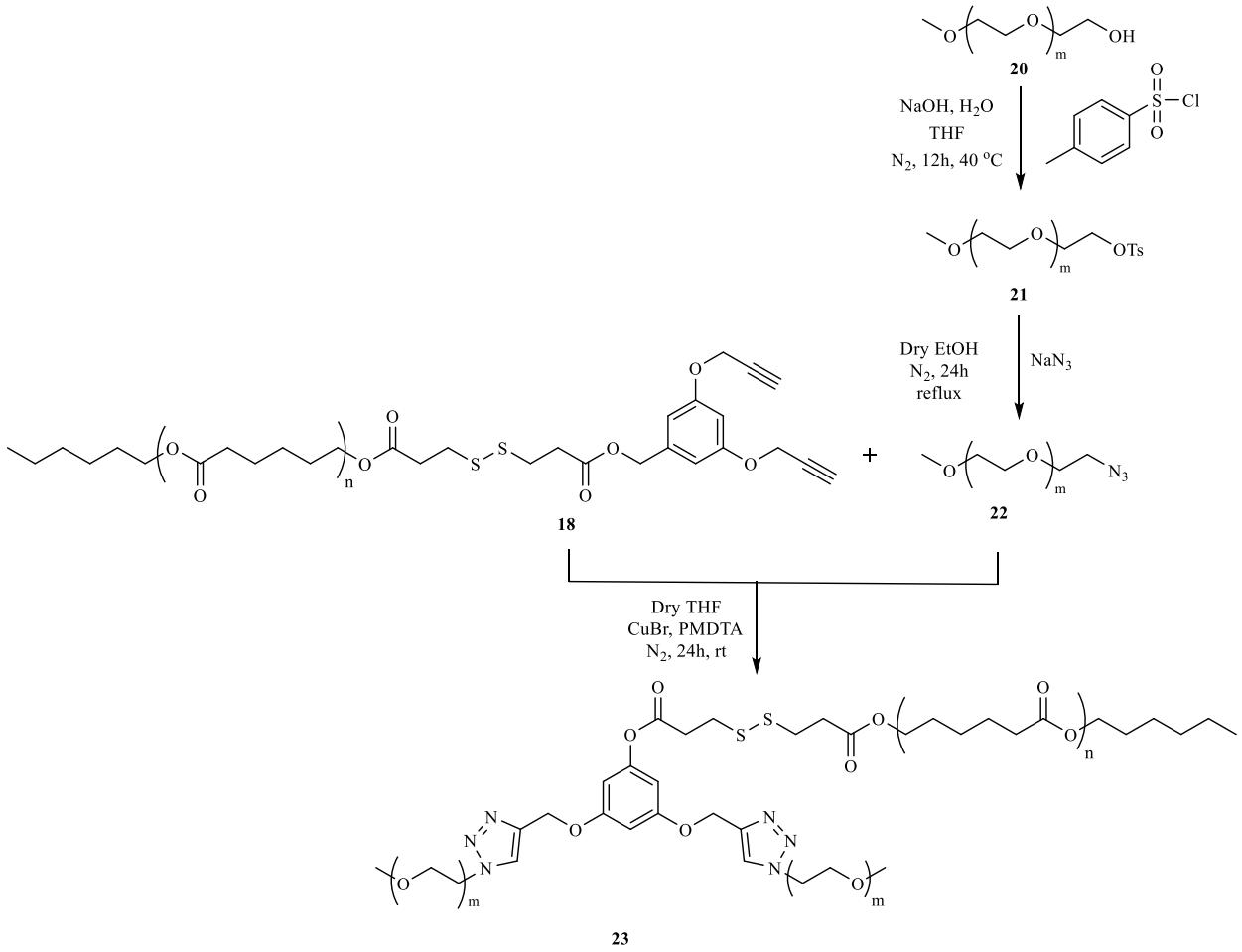

Scheme A.4. Synthesis of μ4.

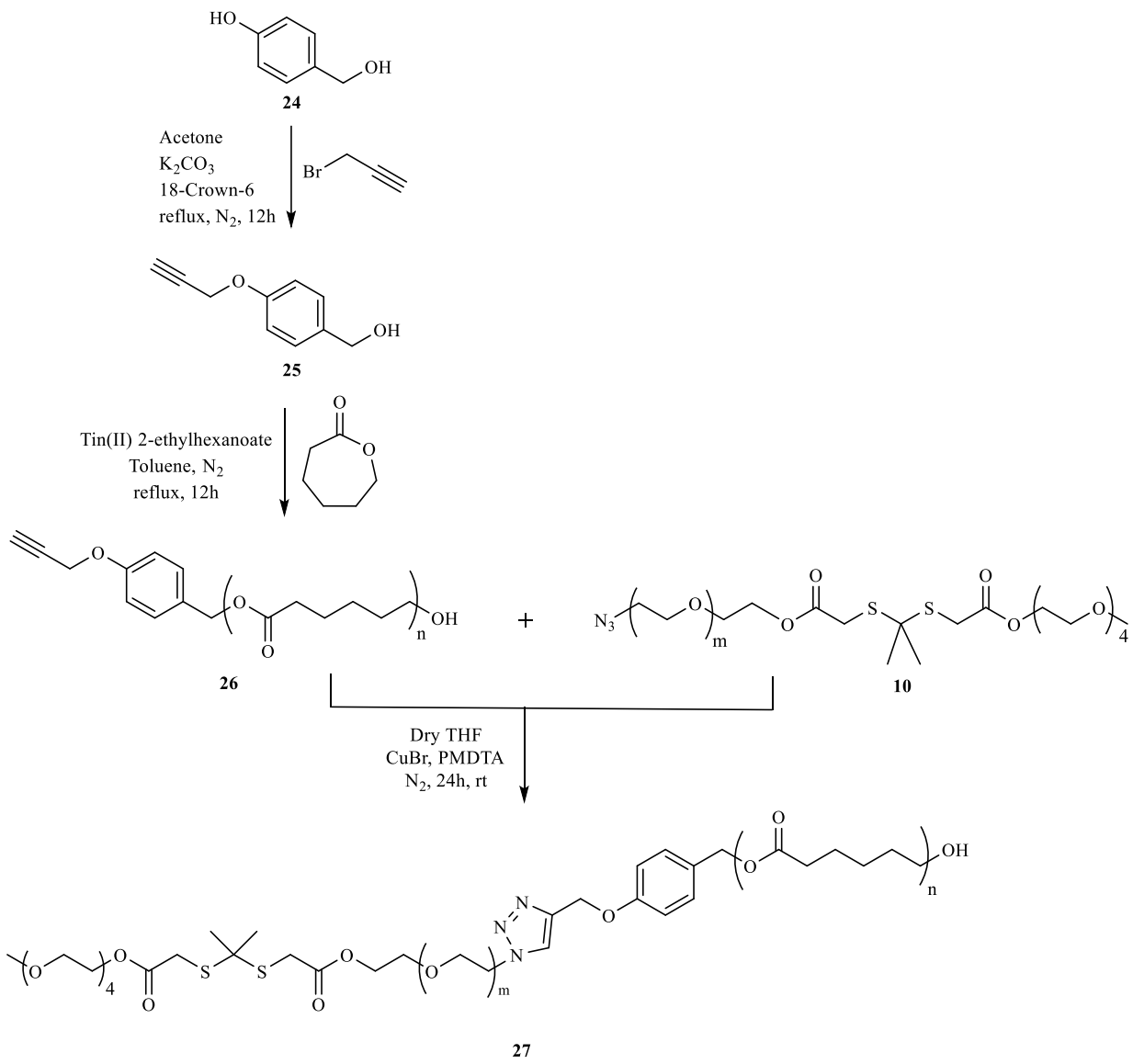

Scheme A.5. Synthesis of b1.

A.2. Supplementary Tables & Figures

Table A.1. Characterization of miktoarm star polymer building blocks

Building Block	Molar Mass (MS)[1]	Molar Mass (NMR)[2]	DP (NMR)[3]	DP (MS)	*Đ* (MS)	*Đ* (GPC)
DPB-PCL, **3**	2839	3306	29	25	1.17	1.75
N_3-PEG-TK-TEG, **10**	2371	2684	61	54	1.01	1.09
DS-Hex, **14**	294	N/A	N/A	N/A	N/A	N/A
DPB-DS-PCL-Hx, **18**	2464	3648	32	22	1.08	1.39
mPEG-N_3, **22**	2133	2112	48	48	1.01	1.06
4PB-PCL, **26**	2037	1938	17	18	1.04	1.55

[1]Polymer building blocks analyzed using MALDI-TOF, DS-Hex analyzed using ESI.

[2]Molar masses calculated based on repeating unit molar mass and DP (NMR).

[3]Number of PEG repeating unit protons compared to overlapping CH_2-N_3 and OCH_3 protons at 3.38 ppm. Number of PCL repeating unit protons for (-CH_2-OOC-)$_n$ measured against Ar-CH_2-O protons at 5.07 ppm in DPB-PCL and 4PB-PCL and against CH_2-CH_2-S-S protons in DPB-DS-PCL-Hx at 2.72-2.99 ppm.

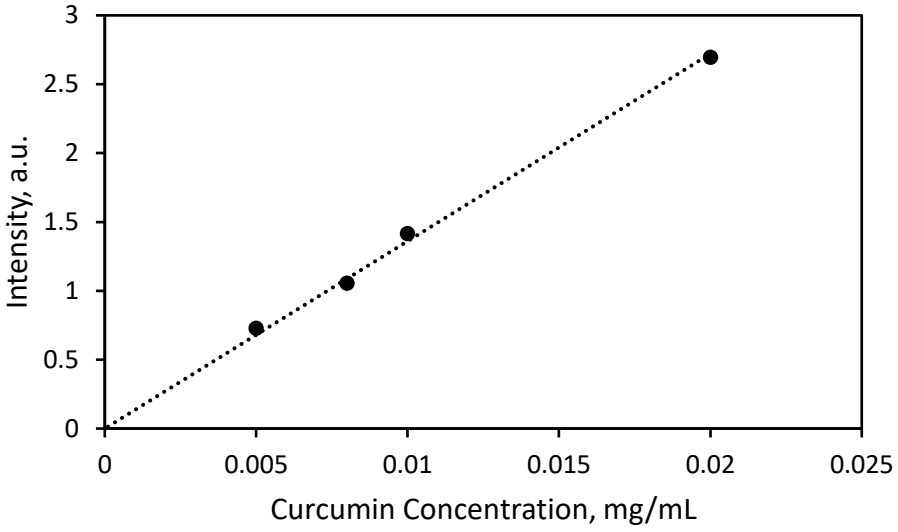

Figure A.1. Standard curve for curcumin concentration at λ = 424 nm.

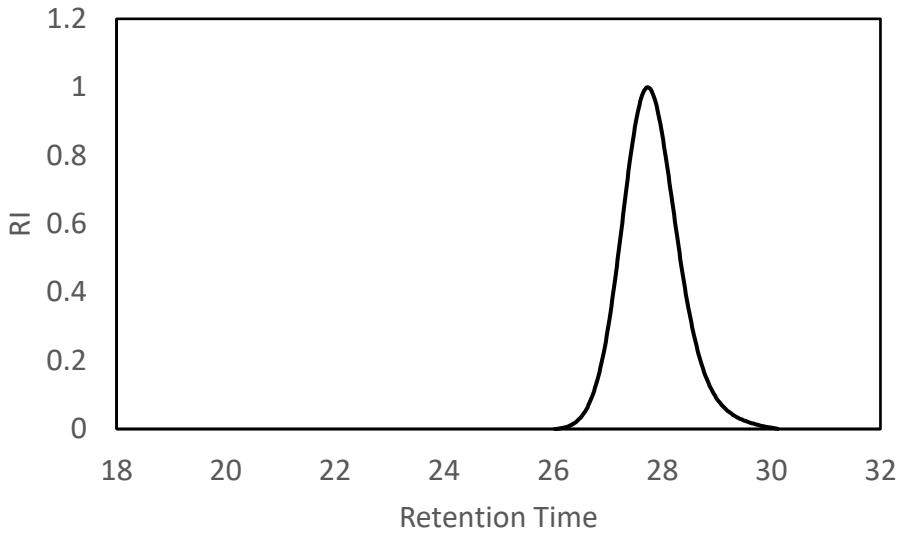

Figure A.2. GPC trace of PEG-N_3 (**6**). Retention time = 27.725 min, $Đ$ = 1.06.

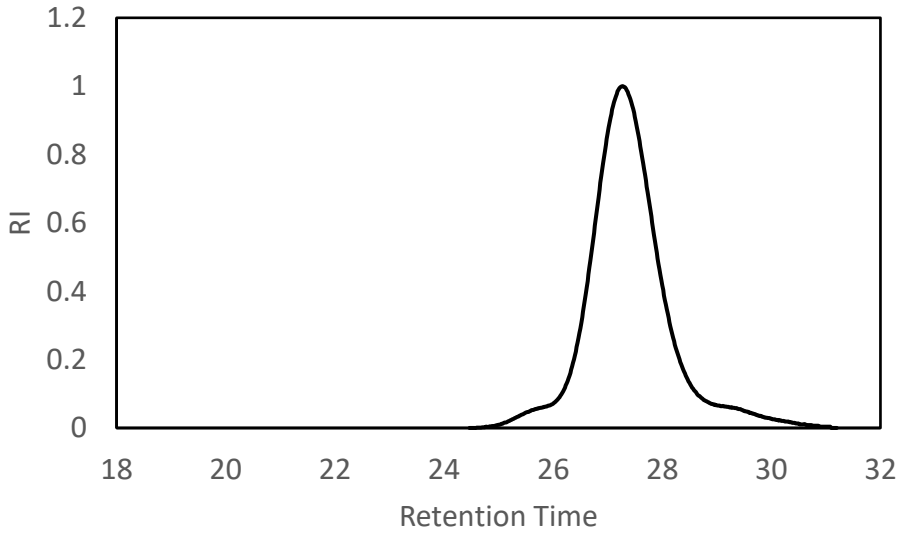

Figure A.3. GPC trace of N_3-PEG-TK-TEG (**10**). Retention time = 27.266 min, $Đ$ = 1.09.

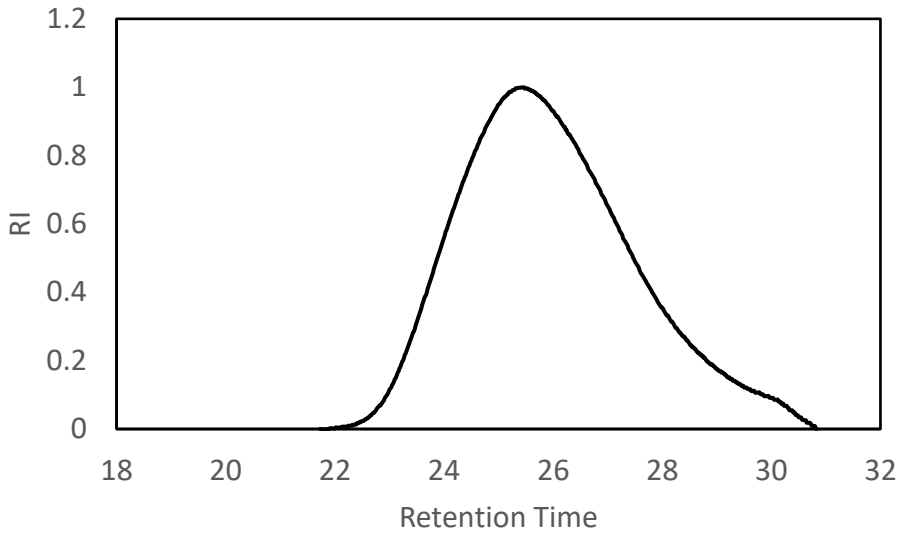

Figure A.4. GPC trace DPB-PCL (**3**). Retention time = 25.317 min, $Đ$ = 1.75.

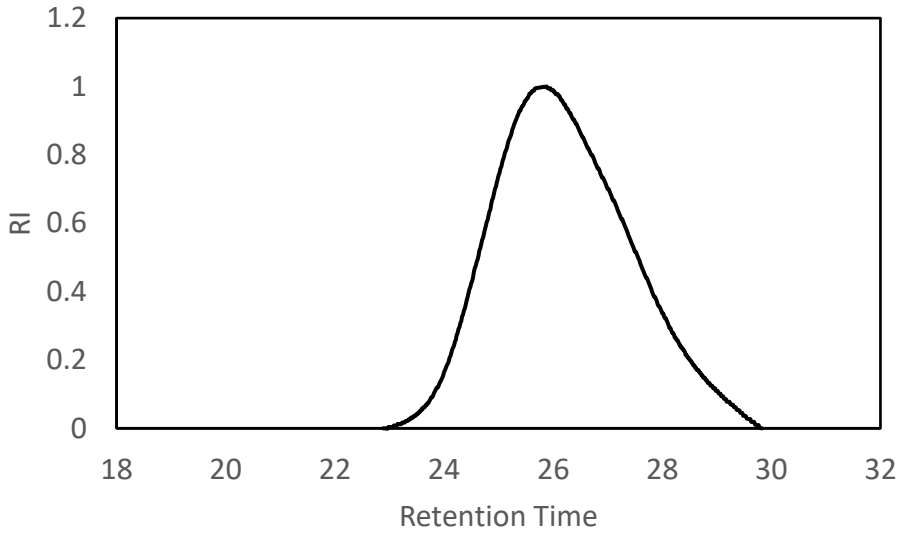

Figure A.5. GPC trace DPB-DS-PCL-Hx (**18**). Retention time = 25.667 min, $Đ$ = 1.39.

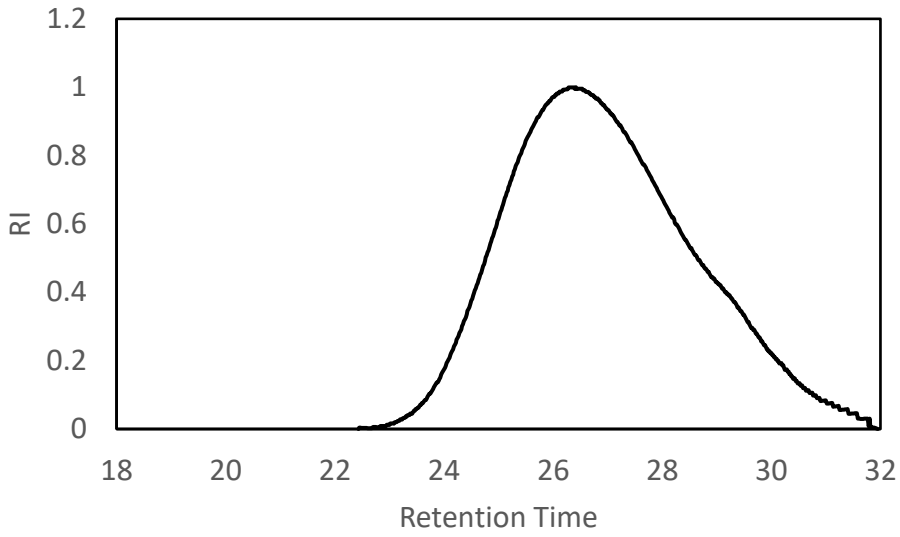

Figure A.6. GPC trace 4PB-PCL (**26**). Retention time = 26.283 min, $Đ$ = 1.55.

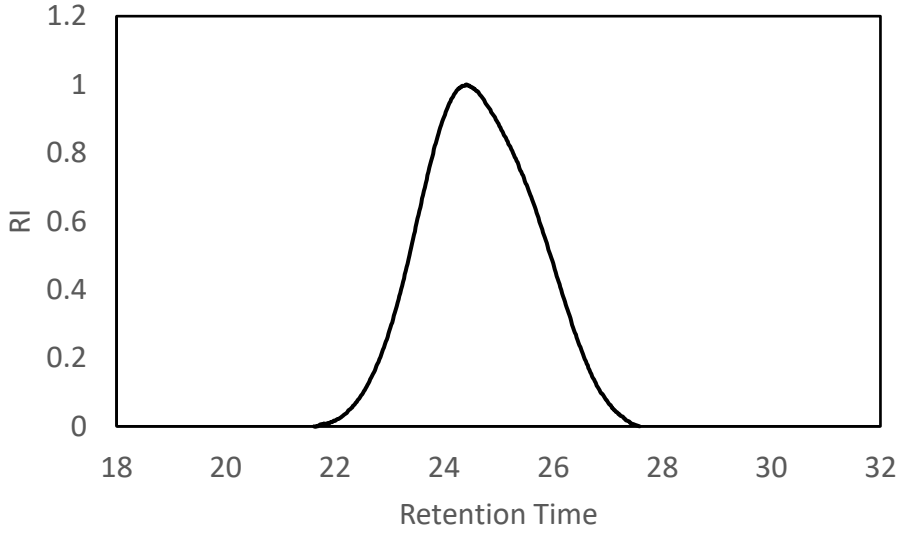

Figure A.7. GPC trace of µ1 (**11**). Retention time = 23.950 min, $Đ$ = 1.34.

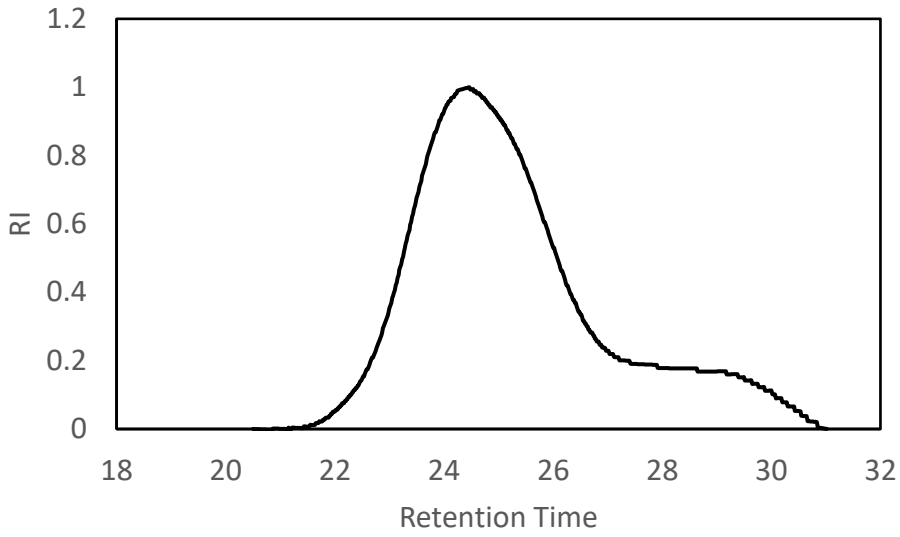

Figure A.8. GPC trace of μ2 (**15**). Retention time = 24.250 min, $Đ$ = 1.36.

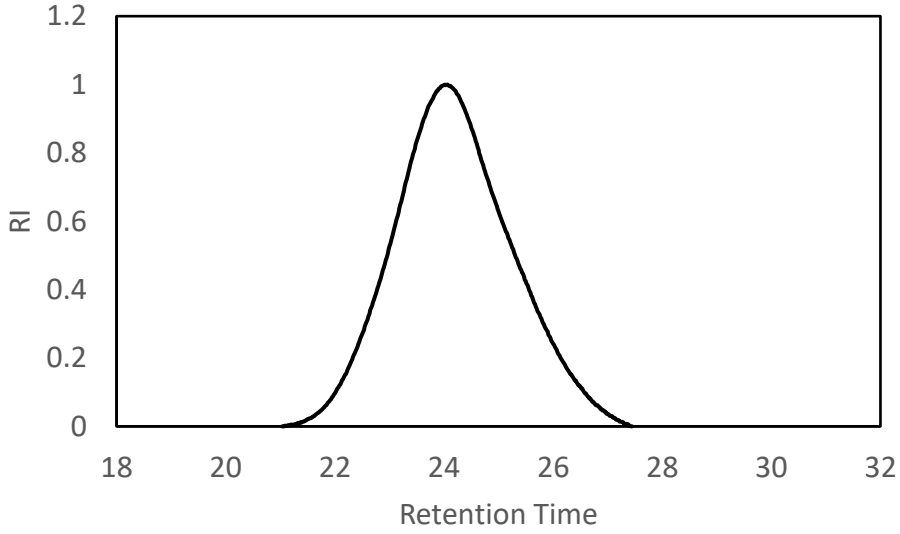

Figure A.9. GPC trace of μ3 (**19**). Retention time = 23.950 min, $Đ$ = 1.39.

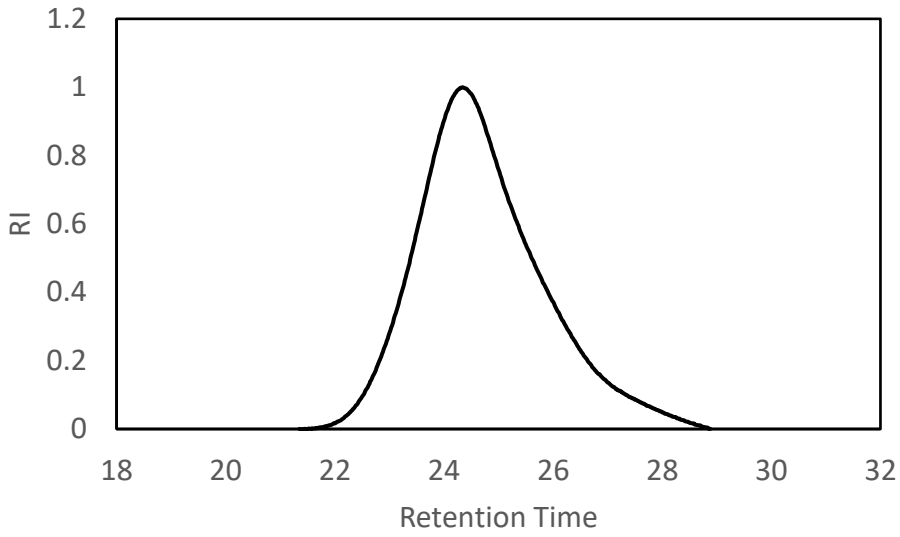

Figure A.10. GPC trace of μ4 (**23**). Retention time = 24.300 min, $Đ$ = 1.36.

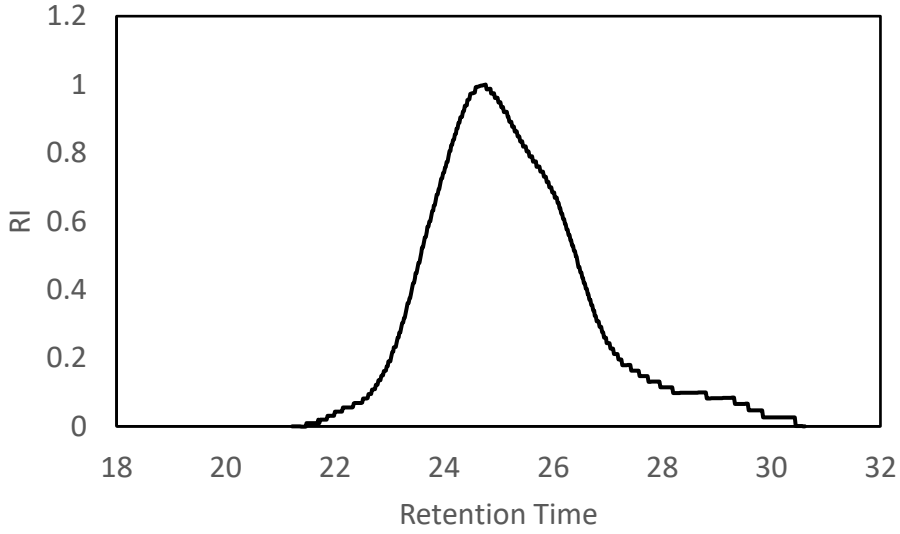

Figure A.11. GPC trace of b1 (**27**). Retention time = 24.583 min, $Đ$ = 1.36.

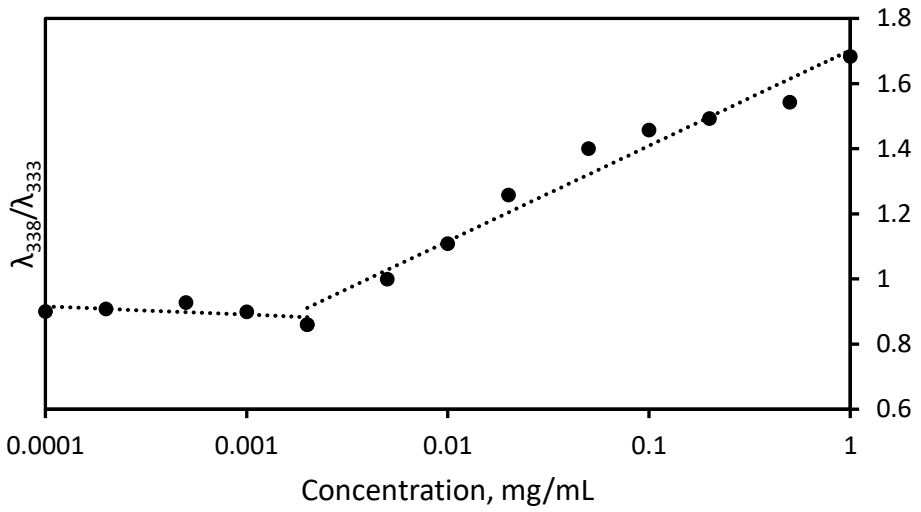

Figure A.12. Critical micelle concentration (CMC) determination of AB_2 miktoarm micelle μ1.

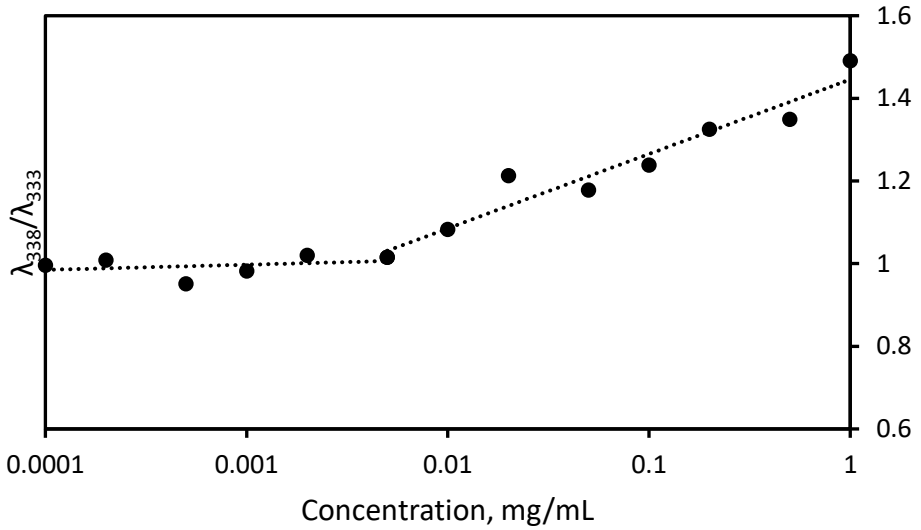

Figure A.13. Critical micelle concentration (CMC) determination of AB_2 miktoarm micelle μ2.

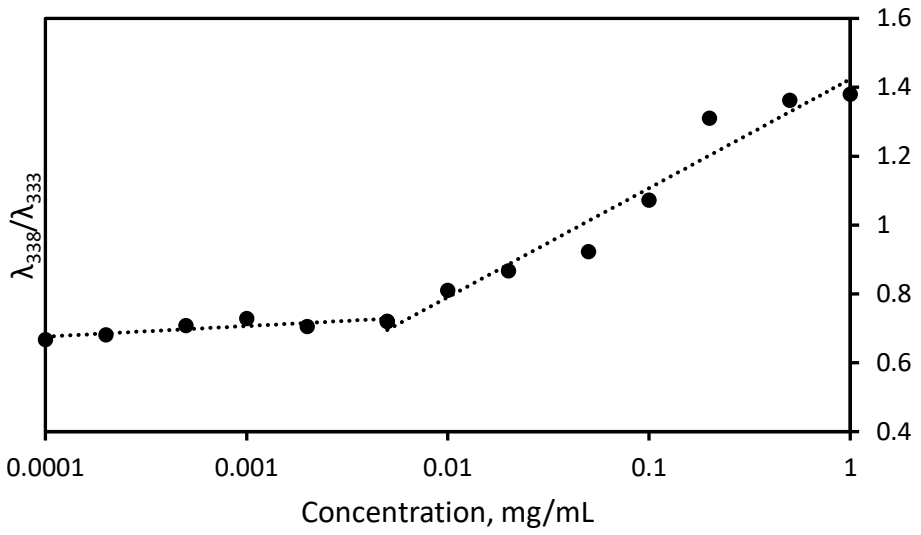

Figure A.14. Critical micelle concentration (CMC) determination of AB_2 miktoarm micelle μ3.

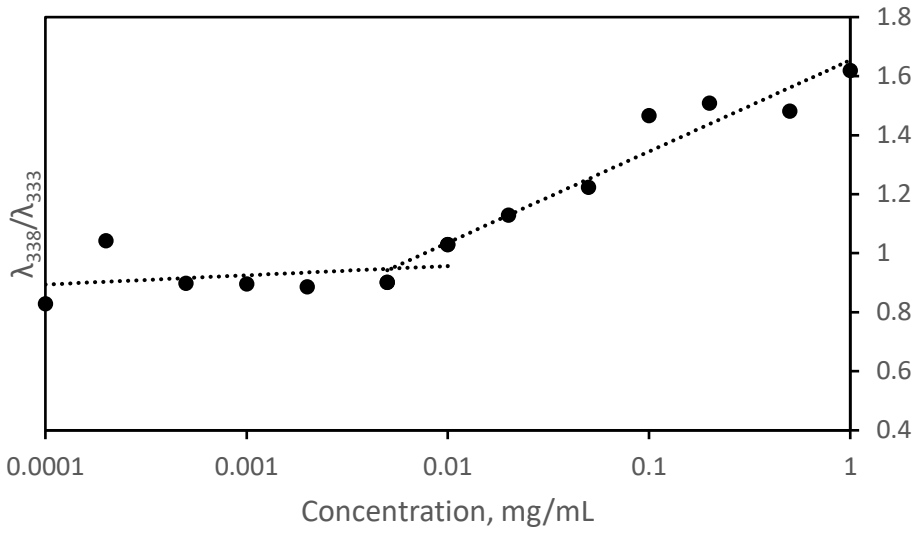

Figure A.15. Critical micelle concentration (CMC) determination of AB_2 miktoarm micelle μ4.

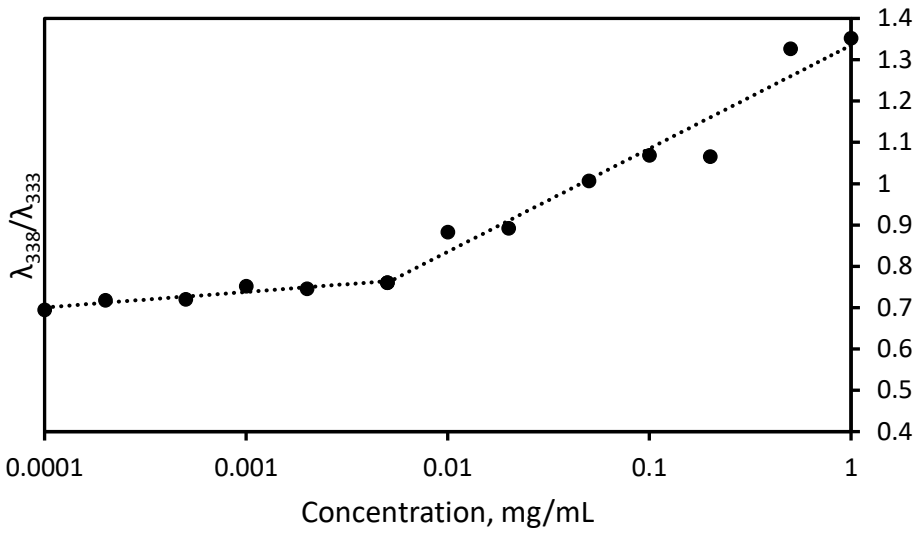

Figure A.16. Critical micelle concentration (CMC) determination of diblock co-polymer micelle b1.

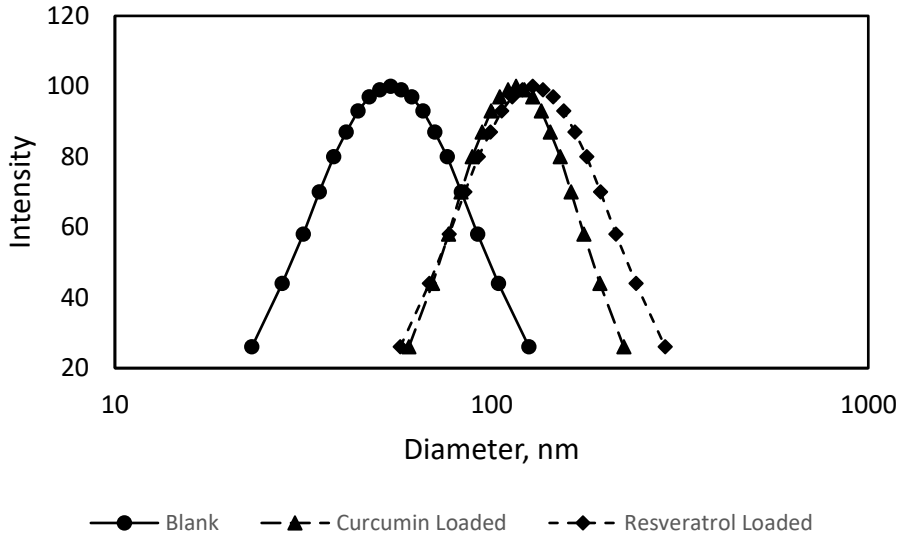

Figure A.17. DLS spectra of blank and drug loaded miktoarm µ1 micelles.

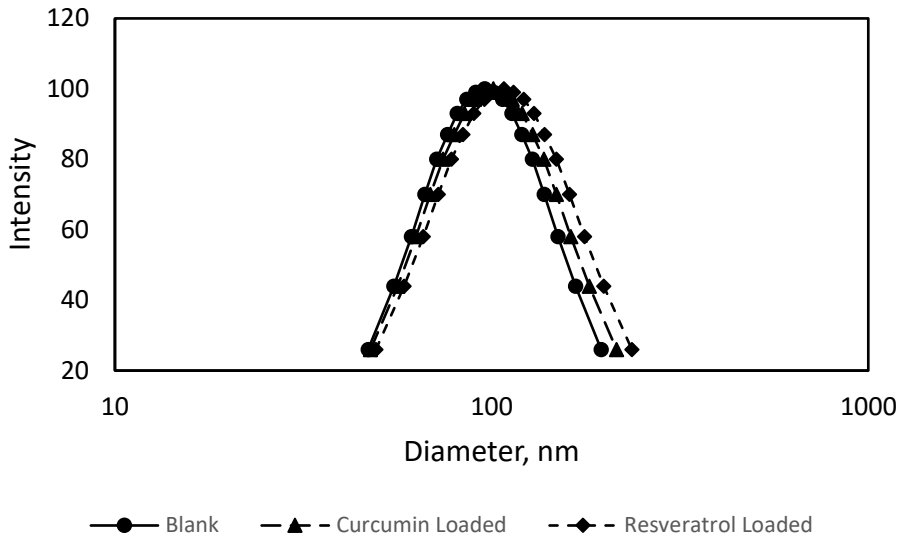

Figure A.18. DLS spectra of blank and drug loaded miktoarm μ2 micelles.

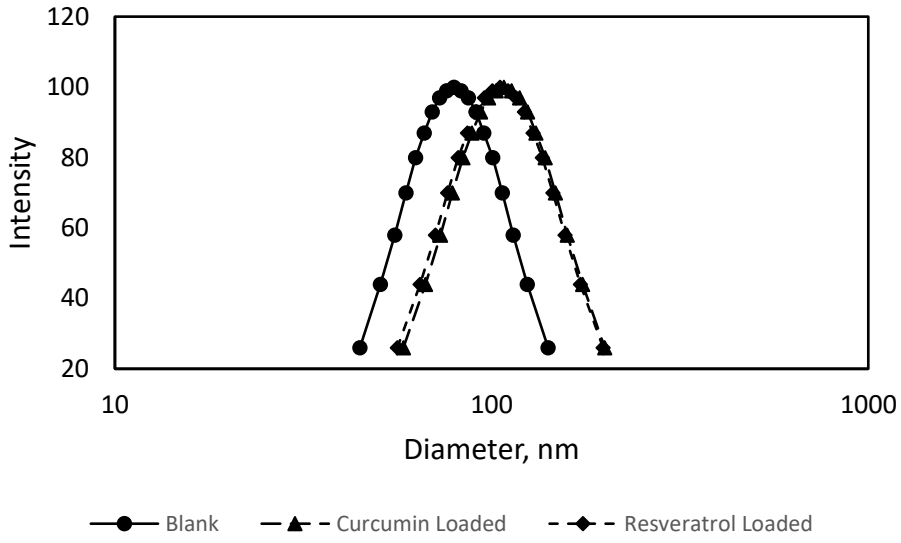

Figure A.19. DLS spectra of blank and drug loaded miktoarm μ3 micelles.

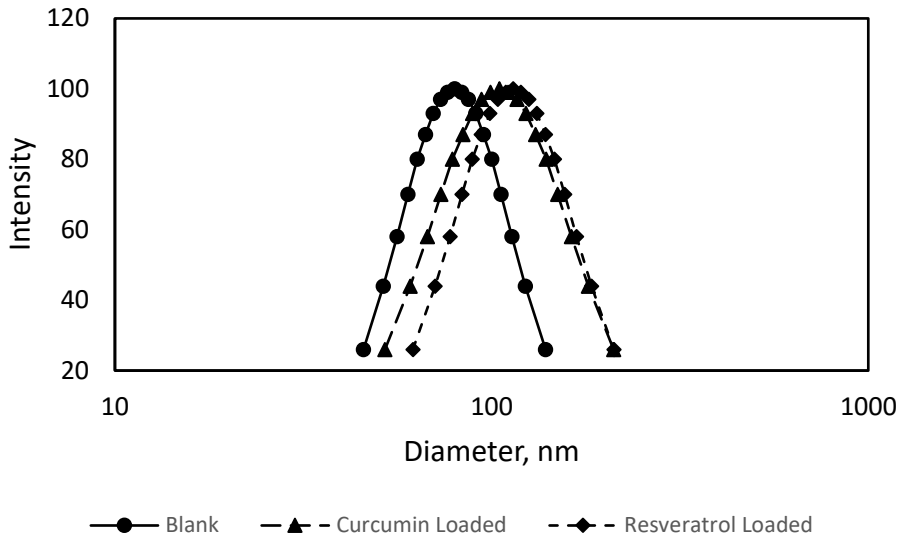

Figure A.20. DLS spectra of blank and drug loaded miktoarm μ4 micelles.

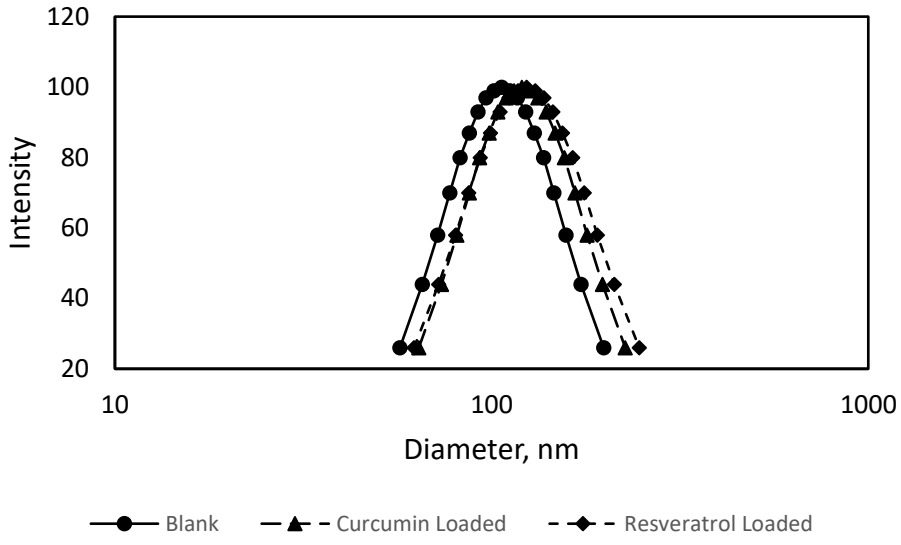

Figure A.21. DLS spectra of blank and drug loaded diblock copolymer b1 micelles.

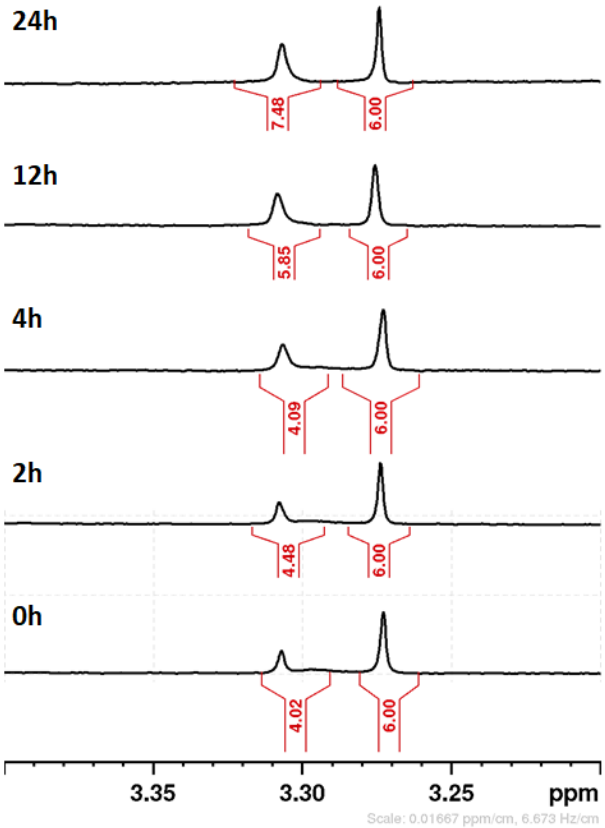

Figure A.22. Integrations of µ1 thioketal C*H*$_2$ (3.31 ppm) and PEG-OC*H*$_3$ (3.27 ppm) peaks in D_2O after incubation with H_2O_2 over time.

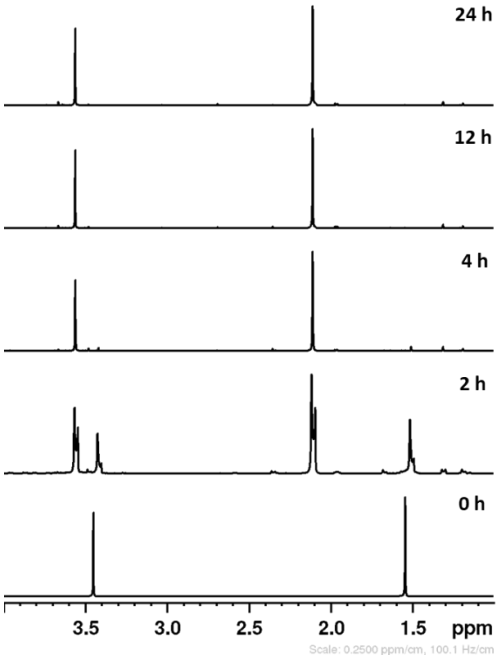

Figure A.23. Reaction of thioketal diacid (TKDA) with H_2O_2 in D_2O monitored by ^{1}H NMR over 24 hours.

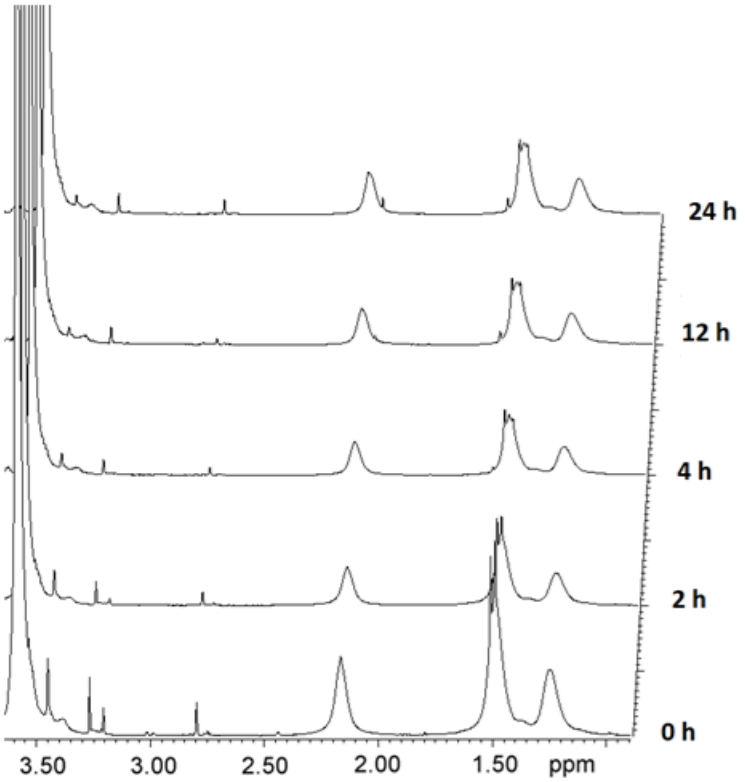

Figure A.24. Reaction of diblock copolymer b1 with H_2O_2 in D_2O monitored by ^1H NMR over 24 hours.

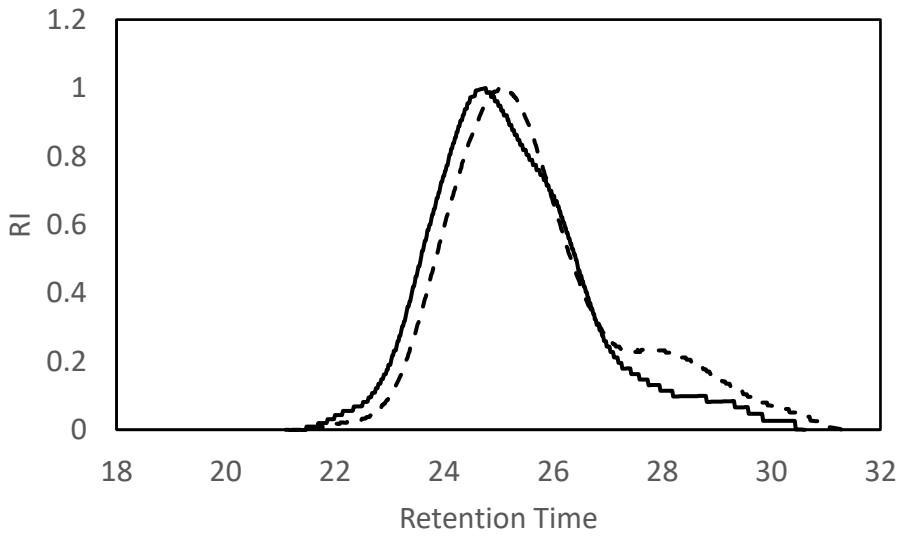

Figure A.25. GPC traces of b1 and b1 treated with 200 mM H_2O_2 over 24 hours.

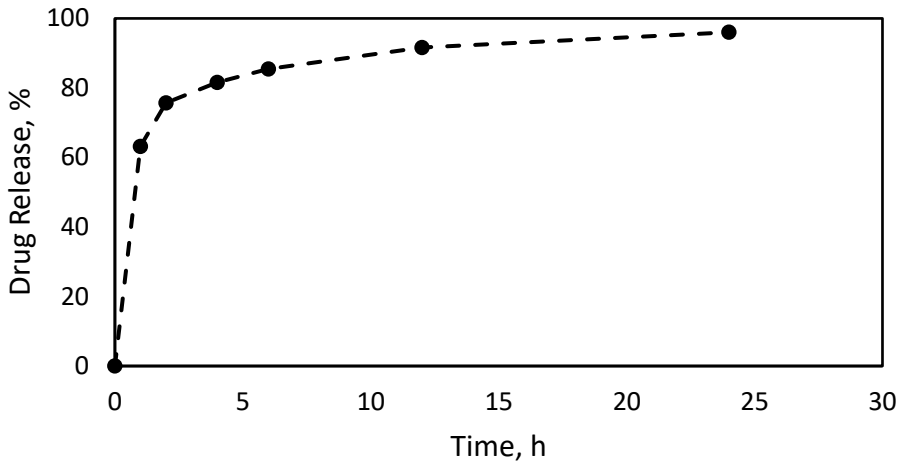

Figure A.26. Free drug release profiles of curcumin. 1 mg/mL drug solution in a 45/40/15 ratio of water/dimethylacetamide/PEG_{750} was dialyzed against pH 7.4 PBS buffer at 37 °C over 24 hours.

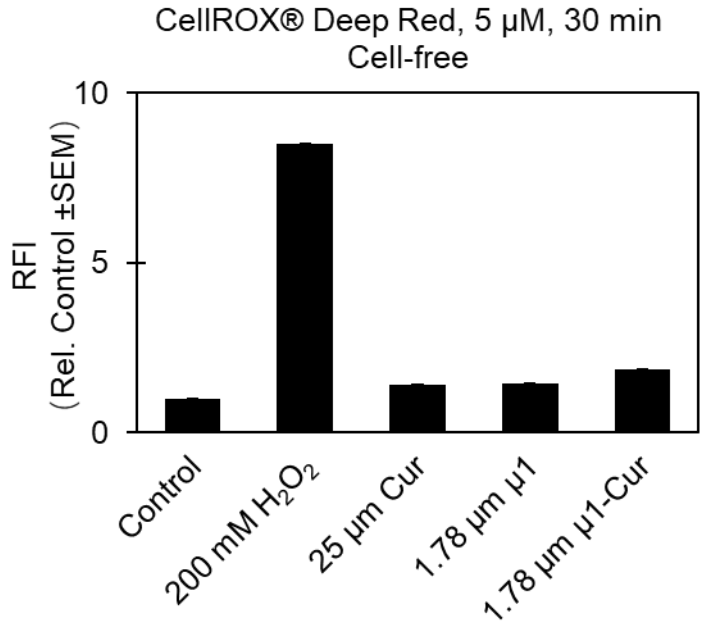

Figure A.27. The cell-free media were treated with 5 µM CellROX Deep Red reagent (C10422, ThermoFisher, Ex/Em. = 640/665 nm) for 30 minutes. The ROS-responsive micelles (µ1, 1.78 µM) were loaded with 7.82 µM of curcumin. The relative fluorescence intensity to the control (distilled H_2O) was quantified using a spectrofluoremeter at an emission wavelength of 665 nm.

A.3. NMR and Mass Spectra

(3,5-bis(prop-2-yn-1-yloxy)phenyl)methanol (DPBA), 2

H-NMR ($CDCl_3$)

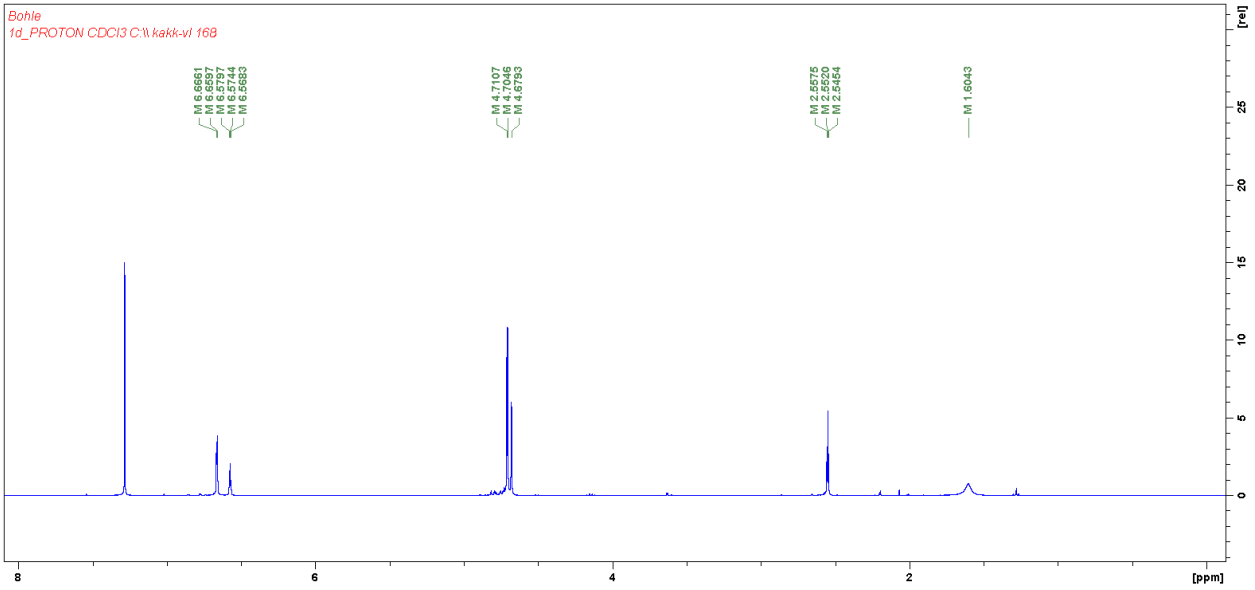

$^{13}C\{^1H\}$-NMR ($CDCl_3$)

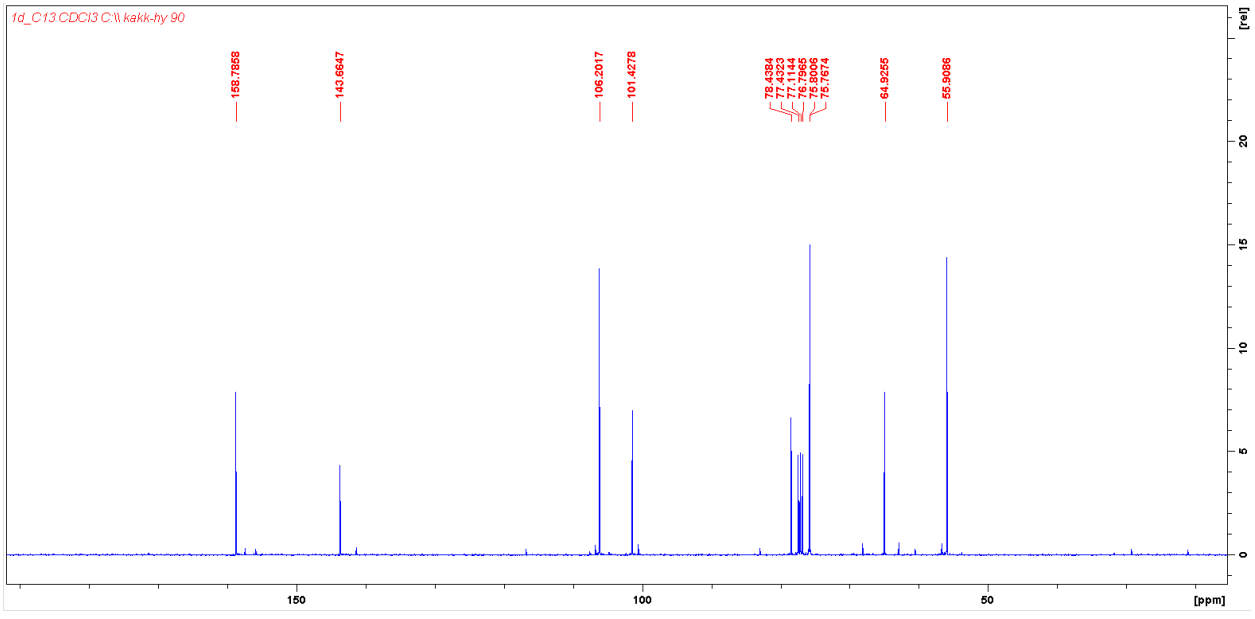

3,5-bis(prop-2-yn-1-yloxy)benzyl PCL (DPB-PCL), 3

H-NMR ($CDCl_3$)

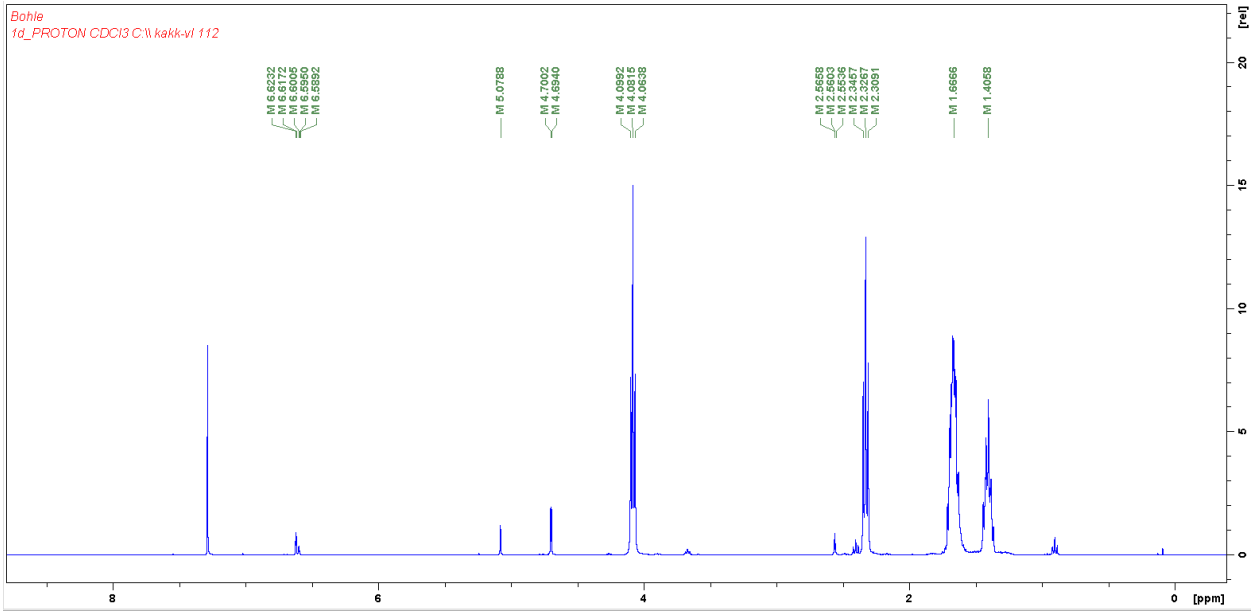

$^{13}C\{^1H\}$-NMR ($CDCl_3$)

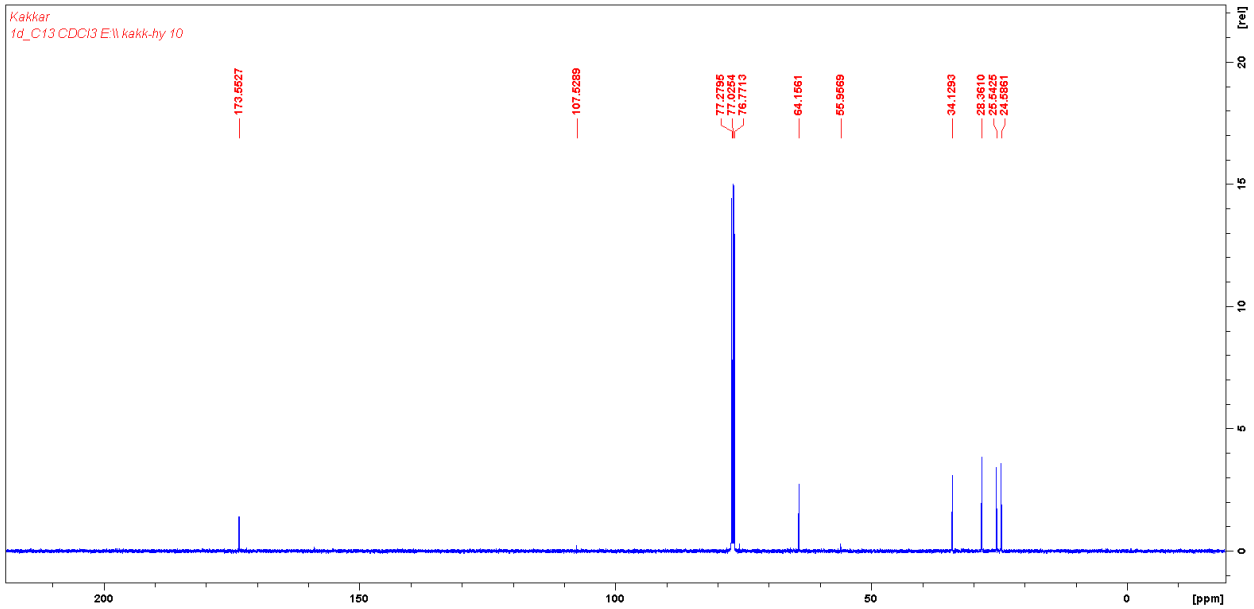

MALDI-TOF

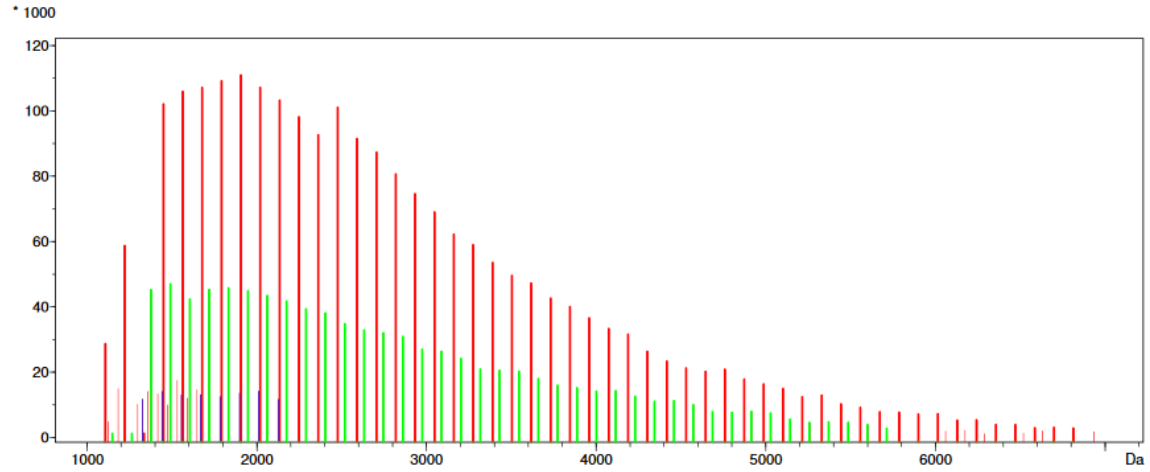

n	ser.	rep.unit	resid.	end1	end2	cation	Mn	Mw	pd	DP	% I.	cnt
1	1	114.000	8.76012	71.0000	209.000	Na	2839.05	3321.40	1.16990	24.9040	64.1	51
2	2	114.000	0.41415	71.0000	209.000	Na	1705.96	1744.95	1.02286	14.9646	3.2	8
3	3	114.000	50.3318	71.0000	209.000	Na	2751.17	3175.09	1.15409	24.1331	26.7	41

PEG-OTs, 5

^{1}H-NMR ($CDCl_3$)

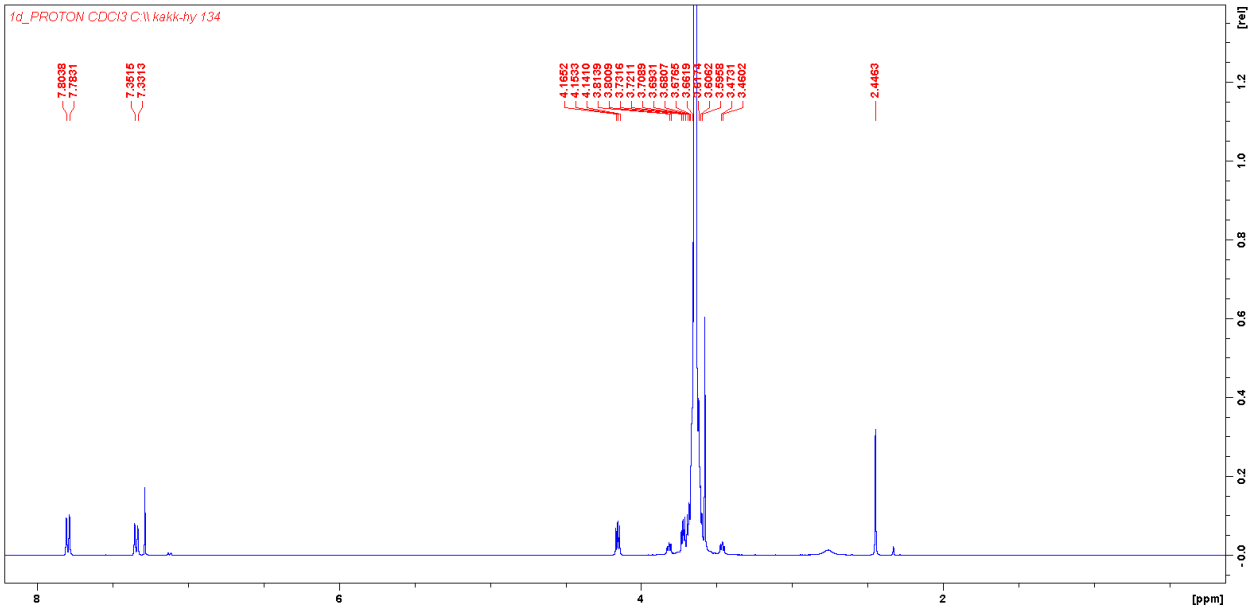

$^{13}C\{^{1}H\}$-NMR ($CDCl_3$)

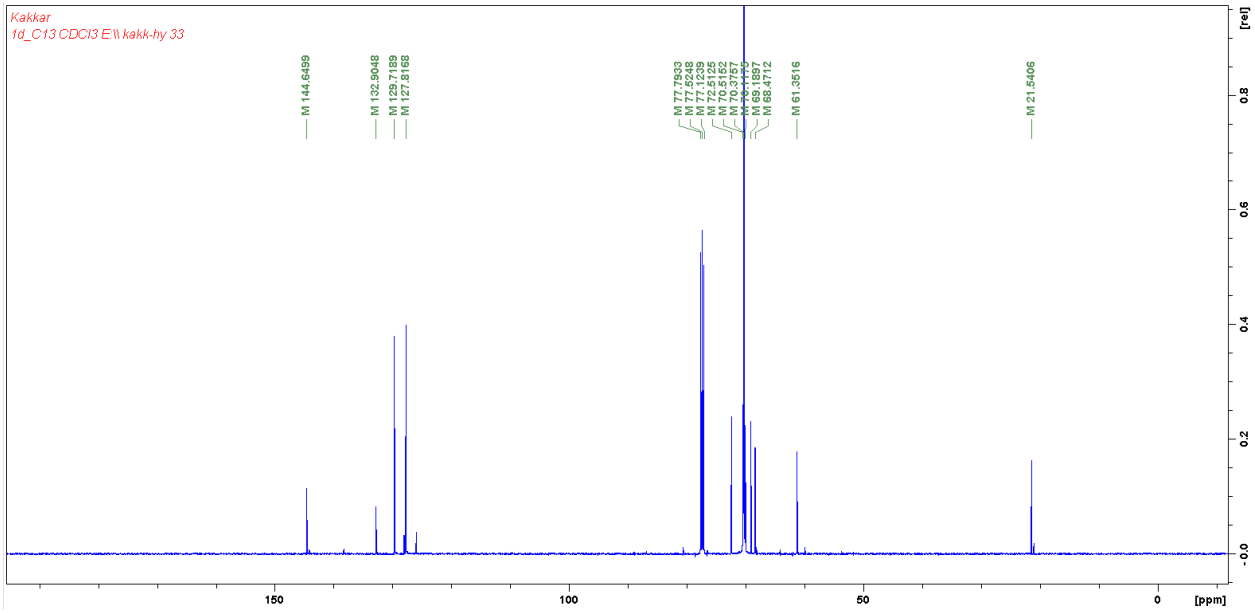

PEG-N_3, 6

H-NMR ($CDCl_3$)

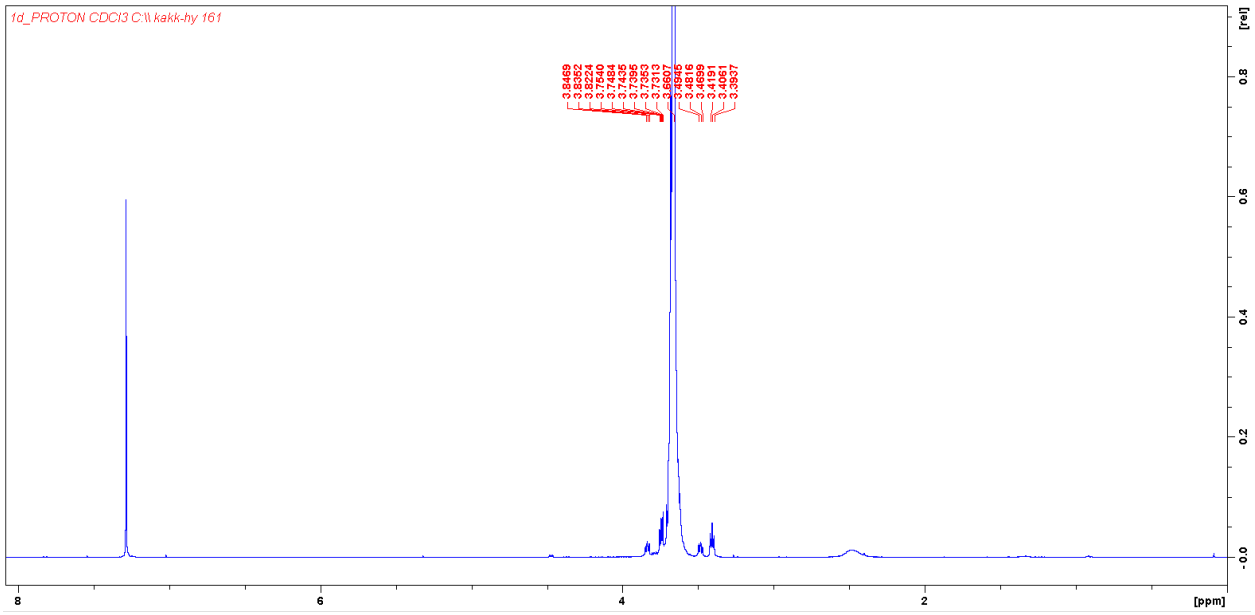

$^{13}C\{^{1}H\}$-NMR ($CDCl_3$)

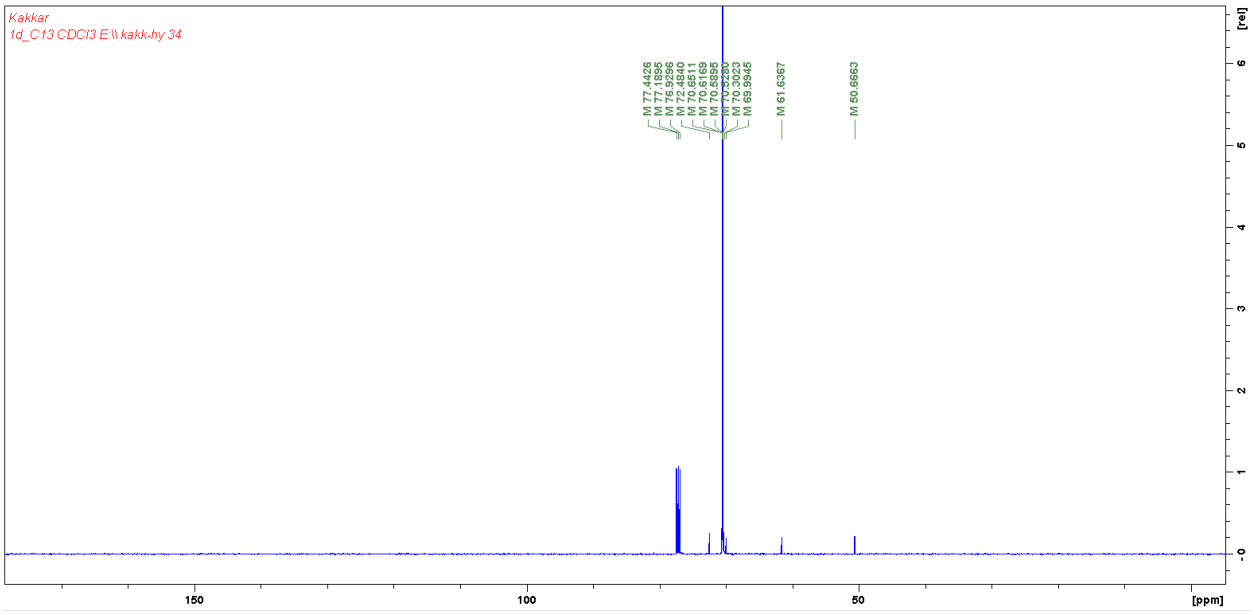

2,2'-(propane-2,2-diylbis(sulfanediyl))diacetic acid (TKDA), 8

H-NMR ($CDCl_3$)

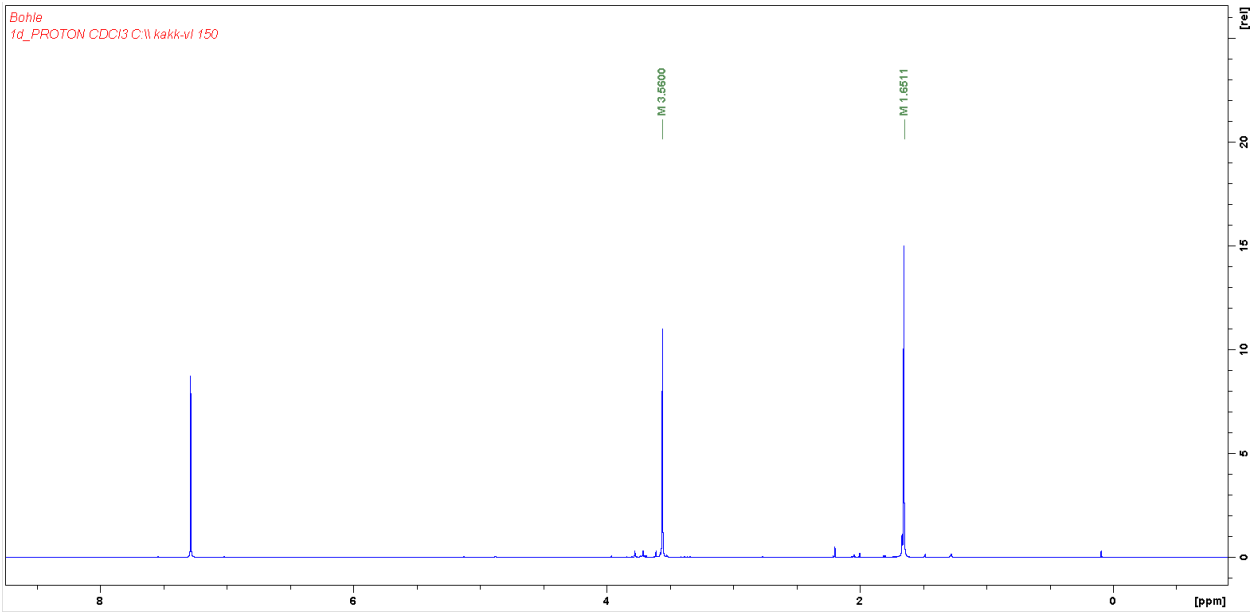

$^{13}C\{^{1}H\}$-NMR (DMSO-d6)

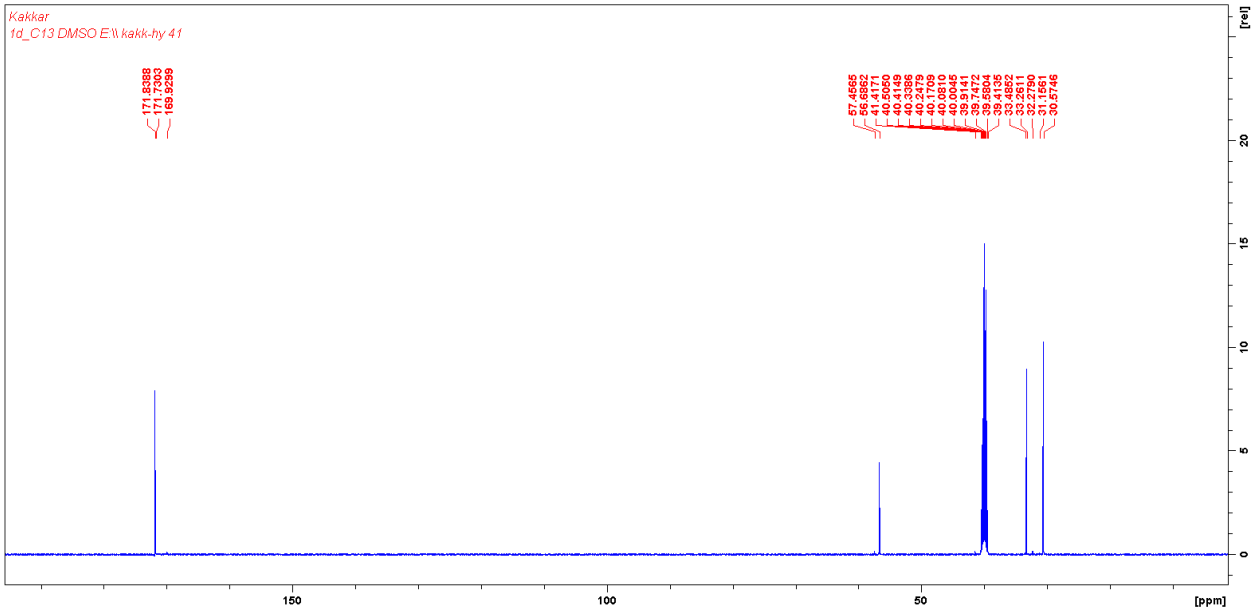

18,18-dimethyl-15-oxo-2,5,8,11,14-pentaoxa-17,19-dithiahenicosan-21-oic acid (TK-TEG), 9

H-NMR ($CDCl_3$)

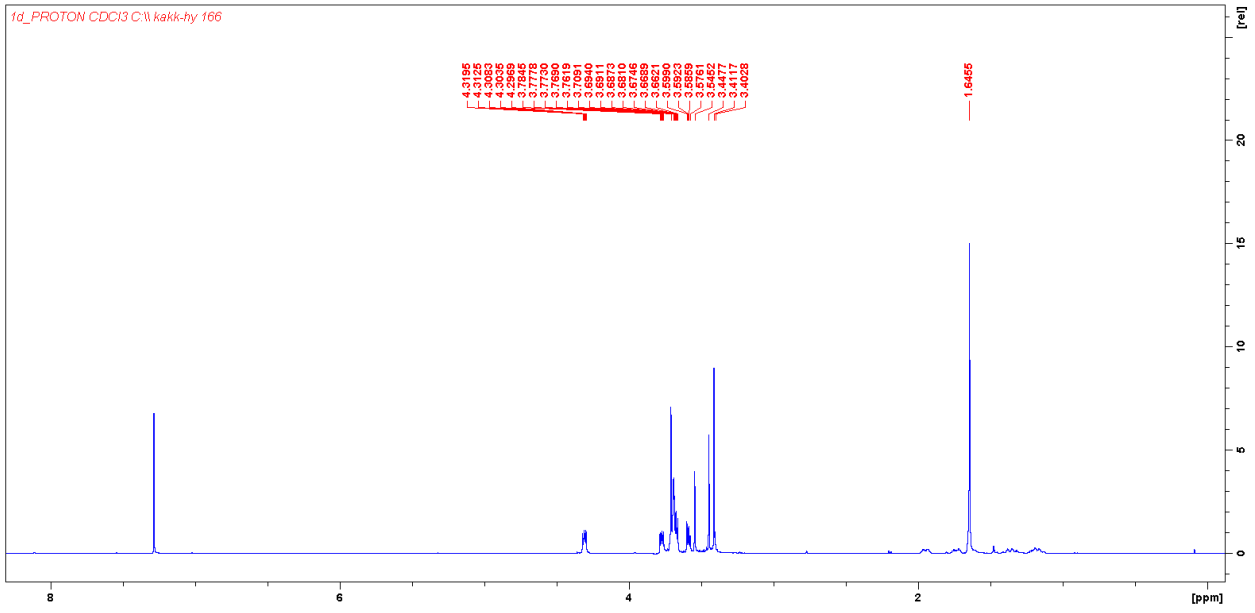

$^{13}C\{^{1}H\}$-NMR ($CDCl_3$)

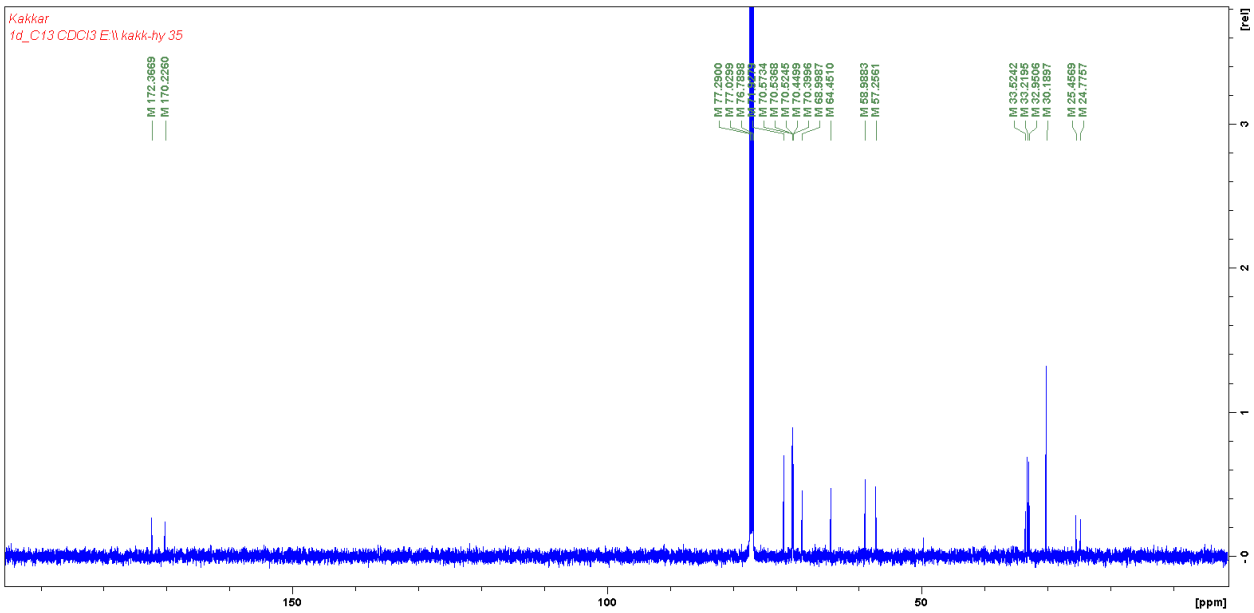

ESI-MS

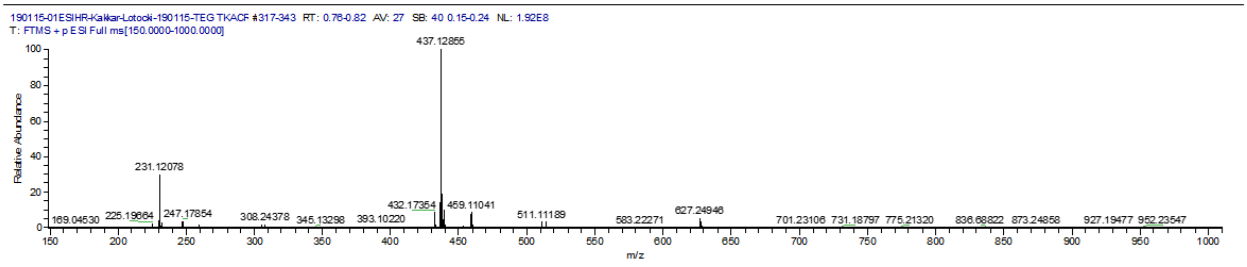

190115-01ESIHR-Kakkar-Lotocki-190115-TEG TKACR#317-343 RT: 0.76-0.82 AV: 27
SB: 40 0.15-0.24
T: FTMS + p ESI Full ms [150.0000-1000.0000]
m/z= 437.09723-437.14661

m/z	Intensity	Relative	Resolution	Charge	Theo. Mass	Delta (ppm)	RDB equiv.	Composition
437.12855	195407968.0	100.00	25542.44	1.00	437.12743	2.56	1.5	$C_{16}H_{30}O_8NaS_2$
					437.12984	-2.95	4.5	$C_{18}H_{29}O_6S_2$

N_3-PEG-TK-TEG, 10

H-NMR ($CDCl_3$)

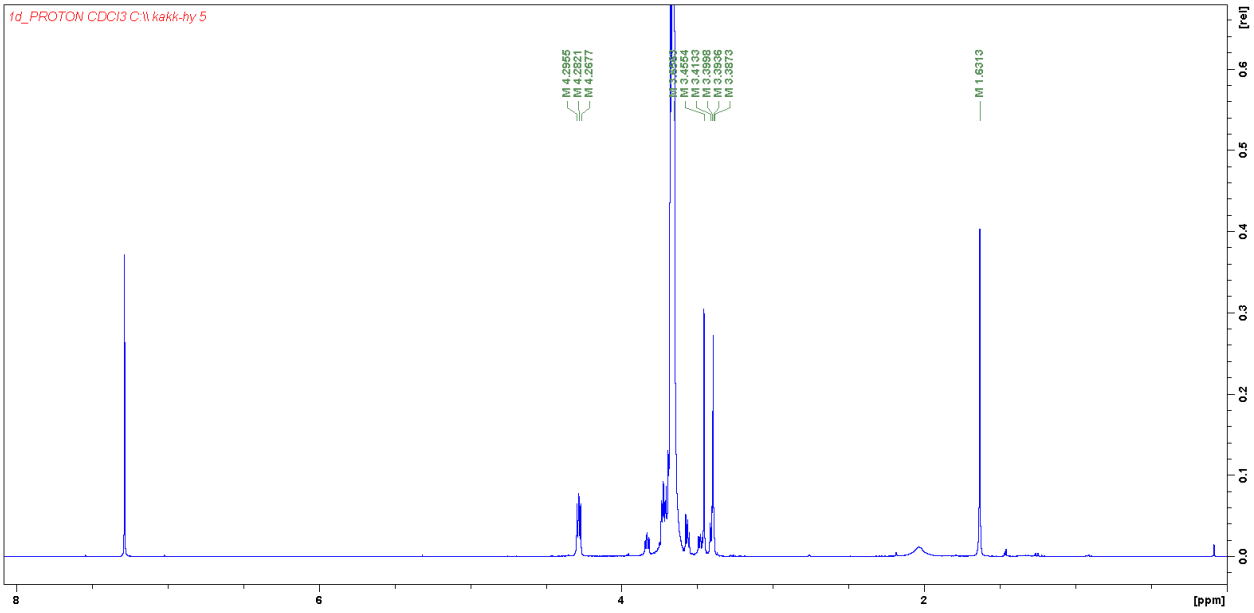

$^{13}C\{^1H\}$-NMR ($CDCl_3$)

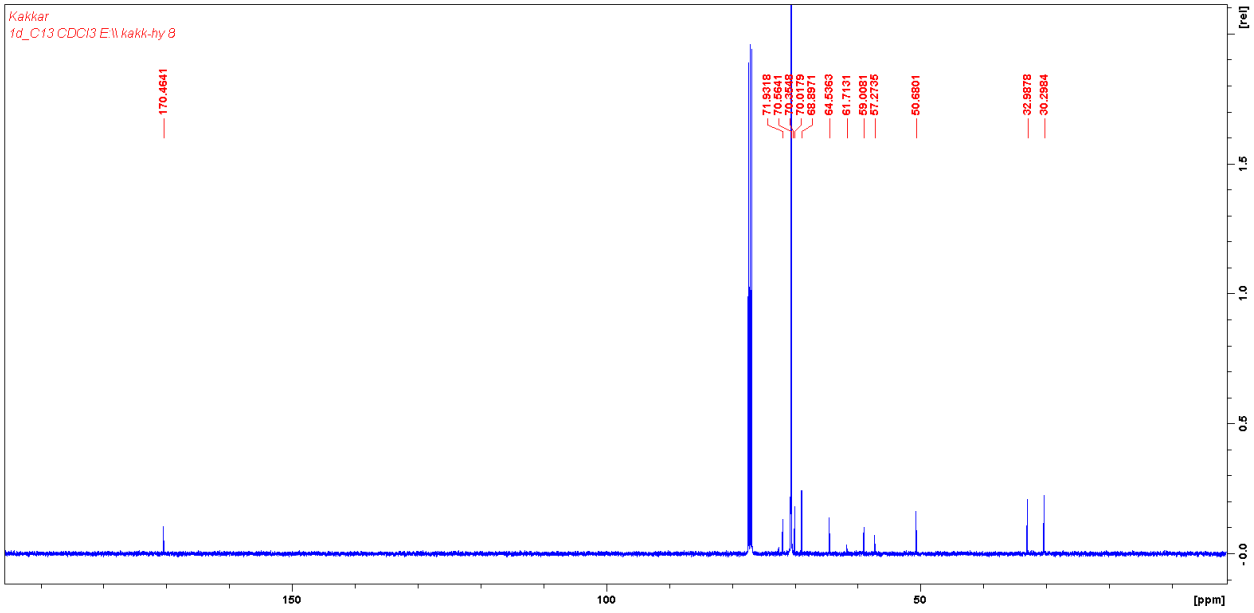

MALDI-TOF

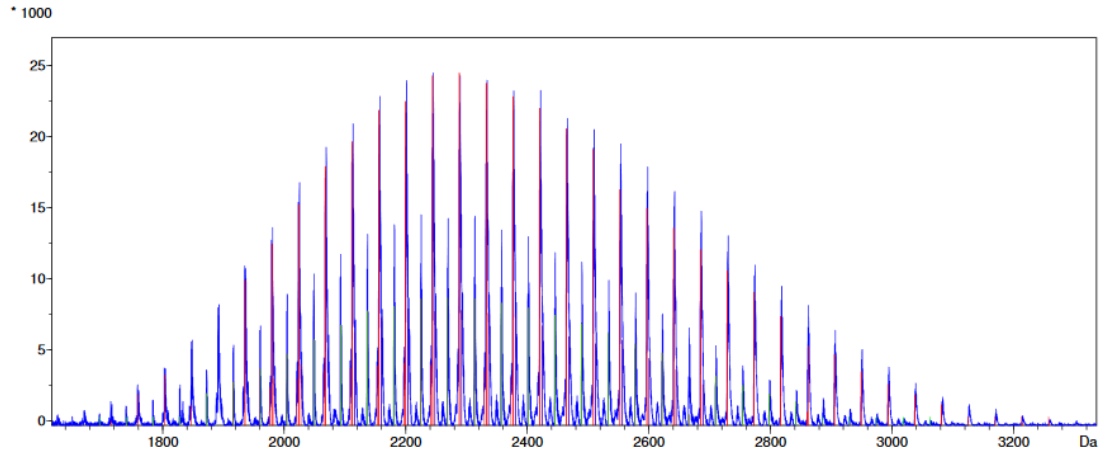

n	ser.	rep.unit	resid.	end1	end2	cation	Mn	Mw	pd	DP	% I.	cnt
1	1	PEG	0.65491	CH3	70.0000	H	2371.85	2400.18	1.01194	53.8736	57.9	31
2	2	PEG	4.47109	CH3	70.0000	H	2364.21	2375.43	1.00474	53.7002	13.6	14
3	3	PEG	3.56838	CH3	70.0000	Na	2293.35	2318.34	1.01090	52.0906	20.1	32

μ(PEG-TK-TEG)$_2$PCL (μ1), 11

H-NMR ($CDCl_3$)

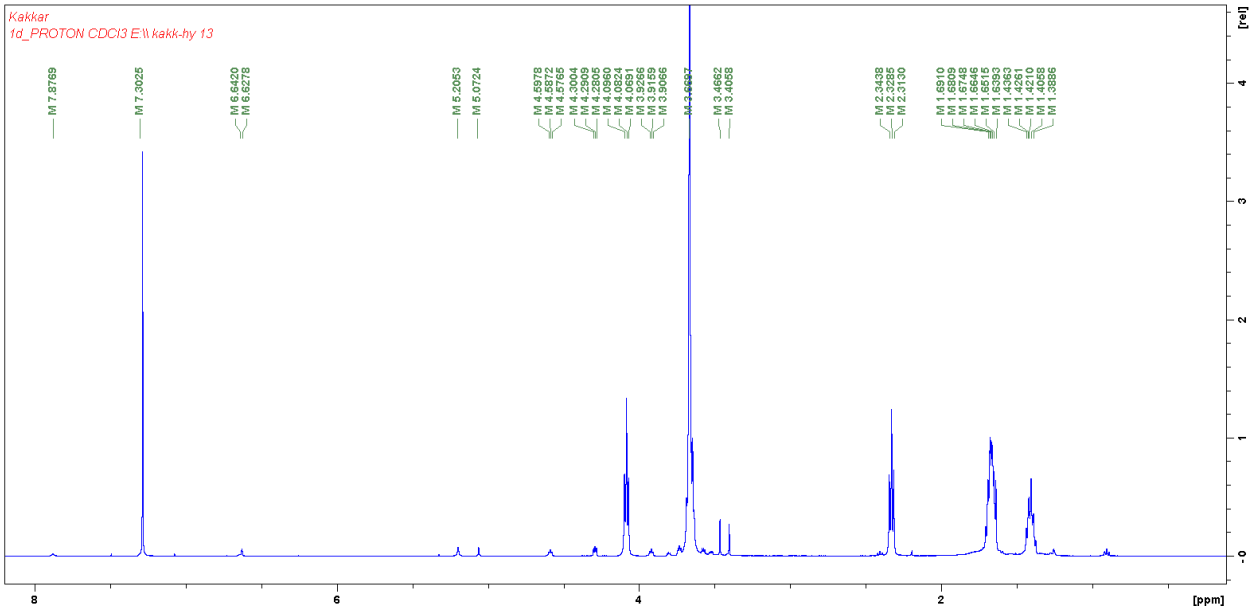

$^{13}C\{^{1}H\}$-NMR ($CDCl_3$)

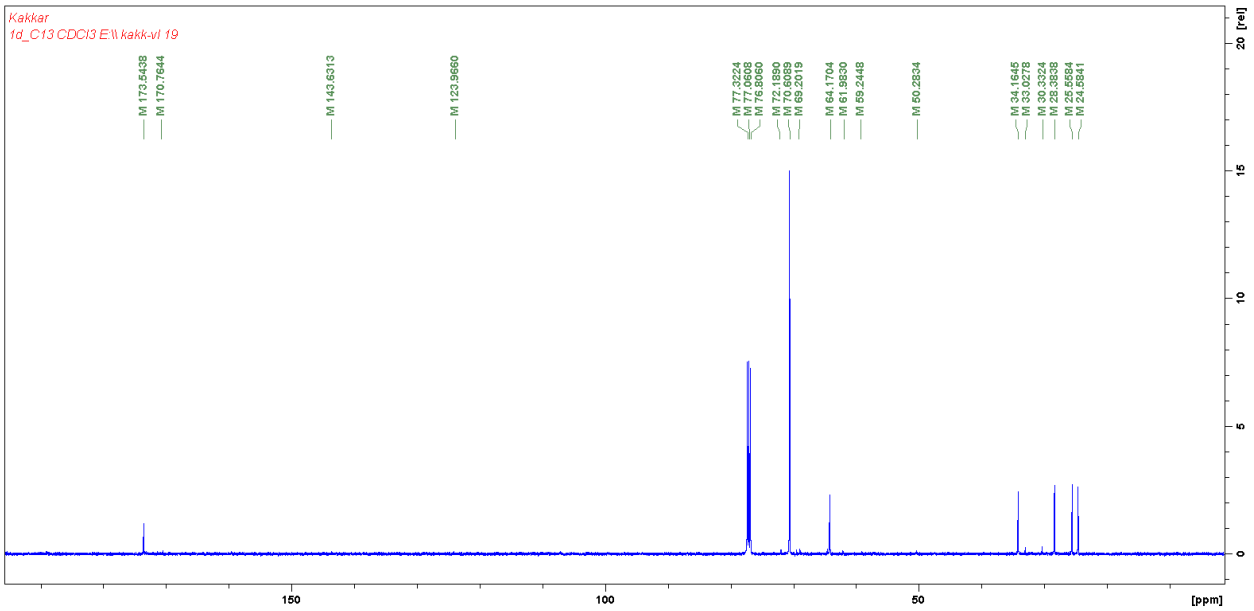

3-((3-(hexyloxy)-3-oxopropyl)disulfaneyl)propanoic acid (DS-Hex), 14

H-NMR ($CDCl_3$)

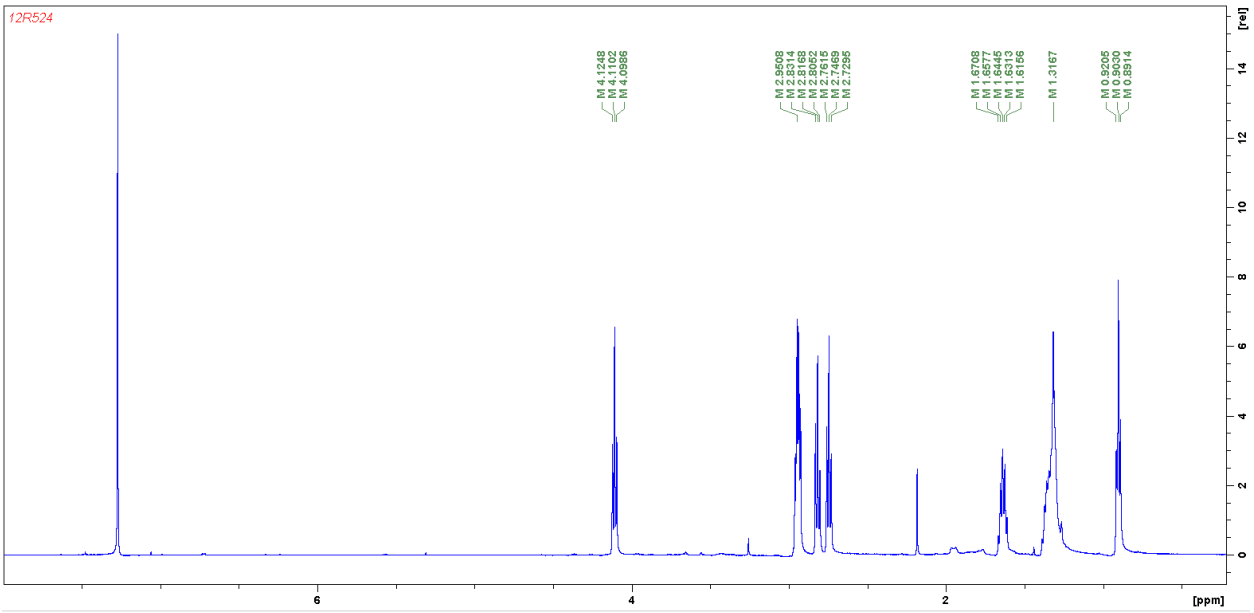

$^{13}C\{^{1}H\}$-NMR ($CDCl_3$)

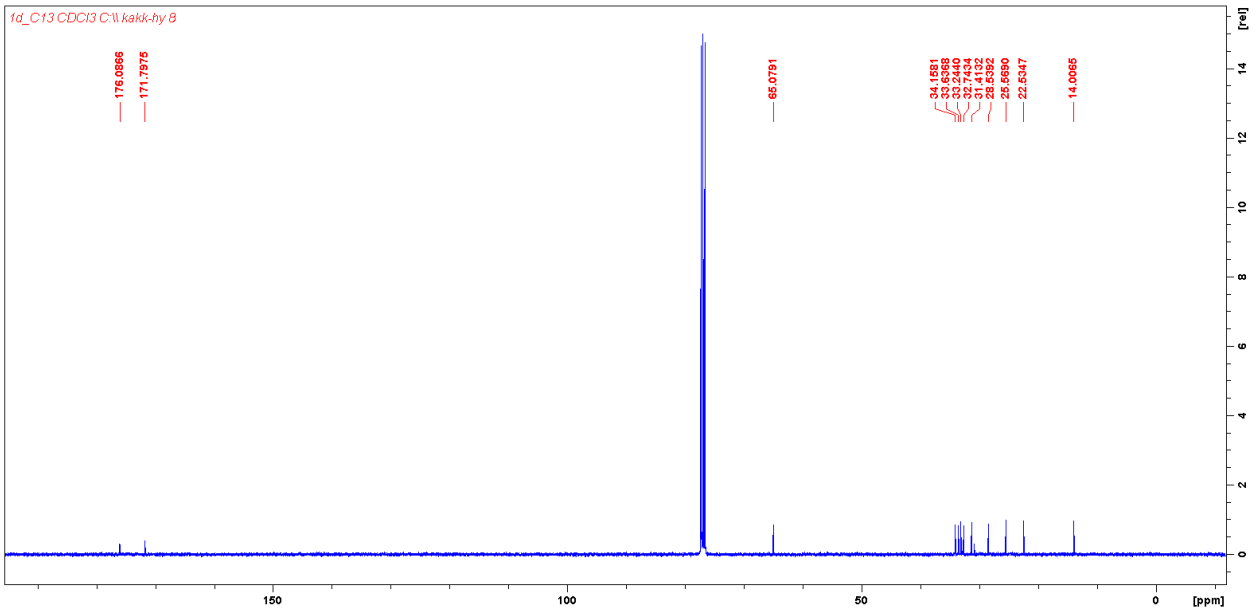

ESI-MS

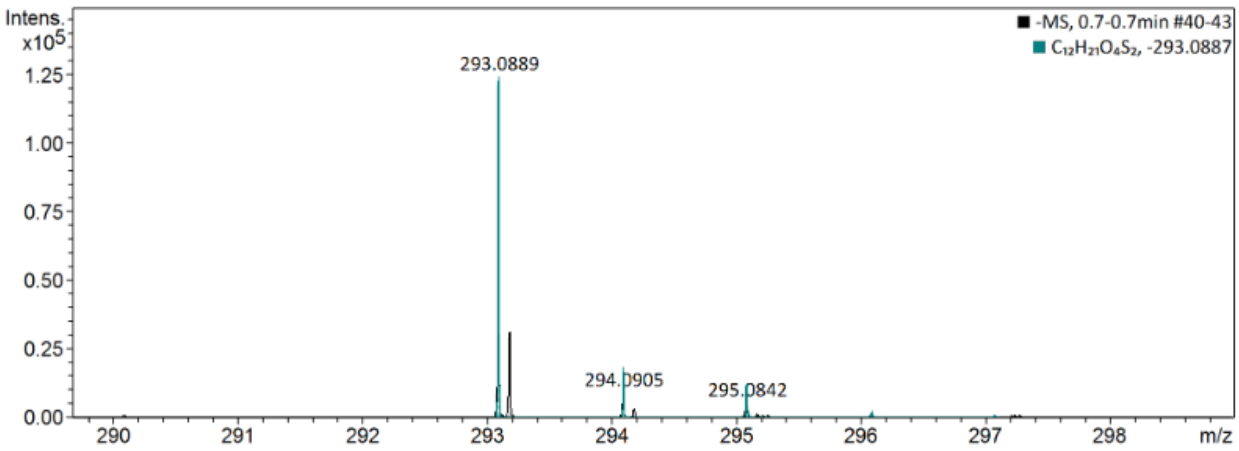

Meas. m/z	#	Ion Formula	m/z	err [ppm]	mSigma	# mSigma	Score	rdb	e⁻ Conf	N-Rule
293.0889	1	C12H21O4S2	293.0887	-0.6	51.3	1	100.00	2.5	even	ok

μ(PEG-TK-TEG)$_2$PCL-DS (μ2), 15

H-NMR ($CDCl_3$)

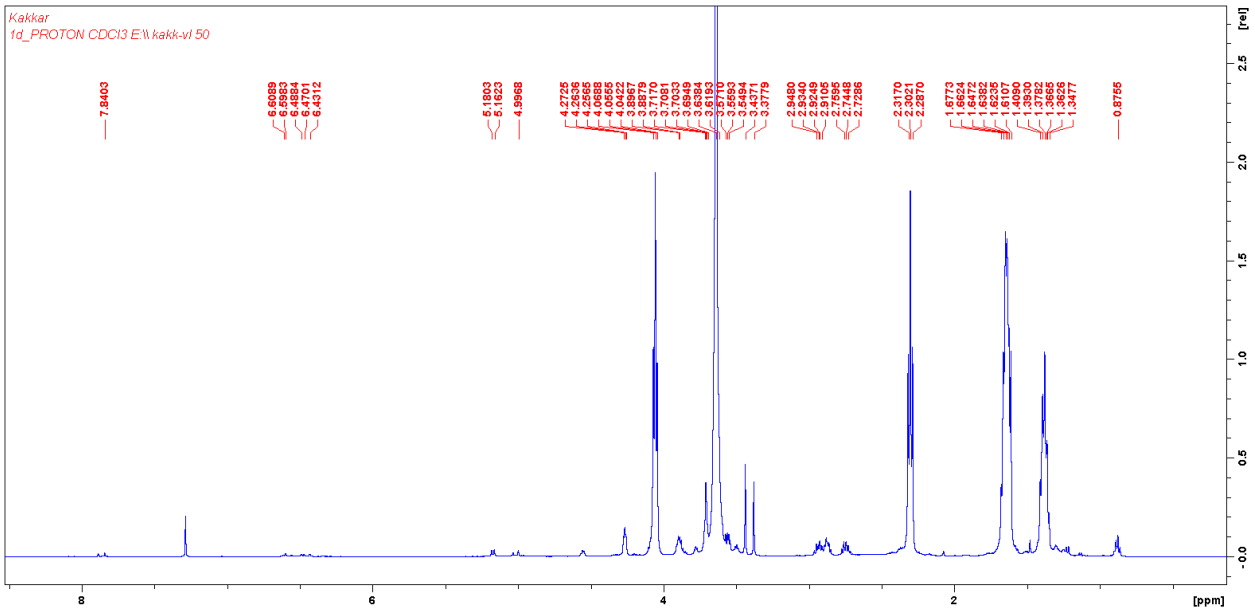

$^{13}C\{^1H\}$-NMR ($CDCl_3$)

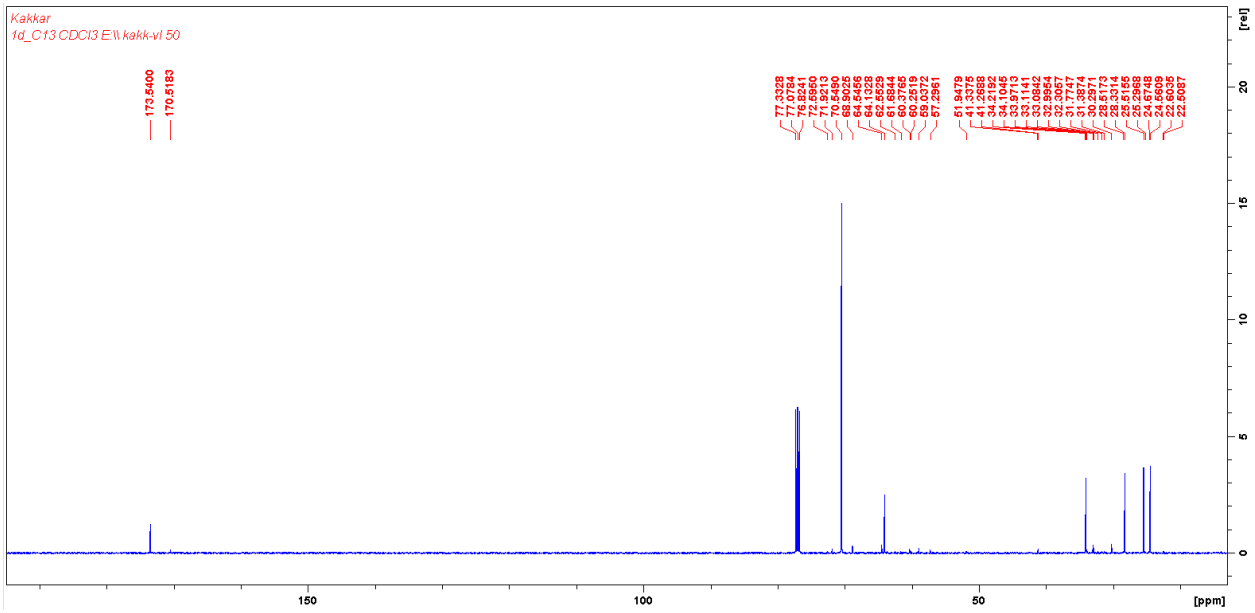

PCL-Hx, 16

H-NMR ($CDCl_3$)

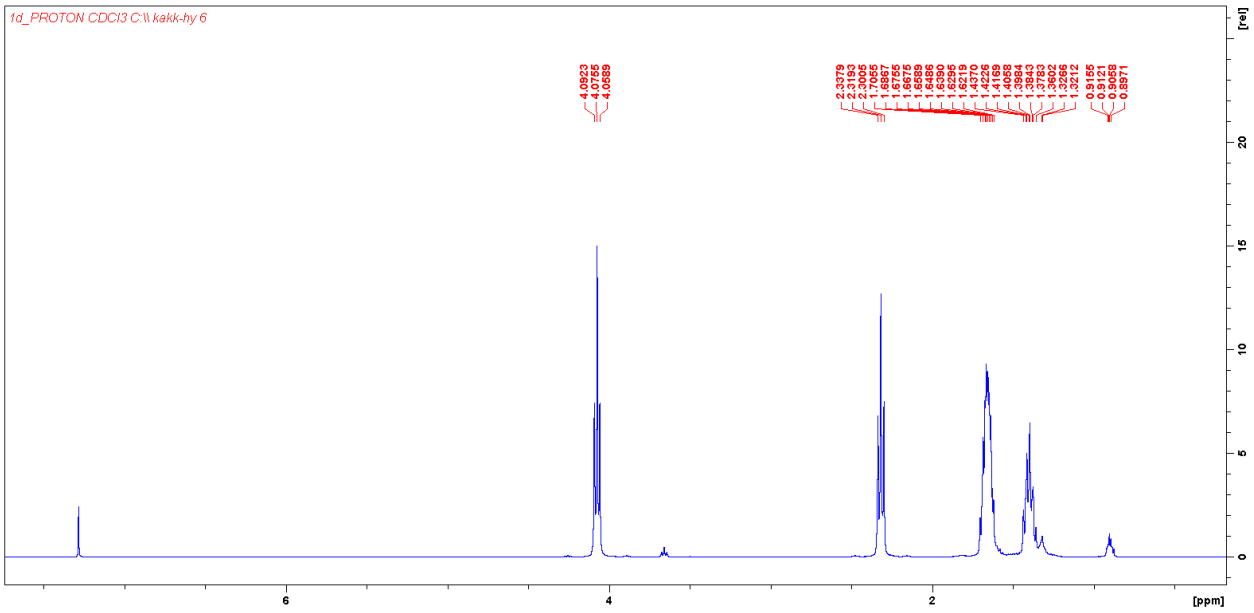

$^{13}C\{^1H\}$-NMR ($CDCl_3$)

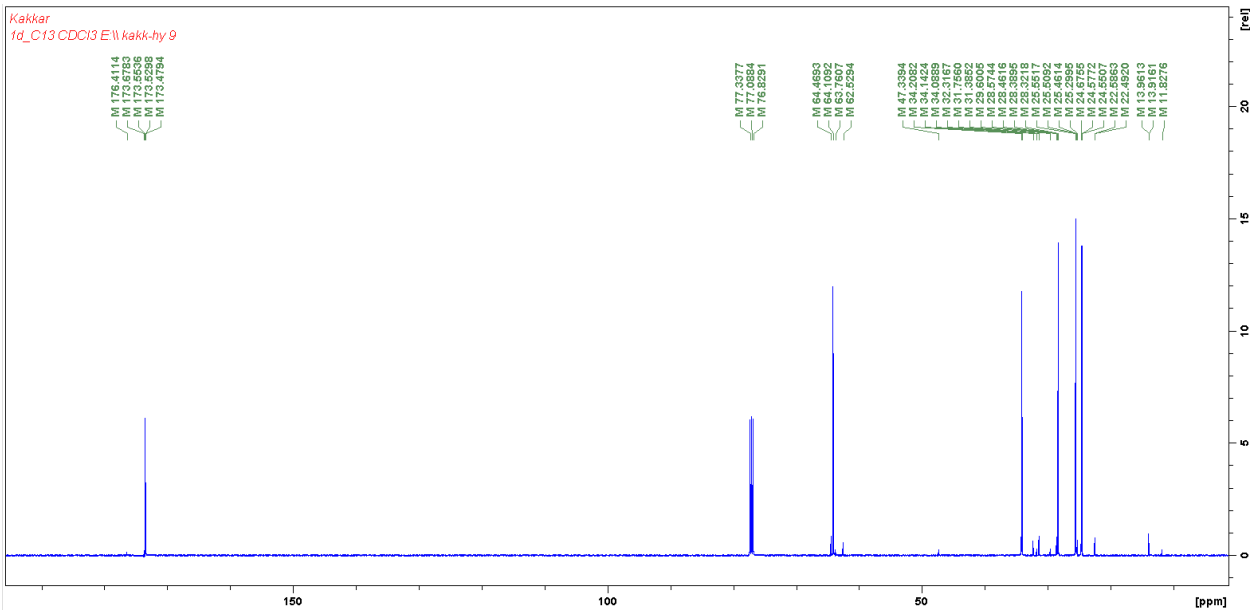

DS-PCL-Hx, 17

H-NMR ($CDCl_3$)

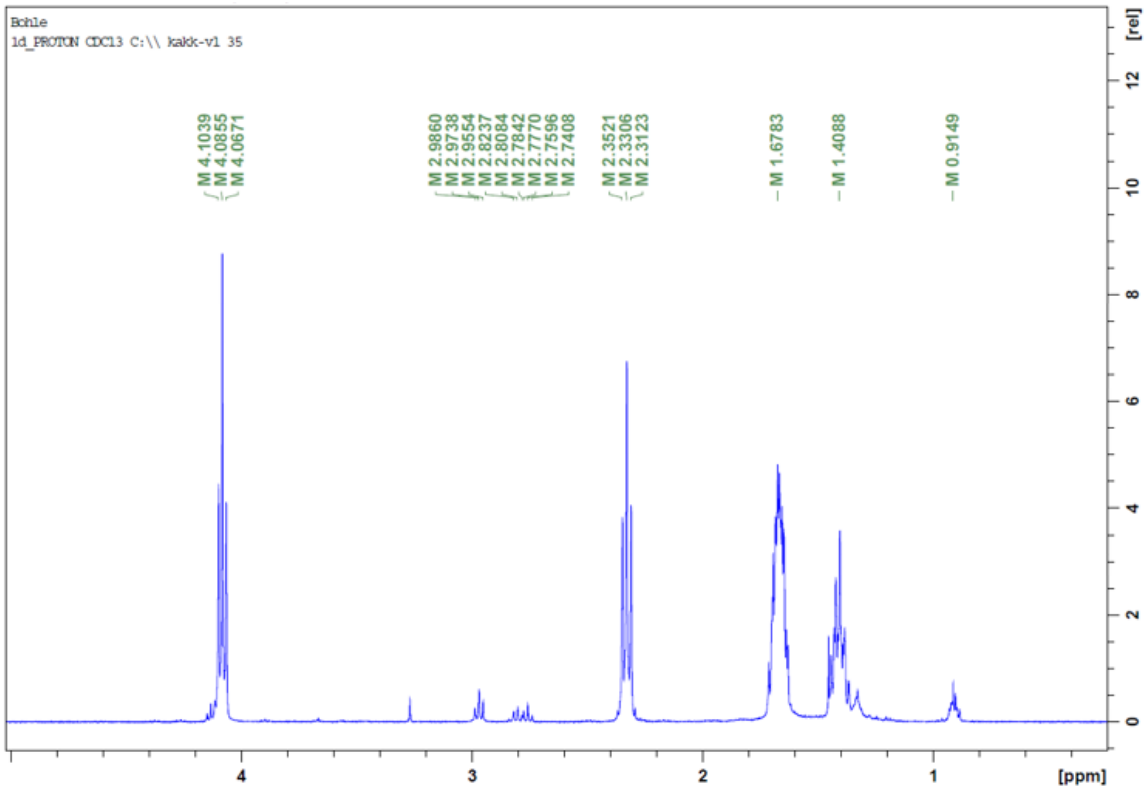

$^{13}C\{^1H\}$-NMR ($CDCl_3$)

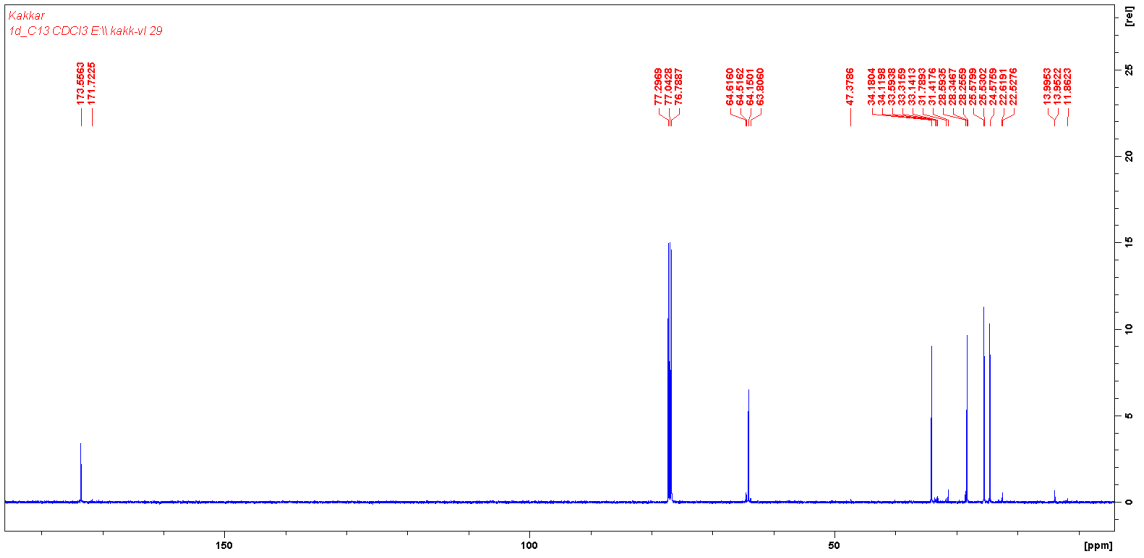

MALDI-TOF

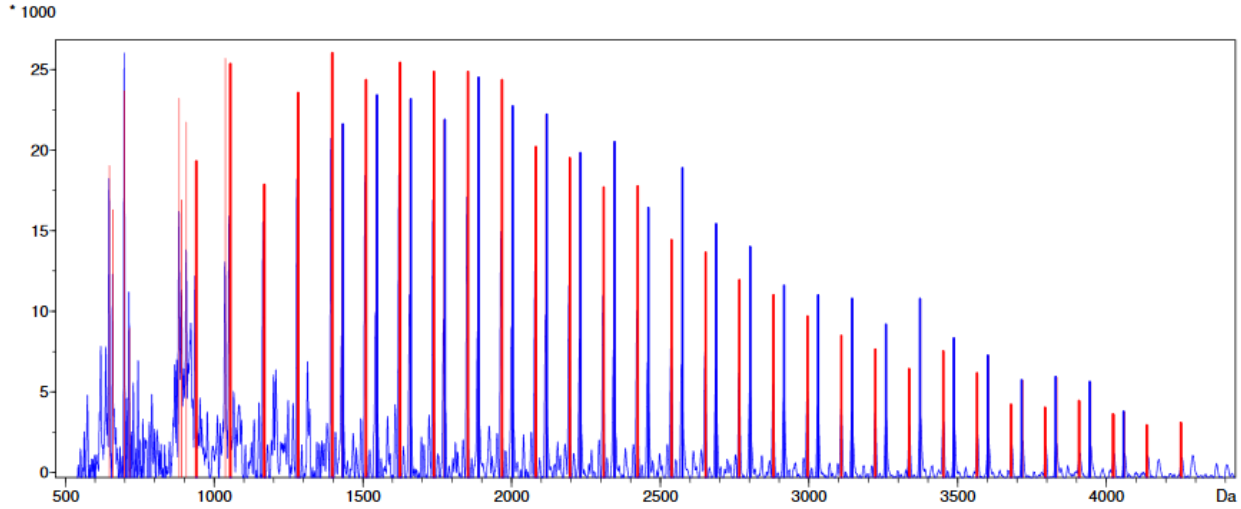

n	ser.	rep.unit	resid.	end1	end2	cation	Mn	Mw	pd	DP	% I.	cnt
1	1	114.000	48.1984	101.000	199.000	Na	2058.17	2379.46	1.15610	18.0541	45.8	30
2	2	114.000	84.1993	101.000	199.000	Na	2378.79	2585.45	1.08688	20.8666	37.7	24

DPB-DS-PCL-Hx, 18

H-NMR ($CDCl_3$)

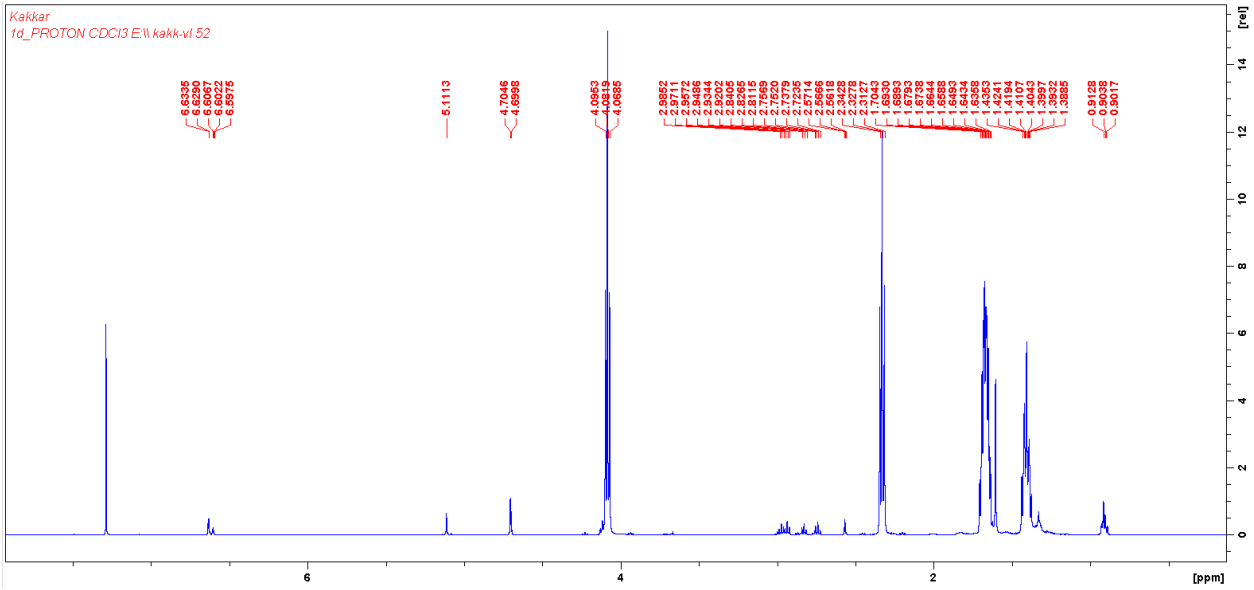

$^{13}C\{^{1}H\}$-NMR ($CDCl_3$)

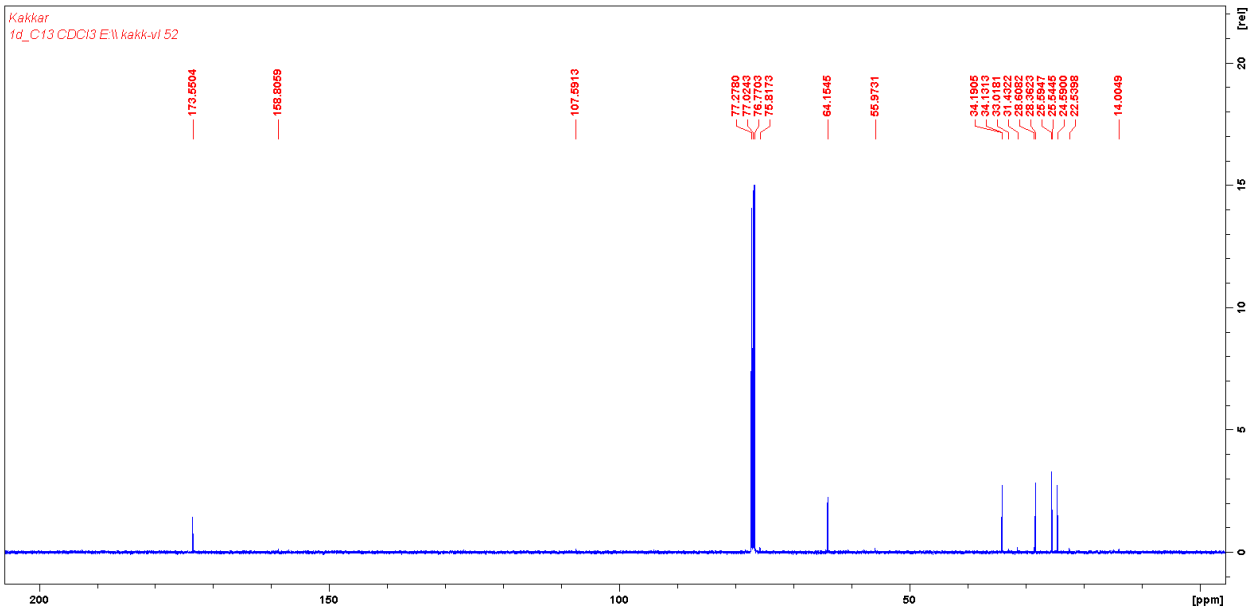

MALDI-TOF

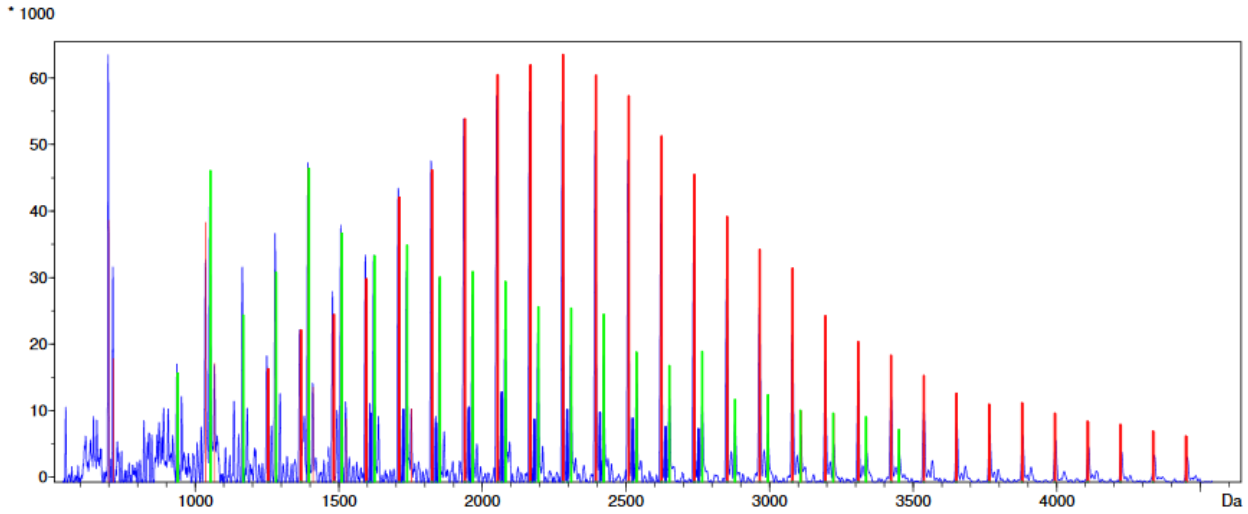

n	ser.	rep.unit	resid.	end1	end2	cation	Mn	Mw	pd	DP	% I.	cnt
1	1	114.000	56.1079	85.0000	407.000	Na	2464.48	2671.70	1.08408	21.6183	52.4	29
2	2	114.000	69.9427	85.0000	407.000	Na	2133.46	2190.40	1.02669	18.7146	6.4	11
3	3	114.000	83.3103	85.0000	407.000	Na	1899.53	2126.34	1.11941	16.6625	32.4	23

μ(PEG-TK-TEG)$_2$DS-PCL (μ3), 19

H-NMR ($CDCl_3$)

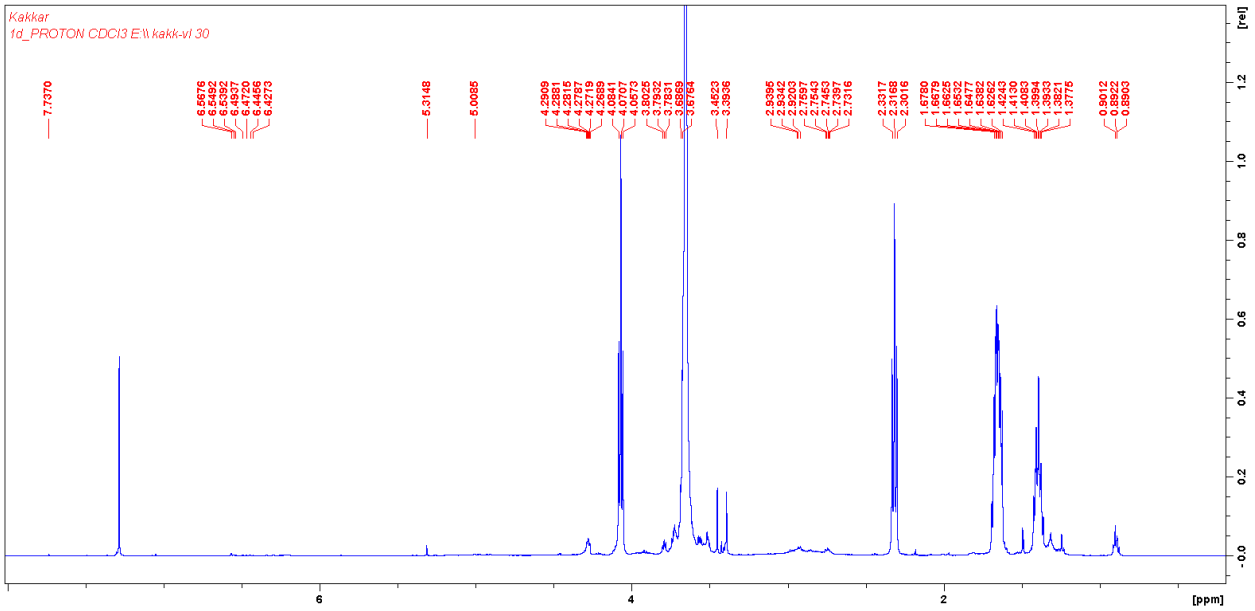

$^{13}C\{^1H\}$-NMR ($CDCl_3$)

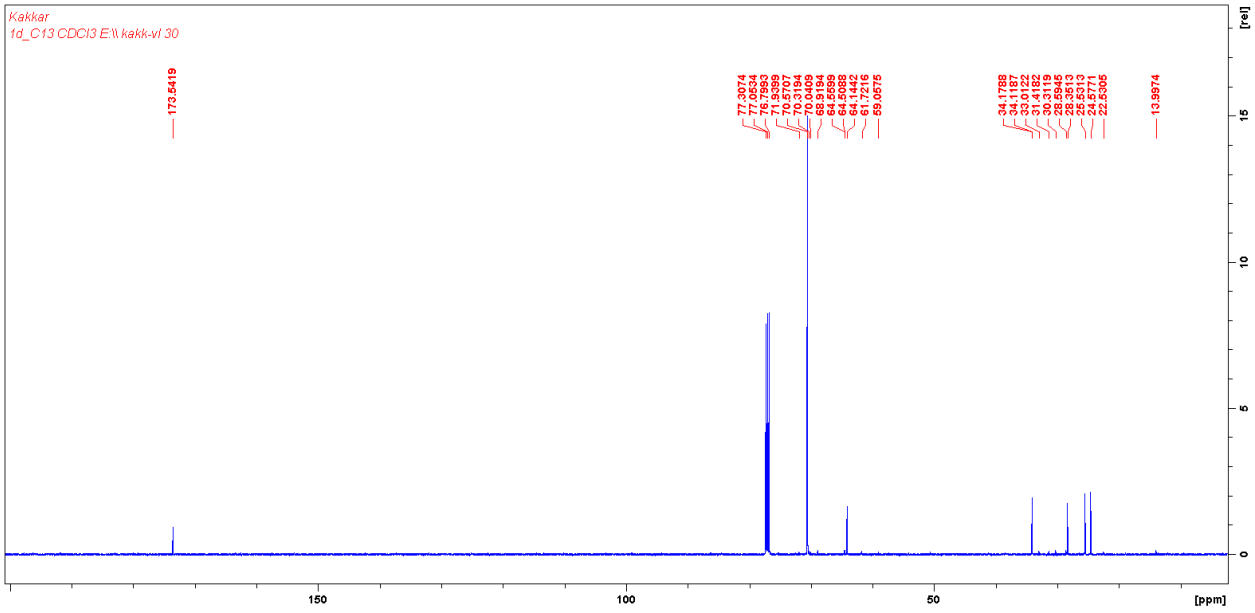

mPEG-OTs, 21

H-NMR ($CDCl_3$)

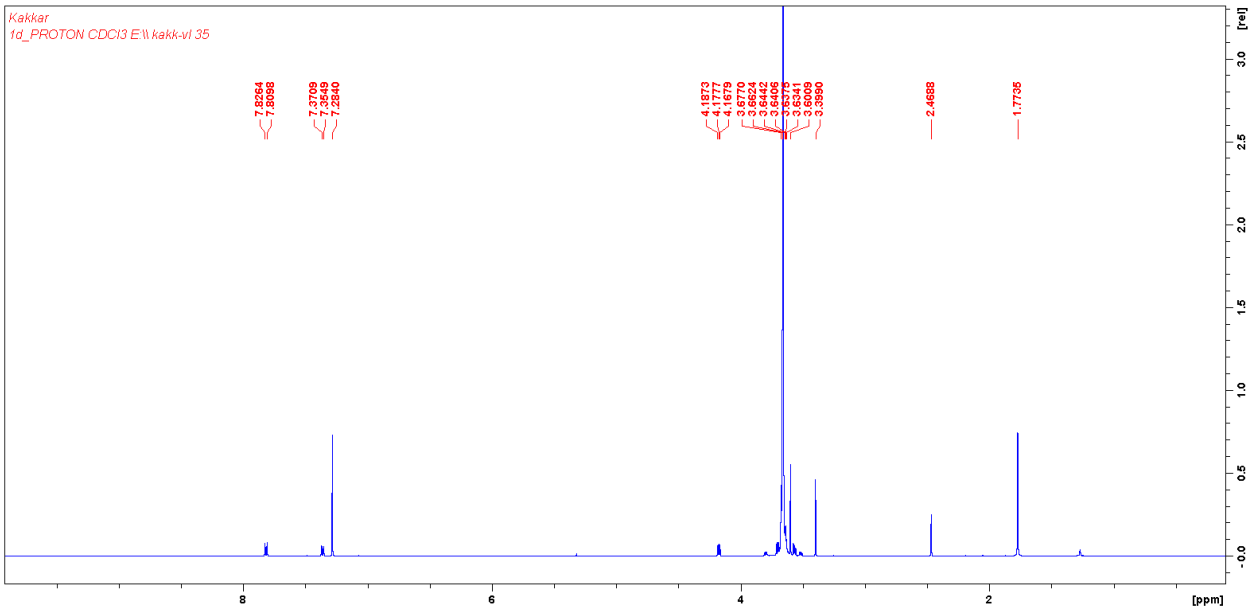

mPEG-N_3, 22

H-NMR ($CDCl_3$)

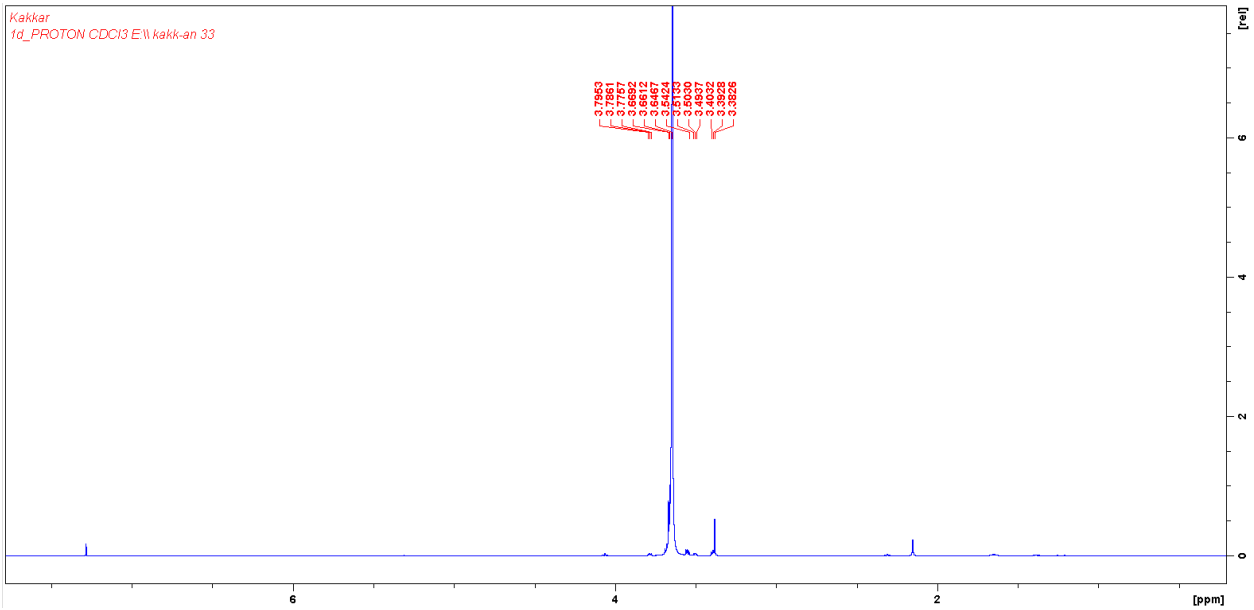

$^{13}C\{^{1}H\}$-NMR ($CDCl_3$)

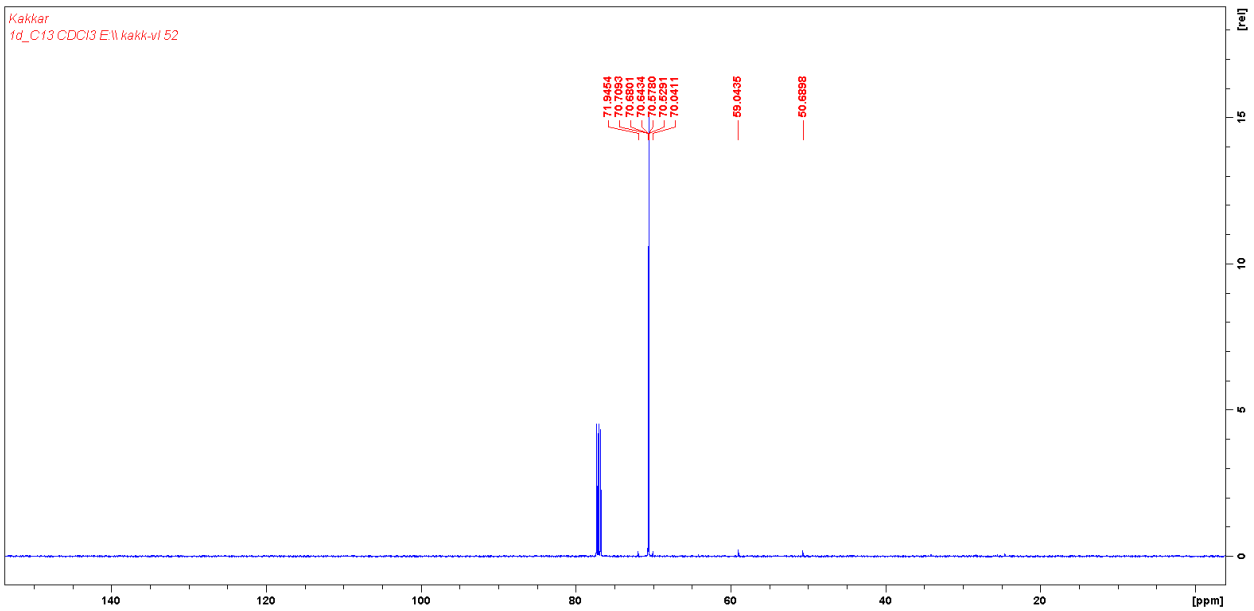

μ$(PEG)_2$DS-PCL (μ4), 23

H-NMR ($CDCl_3$)

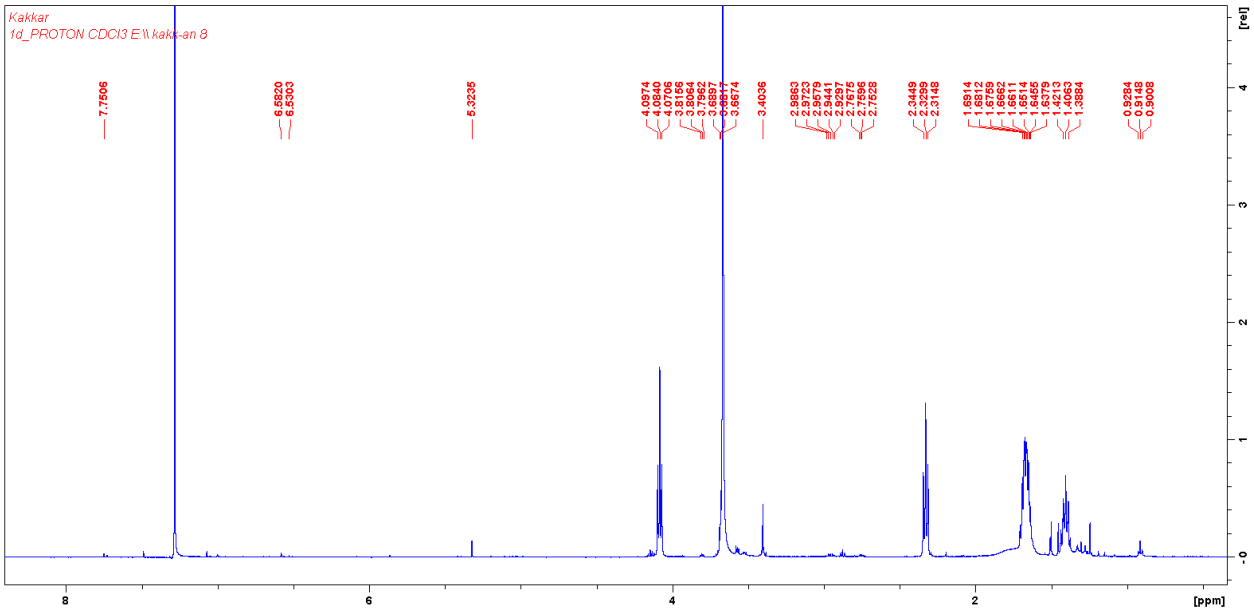

$^{13}C\{^{1}H\}$-NMR ($CDCl_3$)

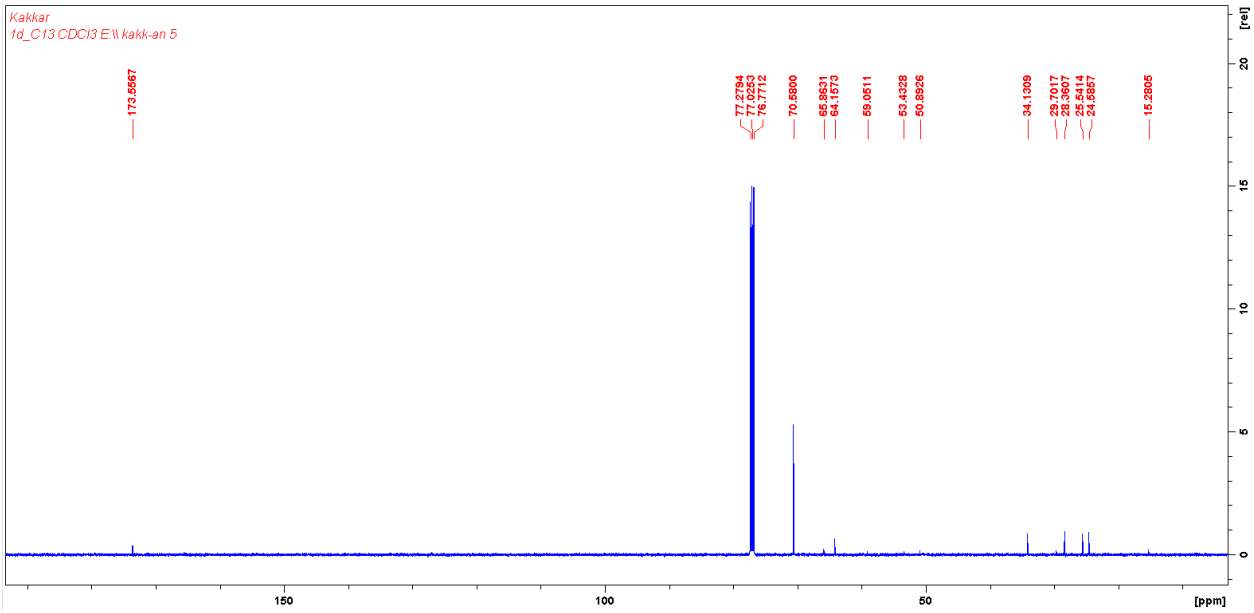

(4-(prop-2-yn-1-yloxy)phenyl)methanol (4PBA), 25

H-NMR ($CDCl_3$)

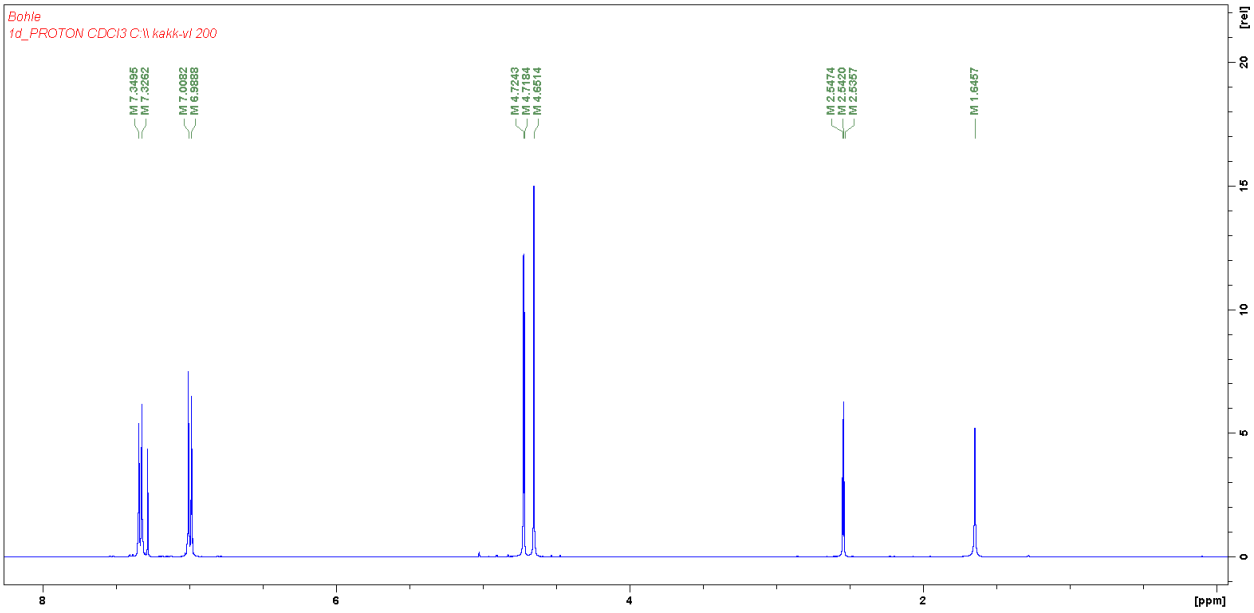

4-(prop-2-yn-1-yloxy)benzyl PCL (4PB-PCL), 26

H-NMR ($CDCl_3$)

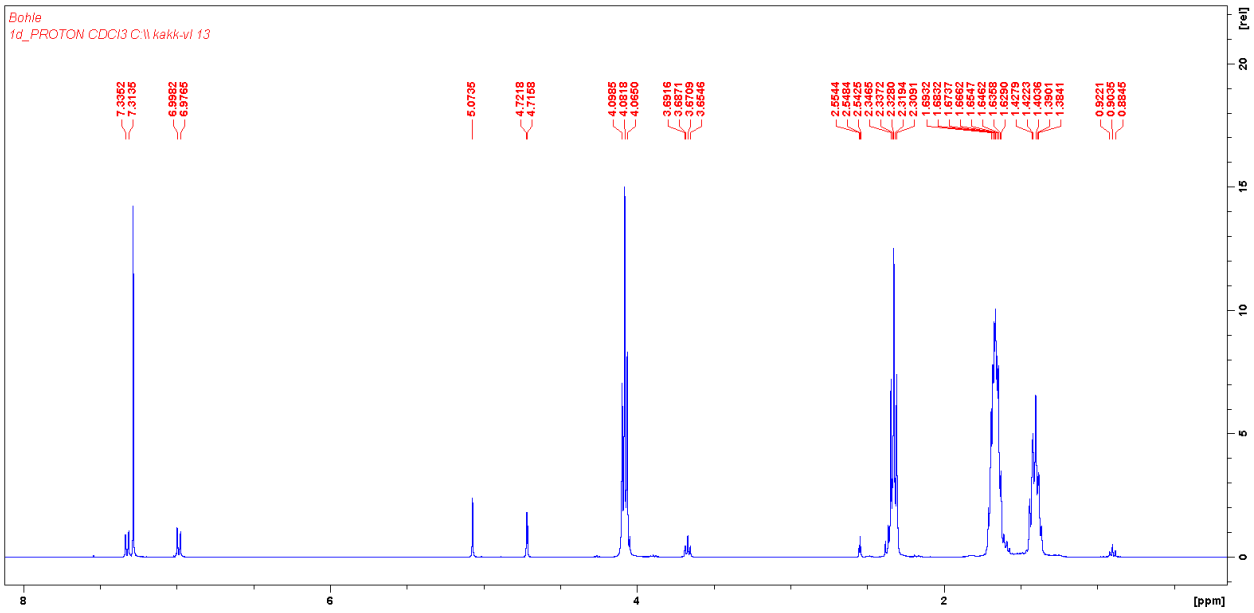

$^{13}C\{^1H\}$-NMR ($CDCl_3$)

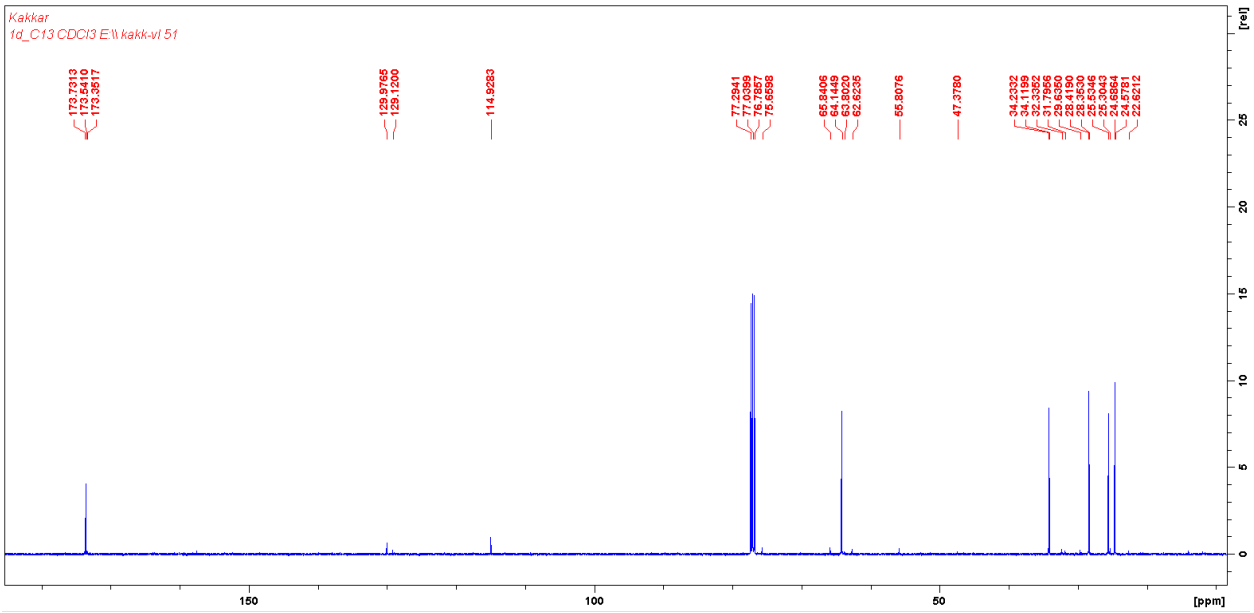

MALDI-TOF

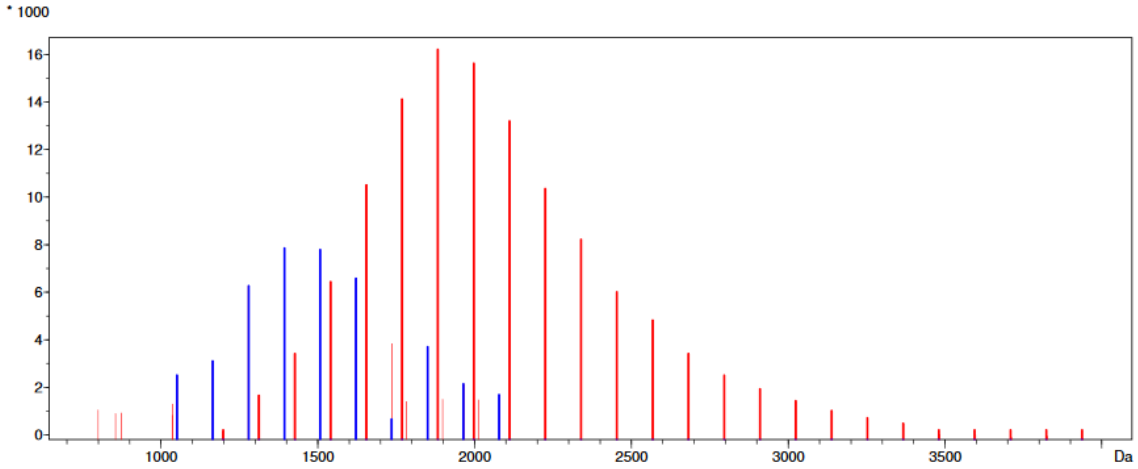

n	ser.	rep.unit	resid.	end1	end2	cation	Mn	Mw	pd	DP	% I.	cnt
1	1	114.000	2.07903	101.000	145.000	K	2036.85	2126.42	1.04398	17.8671	68.1	25
2	2	114.000	6.74983	101.000	145.000	H	1499.48	1546.06	1.03106	13.1533	23.7	10

(PEG-TK-TEG)-*block*-PCL (b1), 27

H-NMR ($CDCl_3$)

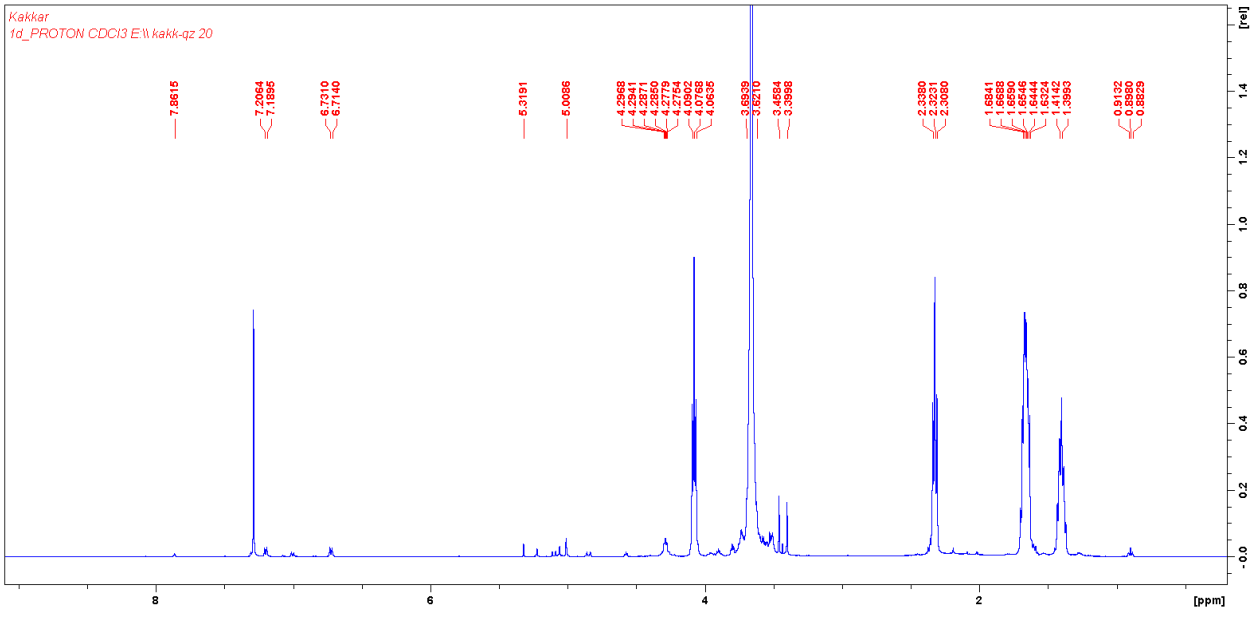

$^{13}C\{^{1}H\}$-NMR ($CDCl_3$)

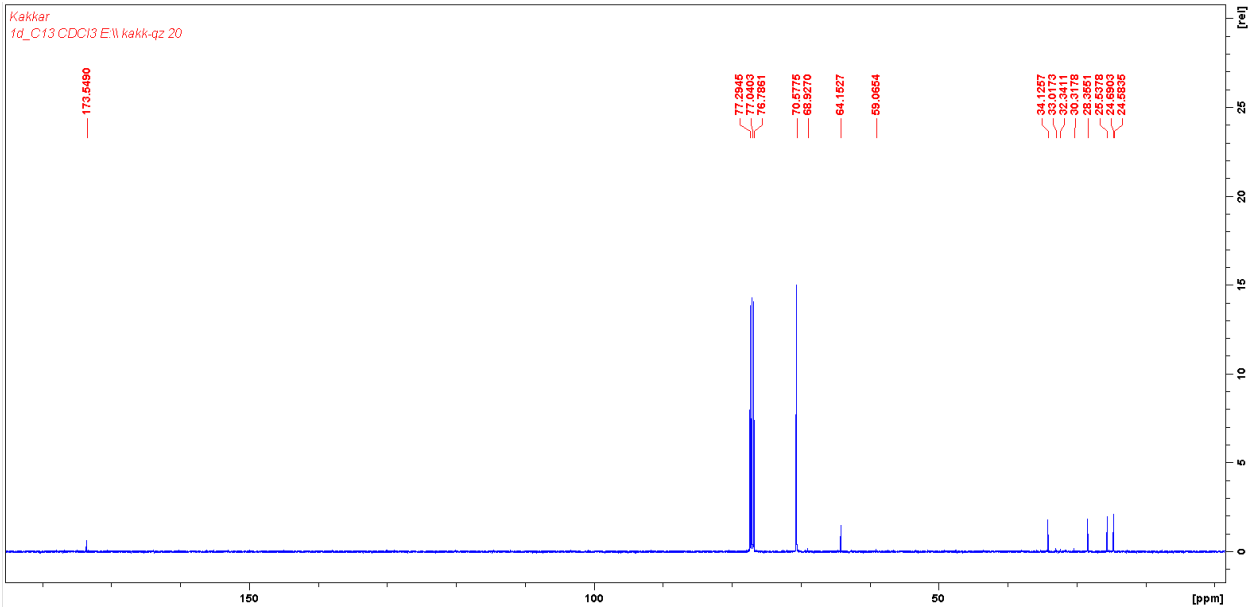

Appendix B

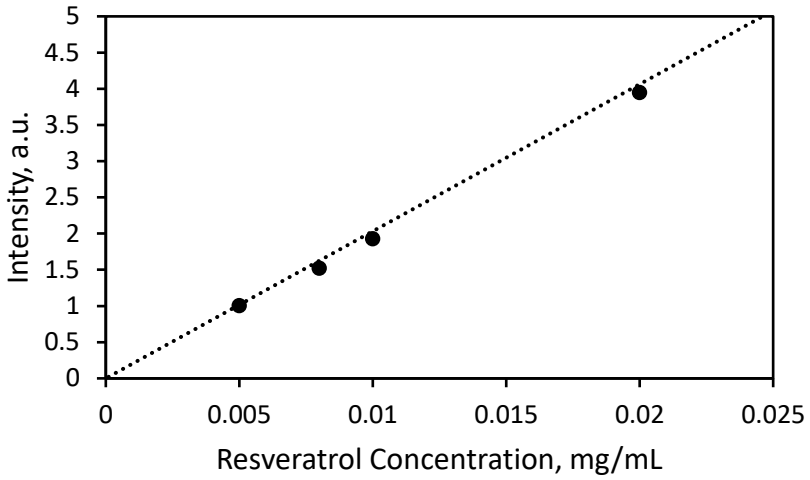

Figure B.1 Standard curve for resveratrol concentration at λ = 324 nm

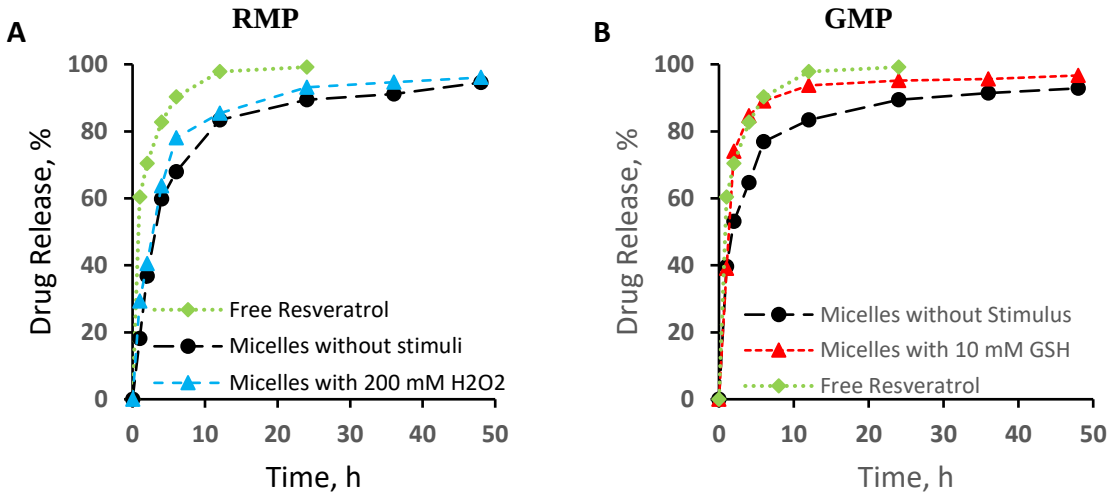

Figure B.2 Release profiles of resveratrol loaded (A) RMP and (B) GMP over 48 hours of dialysis against pH 7.4 PBS. The buffer and dialyzed solutions contained 200 mM H_2O_2 or 10 mM GSH in stimulus responsive studies.

Appendix C

C.1. Supplementary Tables & Figures

Table C.1. Characterization of miktoarm star polymer building blocks

Polymer Segment	Molar Mass (MALDI-TOF)[1]	Molar Mass (NMR)[2]	DP (NMR)	DP (MALDI-TOF)	*Đ* (MALDI-TOF)	*Đ* (GPC)
DPB-PCL', **2**	1994	2841	23	17.50	1.10	1.21
N_3-PEG-TK-TrEG, **5**	2397	2684	54	54.42	1.03	1.05

[1]N_3-PEG-TK-T**r**EG and DPB-PCL' analyzed using M_n given by MALDI-TOF.
[2]Molar masses calculated based on repeating unit molar mass and DP (NMR).

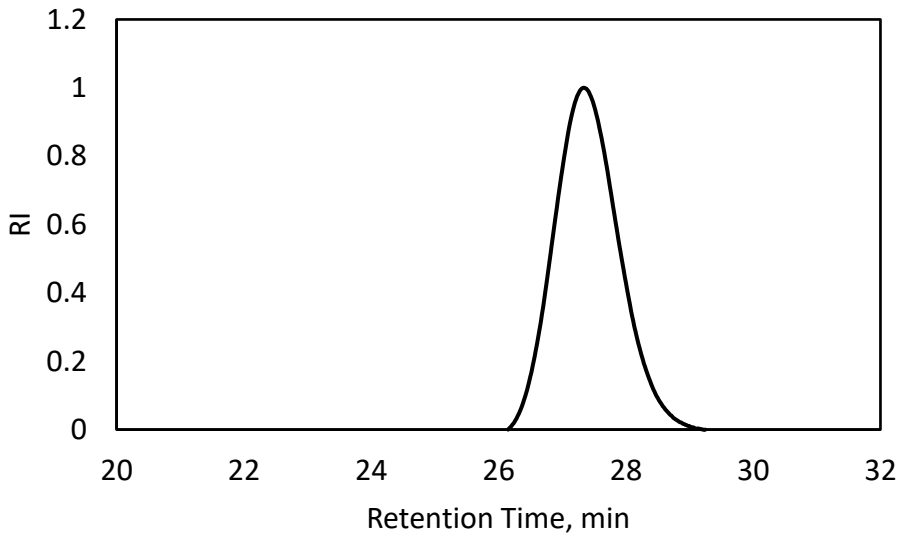

Figure C.1. GPC trace of N_3-PEG-TK-TrEG. Retention time = 27.325 min, *Đ* = 1.05.

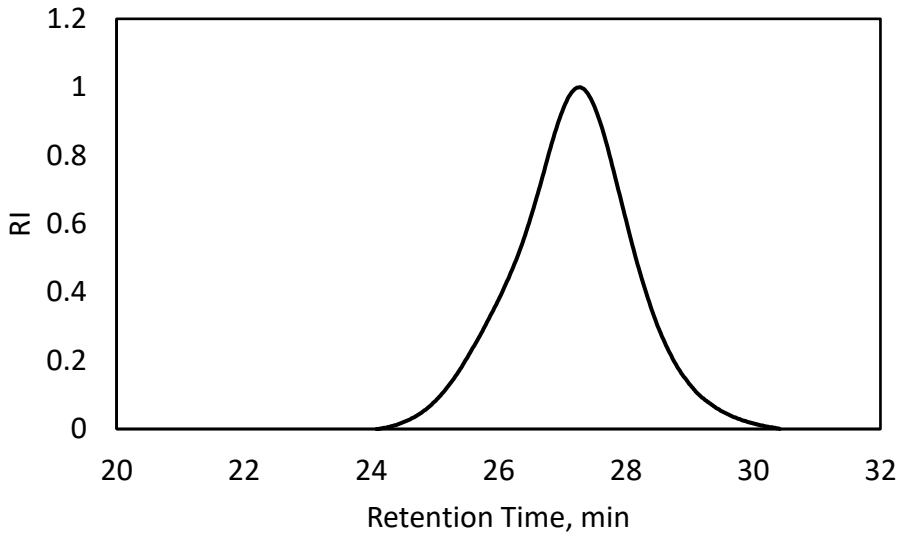

Figure C.2. GPC trace of DPB-PCL'. Retention time = 27.253 min, $Đ$ = 1.21.

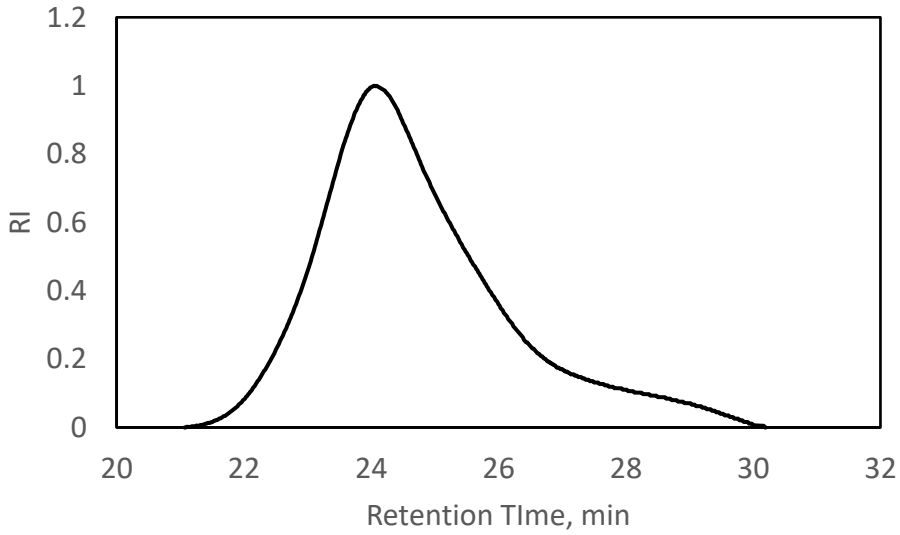

Figure C.3. GPC trace of μ1B. Retention time = 23.983 min, $Đ$ = 1.39.

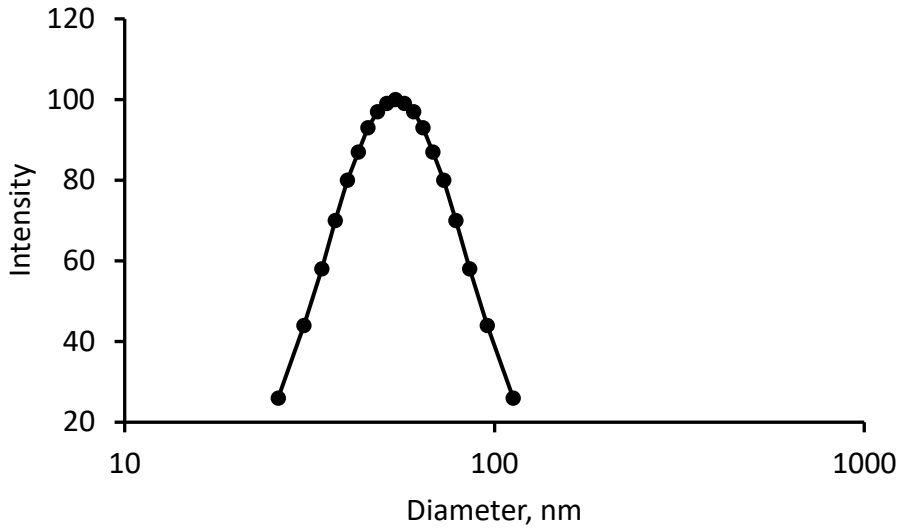

Figure C.4. Size distribution of self-assembled μ1B micelles measured by DLS.

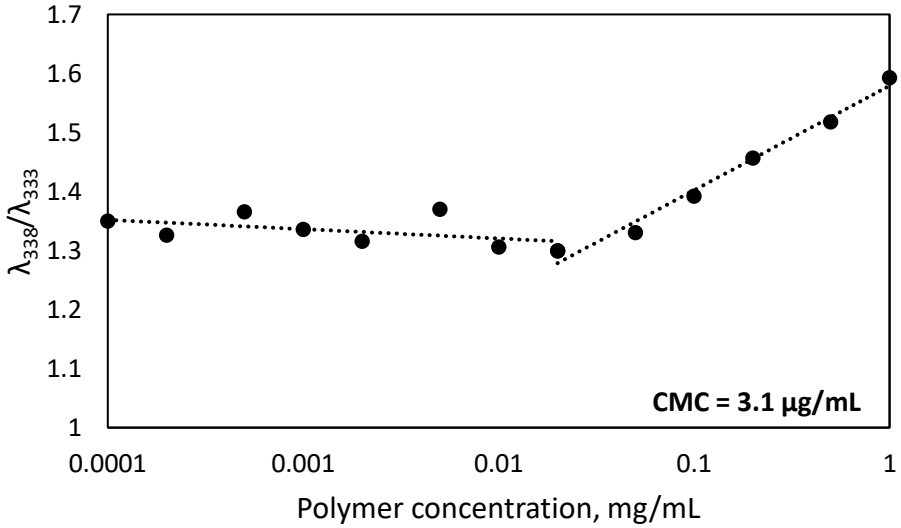

Figure C.5. Critical micelle concentration (CMC) determination of AB_2 miktoarm micelle μ1B.

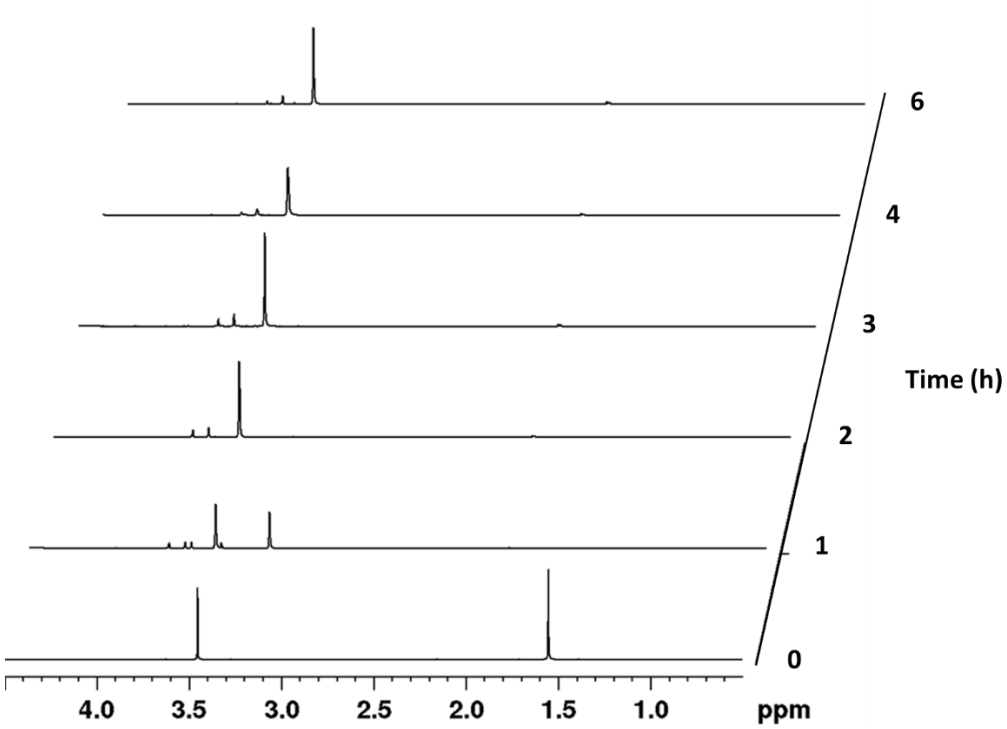

Figure C.6. NMR spectra of mercaptoacetic acid reacting with H_2O_2 in D_2O over time.

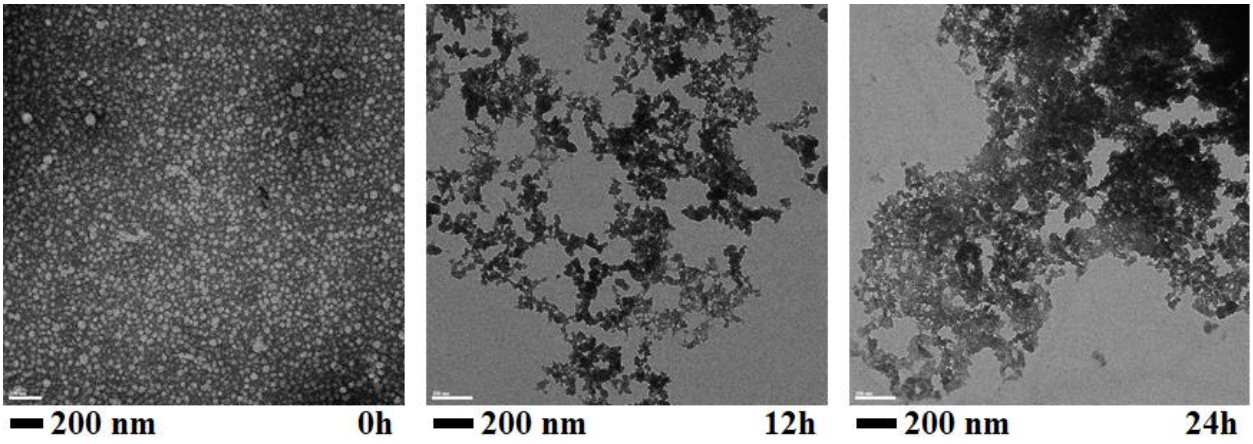

Figure C.7. TEM micrographs of μ1B micelles after (A) 0, (B) 12, and (C) 24 hours of 200 mM H2O2 treatment.

C.2 NMR and Mass Spectra

3,5-bis(prop-2-yn-1-yloxy)benzyl PCL (DPB-PCL'), 2

H-NMR ($CDCl_3$)

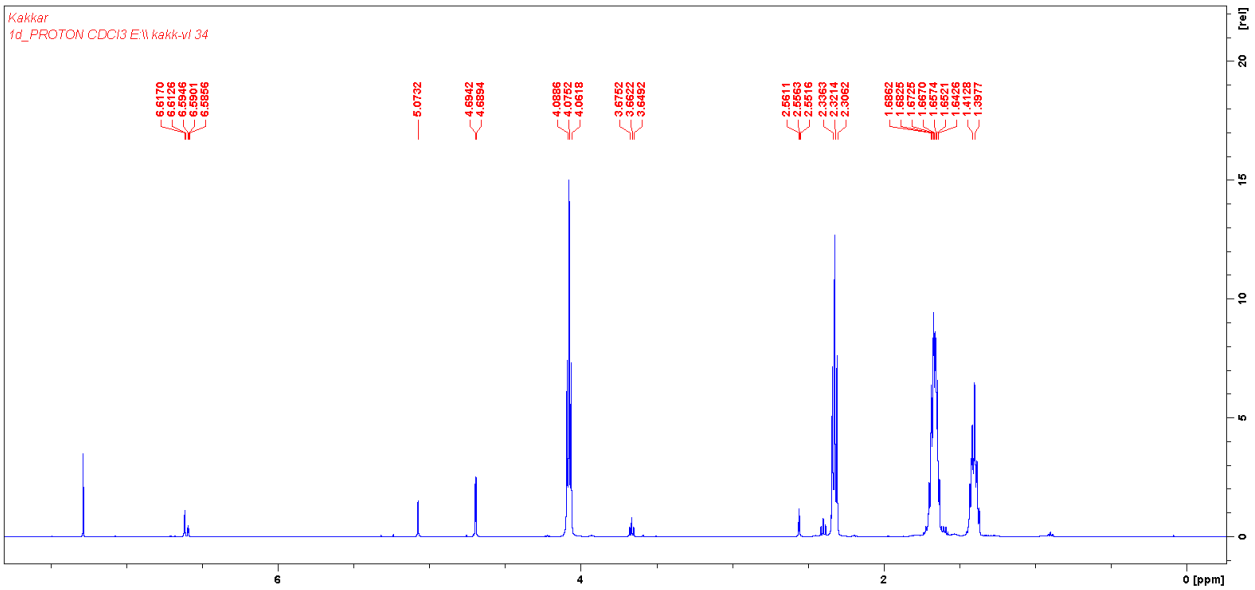

$^{13}C\{^1H\}$-NMR ($CDCl_3$)

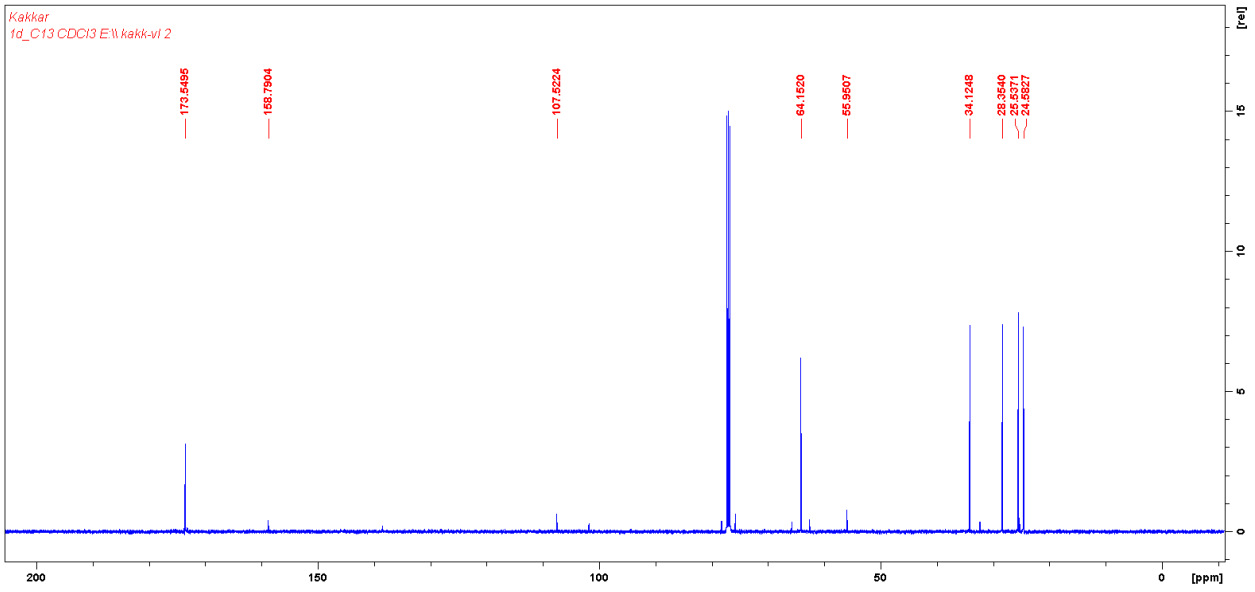

MALDI-TOF

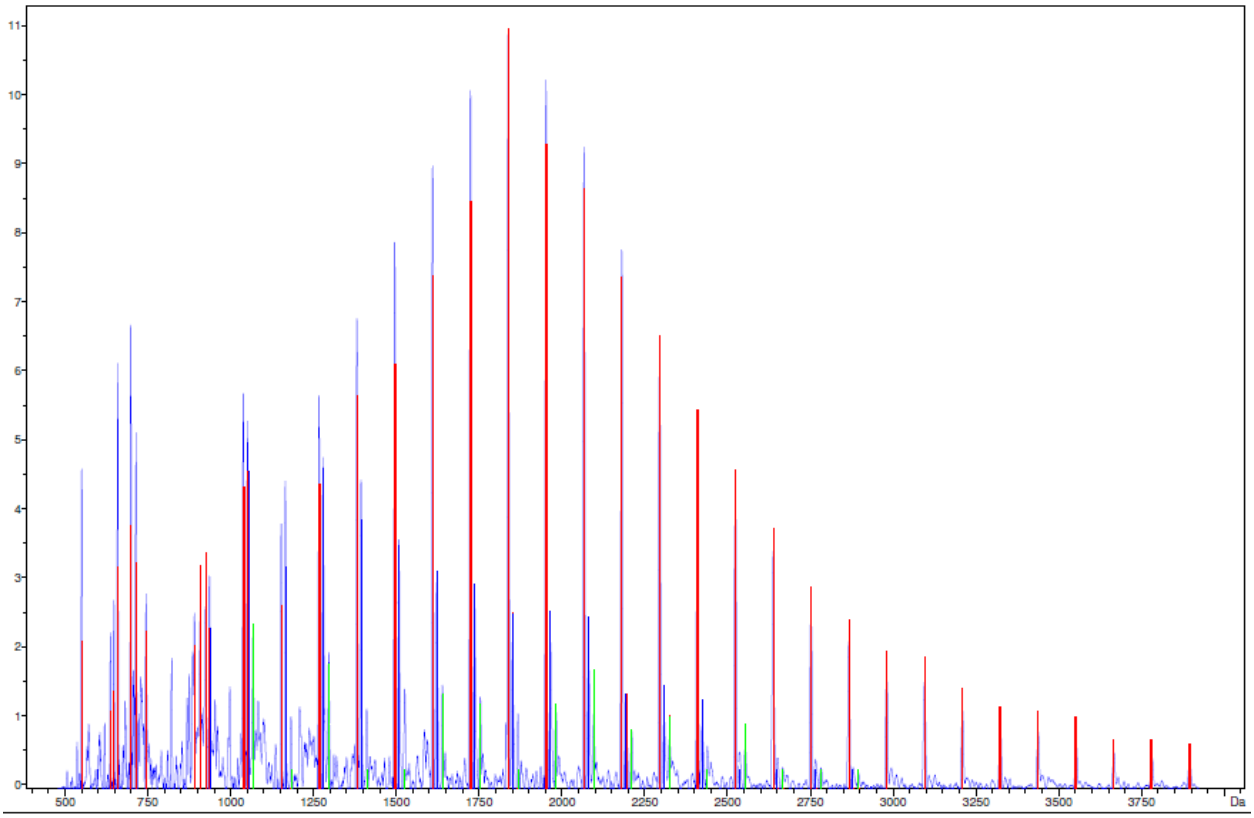

n	ser.	rep.unit	resid.	end1	end2	cation	Mn	Mw	pd	DP	% I.	cnt
1	1	114.000	4.23258	OH	199.000	Na	1994.45	2193.25	1.09968	17.4951	60.6	27
2	2	114.000	0.54948	OH	199.000	K	1514.55	1627.52	1.07459	13.2855	20.9	18
3	3	114.000	16.8824	OH	199.000	K	1714.45	1849.32	1.07867	15.0390	6.5	17

15,15-dimethyl-12-oxo-2,5,8,11-tetraoxa-14,16-dithiaoctadecan-18-oic acid (TK-TrEG), 4

H-NMR ($CDCl_3$)

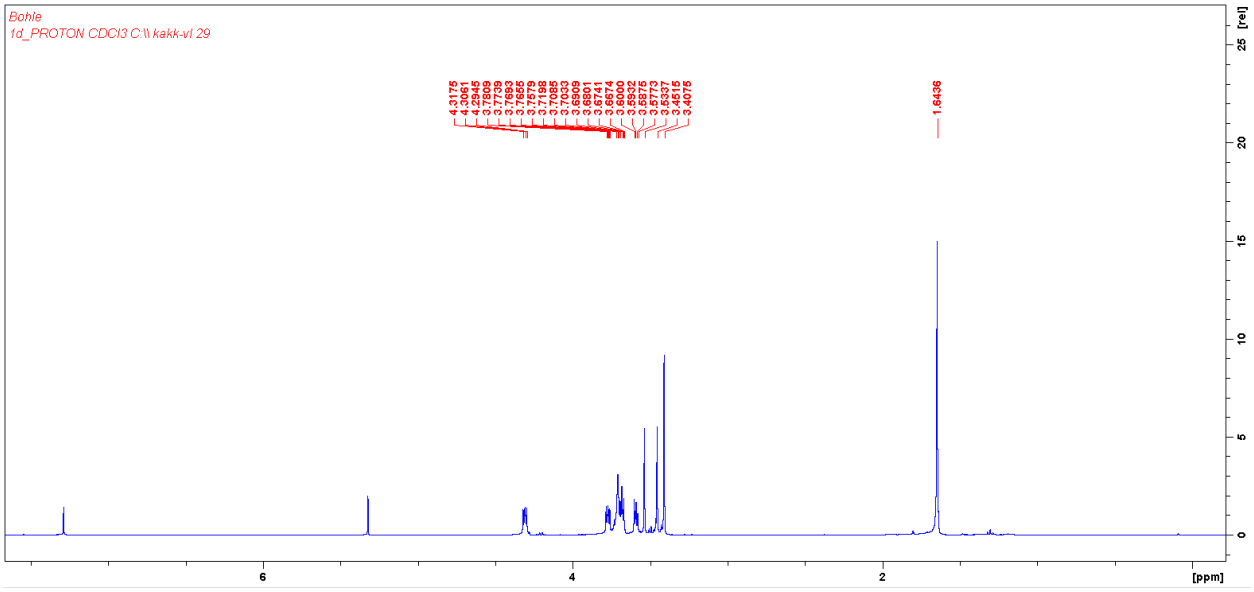

$^{13}C\{^1H\}$-NMR ($CDCl_3$)

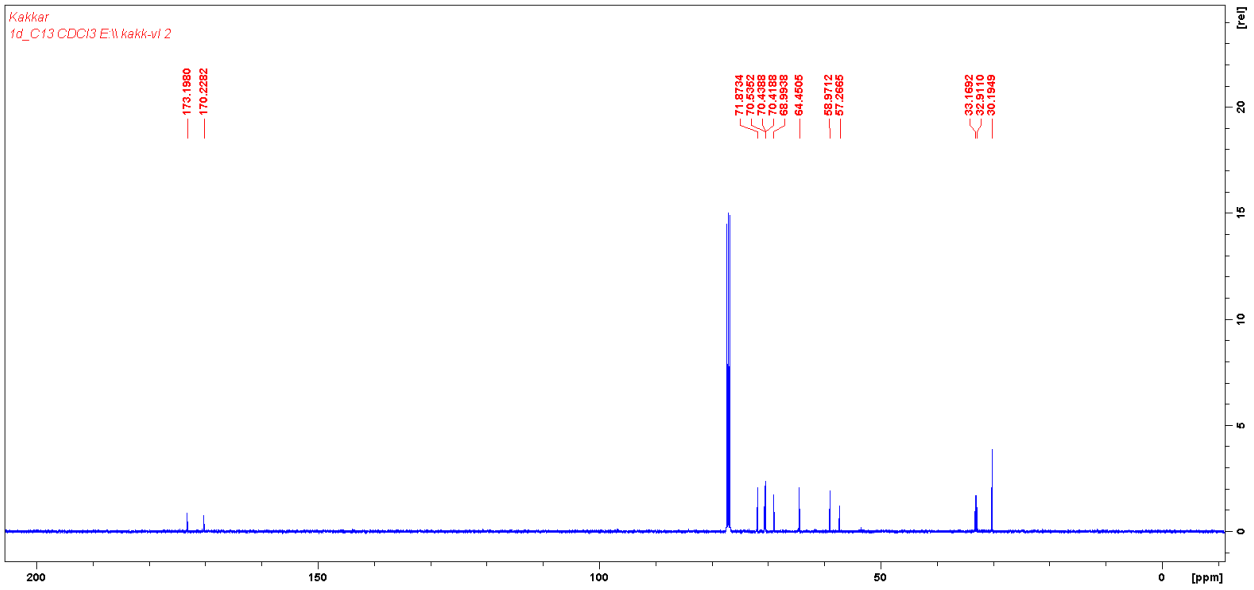

ESI

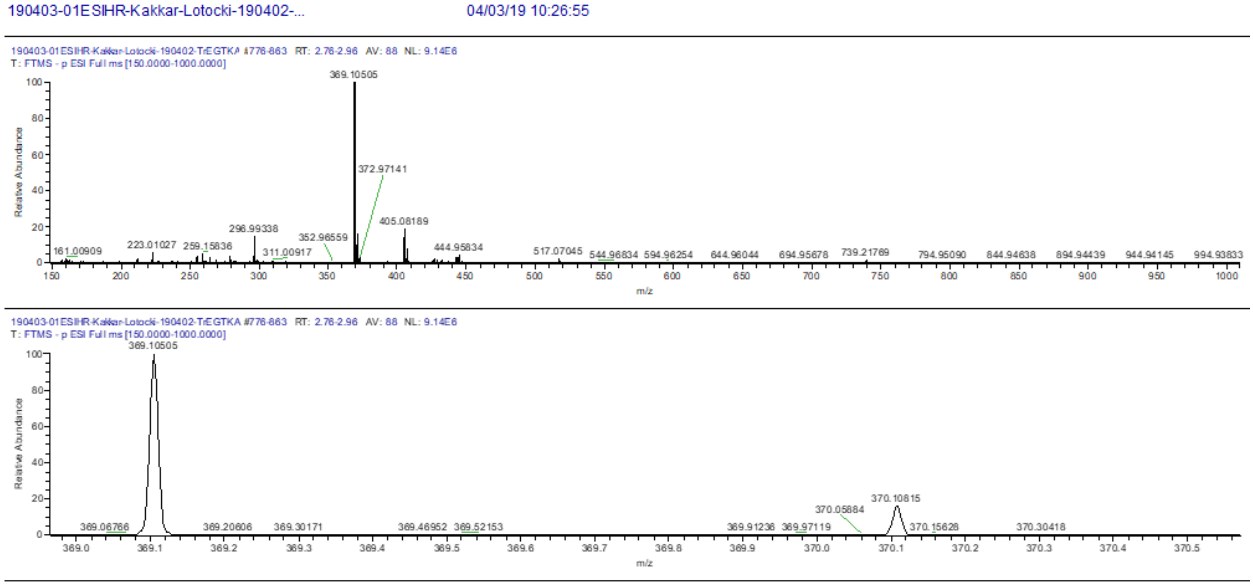

190403-01ESIHR-Kakkar-Lotocki-190402-TrEGTKA#1066 RT: 3.48
T: FTMS - p ESI Full ms [150.0000-1000.0000]
m/z= 369.08868-369.12626

m/z	Intensity	Relative	Resolution	Charge	Theo. Mass	Delta (ppm)	RDB equiv.	Composition
369.10513	3701882.0	100.00	29606.00	1.00	369.10472	1.13	2.5	$C_{14}H_{25}O_7S_2$
					369.10403	3.00	12.0	$C_{20}H_{19}O_4NS$

N_3-PEG-TK-TrEG, 5

H-NMR ($CDCl_3$)

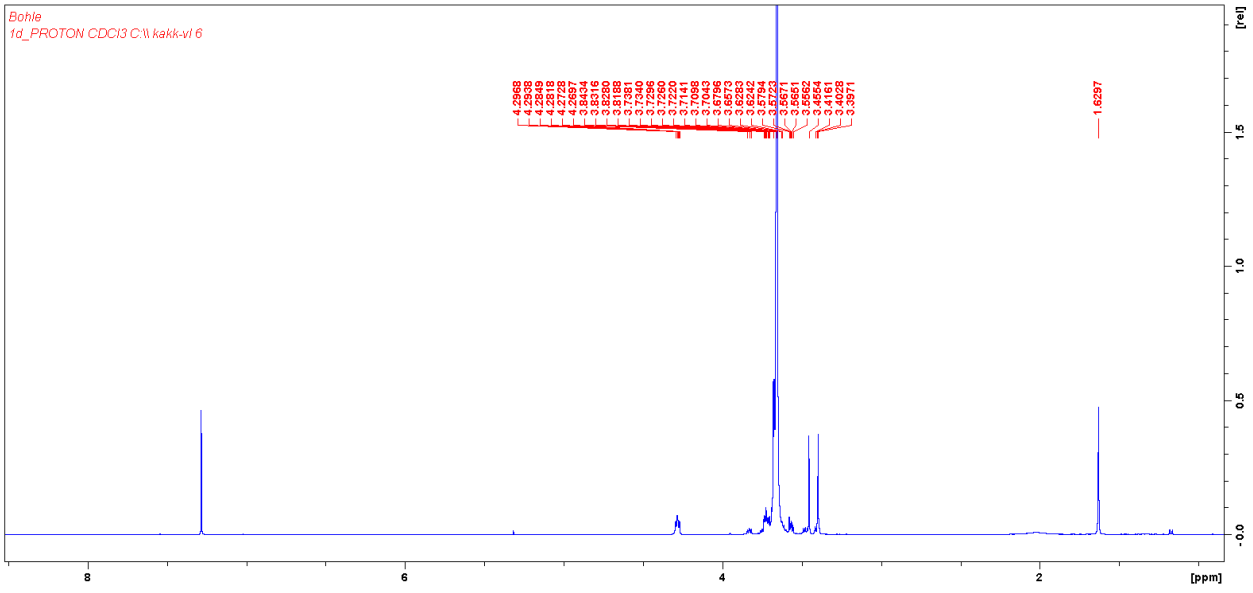

$^{13}C\{^{1}H\}$-NMR ($CDCl_3$)

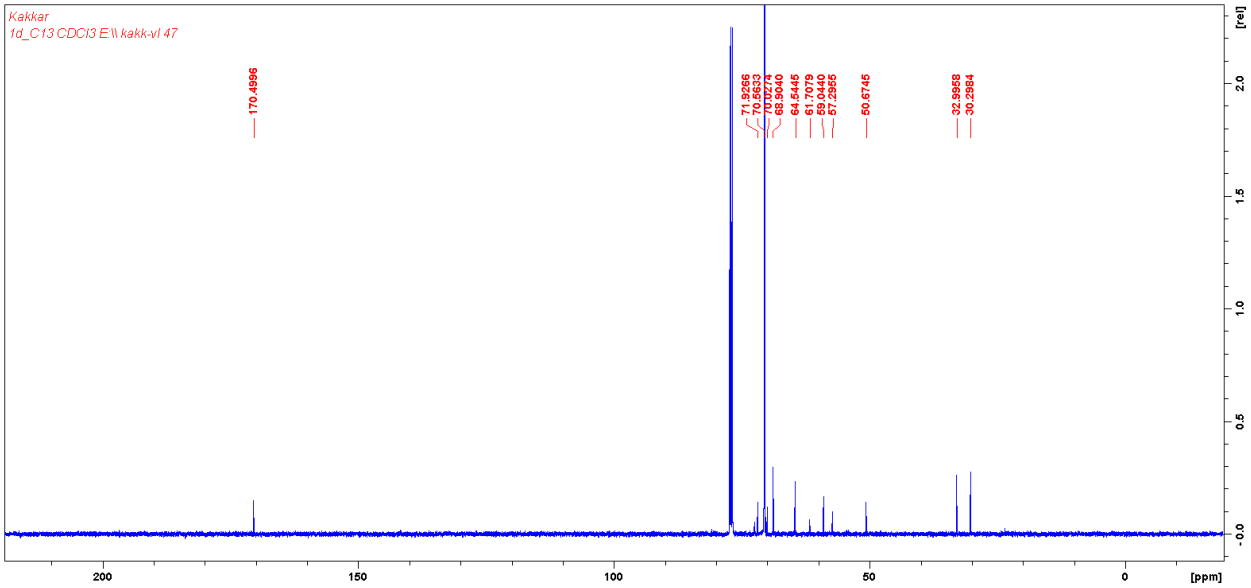

MALDI-TOF

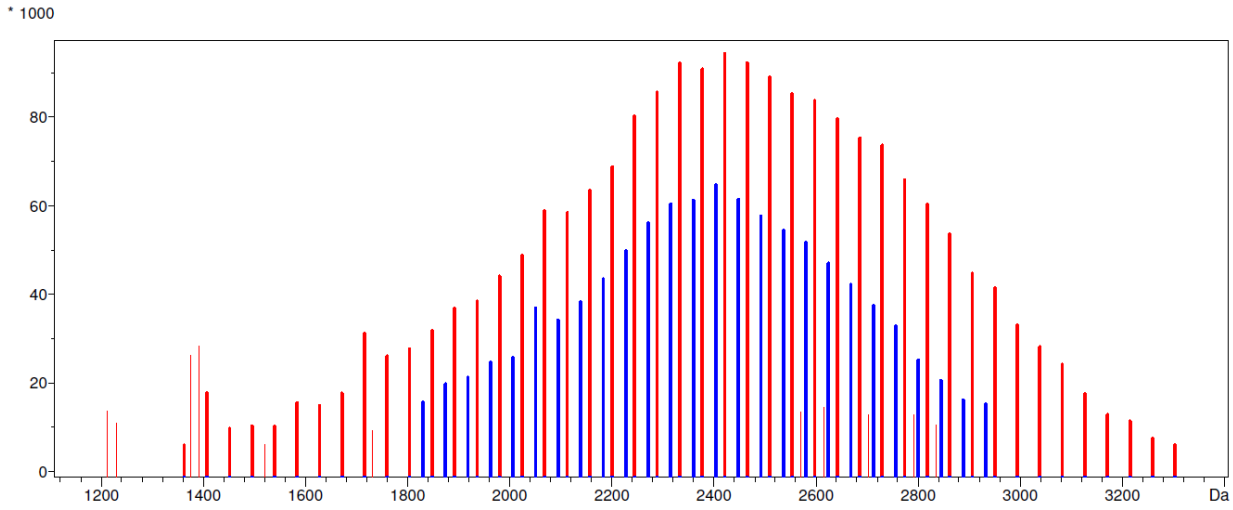

n	ser.	rep.unit	resid.	end1	end2	cation	Mn	Mw	pd	DP	% I.	cnt
1	1	PEG	41.8859	369.474	70.0733	H	2397.41	2465.26	1.02830	54.4216	63.5	45
2	2	PEG	24.3713	369.474	70.0733	H	2387.51	2417.85	1.01271	54.1968	31.3	26

μ(PEG-TK-TrEG)$_2$PCL (μ1B), 6

H-NMR ($CDCl_3$)

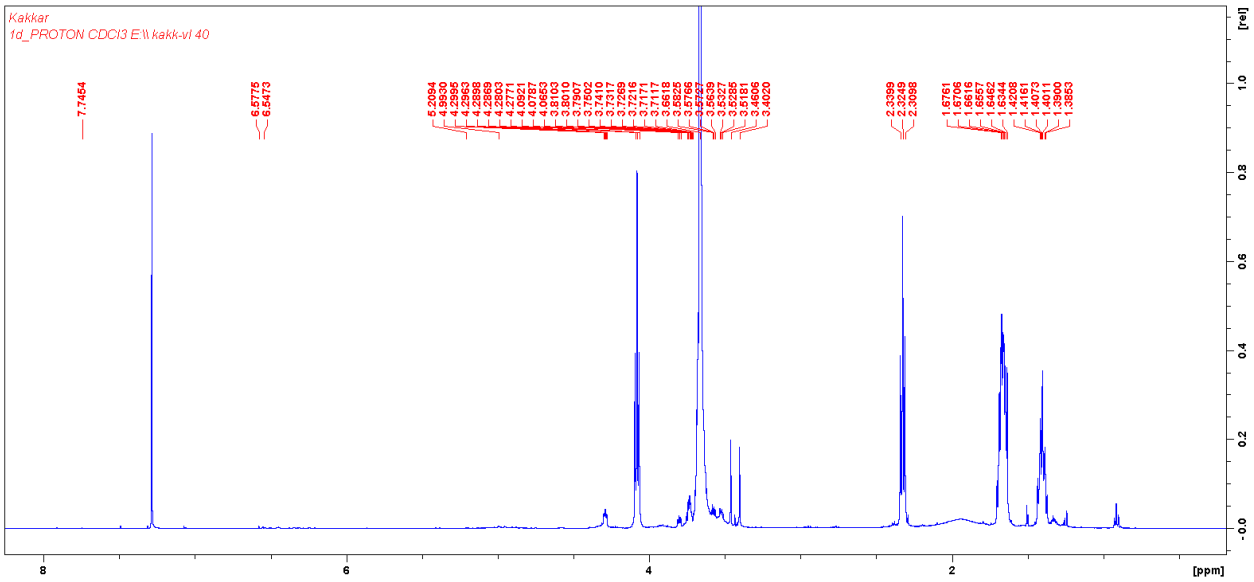

$^{13}C\{^1H\}$-NMR ($CDCl_3$)

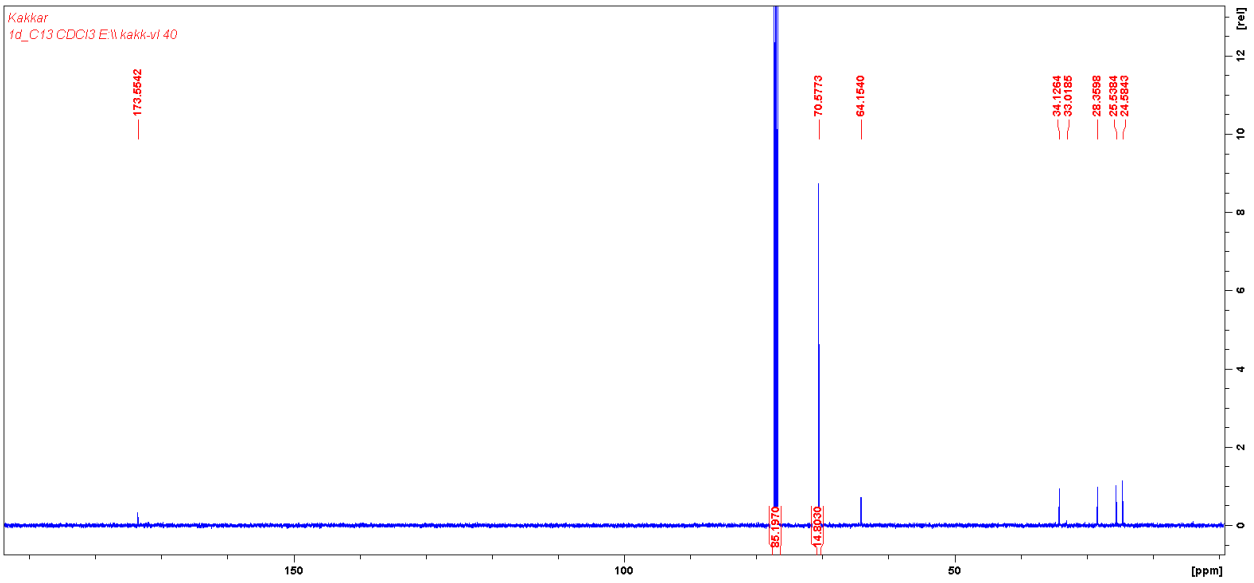

Journal of Materials Chemistry B

ROYAL SOCIETY OF CHEMISTRY

PAPER

View Article Online
View Journal | View Issue

Cite this: J. Mater. Chem. B, 2020, 8, 7275

Facile design of autogenous stimuli-responsive chitosan/hyaluronic acid nanoparticles for efficient small molecules to protein delivery†

Parinaz Sabourian,[ab] Jeff Ji,[c] Victor Lotocki,[a] Alexandre Moquin,[ac] Ramez Hanna,[a] Masoud Frounchi,*[b] Dusica Maysinger*[c] and Ashok Kakkar*[a]

Received 22nd March 2020,
Accepted 30th June 2020

DOI: 10.1039/d0tb00772b

rsc.li/materials-b

Easily assembled and biocompatible chitosan/hyaluronic acid nanoparticles with multiple stimuli-responsive ability are ideally suited for efficient delivery of therapeutic agents under specific endogenous triggers. We report a simple and versatile strategy to formulate oxidative stress and pH-responsive chitosan/hyaluronic acid nanocarriers with high encapsulation efficiencies of small drug molecules and nerve growth factor protein. This is achieved through invoking the dual role of a thioketal-based weak organic acid to disperse and functionalize low molecular weight chitosan in one-pot. Thioketal embedded chitosan/hyaluronic acid nanostructures respond to oxidative stress and show controlled release of quercetin, curcumin and NGF. Lowering the pH in the buffer solution led to higher quercetin release from NPs than at physiological pH, and mimicked the nanoparticle behavior in the environment of early to late endosomes. Curcumin and quercetin loaded NPs killed glioblastoma cells with high efficiency, and NGF-loaded nanoparticles retained biological activity of the protein and increased peripheral nerve outgrowth in explanted mouse dorsal root ganglia.

Introduction

Elevated oxidative stress and a decrease in intra- and extracellular pH have been commonly associated with neurological disorders and cancer.[1,2] Environment sensing nano-delivery systems which could efficiently encapsulate a variety of cargo and release therapeutic agents in response to endogenous stimuli (reactive oxygen species (ROS) or low pH) constitute a topical area of research in targeted drug delivery.[3–5] Several ROS and pH-responsive entities have been developed and incorporated into polymeric nanoparticles (NPs) including abundant, biocompatible and biodegradable chitosan-based systems.[6–8] For example, (i) phenyl-boronic acid pinacol ester has been used to prepare ROS-responsive polymeric NPs;[9] and (ii) lactose-modified chitosan/hyaluronic acid (HA) colloids scavenged H_2O_2 generated by human neutrophils at pH 6, which mimics an inflamed microenvironment.[10] Despite such efforts,[11–14] significant challenges in developing NPs-based carriers using natural biopolymers embedded with ROS-responsive entities still remain. These issues can be addressed by developing simple synthetic routes to the functionalization of chitosan-based nanocarriers with efficient stimuli-responsive entities, enhancing encapsulation diversity of cargo, and determining their efficacy in controlled therapeutic delivery.

Chitosan, a polysaccharide with easily accessible reactive surface groups, has been widely utilized in varied applications including the pharmaceutical industry.[15,16] Its response to changes in pH, which mimic endogenous environmental variations, has been employed in developing stimuli-responsive drug delivery platforms.[17,18] One of the limitations in developing functionalized chitosan (FCS) based drug-delivery systems is the insolubility of low molecular weight chitosan (CS) in aqueous media at neutral pH. This is generally overcome by dispersing chitosan in an aqueous solution with hydrochloric acid (HCl) or acetic acid, followed by the introduction of specific chemical entities through chitosan's surface OH or NH_2 groups.[19] We sought to mitigate this issue by using biocompatible 2,2′-(propane-2,2-diylbis(sulfanediyl))diacetic acid (thioketal diacid, abbreviated TKDA, Scheme 1) that could assume the dual role of dispersing CS in an aqueous medium, as well as functionalize it with ROS-responsive thioketal entities *via* a facile synthetic methodology. TKDA as a weak organic acid can help reduce solution pH, solubilize CS, and thus eliminate the need to add HCl or acetic acid externally first. Free amine

[a] Department of Chemistry, McGill University, 801 Sherbrooke St. West, Montréal, Québec H3A 0B8, Canada. E-mail: ashok.kakkar@mcgill.ca
[b] Department of Chemical and Petroleum Engineering, Sharif University of Technology, Azadi Avenue, Tehran, Iran
[c] Department of Pharmacology and Therapeutics, McGill University, 3655 Promenade Sir William Osler, Montréal, Québec H3G 1Y6, Canada

† Electronic supplementary information (ESI) available. See DOI: 10.1039/d0tb00772b

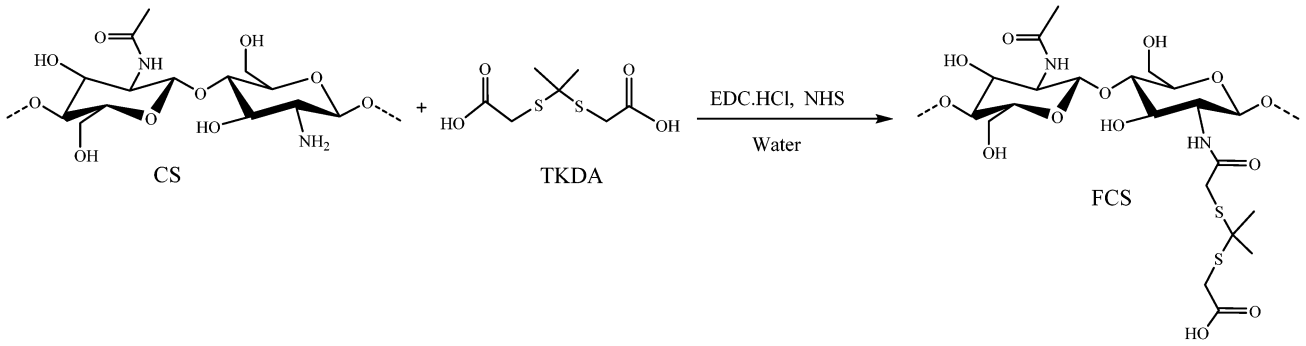

Scheme 1 Functionalization of CS with TKDA.

groups on the backbone of CS could then be used to conjugate TKDA through an amidation reaction.[20–24] The thioketal group of TKDA responds to and breaks down in the presence of ROS commonly found at diseased or injured sites.[25–27] Unfunctionalized chitosan chains also swell upon protonation in the acidic environment of endosomes (pH 3 to 6).[28–30] We report herein a simple and versatile strategy to develop oxidative stress- and pH-responsive NPs through the functionalization of CS with TKDA, a solubilizing and ROS-responsive molecule, and subsequent complexion of FCS with hyaluronic acid (HA). Hyaluronic acid, also known as hyaluronan, is a naturally occurring polysaccharide, which contains *N*-acetyl-D-glucosamine and D-glucoronic acid as the repeat units.[31] Due to the unique and interesting physicochemical properties of this polyanionic macromolecule, including biocompatibility and biodegradability, it has been extensively utilized for a variety of applications in biology.[32,33] It is also commonly employed to prepare stable nanoparticles by ionotropic polyelectrolyte complexation with positively charged chitosan for encapsulation of a variety of active therapeutics in drug delivery applications.[34–37]

Curcumin and quercetin are pluripotent lipophilic compounds that have shown promise in the treatment of multiple types of cancer, but are limited by their low bioavailability and instability in biological media.[38–43] We assessed the effectiveness of FCS/HA NPs to load and deliver these chemotherapeutics in a cell model of glioblastoma (GBM) multiform. To test the versatility of the FCS/HA NPs, we also investigated the delivery of the neurotrophic protein nerve growth factor (NGF) that can promote neuronal regeneration.[44,45] Due to the instability of NGF in biological media, its incorporation into NPs can help prevent hydrolytic and enzymatic degradation.[46–48] ROS-responsive chitosan-based NPs were loaded with curcumin, quercetin and NGF, and tested in both 2D and 3D cultures of GBM and dorsal root ganglia (DRG) cells. We demonstrate that FCS/HA NPs were effective in responding to oxidative stress and pH with enhanced release rates and can deliver a diverse range of cargo of varying size and solubility. Curcumin and quercetin loaded NPs killed GBM cells with high efficiency, and NGF-incorporated nanocarriers markedly increased peripheral nerve outgrowth in explanted mouse DRG.

Experimental

Materials

The following were purchased from (i) CarboSynth: HA (40–50 kDa, CAS: 9012764); and (ii) Sigma Aldrich: CS (50–190 kDa, CAS: 9012764); mercaptoacetic acid (92 g mol^{-1}), 3-dimethyl aminopropyl-*N*′-ethyl carbodiimide hydrochloride (EDC·HCl), *N*-hydroxy succinimide (NHS), fluorescein isothiocyanate (FITC), quercetin (CAS: 117-39-5), metformin (D5035, 165.63 g mol^{-1}), curcumin (08511) and NGF (2.5S, N6009), and used as received. Alexa Fluor® 488 anti-rabbit secondary antibody was purchased from Thermo-Fisher. Rabbit anti-transcription factor EB (TFEB) was purchased from Bethyl Laboratories. Type-II collagenase was purchased from Worthington Biochemical Corporation. β-Tubulin III was purchased from Millipore. U251 cells were obtained from the American Type Culture Collection. Reagents including sodium hydroxide (NaOH), HCl, acetic acid; solvents such as hexanes, dimethyl formamide (DMF), dimethyl sulfoxide (DMSO), acetone, methanol, and deuterated solvents (D_2O, CD_3OD, $CDCl_3$) for proton (^1H) and carbon (^{13}C) nuclear magnetic resonance (NMR), were used as received from Sigma Aldrich.

Instrumentation

NMR spectra were recorded on a Bruker AVIIIHD 400 instrument at 400 MHz. It was equipped with a 5 mm BBFO$^+$ Smart Probe that autotunes to ^1H on one channel. All spectra were collected and analyzed with TopSpin software. Fourier-transform infrared spectroscopy (FTIR) spectra were acquired on a Spectrum Two FT-IR spectrometer equipped with a single bounce diamond Attenuated Total Reflectance (ATR) for solids. The spectra were measured as an average of 32 scans with 4 cm^{-1} resolution with a range of 400 to 4000 cm^{-1}. Size distributions of empty and loaded NPs were determined with a Brookhaven 90 Plus Particle Size Analyzer. All measurements were taken in triplicate at a 90° scattering angle at 25 °C. To analyze the surface charge of NPs for cell affinity, zeta potentials were obtained from aqueous suspensions of NPs using a Zetasizer Nano ZS by Malvern. All the measurements were performed 5 times for each sample at room temperature and an electrical field of 4.9 ± 0.1 V was applied. UV-visible spectra were recorded on a Varian Cary 50 UV-Vis spectrophotometer equipped with nanodrop accessory.

Transmission electron microscopy (TEM) micrographs were recorded using a FEI Tecnai 12 BioTwin 120 kV TEM equipped with an AMT XR80 CCD Camera System located at the Facility for Electron Microscopy Research (FEMR) at McGill University. Fluorescence microscopy was performed on a Leica DMI6000B microscope.

Synthesis of TKDA

TKDA was synthesized from mercaptoacetic acid by an adaptation and modification of a literature procedure.[49] Mercaptoacetic acid (2.00 mL, 28.7 mmol) was dissolved in acetone (4.25 mL, 57.3 mmol) under a nitrogen atmosphere. After cooling in an ice bath, 4 mL of concentrated HCl was added dropwise to the solution, and the reaction mixture was left to stir overnight as the solution came to room temperature. Upon completion, the flask was cooled once more in an ice bath and the precipitate was filtered. The product was washed sequentially with cold water and cold hexanes three times, and then dried *in vacuo*.

^{1}H NMR (400 MHz, D_2O): δ_H (ppm) 1.54 (6H, s, CH_3), 3.44 (4H, s, CH_2). MS: ESI *m*/*z*: (M − H) calculated for $C_7H_{11}O_4S_2$ 223.28 g mol^{-1}, found 223.01 g mol^{-1}.

Dissolution of chitosan using TKDA (DCS)

25 mg of CS and 20 mg of TKDA were added to a round bottom flask containing 1 mL of deuterated water (D_2O). Dissolution of the mixture was noted visually within 10 minutes. A small aliquot of the clear solution was taken for NMR measurements.

Synthesis of FCS

25 mg of CS was added to 1 mL of deionized (DI) water and stirred at room temperature under nitrogen. 20 mg of TKDA, 3.5 mg EDC·HCl, 2 mg NHS and 100 μL of DMF were added sequentially into CS solution. The pH of the solution was measured to be at 4.2. After 24 h stirring at room temperature, acetone with a volumetric ratio of 3 : 1 was added, and the reaction mixture was vacuum filtered. The product was washed 5–6 times with acetone and ether to remove catalysts and unreacted TKDA. The crude FCS was then dialyzed in a 6.5 kDa MWCO membrane against water for 48 h to remove any residual DMF, TKDA, or catalysts. Following the dialysis, the solution was concentrated *in vacuo* and again precipitated in acetone in a 3 : 1 volumetric ratio. The pure product was collected by vacuum filtration and dried *in vacuo*.

Preparation of FCS/HA and CS/HA NPs

NPs were prepared *via* an ionic gelation method.[50] An aqueous 0.25 mg mL^{-1} solution of FCS or CS was prepared (pH was adjusted to 5.5 with TKDA). Upon dissolution, the FCS or CS solution was filtered through a 0.45 μm syringe filter. Separately, an aqueous 0.5 mg mL^{-1} HA solution was prepared and filtered through a 0.22 μm syringe filter. 80 μL of HA solution was added dropwise into 2 mL of FCS or CS solution with a 4% v/v concentration while stirring vigorously for 30 s, until the solution became opaque. The resulting NPs were filtered through a 0.45 μm syringe filter.

Preparation of drug loaded FCS/HA and CS/HA NPs

The procedure for preparing drug loaded NPs was similar to the one used for empty NPs, as described above.[51] 0.25 mg mL^{-1} concentrations of quercetin and curcumin were prepared in 1 mL methanol and acetone, respectively. Equal volumes of FCS or CS and a drug solution were mixed together while stirring at room temperature for 15 min. 80 μL of HA solution (4% v/v of FCS/CS-drug solution) was added dropwise to 2 mL of each mixture while stirring at room temperature for 30 s. The NPs suspensions were then separately filtered using 0.45 μm syringe filters. Finally, the NPs suspensions were ultra-centrifuged using 3 kDa Amicon® Ultra-4 centrifugal tubes at 4500 rpm and 25 °C for 30 min, to separate the free drug for encapsulation efficiency (EE%) and loading capacity (LC%) calculations.

Preparation of FITC-labeled NGF

0.5 mg of NGF was first dissolved in 1 mL of sodium bicarbonate buffer (0.1 M, pH = 8.5). FITC solution was prepared in DMSO with a concentration of 10 mg mL^{-1}, sonicated, and subsequently added into the NGF solution to a concentration of 0.63% v/v. The mixture was then sonicated at room temperature for 90 min in the dark. FITC labeled-NGF was purified from the free dye by three consecutive centrifugations using 3 kDa Amicon® Ultra-4 centrifugal filters and rinsed with fresh sodium bicarbonate buffer. Finally, UV-vis spectra were taken of the supernatant to determine the amount of unlabeled NGF.[52]

Preparation of NGF and NGF-FITC loaded FCS/HA NPs

NGF and NGF-FITC were mixed separately with HA solutions (0.052% w/v NGF/HA). Then, the NGF/HA and NGF-FITC/HA mixtures were added dropwise to FCS solutions (4% v/v) and stirred for 30 seconds. The resulting NP suspensions were filtered through 0.45 μm syringe filters and ultra-centrifuged with 30 kDa microtubes at 14 500 rpm and 25 °C for 20 min to separate free NGF.

Preparation of FITC-labeled FCS

1% w/v of FCS was dispersed in DI water and filtered through a 0.45 μm syringe filter. A 1 mg mL^{-1} FITC solution in DMSO was added to the FCS solution to give a concentration of 1% v/v and the mixture was sonicated at room temperature for 3 hours in the dark. FITC-labeled FCS was obtained by first precipitating it with 0.2 M NaOH and then centrifuging it. It was purified from free dye through repeated washings with (70 : 30 v/v) DMSO/DI water. Finally, DMSO was removed from the FITC-labeled FCS with three consecutive centrifugations using 3 kDa Amicon® Ultra-4 Centrifugal Filters.[51]

Preparation of FITC-labeled FCS/HA NPs

NPs were prepared using an ionic gelation method.[35,50] FITC-labeled FCS solution was diluted in DI water to a concentration of 0.25 mg mL^{-1} while stirring at room temperature. 80 μL of syringe filtered HA solution (0.5 mg mL^{-1}) was then added dropwise into the FITC-labeled FCS solution (to a concentration

of 4% v/v) while vigorously stirring for 30 s until the solution became opaque. NPs were then filtered through a 0.45 μm syringe filter.

Determination of EE% and LC%

Unencapsulated drug amounts were determined by measuring the UV-Vis absorbances of supernatants from centrifuged NP suspensions. The absorbance peaks for free quercetin, curcumin and NGF-FITC, were recorded at $\lambda_{abs.}$ = 255, 437, and 494 nm respectively. To calculate NP cargo loading, an aliquot of the centrifuged NP suspension supernatant was separated, freeze dried for 24 h, its weight was measured, and then it was multiplied by the total volume of the NP suspension.[52] A very small amount of drug precipitated upon adding the drug solution into FCS/CS solution. This precipitate was removed by filtering the nanoparticles through syringe filters. The filtered nanoparticle suspensions were subsequently centrifuged using ultracentrifugation tubes at 4500 rpm. The loading capacity (LC%) and encapsulation efficiencies (EE%) were calculated using UV-Vis absorption spectra of nanoparticle suspensions after syringe filtration, and the supernatant after centrifugation. After removing the supernatant from centrifugation, tubes were rinsed, and the UV-Vis quantification considered these volumes for calculations. The equations for EE% and LC% determinations are given below:

$$\mathrm{EE}\% = \frac{W_\mathrm{i} - W_\mathrm{f}}{W_\mathrm{i}} \times 100 \quad (1)$$

$$\mathrm{LC}\% = \frac{W_\mathrm{i} - W_\mathrm{f}}{W_\mathrm{d}} \times 100 \quad (2)$$

In eqn (1) and (2), W_i, W_f and W_d represent initial drug weight in NPs suspensions, free cargo weight and the weight of dried NPs, respectively.

TEM sample preparation

Carbon coated grids were initially treated in a glow-discharge apparatus at −25 mA for 30 s. A drop (5 μL) of a NP sample was deposited on the grid and left for 1 minute. Excess liquid was absorbed using Whatman filter paper. Then, a drop of uranyl acetate (2%, 5 μL) as a negative stain was deposited and left for 1 minute followed by a similar filter paper treatment. The grids were then left to dry overnight in a Petri dish at room temperature before imaging.[52]

ROS-responsive drug release

Drug release studies from CS/HA and FCS/HA NPs were performed by dialyzing desired volumes of NP suspensions in cellulose dialysis tubes (MWCO = 6–8 kDa), against phosphate buffer saline (PBS) solution (pH = 7.25 adjusted by 1 M citric acid) to prevent cargo degradation. 1% v/v Tween 80 was added to PBS for curcumin release studies. 12.2 μL of 100 μM H_2O_2 was added to 1 mL of each FCS/HA solution, then dialyzed against the PBS solution while stirring at 37 °C. Every 3 h, 3 mL of each PBS solution was taken and replaced with fresh PBS solution to simulate sink conditions inside the body. The released drug was measured *via* UV-visible spectrophotometry at $\lambda_{abs.}$ = 255, 437, and 494 nm for quercetin, curcumin, and NGF-FITC, respectively. For comparison, the hydrophobic drugs (curcumin and quercetin) were dissolved in polyethylene glycol (PEG) 350/DI water/dimethyl acetamide with the ratio of 45 : 40 : 15 v/v/v, and their drug release profiles were measured.[52]

pH-Responsive drug release

Quercetin loaded FCS/HA NPs were dialyzed against PBS solutions as per the ROS-responsive drug release section, except the pH was adjusted to 4.17, 6.14 or 7.25 with 1 M citric acid before dialysis. Every 3 h, 3 mL of each PBS solution was taken and replaced by fresh PBS solutions to simulate sink conditions inside the body. Released quercetin was quantified *via* UV absorption spectrometry at $\lambda_{abs.}$ = 255 nm.

U251 cell culturing

U251 cells were cultured in culturing medium composed of Dulbecco's Modified Eagle's Medium (DMEM) supplemented with 10% fetal bovine serum and 1% 10 000 U mL^{-1} penicillin–streptomycin. Cells were incubated at 37 °C and 5% CO_2.

U251N cell viability

Cells were seeded at 10 000 or 4000 cells per well into 96-well plates (Costar) for 24 or 72 h experiments, respectively. Cells were treated with drugs and or NPs in culturing medium 24 h after seeding. After treatment, cells were fixed in 4% paraformaldehyde for 10 min at room temperature and stained with 10 μM Hoechst 33342. Cells were imaged using fluorescence microscopy and the number of nuclei was analyzed using CellProfiler.[53]

TFEB nuclear translocation in GBM cells

U251 were seeded onto poly-D-lysine coated coverslips at 15 000 cells per coverslip and grown overnight. Cells were treated with drugs and/or NPs in serum free growth media (DMEM + 1% penicillin–streptomycin). Cells were fixed with 4% paraformaldehyde, permeabilized with 0.1% Triton ×-100. Then, blocked with 10% goat serum, incubated in rabbit anti-TFEB (1:1000) for 1 h at room temperature, and labelled with secondary antibody Alexa Fluor 488 goat anti-rabbit (1:500). Cells were labelled with 10 μM Hoechst 33342 and mounted onto microscope slides using Aqua-Poly/mount. Images were taken using a fluorescence microscope and analyzed in ImageJ. The ratio of the mean fluorescence value between the nuclear *vs.* cytosolic TFEB was quantified.

DRG isolation

Thoracic and lumbar DRG were removed from adult (1–2 months) C57BL/6 mice. Isolated DRGs were placed in ice-cold RPMI-1640.

Explant cultures

L1–L5 DRGs were embedded in Matrigel (BD Biosciences) attached to a glass coverslip placed in the well of a 24-well plate and incubated in media (RPMI-1640 + 1% penicillin–streptomycin)

after the Matrigel has solidified. After 24 h, the culture was treated with drugs and/or NPs for 10 days, with half of the media replaced every 3 days. After treatment, 500 μg mL^{-1} MTT was added for 4 h incubation at 37 °C and bright-field images were taken using a 10× objective on an inverted microscope.

Dissociated DRG

Thoracic and lumbar DRGs were incubated in 0.1% type-II collagenase at 37 °C for 30 min followed by incubation in 0.25% trypsin at 37 °C for 30 min. The ganglion was then mechanically triturated using a fire-polished pipette. Dissociated cells were grown on laminin-coated 96-well plates in growth medium (Ham's F12 + nitrogen gas supplement + 1% penicillin–streptomycin). Cells were treated with drugs and/or NPs for 10 days. After treatment, cells were fixed with 4% paraformaldehyde for 20 min at room temperature and labelled with β-tubulin III (1:1000) overnight at 4 °C and stained with AlexaFluor 488 goat-anti mouse (1:500). Images were taken with a fluorescence microscope and neurite length was measured using ImageJ.

FITC-NPs imaging and lysosome labelling

U251 were seeded onto poly-D-lysine coated coverslips at 15 000 cells per coverslip and grown overnight. Cells were treated with FITC-labelled FCS-NP (0.025 mg mL^{-1} FCS, 0.05 mg mL^{-1} HA) for 24 h in serum-free media. After treatment, cells were incubated in 500 nM Lysotracker Red DND-99 for 5 min in the cell incubator. Cells were fixed with 4% PFA, labelled with 10 μM Hoechst 33342 for 10 min at room temperature and mounted onto microscope slides. Images were taken using a fluorescence microscope and analyzed in ImageJ.

Results and discussion

Dispersion and functionalization of chitosan with TKDA

TKDA was prepared from mercaptoacetic acid, and we first examined its ability to solubilize chitosan in an aqueous medium. As mentioned earlier, solubility of chitosan in water is pH dependent, and its dispersion in an aqueous medium is generally achieved by adjusting the pH to 5–6 with HCl, acetic acid, or other common acids.[54–58] Addition of TKDA to an aqueous solution of chitosan easily facilitated its dissolution, and a clear solution was obtained. We also monitored this process using ^{1}H NMR and saw that the CH_2 protons next to the COOH group in TKDA shifted upfield from 3.44 to 3.35 ppm (Fig. 1). This suggests that TKDA addition interferes with the interactions between NH_2 groups of chitosan, possibly through hydrogen bonding. These results infer that the ROS-responsive chitosan can be prepared in one-pot by invoking the dual role of TKDA dispersion and functionalization. The TKDA solubilized chitosan was then employed for the amidation reaction using NHS/EDC·HCl catalysts, and it led to a further upfield shift of TKDA CH_2 protons to 3.27 ppm (Fig. 1). This trend of incremental upfield shifts upon CS/TKDA dissolution and

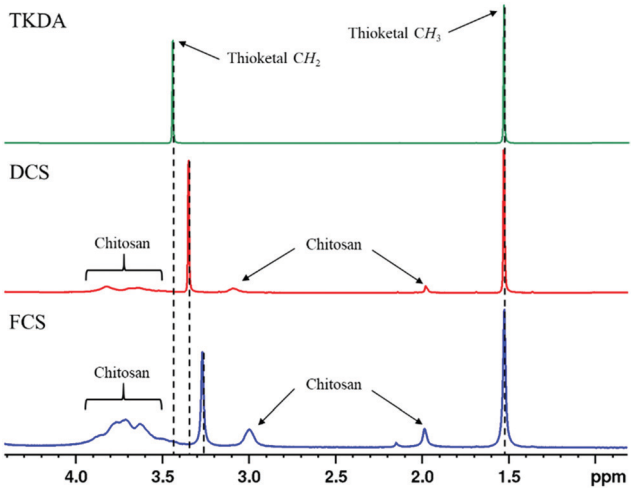

Fig. 1 ^{1}H NMR-observed shifts in D_2O of thioketal CH_2 protons upon chitosan dissolution (DCS), and functionalization (FCS).

functionalization was also confirmed for the *C*OOH and *C*H_2 peaks *via* $^{13}C\{^1H\}$ NMR (Fig. S1, ESI†).[27,59,60]

The chitosan functionalization efficiency was estimated using ^{1}H NMR. In TKDA-assisted DCS, the CH_3 and CH_2 protons of the TKDA appear at 1.53 and 3.35 ppm, respectively. Upon amidation, the CH_2 protons shift further upfield to 3.27, and the corresponding CH_3 protons remain nearly unchanged at 1.52 ppm. To estimate functionalization efficiency, the thioketal CH_3 peak integrations were directly compared to that of the chitosan peak at 2.0 ppm (Fig. 1) between DCS and FCS. These peaks were chosen for their clarity and absence of overlapping peaks in the NMR spectra. Using (i) the same amounts of TKDA to dissolve and covalently link chitosan with ROS-responsive entities; and (ii) chitosan being used as a constant between the samples, functionalization can be consistently measured as the relative amount of TKDA before (DCS) and after (FCS) amidation. Following this method and using eqn (3), the functionalization efficiency was estimated to be 40%.

$$\text{Functionalization } \% = \frac{\text{FCS Int. (1.5 ppm)}/\text{FCS Int. (2.0 ppm)}}{\text{DCS Int. (1.5 ppm)}/\text{DCS Int. (2.0 ppm)}} \quad (3)$$

FCS/HA-based NPs

FCS was subsequently used for the preparation of empty and therapeutic loaded NPs *via* the commonly employed ionic gelation method with HA.[50,54–56] Quercetin and curcumin were chosen as model hydrophobic drugs due to their broad anti-cancer properties but low bioavailability.[39,42,43] In order to establish the versatility of our NPs, we additionally considered encapsulation of a large macromolecule, a NGF, which has been shown to promote neuronal regeneration. Its utility is limited due to its susceptibility to enzymatic and hydrolytic degradation in a biological medium.[44,45,48,61] FCS based NPs showed excellent loading of both quercetin and curcumin with

Table 1 Physical characteristics of FCS/HA and CS/HA NPs

NPs	D_H (nm)	PDI	ζ (mV)	EE (%)	LC (%)
CS/HA	85.8	0.207	+6.3	—	—
FCS/HA	38.6	0.160	−3.8	—	—
Quercetin/CS/HA	500.7	0.302	−5.2	82.3	43.3
Quercetin/FCS/HA	237.6	0.262	−6.6	95.6	46.8
Curcumin/FCS/HA	133.2	0.235	−7.6	95.3	47.6
NGF-FITC/FCS/HA	120.2	0.222	−6.4	72.3	19.9

Notes: pH of each NP solution was 5.6, and the cargo solution concentration was 250 (quercetin/CS/HA; quercetin/FCS/HA; curcumin/FCS/HA), and 500 mg mL^{-1} (NGF-FITC/FCS/HA).

EE% (Table 1) comparable, and in some cases higher than those reported earlier.[62–69] The LC% of CS/HA based NPs prepared *via* the same ionic gelation method was lower for the model drug quercetin (~82%, Table 1). Encapsulation of drug molecules into nanocarriers relies heavily on how efficiently these are dispersed in the nanoparticle internal space, as well as the interactions of the drug molecules with its interior. The latter may be enhanced by loading near the isoelectric point of the cargo, core stabilization, hydrophobic effects, the presence of groups such as COOH, OH *etc.* In carriers prepared by ionic gelation method, charged interactions between chitosan and hyaluronic acid, lead to the formation of nanoparticles, into which therapeutic agents are entrapped.[70,71] We believe that the high EE% and LC% in the FCS/HA NPs reported here, as well as seen in other CS/HA systems,[72,73] are due to a combination of these factors. The covalent functionalization of chitosan with 2,2′-(propane-2,2′-diylbis(sufanediyl)diacetic acid), introduces dimethylthioketal centers, which enhance hydrophobicity of its interior upon nanoparticle formation.[31,74–79] It also introduces free thioketal terminal COOH groups which can participate in interactions including hydrogen bonding. These factors collectively contribute in enhancing loading of hydrophobic drugs into the FCS architecture. The reasons for higher loading in FCS-based NPs may include increased hydrophobicity of the internal collapsed and defined FCS structure. High EE% and LC% of drug loaded FCS/HA NPs is due to the hydrophobicity of thioketal moieties in FCS structure. Thioketal moieties could interact with hydrophobic drugs in the NPs core. Despite the much greater molecular weight of NGF-FITC, its loading into the functionalized NPs still resulted in good EE% of ~72%, possibly due to better interaction of the neuropeptide with the TKDA functionalized internal architecture of the NPs.[80–82]

Dynamic light scattering (DLS), zeta potential and TEM analyses of NPs

FCS/HA NPs with and without pharmaceutical cargo were analysed for their mean hydrodynamic diameters (D_H) and polydispersities by DLS (Table 1 and Fig. S2, ESI†). Owing to their functionalization with TKDA, the empty FCS-based NPs showed a much more compact D_H of 39 nm, as opposed to the less dense CS NPs (D_H of 86 nm).[83–85] Notably, this large difference in size translated well when both systems were loaded with quercetin. For example, while quercetin-loaded FCS/HA NPs had D_H of 238 nm, the size of CS NPs was 501 nm (a more than twofold difference). Considering the size of the porous vasculature around diseased tissue, NPs of sizes ~200 nm are generally accepted to have good permeability and unperturbed function.[86] An investigation of zeta potentials revealed that FCS/HA NPs had mostly negative surface charges (Table 1), and this suggests that interactions between NP core and hydrophobic cargo contribute towards reducing the exposure of the positively charged amine groups of polymer chains on the surface of NPs.[87]

FCS/HA NPs showed spherical morphologies in TEM images (Fig. 2) with compact architectures, as is expected of chitosan/HA structures.[50,83,88] Quercetin, curcumin, and NGF-FITC loaded FCS/HA NPs had mean diameters of 236, 82, and 91 nm respectively, and are in line with or slightly smaller than diameters found by DLS. Smaller size may more likely be due to the dehydration of samples during TEM analyses (Fig. 3). In general, narrow size distributions were observed for all the NPs, except for quercetin-loaded FCS/HA which showed two distinct size populations (Fig. 3C). Notably, the smaller population roughly corresponded to that of empty FCS/HA NPs (Fig. 3D) which suggests that not all NPs get loaded with the drug. On the other hand, complete loading of curcumin and NGF-FITC were confirmed *via* their size distributions and TEM (noted by darker regions inside NPs) (Fig. 2A and B).[89–91] Interestingly, while NGF-FITC loaded NPs had spherical morphology, these also had a porous character (Fig. S3, ESI†).[92]

Stimulus response studies

TKDA employed in this study gets oxidatively cleaved into mercaptoacetic acid and acetone upon exposure to ROS (Scheme 2). We first established a time dependent response

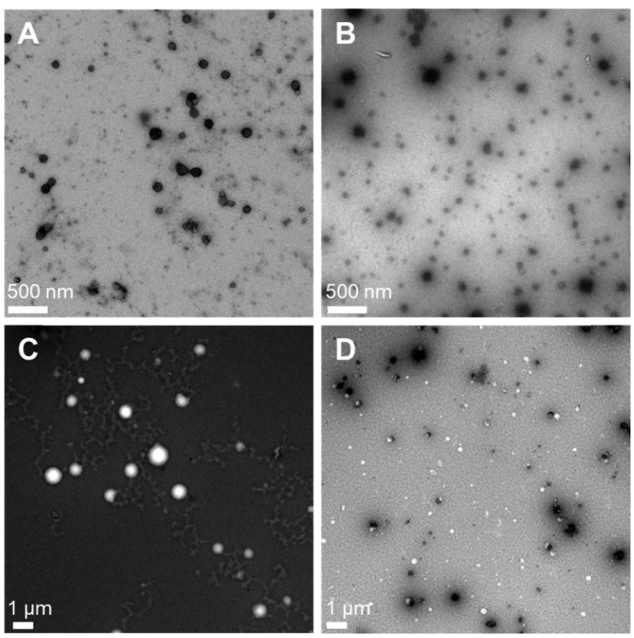

Fig. 2 TEM micrographs of (A) curcumin-, (B) NGF-FITC-, (C) quercetin-loaded FCS/HA NPs, and (D) empty FCS/HA NPs.

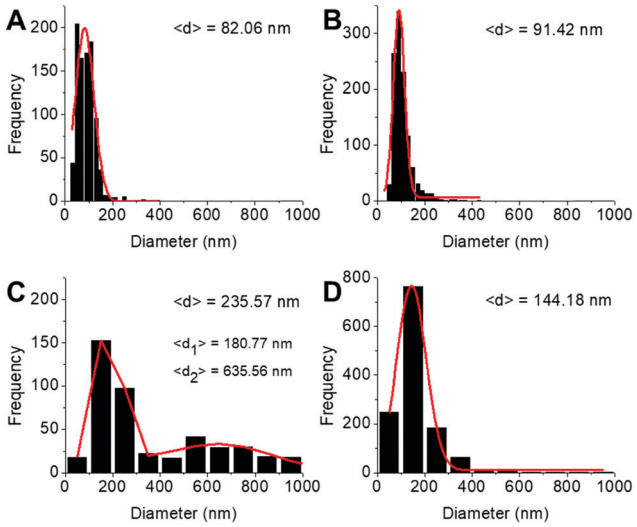

Fig. 3 Size histograms of (A) curcumin-, (B) NGF-FITC-, (C) quercetin-loaded FCS/HA NPs, and (D) empty FCS/HA NPs. Histograms were prepared by measuring around 1000 particles from 6–9 fields of view using ImageJ and Origin 8.

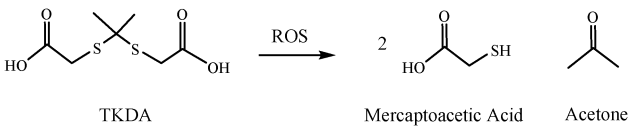

Scheme 2 Oxidative cleavage of TKDA to mercaptoacetic acid and acetone using ROS.

of TKDA to oxidative stress using ^{1}H NMR. To 500 μL of a 20 mg mL^{-1} solution of TKDA in D_2O, 12.2 μL of 200 mM H_2O_2 were added, and its ^{1}H NMR spectrum was recorded at 0 h. The solution was then sonicated at 37 °C and spectra were taken at definite time intervals up to 48 h (Fig. 4A). The thioketal CH_3 peak at 1.54 ppm slowly decreased as the molecule was degraded by ROS, and a characteristic peak for acetone begun to appear at 2.13 ppm. Simultaneously, the thioketal CH_2 peak at 3.44 shifted to 3.55 as free thiol ends were generated.

To ascertain that the ROS-responsive TKDA linker in our FCS/HA NPs retains its oxidative stress response, the functionalized NPs were similarly incubated with H_2O_2 in D_2O, and their response was measured over time *via* ^{1}H NMR (Fig. 4B). A trend akin to what we had observed for TKDA alone above, was seen for the NPs: (i) the cleavage of the thioketal group is accompanied with a decrease in the linker's CH_3 and CH_2 proton peaks at 1.52 and 3.27 ppm respectively, and (ii) an increase of the acetone peak at 2.13 ppm. As expected, TKDA-associated peaks changed more slowly in the case of NPs due to the limited diffusion of H_2O_2 within the FCS/HA NPs.

We subsequently examined the ROS-induced degradation behaviour of FCS/HA NPs by DLS. The NPs were treated with 12.2 μL of 200 mM H_2O_2 and monitored over a 48 hour period while being sonicated at 37 °C (Fig. 5A). Interestingly, two distinct populations emerged as a result of ROS exposure. The cleavage of thioketal linkers in the NPs caused the system to dissociate resulting in the smaller population,[93] which then led to an aggregation of the degraded NP components.

Since CS based NPs are known to swell in low pH environments, we investigated the pH-responsiveness of our FCS/HA (Fig. 5B). As expected, the size distributions of NPs slowly increased up to 800 nm, as the pH was reduced from 6 to 4 to 3 using 1 M citric acid. These conditions mimic the endosome environments at earlier stages, and suggest swelling of FCS/HA NPs upon decreasing pH (due to protonation of amine groups).[94,95]

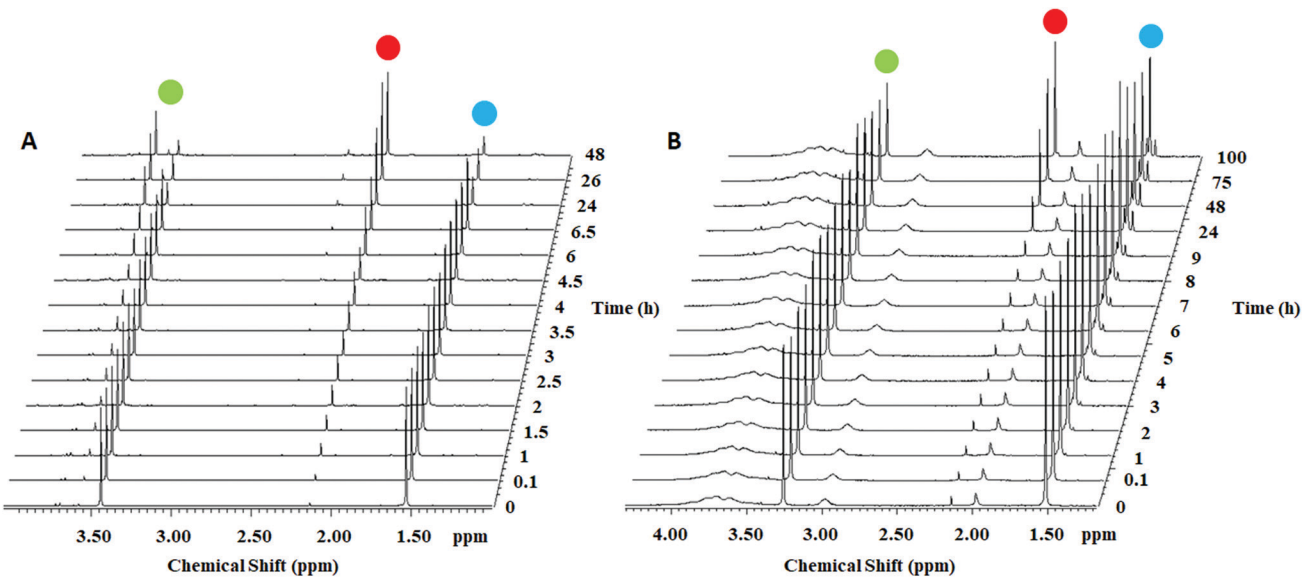

Fig. 4 Time dependent ^{1}H NMR spectra of (A) TKDA and (B) FCS/HA NPs in D_2O, upon incubation with 200 mM H_2O_2, representing ROS-responsive cleavage of thioketal groups (Scheme 2) over time. Green: CH_3, red: acetone and blue: CH_2 peaks.

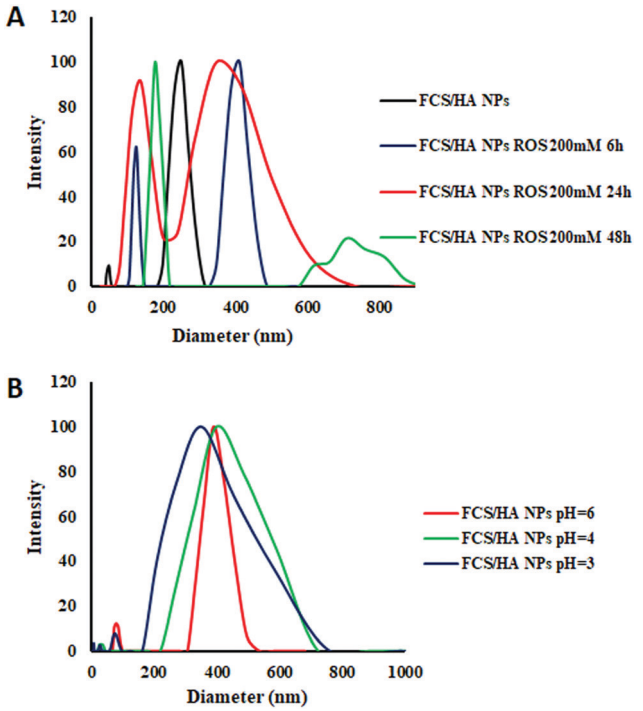

Fig. 5 (A) ROS and (B) pH-responsive behaviour of empty FCS/HA NPs analysed by DLS.

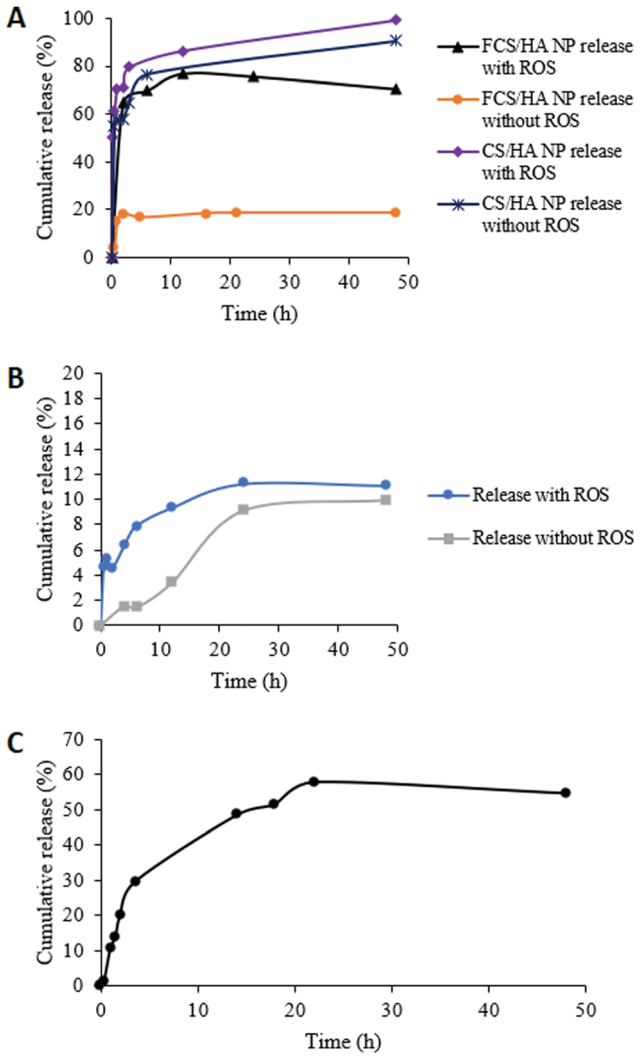

Fig. 6 ROS-responsive release profiles of (A) quercetin from FCS/HA and CS/HA NPs with or without 100 μM of H_2O_2, (B) curcumin from FCS/HA NPs with or without 100 μM of H_2O_2, and (C) NGF-FITC from FCS/HA NPs.

Drug release studies

ROS-response behavior. We subsequently studied the stimulus response of the FCS/HA NPs, and how the ROS-rich environment will influence drug release in these systems. Drug loaded FCS/HA NPs were dialyzed against PBS buffer with a 200 mM concentration of H_2O_2 over 48 hours, and aliquots were taken from the buffer medium to measure the amount of released cargo *via* UV-visible spectroscopy. Quercetin loaded NPs generally saw a burst release within the first 3 hours of dialysis. However, there was a clear and large difference between the final cumulative release of FCS/HA NPs between ROS-exposed and untreated samples (Fig. 6A). Upon exposure to ROS, NPs showed a cumulative release of 70%, which is more than 50% higher than NPs without any treatment with H_2O_2. For comparison, we also evaluated the efficiency of quercetin release from CS/HA NPs with or without exposure to ROS. The unfunctionalized NPs facilitated higher free diffusion of quercetin into the medium, resulting in a slightly faster burst release and significantly higher cumulative release of 90% after 48 hours. This clearly shows that CS functionalization is key in preventing premature drug release, and in limiting side-effects through exposure to non-disease sites. Interestingly, ROS-treated CS/HA NPs showed a slightly higher cumulative release, with nearly 100% of the drug released after 48. This may be due to HA which can act as a weak ROS scavenger.[93]

The curcumin loaded FCS/HA system showed a significantly slower and more sustained release (Fig. 6B). Likely due its higher hydrophobicity,[96–98] curcumin had a cumulative release of about 11% over 48 hours in a H_2O_2-containing medium. This was only marginally higher than the 10% release without ROS treatment.

FCS/HA NPs showed good sustained release (to a maximum of 55%) of NGF-FITC over 48 hours without any stimulus (Fig. 6C). The sustained release, complemented by the absence of a noticeable burst release, indicated the ability of the NPs to protect NGF-FITC from the biological environment until delivery at the targeted disease site. Due to the instability of NGF-FITC to oxidative stress, a stimulus-responsive release study was not conducted.[99,100]

pH-Responsive release. We subsequently examined drug release from FCS/HA NPs at pH 7.25, 6.14 and 4.17, which more closely resemble physiological and endosomal environments (Fig. 7).[95] We had earlier confirmed pH induced swelling of FCS/HA NPs at low pH by DLS (Fig. 5B). In agreement with these results, quercetin release was significantly enhanced from 19% at pH 7.25 to 90% at pH 6.14. Further reduction of pH to 4.17 resulted in no significant improvement in drug

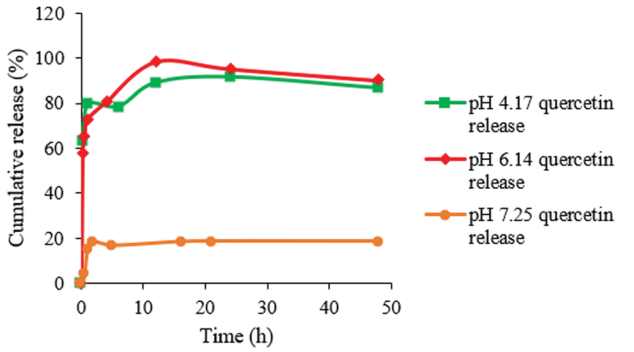

Fig. 7 pH-Responsive release profile of quercetin loaded FCS/HA NPs.

release from that observed at 6.14, and a mostly consistent release profile was maintained. The stability of NGF in aqueous solution at varied pH has been well studied, and it is known to decrease with reduction in pH, leading to degradation.[101,102] To avoid complications in obtaining reliable data, the pH-responsive drug release from NGF-loaded nanoparticles was not investigated.

In vitro biological evaluation

GBM cell cultures and viability. Curcumin and quercetin are natural compounds with chemotherapeutic activity.[43,103] However, their use *in vivo* is limited by their instability and insolubility.[104,105] We used FCS/HA NPs as nanocarriers for the delivery of curcumin and quercetin and tested their anti-cancer activity in an *in vitro* model of GBM multiform (Fig. 8). Free curcumin and curcumin-loaded FCS/HA NPs similarly reduced GBM viability, achieving near 100% cell death after 72 h at 20 μM curcumin, (Fig. 8A and B). Interestingly, quercetin loaded FCS/HA NPs showed 3-fold greater reduction in GBM viability after 72 h at 80 μM quercetin compared to free quercetin (Fig. 8C and D). The slower release of quercetin from FCS/HA NPs may protect the bulk of the quercetin from degradation in biological media while maintaining sufficient concentrations in the media to exert its anti-cancer activity. Given the low pH environment surrounding GBM tumors,[106,107] the pH-responsive FCS/HA NPs may be particularly suited for the targeted delivery of curcumin/quercetin to the tumor microenvironment. At the tumor site, the low solubility of the released curcumin/quercetin may limit its diffusion and subsequently concentrate around the cancerous tissue.

Nuclear translocation in GBM cells. TFEB, a master regulator of autophagy, is often upregulated in cancer cells,[108] and its activation leads to greater lysosomal biogenesis and activation of autophagy. Curcumin and quercetin are known inducers of TFEB activation and nuclear translocation.[109,110] We found comparable TFEB nuclear translocation in GBM treated with curcumin/quercetin FCS/HA NPs or free curcumin/quercetin (Fig. 9). Treatment with curcumin loaded FCS/HA NPs showed reduced TFEB nuclear translocation after 1 h compared to free curcumin (Fig. 9 and Fig. S10, ESI†), although TFEB nuclear

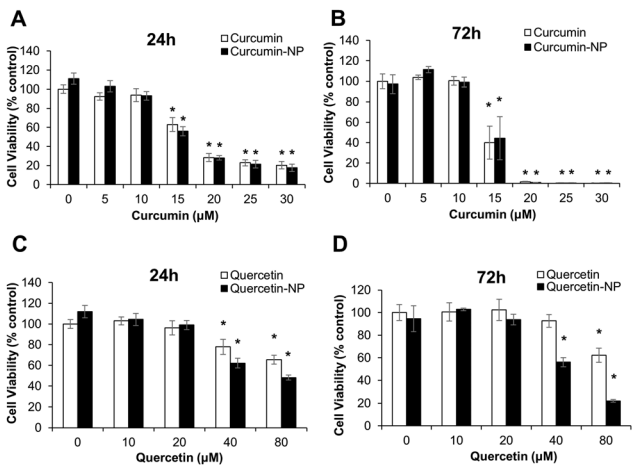

Fig. 8 Curcumin and quercetin loaded FCS/HA NPs kills GBM cells. (A and B) U251N cells were exposed to different concentrations of free-curcumin or curcumin incorporated in nanocarriers for 24 or 72 h. Control media (0 μM drugs) for all treatments with drug-loaded nanocarriers contained only the nanocarrier. (C and D) U251N cell were exposed to different concentrations of free-quercetin or quercetin loaded NPs for 24 h, or 72 h. Cell viability was assessed by counting the number of Hoechst 33342 labelled nuclei after the treatments. Average values were obtained from six measurements (n = 6) and error bars present SEM. * denotes significance at $p < 0.05$ compared to control (0 μM drug).

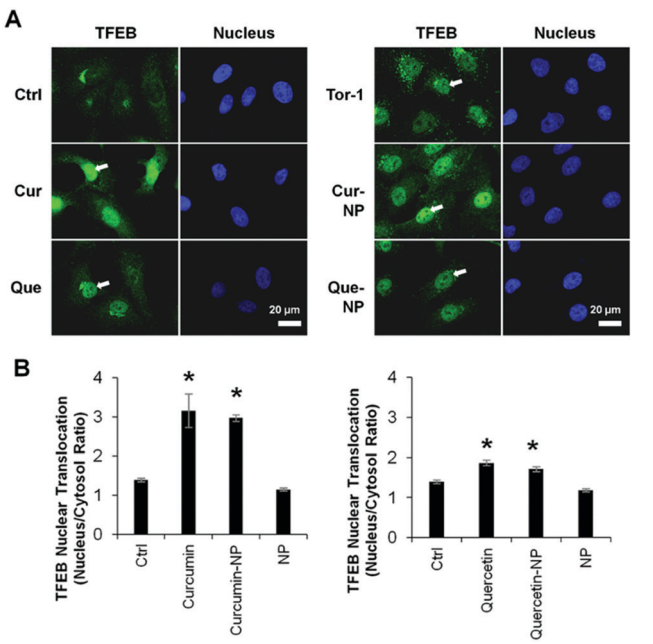

Fig. 9 Curcumin and quercetin loaded FCS/HA NPs increase TFEB nuclear translocation in GBM. U251 cells were switched to serum-free media for 8 h and exposed to 20 μM free curcumin (Cur)/curcumin loaded NPs (Cur-NP), or equivalent empty carrier for 8 h, 50 μM free quercetin (Que)/quercetin loaded NPs (Que-NP) or equivalent empty carrier for 2 h, or 1 μM torin-1 (Tor-1) for 2 h as a positive control for TFEB nuclear translocation. (A) Representative photomicrograph of TFEB and Hoechst 33342 labelled nuclei. (B) Quantification of TFEB nuclear translocation (ratio of average fluorescence of TFEB in the nucleus to cytosol). $N > 49$ cells per condition, error bars = SEM. * denotes significance at $p < 0.05$ compared to control. Arrows points to examples of TFEB nuclear translocation.

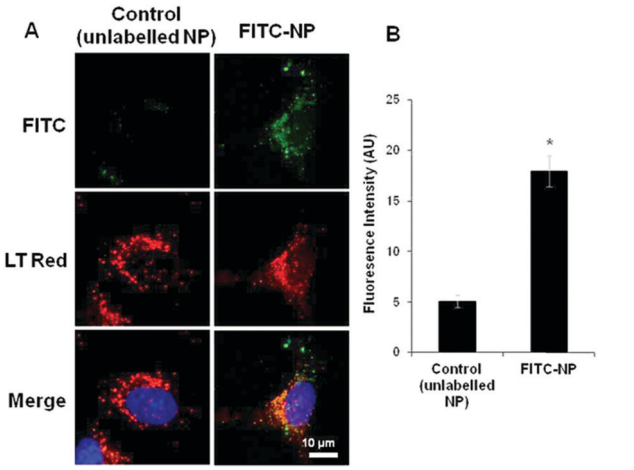

Fig. 10 FITC-labelled FCS/HA NPs co-localize with lysosomes in U251N cells. U251N cells were treated FITC-labelled NPs or equivalent unlabelled NPs for 24 h in serum-free media and stained for lysosomes using Lysotracker Red (LR). (A) Photomicrograph of FITC-NP (green), lysosomes (red), and cell nuclei (blue). (B) Quantification of average FITC fluorescence intensity per cell. $N > 35$ cells per condition, error bars = SEM. * denotes significance at $p < 0.05$ compared to control. FCS/HA NPs can enter the cell and subsequently deliver its cargo after swelling inside the acidic pH environment of the endolysosome and creating a leaky membrane, or through the cleavage of TKDA groups in the presence of ROS which detaches the cargo from the carrier. When the cargo is curcumin, it can exert its actions involving several mechanisms, *e.g.* by binding to the TFEB, enhancing lysosomal biogenesis and inducing cell death in GBM.

translocation became comparable after 8 h. While empty FCS/HA NPs did not induce TFEB nuclear translocation, FITC-labelled FCS/HA NPs uptaken by U251 cells can co-localize with lysosomes after 24 h (Fig. 10). Curcumin activation of TFEB has been associated with autophagic cell death in breast cancer cells.[111] However, inhibition of autophagy has been shown to sensitize cancer cells to the effects of curcumin.[112] Given the pluripotent effects of curcumin, the consequence of TFEB activation in cancer is still under debate.

DRG isolation and explant cultures

To highlight the versatility of FCS/HA NPs as a nanodelivery system, we tested whether FCS/HA NPs can deliver larger proteins as well as small hydrophobic drugs. Chitosan nanostructures have been intensively investigated as biocompatible scaffolds to reconnect peripheral nerves.[113] DRG are sensory nerve bundles that relay sensory input from the periphery (PNS) to the central nervous system (CNS) and are often used to study peripheral nerve regeneration.[114] We tested whether NGF loaded FCS/HA NPs can improve neuronal outgrowth of DRG neurons in 2D monolayers as well as 3D explant cultures (Fig. 11). NGF loaded FCS/HA NPs and free NGF both increased neuronal outgrowth in dissociated DRG cultures (Fig. 11A and B) as well as the density of neuronal extensions in the 3D explants (Fig. 11C). Importantly, unloaded FCS/HA NPs did not reduce neurite outgrowth in any of the models and may be a suitable nanocarriers for slow and sustained release of neurotrophic factors. Future applications could take advantage of the

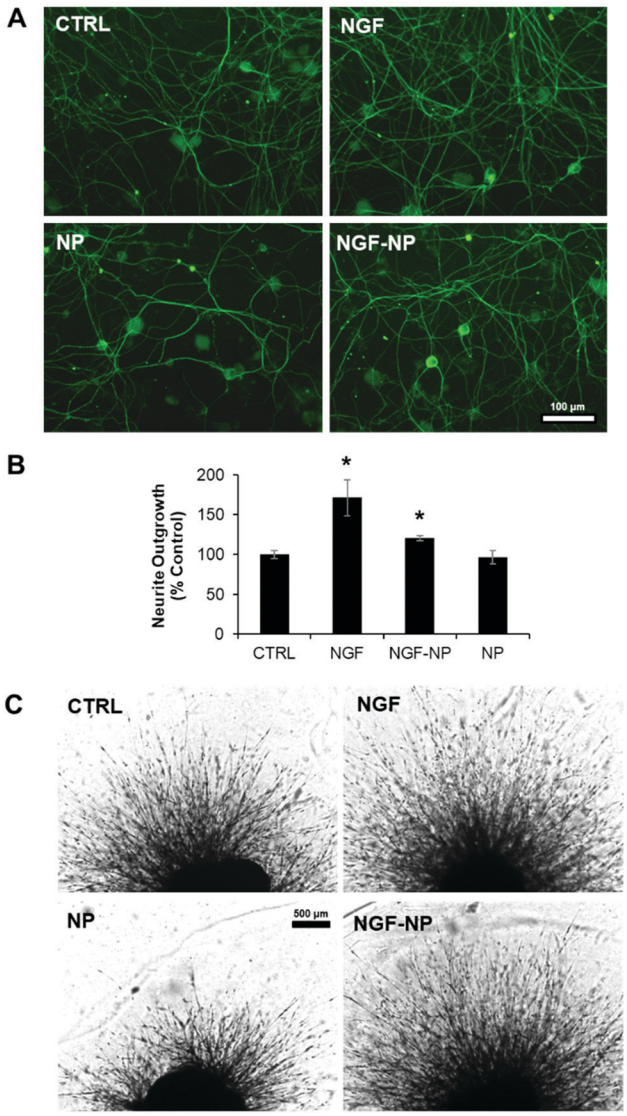

Fig. 11 Effect of NGF loaded FCS/HA NPs on DRG neurite outgrowth. Primary cultures were established from adult (1–2 months) mouse DRGs. Cultures were treated in serum free media containing PBS, 50 ng ml^{-1} free NGF, 50 ng ml^{-1} NGF loaded NPs (NGF-NP), or equivalent unloaded FCS/HA NPs (NP) for 10 days before imaging. (A and B) Immunocytochemistry of dissociated DRG cultures labelled for neuron specific marker BIII-tubulin and quantification of neurite outgrowth. (C) Photomicrograph of DRG explants. Neurite outgrowth in (B) was averaged from $n = 3$ and error bars represent = SEM. * denotes significance at $p < 0.05$ compared to control.

oxidative and pH-responsiveness of the FCS/HA NPs by providing targeted release of therapeutic agents at the site of injury which is enriched in ROS and acidic species due to the local activation of immune cells.[115]

Conclusions

We have developed a versatile one-pot methodology for the aqueous dispersion and functionalization of CS using a biocompatible ROS-responsive weak acid, TKDA. This two-fold role

of TKDA facilitates and simplifies functionalization of CS, and chitosan functionalized with TKDA displays dual stimuli responsive behavior (ROS and pH). This was explored by NMR, DLS and drug release studies in the presence of various concentrations of H_2O_2 and varied pH. FCS/HA NPs had good size distributions with a hydrophobic core and hydrophilic shell structure when assembled with curcumin and quercetin. However, a nanoprecipitate-like structure with what appeared to be pores was observed by TEM in empty FCS/HA NPs and upon loading NGF. Curcumin and quercetin loaded FCS/HA NPs killed GBM cells after 24 and 72 h, and increased TFEB nuclear translocation in GBM cells that is required for tumor cell death. NGF-loaded FCS/HA NPs increased neurite outgrowth compared to control in 3D explant DRG of mouse. FITC-NPs showed higher fluorescence intensity compared to unlabeled NPs. FITC-labeled FCS/HA NPs successfully co-localized with lysosomes in U251N cells which exhibited no toxicity for FITC-NPs over 24 h. This suggests that drug-loaded NPs can be retained inside endosomes for a long time (24 h) after cellular uptake for efficient drug release. Simplification of the design of dual stimuli-responsive FCS-based NPs provides an ideal platform in controlled delivery applications of a diverse range of bioactive agents (drugs, proteins, growth factors *etc.*) with high EE% and LC%. Eventually, these stimuli responsive nanocarriers should be tested in animal models of diseases *in vivo* to assess if they are superior to the unincorporated biologically active agents, and whether they could accelerate cargo release in a desired manner.

Conflicts of interest

There are no conflicts to declare.

Acknowledgements

We would like to thank the Natural Sciences and Engineering Research Council of Canada (NSERC) and the Quebec Centre for Advanced Materials/Centre Québécois sur les Matériaux Fonctionnels (QCAM/CQMF) for financial support.

References

1 D. S. Kelkar, G. Ravikumar, N. Mehendale, S. Singh, A. Joshi, A. K. Sharma, A. Mhetre, A. Rajendran, H. Chakrapani and S. S. Kamat, *Nat. Chem. Biol.*, 2019, **15**, 169–178.
2 E. Niedzielska, I. Smaga, M. Gawlik, A. Moniczewski, P. Stankowicz, J. Pera and M. Filip, *Mol. Neurobiol.*, 2016, **53**, 4094–4125.
3 X. Wu, H. Yang, W. Yang, X. Chen, J. Gao, X. Gong, H. Wang, Y. Duan, D. Wei and J. Chang, *J. Mater. Chem. B*, 2019, **7**, 4734–4750.
4 M. Shi, J. Zhang, Z. Huang, Y. Chen, S. Pan, H. Hu, M. Qiao, D. Chen and X. Zhao, *J. Mater. Chem. B*, 2020, **8**, 1616–1628.
5 P. Sabourian, M. Tavakolian, H. Yazdani, M. Frounchi, T. G. M. van de Ven, D. Maysinger and A. Kakkar, *J. Controlled Release*, 2020, **317**, 216–231.
6 Y. Yao, H. Zhang, Z. Wang, J. Ding, S. Wang, B. Huang, S. Ke and C. Gao, *J. Mater. Chem. B*, 2019, **7**, 5019–5037.
7 C. Chen, W. Yao, W. Sun, T. Guo, H. Lv, X. Wang, H. Ying, Y. Wang and P. Wang, *Int. J. Biol. Macromol.*, 2019, **122**, 1090–1099.
8 Y. Liu, F. Chen, K. Zhang, Q. Wang, Y. Chen and X. Luo, *J. Mater. Chem. B*, 2019, **7**, 3884–3893.
9 B. Yang, Y. Chen and J. Shi, *Chem. Rev.*, 2019, **119**, 4881–4985.
10 F. Vecchies, P. Sacco, E. Decleva, R. Menegazzi, D. Porrelli, I. Donati, G. Turco, S. Paoletti and E. Marsich, *Biomacromolecules*, 2018, **19**, 3936–3944.
11 J. Flynn, E. Durack, M. N. Collins and S. P. Hudson, *J. Mater. Chem. B*, 2020, **8**, 4029–4038.
12 H. Ye, Y. Zhou, X. Liu, Y. Chen, S. Duan, R. Zhu, Y. Liu and L. Yin, *Biomacromolecules*, 2019, **20**, 2441–2463.
13 S. A. Smith, L. I. Selby, A. P. R. Johnston and G. K. Such, *Bioconjugate Chem.*, 2019, **30**, 263–272.
14 D. Kim, K. Shin, S. G. Kwon and T. Hyeon, *Adv. Mater.*, 2018, **30**, 1802309.
15 H. Guo, S. Tan, J. Gao and L. Wang, *J. Mater. Chem. B*, 2020, **8**, 1759–1770.
16 N. Morin-Crini, E. Lichtfouse, G. Torri and G. Crini, *Environ. Chem. Lett.*, 2019, **17**, 1667–1692.
17 W. Wu, L. Luo, Y. Wang, Q. Wu, H.-B. Dai, J.-S. Li, C. Durkan, N. Wang and G.-X. Wang, *Theranostics*, 2018, **8**, 3038–3058.
18 H. Wang, J. Qian and F. Ding, *J. Mater. Chem. B*, 2017, **5**, 6986–7007.
19 A. Barra, Z. Alves, N. M. Ferreira, M. A. Martins, H. Oliveira, L. P. Ferreira, M. M. Cruz, M. d. D. Carvalho, S. M. Neumayer, B. J. Rodriguez, C. Nunes and P. Ferreira, *J. Mater. Chem. B*, 2020, **8**, 1256–1265.
20 W. M. Argüelles-Monal, J. Lizardi-Mendoza, D. Fernández-Quiroz, M. T. Recillas-Mota and M. Montiel-Herrera, *Polymers*, 2018, **10**, 342.
21 D.-K. Ho, S. Frisch, A. Biehl, E. Terriac, C. De Rossi, K. Schwarzkopf, F. Lautenschläger, B. Loretz, X. Murgia and C.-M. Lehr, *Biomacromolecules*, 2018, **19**, 3489–3501.
22 W.-F. Lai and H. C. Shum, *ACS Appl. Mater. Interfaces*, 2015, **7**, 10501–10510.
23 V. K. Thakur and M. K. Thakur, *ACS Sustainable Chem. Eng.*, 2014, **2**, 2637–2652.
24 Q. Xu, C. He, C. Xiao and X. Chen, *Macromol. Biosci.*, 2016, **16**, 635–646.
25 H.-L. Pu, W.-L. Chiang, B. Maiti, Z.-X. Liao, Y.-C. Ho, M. S. Shim, E.-Y. Chuang, Y. Xia and H.-W. Sung, *ACS Nano*, 2014, **8**, 1213–1221.
26 M. S. Shim and Y. Xia, *Angew. Chem., Int. Ed.*, 2013, **52**, 6926–6929.
27 Q. Li, Y. Wen, J. Wen, Y.-P. Zhang, X.-D. Xu, A. Victorious, R. Zavitz and X. Xu, *RSC Adv.*, 2016, **6**, 38984–38989.
28 S. K. Samal, M. Dash, S. Van Vlierberghe, D. L. Kaplan, E. Chiellini, C. van Blitterswijk, L. Moroni and P. Dubruel, *Chem. Soc. Rev.*, 2012, **41**, 7147–7194.

29 W. Zai, W. Chen, Z. Wu, X. Jin, J. Fan, X. Zhang, J. Luan, S. Tang, X. Mei, Q. Hao, H. Liu and D. Ju, *ACS Appl. Mater. Interfaces*, 2019, **11**, 4842–4857.
30 L. Cui, W. Liu, H. Liu, Q. Qin, S. Wu, S. He, X. Pang, C. Zhu and P. Shen, *ACS Appl. Bio Mater.*, 2019, **2**, 1907–1919.
31 F.-Q. Hu, L.-N. Liu, Y.-Z. Du and H. Yuan, *Biomaterials*, 2009, **30**, 6955–6963.
32 G. Huang and H. Huang, *J. Controlled Release*, 2018, **278**, 122–126.
33 M.-Y. Hsiao, A.-C. Lin, W.-H. Liao, T.-G. Wang, C.-H. Hsu, W.-S. Chen and F.-H. Lin, *Sci. Rep.*, 2019, **9**, 4784.
34 S. A. Young, H. Riahinezhad and B. G. Amsden, *J. Mater. Chem. B*, 2019, **7**, 5742–5761.
35 E. Lallana, J. M. Rios de la Rosa, A. Tirella, M. Pelliccia, A. Gennari, I. J. Stratford, S. Puri, M. Ashford and N. Tirelli, *Mol. Pharmaceutics*, 2017, **14**, 2422–2436.
36 A. Almalik, P. J. Day and N. Tirelli, *Macromol. Biosci.*, 2013, **13**, 1671–1680.
37 A. Almalik, H. Benabdelkamel, A. Masood, I. O. Alanazi, I. Alradwan, M. A. Majrashi, A. A. Alfadda, W. M. Alghamdi, H. Alrabiah, N. Tirelli and A. H. Alhasan, *Sci. Rep.*, 2017, **7**, 10542.
38 F. Raza, H. Zafar, X. You, A. Khan, J. Wu and L. Ge, *J. Mater. Chem. B*, 2019, **7**, 7639–7655.
39 N. S. Srivastava and R. A. K. Srivastava, *Phytomedicine*, 2019, **52**, 117–128.
40 S. Kundur, A. Prayag, P. Selvakumar, H. Nguyen, L. McKee, C. Cruz, A. Srinivasan, S. Shoyele and A. Lakshmikuttyamma, *J. Cell. Physiol.*, 2019, **234**, 11103–11118.
41 M. Wang, S. Jiang, L. Zhou, F. Yu, H. Ding, P. Li, M. Zhou and K. Wang, *Int. J. Biol. Sci.*, 2019, **15**, 1200–1214.
42 V. Ravichandiran, K. Masilamani, B. Senthilnathan, A. Maheshwaran, W. Tin Wui and R. Partha, *Curr. Drug Delivery*, 2017, **14**, 1053–1059.
43 J.-Y. Zhang, M.-T. Lin, M.-J. Zhou, T. Yi, Y.-N. Tang, S.-L. Tang, Z.-J. Yang, Z.-Z. Zhao and H.-B. Chen, *Molecules*, 2015, **20**, 11524–11534.
44 H. Kraskiewicz, B. Breen, T. Sargeant, S. McMahon and A. Pandit, *ACS Chem. Neurosci.*, 2013, **4**, 1297–1304.
45 C. Chu, J. Deng, L. Liu, Y. Cao, X. Wei, J. Li and Y. Man, *RSC Adv.*, 2016, **6**, 90856–90872.
46 S. Mondal, S. Ghosh and S. P. Moulik, *J. Photochem. Photobiol., B*, 2016, **158**, 212–218.
47 N. Zilony, M. Rosenberg, L. Holtzman, H. Schori, O. Shefi and E. Segal, *J. Controlled Release*, 2017, **257**, 51–59.
48 S. Razavi, R. Seyedebrahimi and M. Jahromi, *Biochem. Biophys. Res. Commun.*, 2019, **513**, 681–687.
49 C. Yue, C. Zhang, G. Alfranca, Y. Yang, X. Jiang, Y. Yang, F. Pan, J. M. de la Fuente and D. Cui, *Theranostics*, 2016, **6**, 456.
50 Y. Belabassi, J. Moreau, V. Gheran, C. Henoumont, A. Robert, M. Callewaert, G. Rigaux, C. Cadiou, L. Vander Elst, S. Laurent, R. N. Muller, A. Dinischiotu, S. N. Voicu and F. Chuburu, *Biomacromolecules*, 2017, **18**, 2756–2766.
51 W. Fan, W. Yan, Z. Xu and H. Ni, *Colloids Surf., B*, 2012, **95**, 258–265.
52 A. Moquin, J. Ji, K. Neibert, F. M. Winnik and D. Maysinger, *ACS Omega*, 2018, **3**, 13882–13893.
53 A. E. Carpenter, T. R. Jones, M. R. Lamprecht, C. Clarke, I. H. Kang, O. Friman, D. A. Guertin, J. H. Chang, R. A. Lindquist and J. Moffat, *Genome Biol.*, 2006, **7**, R100.
54 X. Liu, W. Xia, Q. Jiang, Y. Xu and P. Yu, *J. Agric. Food Chem.*, 2014, **62**, 297–303.
55 Y. Chen, V. Javvaji, I. C. MacIntire and S. R. Raghavan, *Langmuir*, 2013, **29**, 15302–15308.
56 Q. Chen, A. Xu, Z. Li, J. Wang and S. Zhang, *Green Chem.*, 2011, **13**, 3446–3452.
57 N. C. Minh, V. H. Nguyen, S. Schwarz, W. F. Stevens and T. S. Trung, *Int. J. Biol. Macromol.*, 2019, **121**, 718–726.
58 G. Romanazzi, F. M. Gabler, D. Margosan, B. E. Mackey and J. L. Smilanick, *Phytopathology*, 2009, **99**, 1028–1036.
59 X. Ling, S. Zhang, P. Shao, P. Wang, X. Ma and M. Bai, *Tetrahedron Lett.*, 2015, **56**, 5242–5244.
60 S. Bashir, Y. Y. Teo, S. Naeem, S. Ramesh and K. Ramesh, *PLoS One*, 2017, **12**, e0179250.
61 J.-M. Péan, M.-C. Venier-Julienne, F. Boury, P. Menei, B. Denizot and J.-P. Benoit, *J. Controlled Release*, 1998, **56**, 175–187.
62 J. Rashedi, A. Ghorbani Haghjo, M. Mesgari Abbasi, A. Dastranj Tabrizi, S. Yaqoubi, D. Sanajou, Z. Ashrafi Jigheh, A. Namvaran, A. Mohammadi, J. Mohammadi Khoshraj and B. Baradaran, *Adv. Pharm. Bull.*, 2019, **9**, 409–415.
63 M. P. Souza, A. F. M. Vaz, M. T. S. Correia, M. A. Cerqueira, A. A. Vicente and M. G. Carneiro-da-Cunha, *Food Bioprocess Technol.*, 2014, **7**, 1149–1159.
64 H.-K. Ha, J. W. Kim, M.-R. Lee and W.-J. Lee, *Food Res. Int.*, 2013, **52**, 82–90.
65 W. Nan, L. Ding, H. Chen, F. U. Khan, L. Yu, X. Sui and X. Shi, *Front. Pharmacol.*, 2018, **9**, 826.
66 R. Yang, Y. Zheng, Q. Wang and L. Zhao, *Nanoscale Res. Lett.*, 2018, **13**, 330.
67 L. Duse, E. Baghdan, S. R. Pinnapireddy, K. H. Engelhardt, J. Jedelská, J. Schaefer, P. Quendt and U. Bakowsky, *Phys. Status Solidi A*, 2018, **215**, 1700709.
68 K. Md. Asad, Z. Md, H. M. Syed, A. Irfan and A. R. Md. Moshahid, *Anti-Cancer Agents Med. Chem.*, 2018, **18**, 1131–1137.
69 R. Mirnejad, M. A. Mofazzal Jahromi, S. Al-Musawi, M. Pirestani, M. Fasihi Ramandi, K. Ahmadi, H. Rajayi, Z. Mohammad Hassan and M. Kamali, *Iran. J. Biotechnol.*, 2014, **12**, 1–8.
70 Q. Gan and T. Wang, *Colloids Surf., B*, 2007, **59**, 24–34.
71 Y. Xu and Y. Du, *Int. J. Pharm.*, 2003, **250**, 215–226.
72 L. Yang, S. Gao, S. Asghar, G. Liu, J. Song, X. Wang, Q. Ping, C. Zhang and Y. Xiao, *Int. J. Biol. Macromol.*, 2015, **72**, 1391–1401.
73 Y. Xu, S. Asghar, L. Yang, Z. Chen, H. Li, W. Shi, Y. Li, Q. Shi, Q. Ping and Y. Xiao, *Int. J. Biol. Macromol.*, 2017, **102**, 1083–1091.
74 Y. H. Kim, S. H. Gihm, C. R. Park, K. Y. Lee, T. W. Kim, I. C. Kwon, H. Chung and S. Y. Jeong, *Bioconjugate Chem.*, 2001, **12**, 932–938.

75 Y. J. Son, J.-S. Jang, Y. W. Cho, H. Chung, R.-W. Park, I. C. Kwon, I.-S. Kim, J. Y. Park, S. B. Seo, C. R. Park and S. Y. Jeong, *J. Controlled Release*, 2003, **91**, 135–145.
76 P. Opanasopit, T. Ngawhirunpat, A. Chaidedgumjorn, T. Rojanarata, A. Apirakaramwong, S. Phongying, C. Choochottiros and S. Chirachanchai, *Eur. J. Pharm. Biopharm.*, 2006, **64**, 269–276.
77 X. Xiangyang, L. Ling, Z. Jianping, L. Shiyue, Y. Jie, Y. Xiaojin and R. Jinsheng, *Colloids Surf., B*, 2007, **55**, 222–228.
78 Y.-S. Wang, L.-R. Liu, Q. Jiang and Q.-Q. Zhang, *Eur. Polym. J.*, 2007, **43**, 43–51.
79 M. Chen, Y. Liu, W. Yang, X. Li, L. Liu, Z. Zhou, Y. Wang, R. Li and Q. Zhang, *Carbohydr. Polym.*, 2011, **84**, 1244–1251.
80 A. M. Jonker, D. W. P. M. Löwik and J. C. M. van Hest, *Chem. Mater.*, 2012, **24**, 759–773.
81 F. Raza, H. Zafar, Y. Zhu, Y. Ren, A. Ullah, A. U. Khan, X. He, H. Han, M. Aquib, K. O. Boakye-Yiadom and L. Ge, *Pharmaceutics*, 2018, **10**, 16.
82 Y.-Z. Zhao, X. Jiang, J. Xiao, Q. Lin, W.-Z. Yu, F.-R. Tian, K.-L. Mao, W. Yang, H. L. Wong and C.-T. Lu, *Acta Biomater.*, 2016, **29**, 71–80.
83 S. Mavila, O. Eivgi, I. Berkovich and N. G. Lemcoff, *Chem. Rev.*, 2016, **116**, 878–961.
84 K. Kajiwara and W. Burchard, *Polymer*, 1981, **22**, 1621–1628.
85 J. E. Martin and B. E. Eichinger, *Macromolecules*, 1983, **16**, 1345–1350.
86 S. M. Moghimi, A. C. Hunter and J. C. Murray, *Pharmacol. Rev.*, 2001, **53**, 283.
87 N. M. Zaki, A. Nasti and N. Tirelli, *Macromol. Biosci.*, 2011, **11**, 1747–1760.
88 E. H. Mejia, H. Contreras, E. Delgado and G. Quintana, *Int. J. Chem. Eng.*, 2019, 3085691.
89 G. Loch-Neckel, L. Santos-Bubniak, L. Mazzarino, A. V. Jacques, B. Moccelin, M. C. Santos-Silva and E. Lemos-Senna, *J. Pharm. Sci.*, 2015, **104**, 3524–3534.
90 S. K. Chinnaiyan, K. Deivasigamani and V. R. Gadela, *Int. J. Biol. Macromol.*, 2019, **125**, 278–289.
91 B. Mili, K. Das, A. Kumar, A. C. Saxena, P. Singh, S. Ghosh and S. Bag, *J. Mater. Sci.: Mater. Med.*, 2017, **29**, 4.
92 E. B. Mirzaei, A. S. A. Ramazani, M. Shafiee and M. Danaei, *Int. J. Polym. Mater.*, 2013, **62**, 605–611.
93 H. Sato, T. Takahashi, H. Ide, T. Fukushima, M. Tabata, F. Sekine, K. Kobayashi, M. Negishi and Y. Niwa, *Arthritis Rheum.*, 1988, **31**, 63–71.
94 Y. Liu, C. Zhou, W. Wang, J. Yang, H. Wang, W. Hong and Y. Huang, *Mol. Pharmaceutics*, 2016, **13**, 4209–4221.
95 N. Kongkatigumjorn, S. A. Smith, M. Chen, K. Fang, S. Yang, E. R. Gillies, A. P. R. Johnston and G. K. Such, *ACS Appl. Nano Mater.*, 2018, **1**, 3164–3173.
96 D. S. Wishart, C. Knox, A. C. Guo, S. Shrivastava, M. Hassanali, P. Stothard, Z. Chang and J. Woolsey, *Nucleic Acids Res.*, 2006, **34**, D668–D672.
97 D. S. Wishart, Y. D. Feunang, A. C. Guo, E. J. Lo, A. Marcu, J. R. Grant, T. Sajed, D. Johnson, C. Li, Z. Sayeeda, N. Assempour, I. Iynkkaran, Y. Liu, A. Maciejewski, N. Gale, A. Wilson, L. Chin, R. Cummings, D. Le, A. Pon, C. Knox and M. Wilson, *Nucleic Acids Res.*, 2018, **46**, D1074–D1082.
98 I. V. Tetko, J. Gasteiger, R. Todeschini, A. Mauri, D. Livingstone, P. Ertl, V. A. Palyulin, E. V. Radchenko, N. S. Zefirov, A. S. Makarenko, V. Y. Tanchuk and V. V. Prokopenko, *J. Comput.-Aided Mol. Des.*, 2005, **19**, 453–463.
99 I. Dewald, O. Isakin, J. Schubert, T. Kraus and M. Chanana, *J. Phys. Chem. C*, 2015, **119**, 25482–25492.
100 Z. Pan, D. Sampath, G. Jackson, K. Werrbach-Perez and R. Perez-Polo, in *Brain Plasticity: Development and Aging*, ed. G. Filogamo, A. Vernadakis, F. Gremo, A. M. Privat and P. S. Timiras, Springer US, Boston, MA, 1997, pp. 173–193, DOI: 10.1007/978-1-4757-9551-6_13.
101 M. Eng, V. Ling, J. A. Briggs, K. Souza, E. Canova-Davis, M. F. Powell and L. R. De Young, *Anal. Chem.*, 1997, **69**, 4184–4190.
102 P. C. Pagadala, L. A. Dvorak and K. E. Neet, *Proc. Natl. Acad. Sci. U. S. A.*, 2006, **103**, 17939–17943.
103 C. Moorthi and K. Kathiresan, *J. Med. Hypotheses Ideas*, 2013, **7**, 15–20.
104 J. Li, G. H. Shin, I. W. Lee, X. Chen and H. J. Park, *Food Hydrocolloids*, 2016, **56**, 41–49.
105 N. Ghayour, S. M. H. Hosseini, M. H. Eskandari, S. Esteghlal, A.-R. Nekoei, H. Hashemi Gahruie, M. Tatar and F. Naghibalhossaini, *Food Hydrocolloids*, 2019, **87**, 394–403.
106 A. Honasoge and H. Sontheimer, *Front. Physiol.*, 2013, **4**, 316.
107 J. U. Rao, D. Coman, J. J. Walsh, M. M. Ali, Y. Huang and F. Hyder, *Sci. Rep.*, 2017, **7**, 7865.
108 L.-m. Fang, B. Li, J.-j. Guan, H.-d. Xu, G.-h. Shen, Q.-g. Gao and Z.-h. Qin, *Acta Pharmacol. Sin.*, 2017, **38**, 1305.
109 J.-X. Song, Y.-R. Sun, I. Peluso, Y. Zeng, X. Yu, J.-H. Lu, Z. Xu, M.-Z. Wang, L.-F. Liu and Y.-Y. Huang, *Autophagy*, 2016, **12**, 1372–1389.
110 Y. Huang, Y. Chen, A. M. Shaw, H. Goldfine, J. Tian and J. Cai, *Oxid. Med. Cell. Longevity*, 2018, 5073420.
111 K. Wang, C. Zhang, J. Bao, X. Jia, Y. Liang, X. Wang, M. Chen, H. Su, P. Li and J.-B. Wan, *Sci. Rep.*, 2016, **6**, 26064.
112 J. Zhang, J. Wang, J. Xu, Y. Lu, J. Jiang, L. Wang, H.-M. Shen and D. Xia, *Oncotarget*, 2016, **7**, 75659.
113 C. Meyer, L. Stenberg, F. Gonzalez-Perez, S. Wrobel, G. Ronchi, E. Udina, S. Suganuma, S. Geuna, X. Navarro, L. B. Dahlin, C. Grothe and K. Haastert-Talini, *Biomaterials*, 2016, **76**, 33–51.
114 F.-Q. Zhou, *J. Visualized Exp.*, 2012, e4141.
115 Y.-w. Hu, Y.-z. Du, N. Liu, X. Liu, T.-t. Meng, B.-l. Cheng, J.-b. He, J. You, H. Yuan and F.-q. Hu, *J. Controlled Release*, 2015, **206**, 91–100.

Electronic Supporting Information

Facile design of autogenous stimuli-responsive chitosan/hyaluronic acid nanoparticles for efficient small molecules to protein delivery

Parinaz Sabourian,[a,b] Jeff Ji,[c] Victor Lotocki,[a] Alexandre Moquin,[a,c] Ramez Hanna,[a] Masoud Frounchi,[b,*] Dusica Maysinger,[c,*] Ashok Kakkar[a,*]

[a] Department of Chemistry, McGill University, 801 Sherbrooke St. West, Montreal, Quebec H3A 0B8 Canada

[b] Department of Chemical and Petroleum Engineering, Sharif University of Technology, Azadi Avenue, Tehran, Iran

[c] Department of Pharmacology and Therapeutics, McGill University, 3655 Promenade Sir William Osler, Montreal, Quebec H3G 1Y6 Canada

[*]**Corresponding Authors:** ashok.kakkar@mcgill.ca; dusica.maysinger@mcgill.ca; frounchi@sharif.edu

Table of Contents

1. ^{13}C NMR Analysis of DCS/FCS (Fig. S1) 2
2. Dynamic light scattering (DLS) analyses (Fig. S2) 3
3. TEM micrograph of porous NGF-FITC FCS/HA NP (Fig. S3) 4
4. Comparison of reactive oxygen species (ROS)-responsive behavior of thioketal diacid (TKDA) and FCS (Fig. S4) 4
5. Free Drug Release Profiles (Fig. S5-S6) 5
6. Evaluation of drug stability in the presence of ROS (Fig. S7) 6
7. UV-visible spectra of cargo compounds and derived standard curves (Fig. S8-9) 7
8. Transcription factor EB (TFEB) nuclear translocation in glioblastoma (GBM) cells (Fig. S10) 10
9. Nuclear magnetic resonance (NMR) data 11
10. ^{1}H NMR spectra (Fig. S11) 12

1. $^{13}C\{^{1}H\}$ NMR Analyses of DCS/FCS

Dissolution (DCS) and functionalization (FCS) of chitosan using TKDA was analyzed through ^{13}C NMR. In DCS, the TKDA *C*OOH peak showed a downfield shift from 175.2 ppm to 176.8 ppm. Similarly, the peak from the adjacent *C*H_2 is shifted downfield from 32.8 ppm to 34.3 ppm, while the other TKDA peaks remained consistent. Chemical coupling of TKDA to LCS to yield FCS further shifts the *C*OOH peak downfield to 178.3 ppm and the *C*H_2 peak to 35.7 ppm (Figure S1).

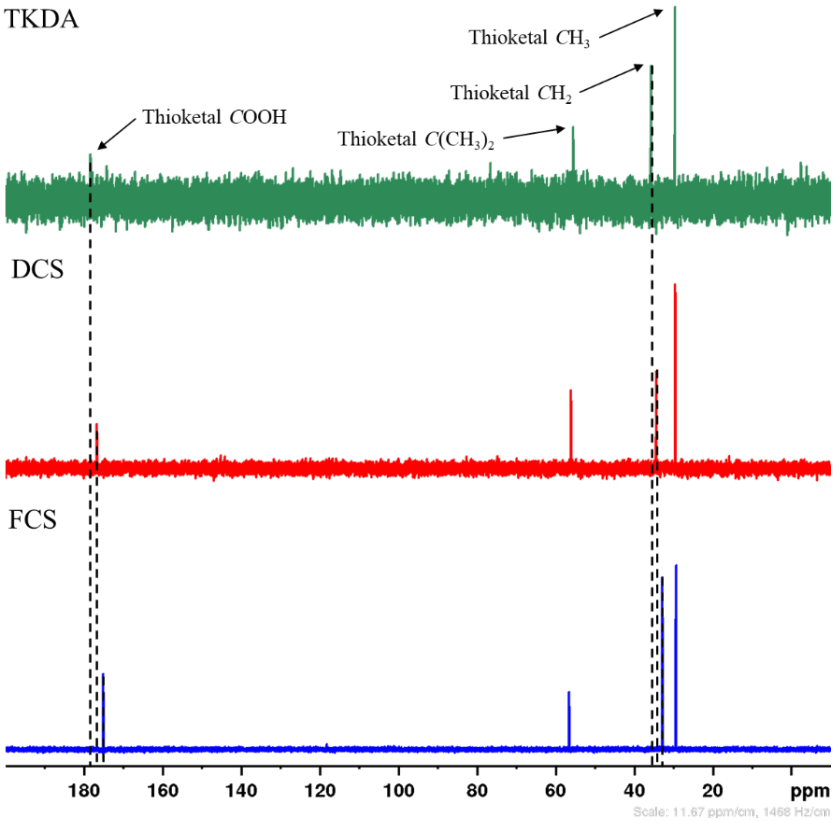

Fig. S1. ^{13}C NMR spectra of TKDA, DCS and FCS prepared by TKDA route.

2. Dynamic light scattering (DLS) analyses

Size distributions and mean hydrodynamic diameters of empty and drug loaded FCS/hyaluronic acid (HA) nanoparticles (NPs) are shown in Fig. S2.

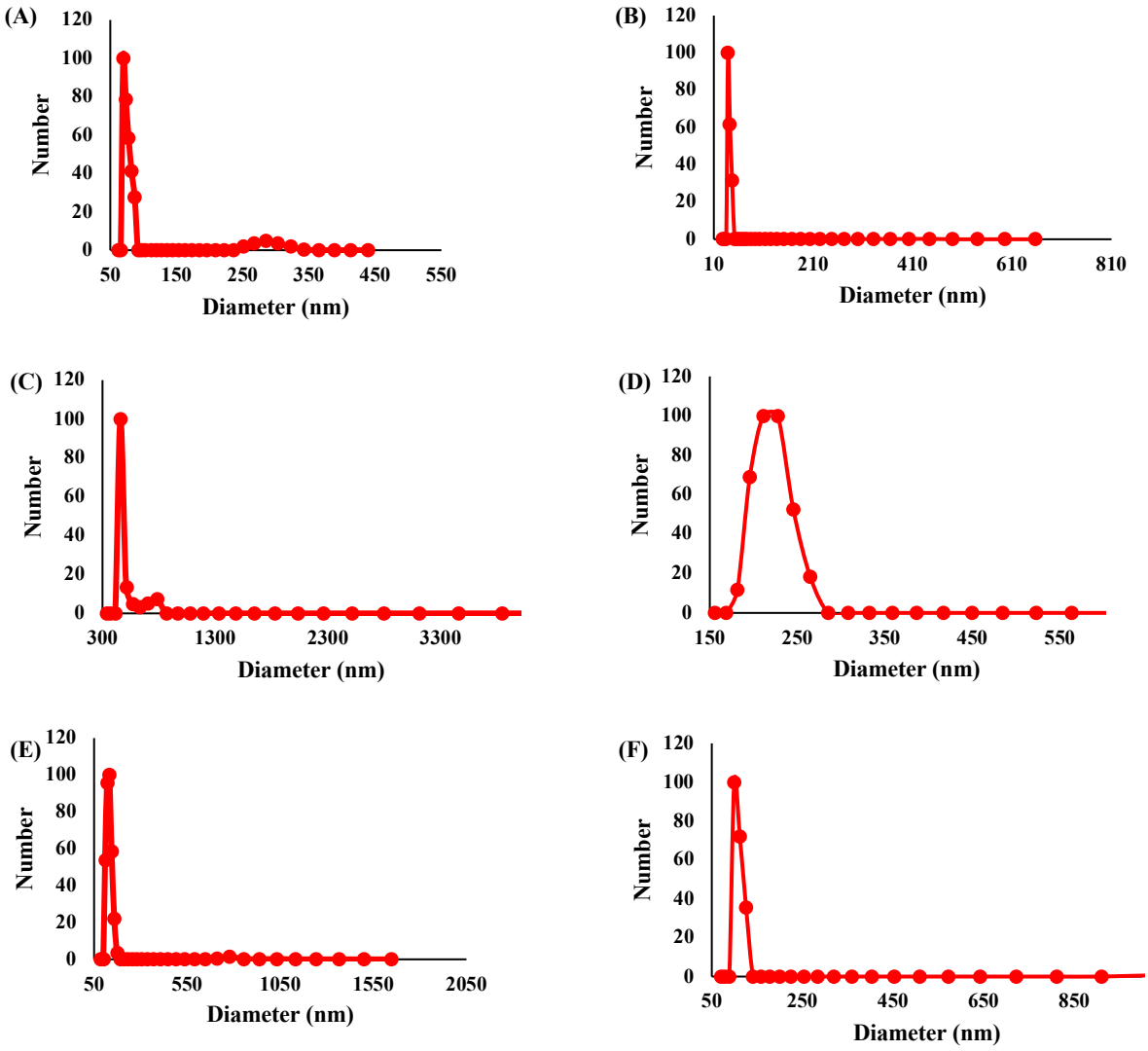

Fig. S2. DLS plots of size distributions for (A) CS/HA, (B) FCS/HA, (C) quercetin loaded CS/HA, (D) quercetin loaded FCS/HA, (E) curcumin loaded FCS/HA and (F) nerve growth factor-fluorescein isothiocyanate (NGF-FITC) loaded FCS/HA NPs.

3. TEM micrograph of porous NGF-FITC FCS/HA NP (Fig. S4)

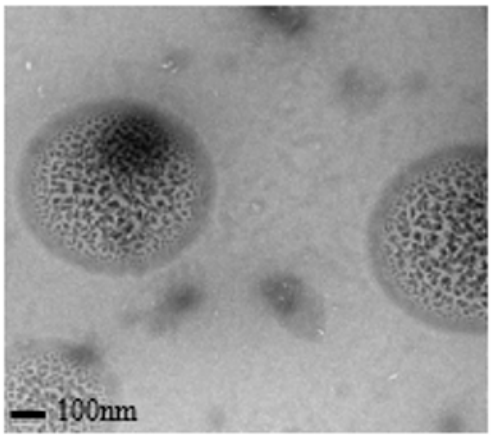

Fig. S3. NGF-FITC loaded FCS/HA porous nanospheres.

4. ROS-responsive behavior of TKDA and FCS

ROS-responsive behavior of the TKDA entity in FCS is exhibited in Fig. S4. The gradually increasing acetone peak over time is shown in top left of each spectrum with red color, as well as formation of SH group was observed between 1.6-1.7 ppm. Time dependent ^{1}H NMR spectra confirmed that TKDA as a ROS-responsive moiety in FCS responded to a small amount of hydrogen peroxide (12.2 µl of 200 mM H_2O_2).

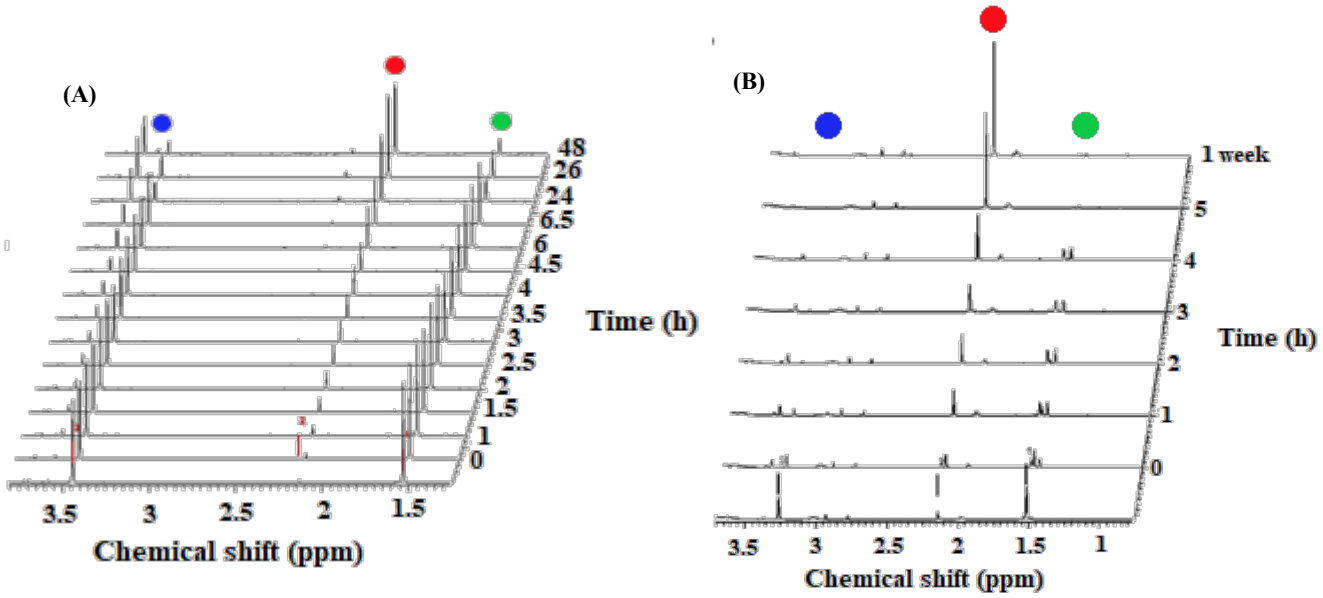

Fig. S4. Time dependent ^{1}H NMR spectra of (A) TKDA and (B) FCS responding to ROS. Green: C*H*$_3$, red: acetone and blue: C*H*$_2$ peaks.

5. Free Drug Release Profiles

As a control for NP-mediated drug release, both quercetin (Fig. S5) and curcumin (Fig. S6) were dissolved in a PEG_{350}/water/dimethyl acetamide mixture with a ratio of 45:40:15 v/v/v, and their drug release profiles were measured.

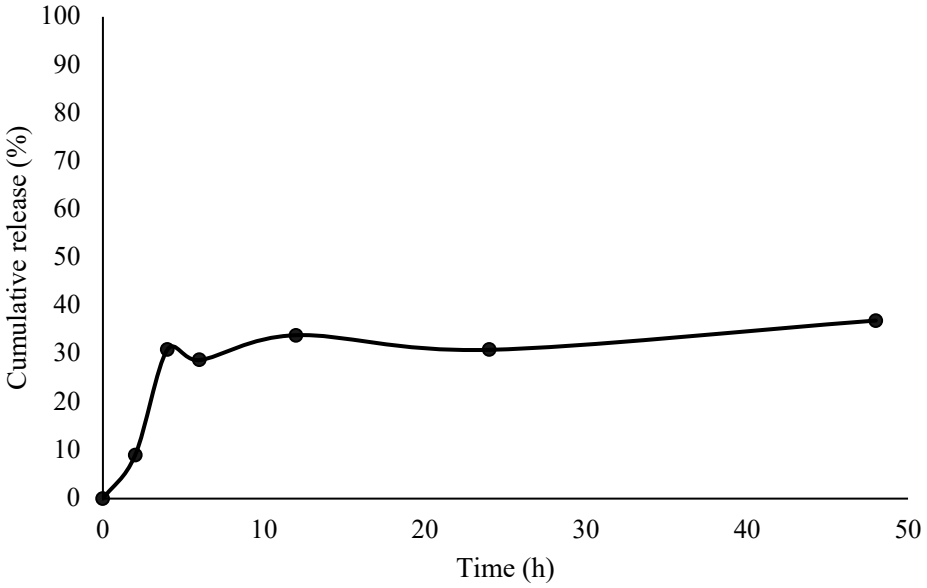

Fig. S5 Free cumulative quercetin release over 48 hours of dialysis time.

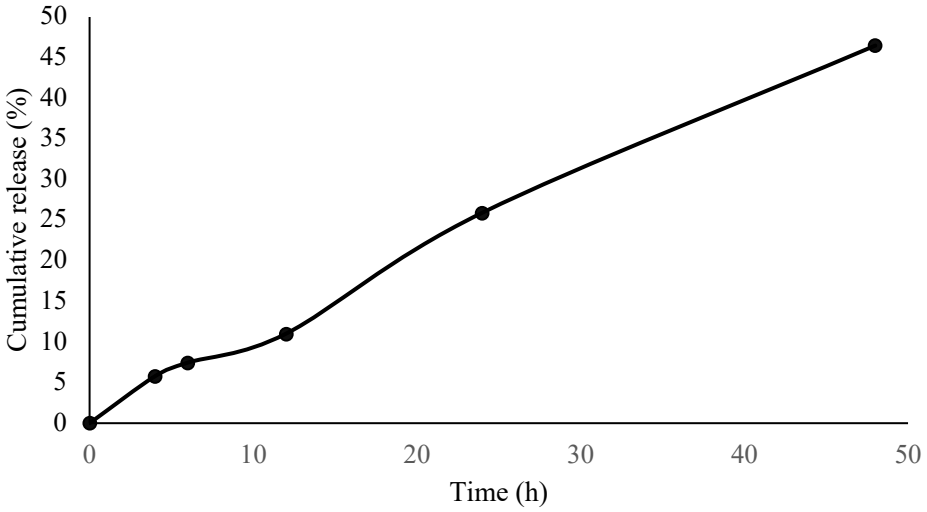

Fig. S6 Free cumulative curcumin release over 48 hours of dialysis time.

6. Evaluation of drug stability in the presence of ROS

To study stability of quercetin in a ROS medium, it was dissolved in methanol at a 0.25 mg/mL concentration. UV-Vis absorption spectra were recorded on a Varian Cary 50 UV-Vis spectrophotometer without H_2O_2, with 100 µM H_2O_2, at zero time and after 24h. Quercetin didn't show any difference in UV absorption peaks (at λ = 255 and 372 nm) after adding 100 µM H_2O_2, but after 24h small changes in UV absorption were observed (Fig. S7).

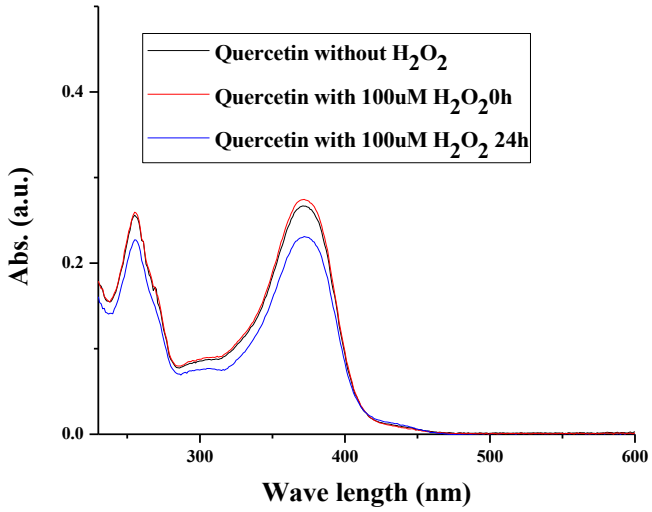

Fig. S7. Stability quercetin in the presence of 100 µM H_2O_2 at zero time and after 24h.

7. UV-visible spectra of cargo compounds and derived standard curves

UV-Vis spectra of different drug molecules and NGF-FITC are shown in Fig. S8. Fig. S9 showed calibration curves of curcumin, NGF-FITC and quercetin solutions with different determined concentrations.

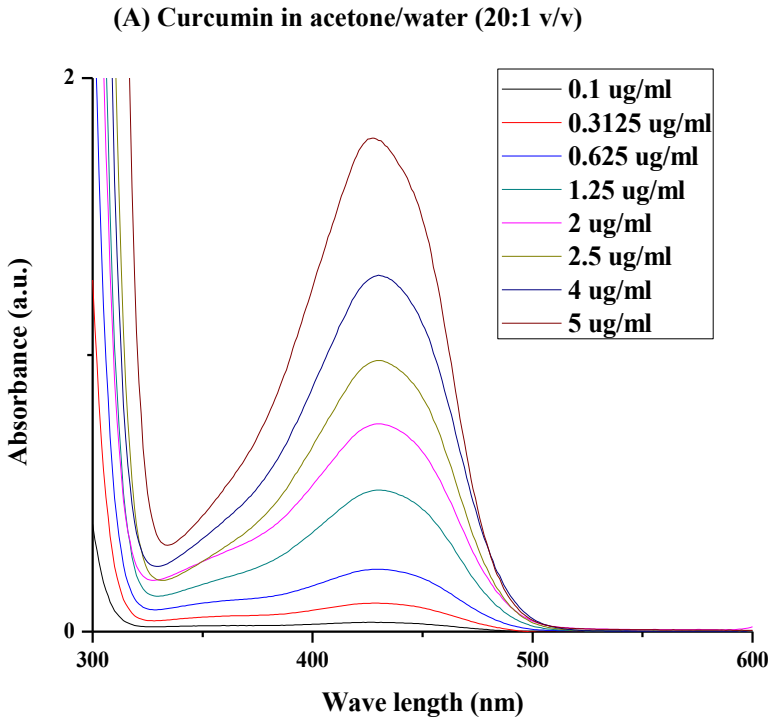

(B) NGF-FITC in water/sodium bicarbonate buffer (20:1 v/v)

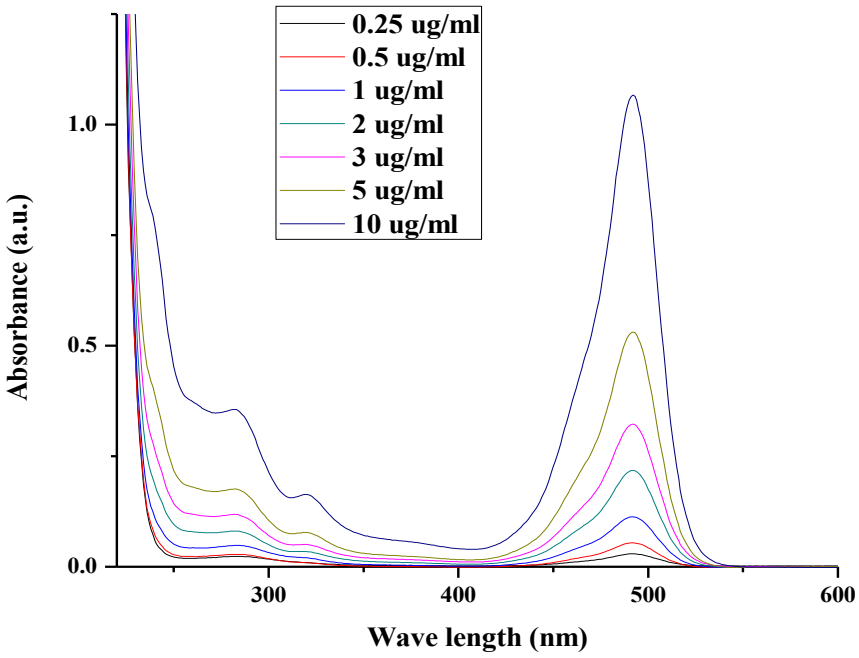

(C) Quercetin in methanol/water (20:1 v/v)

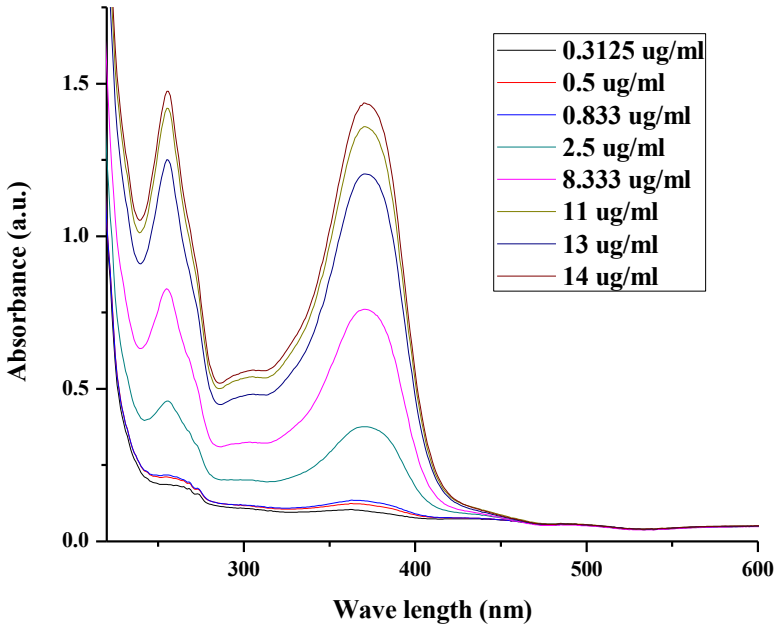

Fig. S8. UV-visible spectra of (A) curcumin, (B) NGF-FITC and (C) quercetin taken to prepare standard curves for each compound

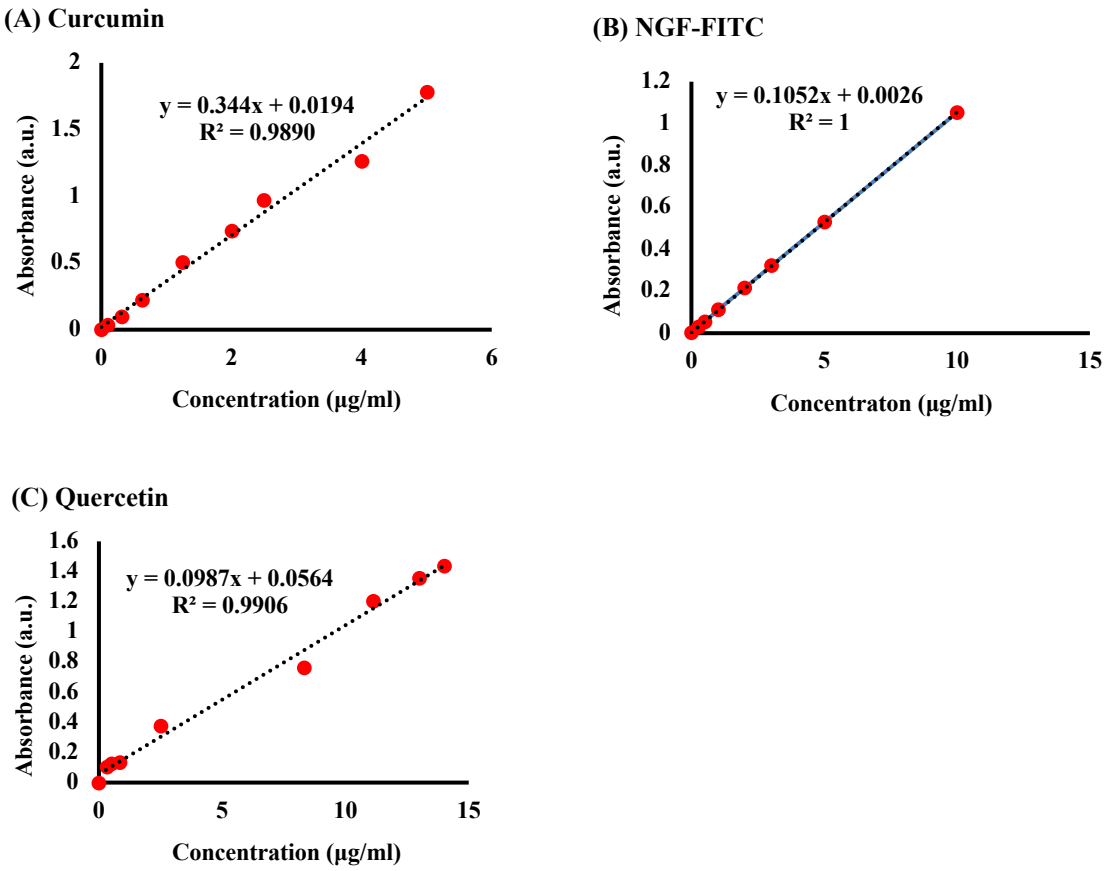

Fig. S9. Calibration curves of (A) curcumin, (B) NGF-FITC and (C) quercetin solutions based on UV-visible spectrophotometry at λ= 437, 494 and 255 nm, respectively.

8. Transcription factor EB (TFEB) nuclear translocation in glioblastoma (GBM) cells

We found comparable TFEB nuclear translocation in GBM treated with curcumin loaded FCS/HA NPs or free curcumin (Fig. S10). Treatment with curcumin loaded FCS/HA NPs showed reduced TFEB nuclear translocation after 1h compared to free curcumin (Fig. S10A-B), although TFEB nuclear translocation became comparable after 8h. Empty FITC-labelled FCS/HA NPs did not induce TFEB nuclear translocation.

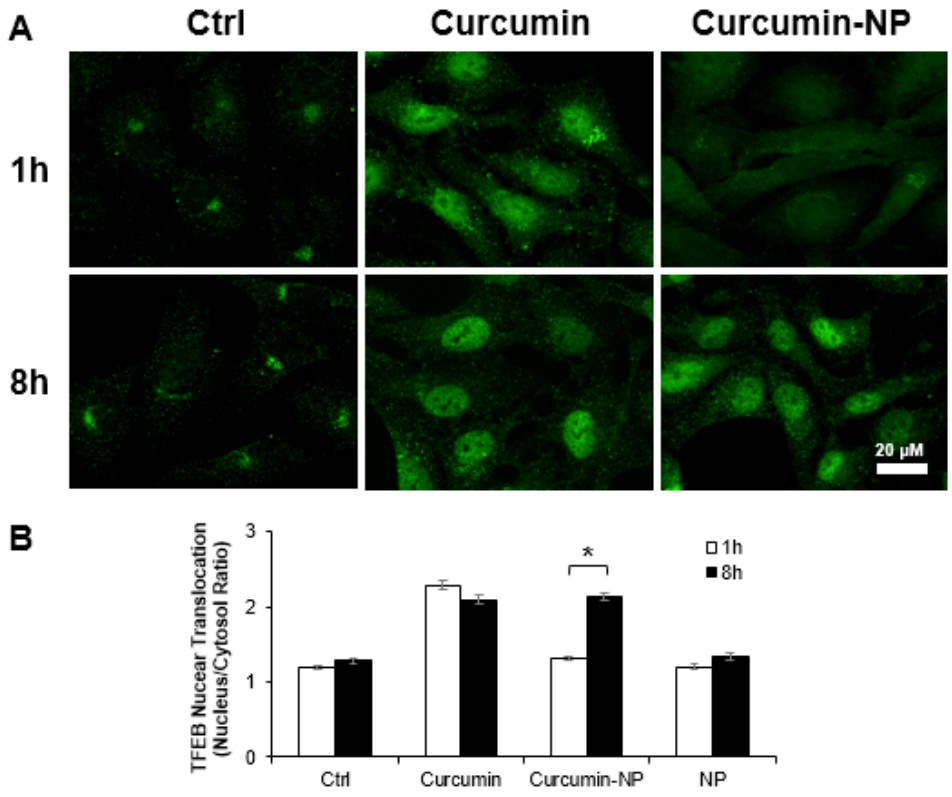

Fig. S10. Intracellular curcumin enhances the fluorescence of nuclear TFEB after 8h. U251 cells were treated with 20 μM free curcumin/curcumin loaded NPs, or equivalent empty FCS/HA NPs for 1h and 8h in serum-free media. (A) Representative photomicrograph of TFEB. (B) Quantification of TFEB nuclear translocation (ratio of average fluorescence of TFEB in the nucleus to cytosol). N>36 cells per condition, error bars = SEM. * denotes significance at $p < 0.05$ comparing 1h to 8h. This highlights the delay in TFEB nuclear translocation in curcumin-NP compared to free curcumin.

9. Nuclear magnetic resonance (NMR) data

CS

^{1}H NMR (400 MHz, D_2O): δ_H (ppm) 1.91 (1059H, s, CH_3), 3.04 (706H, brs, CH), 3.44-3.78 (3530H, m, CH, CH_2), 4.75 (706H, s, CH)

^{13}C NMR (400 MHz, D_2O): δ_C (ppm) 30.19 (353C, CH_3), 59.96 (706C, CH), 69.83 (706C, CH_2), 74.64 (706C, CH), 76.16 (706C, CH), 88.70 (706C, CH), 97.25 (706C, CH), 130.9 (353C, CONH)

TKDA

^{1}H NMR (400 MHz, D_2O): δ_H (ppm) 1.54 (6H, s, CH_3), 3.44 (4H, s, CH_2).

^{13}C NMR (500 MHz, D_2O): δ_C (ppm) 29.4, 32.8, 56.5, 175.2.

DCS

^{1}H NMR (400 MHz, D_2O): δ_H (ppm) 1.53 (6H, s, CH_3), 1.98 (1059H, s, CH_3), 3.09 (706H, brs, CH), 3.35 (4H, s, CH_2), 3.49-3.83 (3530H, m, CH, CH_2), 4.80 (706H, s, CH)

FCS

^{1}H NMR (400 MHz, D_2O): δ_H (ppm) 1.52 (6H, s, CH_3), 1.99 (1059H, s, CH_3), 3.00 (706H, brs, CH), 3.27 (4H, s, CH_2), 3.63-3.80 (3530H, m, CH, CH_2), 4.75 (706H, s, CH)

10. ^{1}H NMR Spectra

CS: ^{1}H NMR (D_2O)

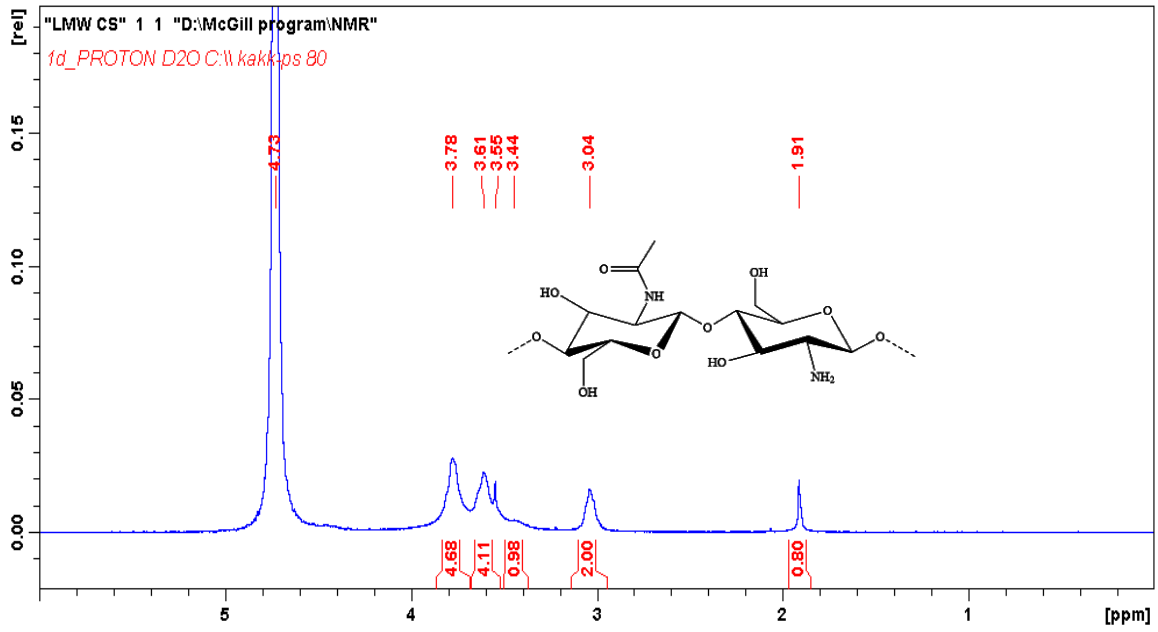

TKDA: ^{1}H NMR (D_2O)

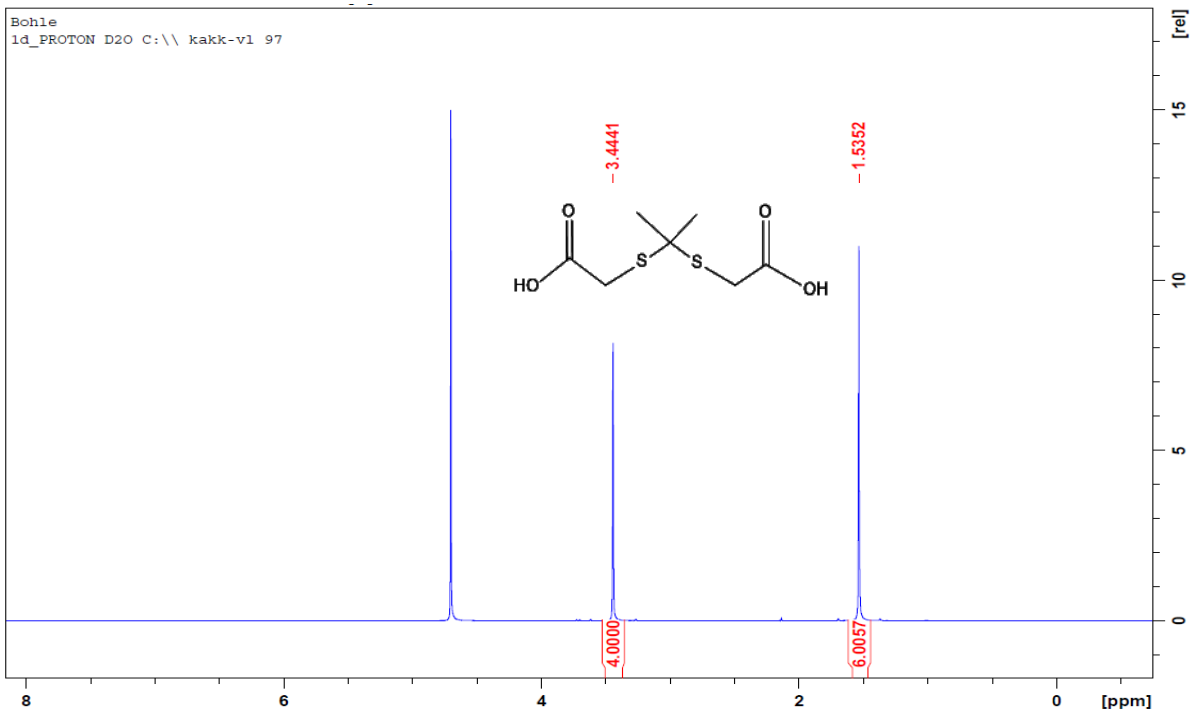

DCS: ^{1}H NMR (D_2O)

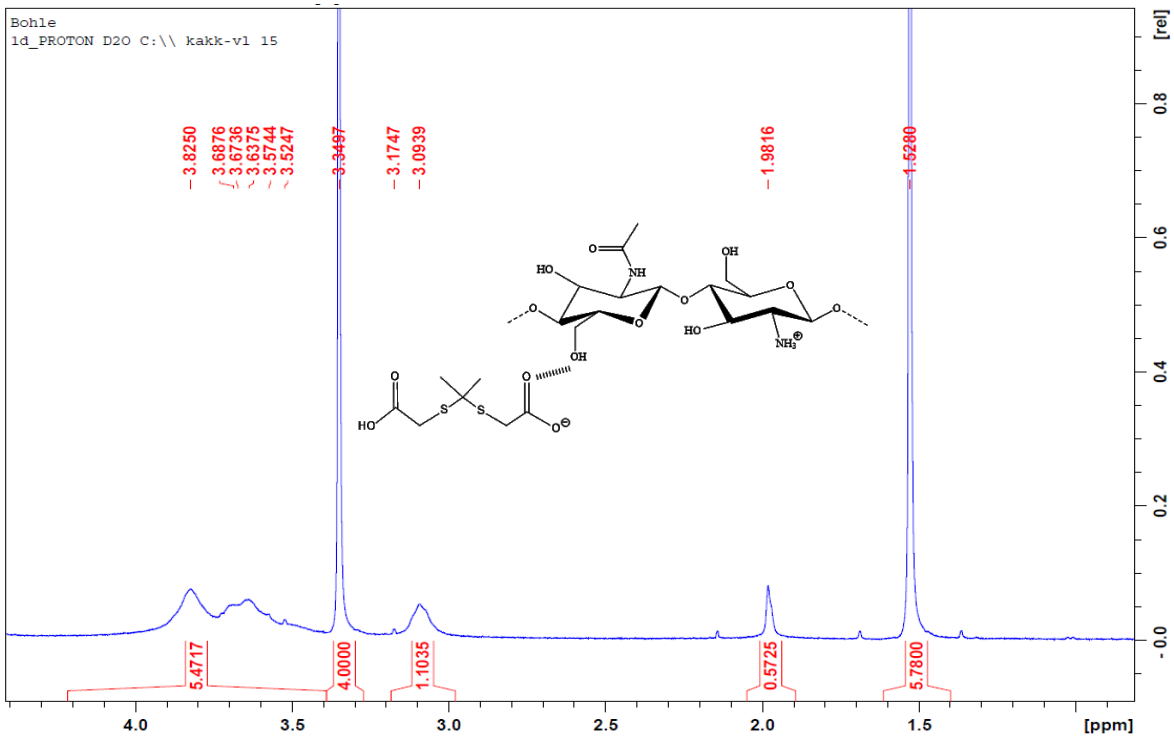

FCS: ^{1}H NMR (D_2O)

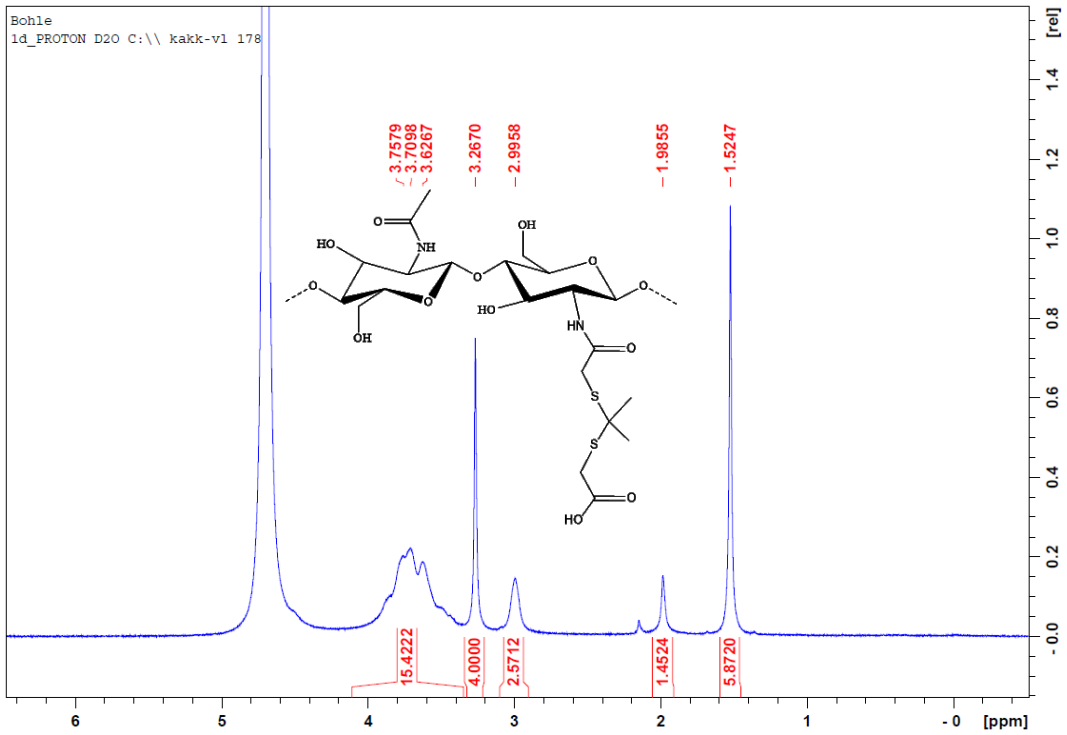

Fig. S11. ^{1}H NMR spectra obtained using Bruker AVIIIHD 400 instrument (400 MHz).